High light induced changes in metabolites, lipids and thylakoid supercomplexes organisation of cyclic electron transport deficient mutant of *Chlamydomonas reinhardtii*

Thesis submitted for the degree of Doctor of Philosophy

By

Nisha Chouhan



Department of Plant Sciences
School of life sciences
University of Hyderabad
Hyderabad, Telangana India



Department of Plant Sciences School of Life Sciences University of Hyderabad Hyderabad 500046



DECLARATION

I, Nisha Chouhan, hereby declare that this thesis entitled "High light induced changes in metabolites, lipids and thylakoid supercomplexes organisation of cyclic electron transport deficient mutant of *Chlamydomonas reinhardtii*" submitted by me under the guidance and supervision of Professor S. Rajagopal is original and independent research work. I also declare that it has not been submitted previously in part or in full to this University or Institution for the award of any degree or diploma.

Date: 23/05/2022

Nisha Chouhan

(Regd. No: 16LPPH10)

rof. S. Rajagobal 23/05/2022 (Supervisor)

Prof. S. RAJAGOPAL

Prof. S. RAJAGOPAL

Dept. of Plant Sciences
School of Life Sciences
School of Lyderabad
University of Hyderabad
Hyderabad-500 046.



Department of Plant Sciences School of Life Sciences University of Hyderabad Hyderabad 500046



CERTIFICATE

This is to certify that the thesis "High light-induced changes the metabolites, lipids and thylakoid supercomplexes organisation of cyclic electron transport deficient mutant of *Chlamydomonas reinhardtii*" submitted by Mrs. Nisha Chouhan bearing registration number 16LPPH10 in partial fulfillment of the requirements for the award of Doctor of Philosophy in Plant Sciences, in the Department of Plant Sciences, School Life Sciences, University of Hyderabad is a record of bonafide work carried out by her under my supervision and guidance. This thesis is free from plagiarism and has not been submitted in part or in full to this or any other University or Institution for the award of any degree or diploma.

Parts of the thesis have been:

- A. Published in the following publication:
 - 1. Front. Plant Sci. 12:752634
 - 2. Photosynth Res. 2020 Dec;146(1-3):247-258
 - 3. Photosynth Res. 2019 Mar;139(1-3):253-266
- B. Presented in the following conferences:
 - 1. Poster presentation in "8th international conference on "photosynthesis and hydrogen energy research for sustainability 2017" at University of Hyderabad, Hyderabad, India; from October 30th November 3rd, 2017.
 - 2. Oral presentation in Plant Science colloquium 2022 at University of Hyderabad, Hyderabad, India.
 - 3. Oral presentation via webinar in Indo-Japan Binational meeting (2022) at the University of Hyderabad, Hyderabad, India

Further, the student has passed the following courses towards the fulfillment of the coursework requirement for Ph.D.

S.No.	Course Code	Name	Credits	Pass/Fail
1	PL801	Analytical Techniques	4	Pass
2	PL802	Research ethics, Data Analysis and biostatistics and management	3	Pass
1	PL803	Lab work & Seminar	5	Pass

Supervisor

Prof. S. RAJAGOPOS Prof. S. Plant Sciences Dept. of Plant Sciences School of Life Sciences School of Life Sciences University of Hyderabad University of Hyderabad Head of the Department

HEAD
Dept. of Plant Sciences
School of Life Sciences
University of Hyderabad
Hyderabad-500 646 IND18

Dean of the School

School of Life Sciences University of Hyderabad Hyderabad-500 046.



Department of Plant Sciences School of Life Sciences University of Hyderabad Hyderabad 500046



Plagiarism Free Certificate

This is to certify that similarity index of this thesis has been checked by the library of University of Hyderabad is 33 %. Out of this 26 % similarity has been found to be identify from the candidate own publication which forms the major part of the thesis. The details of student publication are as follows.

Autophagy induced accumulation of lipids in pgrl1 and pgr5 of Chlamydomonas reinhardtii under high light (Chapter 4).

About 7 % similarity was identify from the external source in the present thesis which is according to prescribed regulations of the university. All the publications related to thesis have been appended at the end of the thesis. Hence, the present thesis considered to be plagiarism free.

Supervisor

Prof. S. RAJAGOPAL
Prof. S. RAJAGOPAL
Dept. of Plant Sciences
School of Life Sciences
School of Life Sciences
University of Hyderabad
Hyderabad-500 046.

This Thesis is dedicated to my Beloved Parents & my husband



Acknowledgment

I would like to express my deep gratitude to my supervisor Prof. S. Rajagopal for guidance, enthusiastic encouragement, and useful critiques of this research work. Continually and convincingly conveyed a spirit of adventure regarding research and scholarship. Without his guidance and persistent help, this Ph.D. would not have been possible

I also thank my Doctoral committee member Prof. Ch. Venkataramana and Prof. Naresh Babu V. Sepuri for their valuable suggestion and encouragement.

I thank the present and former Deans, Prof. S. Dayananda, Prof. K.V.A. Ramaiah and Prof. P. Reddana, School of Life Sciences, for allowing me to school facilities.

I thank present and former Head of Department Prof. G. Padmaja and Prof. Ch. Venkataramana for allowing me to use school and department facilities.

My sincere thanks to my host supervisor Prof. Yuichiro Takahashi for scientific discussion, Dr. Shin-Ichiro Ozawa and Dr. Hiroshi Khudawa, and Miyuki Ishihara san for teaching and guiding me during my visit to Okayama University, Japan.

I would like to thank Dr. Jagadish Gupta and his students Ms. Aprajita Roy and Ms. Pooja Singh from NIPGR for metabolomic analysis.

I would like to thank Prof. Gilles Peltier (CEA-CNRS- Aix Marseille University, France) and Prof. Michael Hippler (University of Munster) for providing *pgrl1* and *pgr5* strains.

I would like to thank my lab mates Drs. Sai Kiran, Elsin Raju, Aparna, Srilatha Nama, Shreya, Ranay, Jayendra, Yusuf, Jyoti Ranjan and Pavitra. My sincere thanks to Mr. Ganesh for their cooperation and assistance in the lab. I thank Dr. Suresh Marriboina for helping me in the analysis of metabolomic analysis data.

I especially thank my friends Minu, Sangeeta, Priyanka, Jahnbi, Rakhee, Dipti, and all my friends in life sciences for their moral support and encouragement when I needed them.

I thank faculty members of the school of life sciences for their support and encouragement. Sincere thanks to the non-teaching and technical staff of the School of Life Sciences. I thank the school of Life Science instrument facility and plant sciences instrument facility. I also thank Dashrath for helping me in the confocal microscopy & ultracentrifugation facility and other office staff.

My sincere thanks to DBT-JRF-SRF for the fellowship and financial support for my Ph.D. and to the lab. I also thank infrastructure grant to the department of plant sciences, school of life science. I thank the funding agencies of lab, DBT- Builder, UGC-SAP, DST-FIST, IOE, DBT, SERB, UGC-ISF, JST, CSIR, and DST. I also thank SERB-OVDF for providing me opportunities to visit overseas (Okayama university Japan) for my work. I also thank JST for allowing me to work in Japan.

Finally, I thank my parents, my husband, brother, sister, and my in-laws for their everlasting love and moral support.

Content

Chapter 1. General introduction Page Nos.		
1 1	NC 1	1.7
1.1	Microalgae	17
1.2	Photosynthesis	18
1.3	PSI-LHCI and PSII-LHCII supercomplexes organization	21
1 1	in microalgae light- in harvesting systems	24
1.4	Reactive oxygen species	24
1.5	Autophagy	26
1.6	Algal fuels	28
1.7	Biofuels and photosynthesis	30
1.8	Lipid composition in microalgae	31
1.9	Carotenoids and xanthophyll	34
1.10	Metabolism	36
1.11	Abiotic stress	38
1.12	Strains of <i>C. reinhardtii</i>	39
1.13	The objective of the study	40
Chap	ter 2. Materials and methods	42-54
2.1	Model organism C. reinhardtii description	42
2.2	Strains and culture conditions	42
2.3	Spectrophotometric measurement	42
2.4	Biomass determination	43
2.5	ROS detection by confocal microscopy	43
2.6	Transmission electron microscopy	44
2.7	Localization of ATG8 from immunofluorescence microscopy	44
2.8	Lipid body analysis by Nile red	45
2.9	Nile Red visible light assay for Triacylglycerol	45
2.10	Flow cytometry measurements	46
2.11	Total starch quantification	46
2.12	Lipid analysis and quantification	46
2.13	FAME analysis of total lipid	47
2.14	Isolation of thylakoid membrane	48
2.15	Sucrose density gradient (SDG) ultracentrifugation	49
2.16	Measurements of circular dichroism spectroscopy	49
2.17	Pigment content determination by HPLC of cells/thylakoids/SDG fraction	50
2.18	Immunoblot analysis	50
2.19	Spectroscopy	51
2.20	Observation of aggregation	51
2.21	RNA isolation and cDNA synthesis	52
2.22	Quantitative real-time PCR	52
2.23	The extraction method and sample preparation of metabolites	53
2.24	Mass spectrometry analysis	54
2.25	Total protein quantification	54
2 26	Statistical analysis	5/

in high light from pgrl1 and pgr5 mutants of Chlamydomonas reinhardtii				
3.1 Introducti	on	57-59		
3.2 Results				
3.2.1	Growth and pigment analysis under high light	59		
3.2.2	ROS induction in high light	61		
3.2.3	Characterization of the supercomplexes isolated from sucrose densi	ty		
	Gradient	62		
3.2.4	77k fluorescence emission spectra data analysis	64		
3.2.5	Absorption spectra analysis of SDG fractions	66		
3.2.6	Pigment-protein interaction studies from visible circular			
	dichroism spectra	68		
3.2.7	Conformational change in the secondary structure under high light	70		
3.2.8	Carotenoid derivatives change under high light grown cells	70		
3.2.9	Carotenoid derivatives in thylakoids	72		
	Carotenoid associated pigments with LHCII trimers (F1 fractions)	73		
3.2.11	Carotenoid associated pigments of PSII-LHCII	7.4		
2 2 12	supercomplex (F2 fraction)	74		
3.2.12	Carotenoid associated pigments of PSI-LHCI supercomplex (F3 fraction)	74		
3.2.13		/4		
3.2.13	pathway under high light	76		
3 2 14	Immunoblot analysis of SDG fractions	77		
	Confocal image of aggregated cells and immunoblots	, ,		
3.2.13.	of unsolubilized thylakoids	79		
3.3 Discussion	1	81-84		
3.4 Conclusion	n	85-86		
Chapter 4. Aı	utophagy induced accumulation of lipids in pgrl1 and pgr5 of			
Chlamydomoi	nas reinhardtii under high light	88-102		
4.1 Introducti	on	88-90		
4.2 Results				
4.2.1	Cellular localization of ATG8	90		
4.2.2		92		
4.2.3	Neutral lipid identification by NR fluorescence	94		
4.2.4	Neutral lipid and membrane lipid analysis by TLC	95		
4.2.5 Transmission electron microscopy studies		96		
4.2.6	± •	98		
	Protein analysis by immunoblot	99		
4.2.8	Fatty acid composition under high light conditions	100		
4.2.9 Neutral lipid and membrane Lipid Analysis		102		

4.3 Discussion		
4.3.1 4.3.2 4.3.3	High light induces reactive oxygen species and autophagy in <i>C. reinhardtii</i> High light induces a high amount of lipid in <i>C. reinhardtii</i> High light alters the fatty acid composition in <i>C. reinhardtii</i>	104 106 108
4.4 Conclusio	n	108
Chapter 5. Id	entification and characterization of metabolomics profile	
from cyclic el	lectron transport mutants	110-133
5.1 Introduction	on	110-112
5.2 Results		112-124
5.2.1 5.2.2 5.2.3	Metabolites profiling and PCA analysis The pathway enrichment analysis under HL Correlation-based clustering among the metabolites	112 116
5.2.4 5.2.5	in <i>C. reinhardtii</i> Network analysis of <i>C. reinahrdtii</i> under HL Differential expression of genes associated with	119 122
	TCA cycle under HL in <i>C. reinhardtii</i>	124
5.3 Discussion		126-132
5.3.1 5.3.2 5.3.3	Enhancement of carbohydrate, fatty acids, and organic acids under HL	126 127 128
5.3.4 5.3.5	The study of metabolite correlations yields new insights HL induced changes in expression of the gene of TCA cycle and TCA metabolites	130 131
5.4 Conclusion		
Chapter 6 SU	JMMARY	147-149
Bibliography		

List of Figures

Figure 1.1	Schematic re	epresentation	of <i>C</i> .	reinhardtii
------------	--------------	---------------	---------------	-------------

- **Figure 1.2** Schematic diagram of linear electron transport of *C. reinhardtii*
- Figure 1.3 Schematic diagram of cyclic electron transport of *C. reinhardtii*
- **Figure 1.4** Supramolecular organization of PSII-LHCII supercomplex of *C. reinhardtii*
- **Figure 1.5** Supramolecular organization of PSI-LHCI supercomplex of *C. reinhardtii*
- **Figure 1.6** Schematic representation of the production of reactive oxygen species from different organelles
- **Figure 1.7** The pathway of autophagy in *C. reinhardtii*
- **Figure 1.8** Schematic representation of the major TAG biosynthesis pathways in *C. reinahrdtii*
- Figure 1.9 Thylakoid lipids association with PSII and pathway of polar lipid synthesis
- Figure 1.10 Carotenoid biosynthetic pathway in C. reinhardtii
- **Figure 1.11** Schematic diagram showing the interaction networks of photosynthesis and metabolism in *C. reinhardtii*
- Figure 3.1 Cell growth and dry biomass were monitored from cells grown under normal light and high light conditions
- Figure 3.2 Chlorophyll and carotenoid content were quantified from cells grown under normal and high light conditions
- Figure 3.3 Total Reactive oxygen species were measured with H2DCFDA
- **Figure 3.4** Fractionation of major thylakoid membrane complexes of WT, *pgrl1*, and *pgr5* of *C. reinhardtii*
- **Figure 3.5** 77k fluorescence emission spectra of thylakoids
- **Figure 3.6** 77k fluorescence emission spectra of SDG fractions
- **Figure 3.7** Absorbance spectra of pigment binding complexes isolated from *C. reinhardtii*
- **Figure 3.8** Visible Circular dichroism spectra of pigment binding complexes isolated from *C. reinhardtii*
- **Figure 3.9** Circular dichroism spectra of secondary structure
- Figure 3.10 Pigment composition of thylakoids and Chlorophyll content of SDG fractions
- **Figure 3.11** Pigment composition of SDG fractions of WT, *pgrl1*, and *pgr5* under normal and high light
- **Figure 3.12** Real-time PCR of WT, *pgrl1*, and *pgr5* of *C. reinhardtii* under normal and high light
- **Figure 3.13** Immunoblots of SDG fractions of WT, *pgrl1*, and *pgr5* mutant strains under normal and high light
- Figure 3.14 Confocal image of aggregated cells and Immunoblots of unsolubilized cells
- **Figure 4.1** Autophagy (ATG)8 accumulation in C. reinhardtii cells under high light conditions
- **Figure 4.2** Lipid droplets were identified through confocal microscopy and FACs analysis
- Figure 4.3 Neutral lipid content is quantified from the cells grown under normal and high light
- **Figure 4.4** Alteration of membrane lipid and TAG in *C. reinhardtii* cells grown under normal and high light conditions
- Figure 4.5 Ultrastructure analysis of *C. reinhardtii* cells during normal and high light
- Figure 4.6 Ultrastructure analysis of Chlamydomonas cells during normal and high light
- Figure 4.7 Total carbohydrate content quantified by Anthrone method from the cells

	grown under normal to high light conditions
Figure 4.8	Protein identification from western blot analysis
Figure 4.9	Changes in lipid composition of <i>C. reinhardtii</i> cells grown under high light conditions.
Figure 5.1	A heat map showing the significantly changing metabolites
Figure 5.2	Principle component analysis (PCA plot)of the metabolites
Figure 5.3	Analysis of metabolic pathways of WT, <i>pgrl1</i> , and <i>pgr5</i> under control and high light
Figure 5.4	Analysis of metabolic pathways of WT, pgrl1, and pgr5 under high light
Figure 5.5	Metabolites – metabolites correlation heat map hierarchical clustering of WT, <i>pgrl1</i> , and <i>pgr5</i> under normal and HL
Figure 5.6	Metabolite – metabolites correlation heat map hierarchical clustering of WT, <i>pgrl1</i> and <i>pgr5</i> under HL
Figure 5.7	Correlation network of metabolites based on Pearson's coefficient
Figure 5.8	The relative content of TCA cycle intermediate of cells of WT, pgrl1, and pgr5
Figure 5.9	An overview of the proposed metabolite change in <i>C. reinhardtii</i> under High light conditions

List of Tables

Chapter 2		
	Table 2.1	Internal standard mix for total fatty acid
	Table 2.2	Primers used for qRT-PCR analysis
Chapter 3		
	Table 3.1	Carotenoid content of <i>C. reinhardtii</i> under normal and high light
		conditions
	Table 4.1	,
		conditions
Chpater 5		
	Table 5.1	Relative concentration and fold changes of major metabolites in
		WT under normal and high light in C. reinhardtii
	Table 5.2	Relative concentration and fold changes of major metabolites in
		pgrl1 under normal and high light in C. reinhardtii
	Table 5.3	Relative concentration and fold changes of major metabolites in
		pgr5 under normal and high light in C. reinhardtii
	Table 5.4	Relative concentration and fold changes of major metabolites in WT
		and pgrl1 under high light in C. reinhardtii
	Table 5.5	Relative concentration and fold changes of major metabolites of
		WT and pgr5 under high light in C. reinhardtii
	Table 5.6	Relative concentration and fold changes of major metabolites of
		pgrl1 and pgr5 under high light in C. reinhardtii

Abbreviations

ACN Acetonitrile
ACE Acetamide
Aris Aristeromycin

ATP Adenosine triphosphate
ATG Autophagy-related genes

BA Boric acid

BHB 3-Hydroxybutyric acid
BSA Bovine serum albumin
β-DM n-dodecyl -D-maltoside

CA Citric acid
Carb Carbamic acid

CBLP Guanidine nucleotide-binding protein beta subunit -like

Chry Chrysanthemol alcohal

CBB Calvin-Benson-Bassham cycle
CET Cyclic electron transport

Chl Chlorophyll
CAC Citric acid cycle
Chl Chlorophyll
CD Circular dichroism
CO₂ Carbon dioxide

Cyt b6f Cytochrome b6f complex

DAG Diacylglycerol

DGAT Diacylglycerol acyltransferase DGDG Digalactosyldiacylglycerol

DGD1 Digalactosyldiacylglycerol synthase

DNA Deoxyribonucleic acid

DP D-pinitol
DTT Dithio-threitol
DW Dry weight
Ela Ellagic acid

ER Endoplasmic reticulum

Erg Ergosterol
MEA Ethanolamine
FA Fumaric acid

FAME Fatty acid methyl esters

FACS Fluorescent activated cell sorter

Fd Ferridoxin
Fru Fructose

FNR Ferredoxin NADP reductase

GA Glycolic acid

GA3P Glycerol 3 phosphate

GAPDH4 Glyceraldehyde 3-phosphate dehydrogenase

Gg Glyceryl-glycoside

GLY Glycine

Glu Glutamate

GGP Glucose 6 phosphate
GC Gas chromatography
GHB Gama-hydroxybutyrate

HL High light

H₂O₂ Hydrogen peroxide IPP Inositol pentaphosphate

I1P D-myo-Inositol-1-monophosphate

Ile L-Isoleucine
77K 77Kelvin
LA Lactic acid
L-Ala L- alanine
L-Val L-Valine

LET Linear electron transport

LC/MS Liquid chromatography/mass spectrometry

LHCI Light-harvesting complexes I
LHCII Light-harvesting complexes II
LHCSR3 Light-harvesting stress related

H₂DCFDA 2,7-dichlorodihydrofluorescein diacetate HPLC High performance liquid chromatography

Ma Malic acid

3MA methoxyamphetamine MA N-methyl-acetamide

MGD1 Monogalactosyldiacylglycerol synthase

MGDG Monogalactosyldiacylglycerol

MP Monopalmitoyl serinol

MSTFA N-methyl-N-(trimethylsilyl) trifluoroacetamide

MUFA Monounsaturated fatty acid NAA N-Acetyl-beta-alanine

NADPH Nicotinamide adenin dinucleotide phosphate

NALA N-acetyl-L-aspartic acid

NPHY Neophytadiene

NPQ Non photochemical quenching

NR Nile red

PB 1-(3-Pyridinyl)-1,4-butanediol

PC Plastocynin
PEC Palmitic acid
Phy Phytol
Put Putrescine

PBS Phosphate saline buffer

PSI Photosystem I PSII Photosystem II

PGR5 Proton gradient regulation5

PGRL1 PGR5- like photosynthetic phenotype

PE Phosphatidylethanolamine

PAG Palmitoyl serinol
PA Propionic acid

PAPE Phosphoric acid propyl ester

PEP Phosphoenolpyruvate

PPM 2-Phenyl-1,3-propanediol monocarbamate

Phe L-Phenylalanine PQ Plastoquinone

PDAT Phospholipid: diacylglycerol acyltransferase

PUFA Polyunsaturated fatty acids

PG Phosphoglycerol

Pro Proline Rib Ribitol

Ribf Ribofuranose

ROS Reactive oxygen species

RNA Ribonucleic acid
RT Room Temperature

RT-PCR Realtime Polymerase chain reaction

O₂• Superoxide anion radical

OH' Hydroxyl radical

O₂ Oxygen

¹O₂ Singlet oxygen

OEC Oxygen evolving complexes

OD Optical density

Ser Serine Sil Silanol

¹Chl* Singlet chlorophyll SFA Saturated fatty acid

SQDG Sulfoquinovosyldiacylglycerol

Sta6 Starchless

TAG Triacylglycerides
TAP Tris-acetate phosphate
TCA Tri-carboxylic acid

3Chl* Triplet chlorophyll
ThA Threonic acid
Thr Threonine

TLC Thin layer chromatography

TEM Transmission electron microscopy

TG Trigallic acid

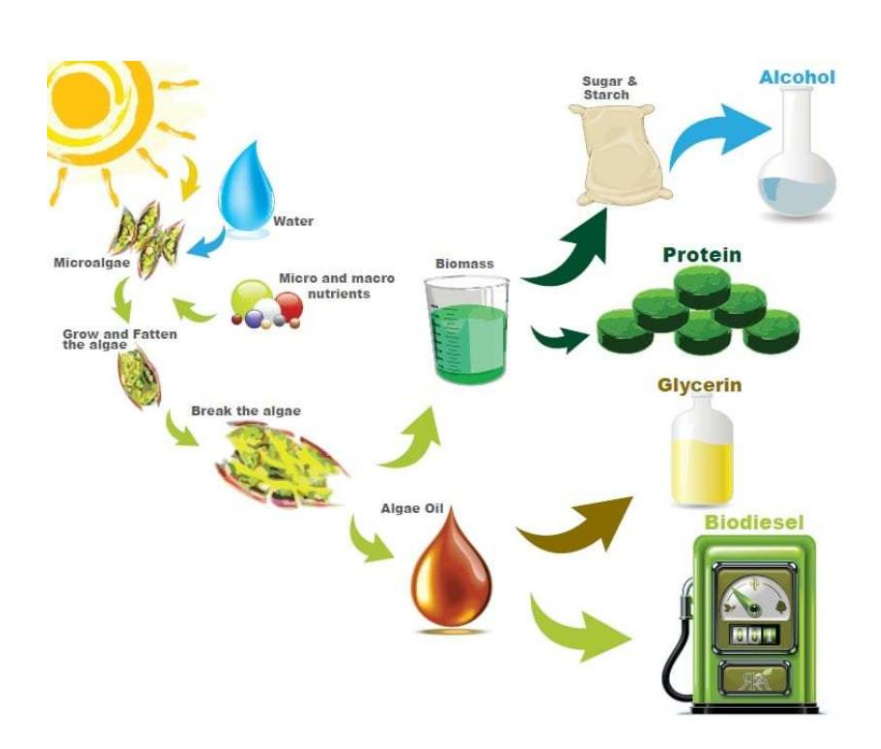
Uracil Uracil
Urd Urdinine
Urea Urea

UMP Uridine5- monophosphate

WT Wild type

Chapter 1

Introduction



1.1 Microalgae

Microalgae are microscopic organisms that are classified under eukaryotes as well as prokaryotes. They are found in both saline and freshwater habitats and are capable of performing photosynthesis, reducing carbon dioxide (CO₂) into sugars. The organisms are also known to tolerate a wide range of temperature, salinity, light, and water conditions. *Chlamydomonas* (*C.*) *reinhardtii* is a single-cell green microalga with a diameter of around 10 μm and contains two cilia (Figure 1.1). It is a biological model organism that's been studied extensively, owing to its efficiency of cultivation and gene manipulation. Being photosynthetic algae, *C. reinhardtii* can grow photoautotrophically; however, they can indeed grow in the dark if supplemented with organic carbon.

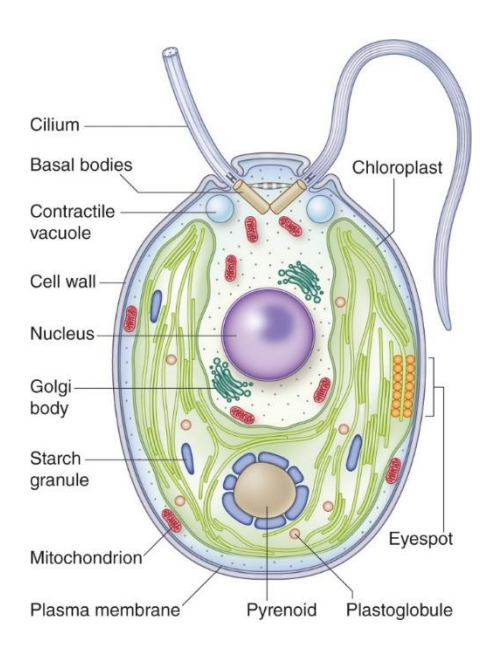


Figure 1.1 Schematic representation of C. reinhardtii. The cells are 10 μm in diameter and have two cilia that confer motility to cells. The large cup-shaded chloroplast covers half of the area of the cell. A single cup-shaped chloroplast takes up a significant amount of space in the cell. The pyrenoid, a structure in which Rubisco is concentrated, is found in this organelle, and the eyespot is located near the cell equator, on the edge of the chloroplast. Water is pumped out of the cell through contractile vacuoles located at the front of the cell to maintain the cytoplasmic water content. The basal bodies are responsible for ciliary assembly and are located at the base of the cilia. A central nucleus, a proteinaceous cell wall, Golgi structures within the cup-shaped portion formed by the chloroplast, and mitochondria are among the cell's other properties. This image is taken from Sasso et al.(2018).

1.2 Photosynthesis

From the beginning of the evolution of life in plants and the formation of the biosphere, light energy has been a critical component (Blankenship et al., 2010). Every living matter is a self-contained system made up of polymers, proteins, carbohydrates, lipids, and nucleic acids. To preserve the integrity and evolution, organisms need to, grow, adapt, and reproduce. This process requires a continuous exchange of energy and substance between the organism and the environment. Living beings derive their energy from solar energy. Therefore an infinite amount of light energy is a necessary condition for the existence of life. Photosynthesis begins with the absorption of light, which triggers a series of light transformation reactions ultimately leading to the formation energy sugars. Photosynthesis is an oxidation-reduction process in which CO₂ is reduced to sugar and water is oxidized to form oxygen in the presence of light. During the conversion of light energy into chemical energy; reducing power nicotinamide adenine dinucleotide phosphate (NADPH) and Adenosine triphosphate (ATP) is generated that drive the carbon fixation process through the Calvin-Benson Bassham (CBB) cycle to form sugars.

The overall reaction of oxygenic photosynthesis can be represented as:

$$6CO_2 + 12H_2O \rightarrow C_6H_{12}O_6 + 6O_2 + 6H_2O$$

In plants and algae, photosynthesis is divided into two stages, light and dark stages. The light stage includes linear electron transport (LET) and cyclic electron transport (CET). In LET, the photons are absorbed by chlorophyll pigments that enclose the reaction core center of photosystem (PS) II. Electrons are excited by the light in the pigment centre P680 at the core of PSII, which is transported to the primary electron acceptor, pheophytin, leaving P680⁺ oxidised. The energy of P680⁺ is used in photolysis. During photolysis electrons from H₂O reduces P680⁺ to P680 and release oxygen along with H+. Plastoquinone accepts an electron from pheophytin and transfers electrons to cytochrome

(Cyt) *b6f* complex. Plastocyanin accepts an electron from (Cyt) *b6f* and delivers it to the luminal side of PSI to pump hydrogen ions from the stroma into the thylakoid. At the same time, a proton gradient (pH) is created across the thylakoid membrane, which provides the proton motive force required for ATP synthesis. The excited electron is then transferred from PSI to ferredoxin and ultimately delivered to the enzyme ferredoxin NADP reductase (FNR), which converts NADP⁺ to NADPH as shown in Figure 1.2. NADPH which is produced during LET is used in the CBB, where CO₂ is fixed to produce sugars.

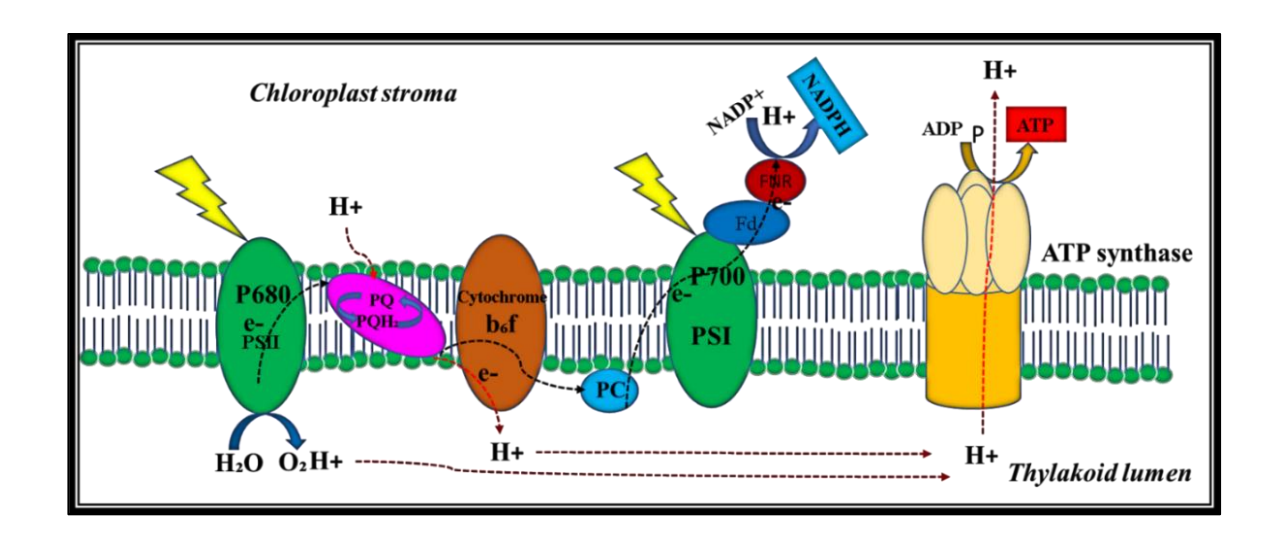


Figure 1.2 Schematic diagram of linear electron transport of *C.* reinhardtii. The electron pathway in photosynthesis is depicted in the diagram below with dotted black arrows. This pathway steps are all paired oxidation-reduction reactions. Water is oxidized as a result of photosystem II (PSII) light response. Electrons travel from photosystem II (PSII) to plastoquinone (PQ), then to cytochromes (Cyt) b6 f, and finally to plastocyanin (PC). Another light reaction stimulate electrons for transfer to ferredoxin (Fd) and then to NADP+ at photosystem I (PSI). Adopted from Simkim et al. (2019).

In CET, a high-energy electron generated by P700, a pigment in the PSI complex, moves in a cyclic pathway. The electron generated in PSI, travels from the primary acceptor to ferredoxin, then to plastoquinone, followed by Cyt *b6f*, and finally to plastocyanin before returning to PSI. The transport chain generates a proton-motive force by pumping H⁺ ions across the membrane, culminating in a concentration gradient that activates ATP synthase. This is known as cyclic photophosphorylation, and it does not create O₂ or NADPH. NADP+, unlike non-cyclic photophosphorylation, does not receive electrons; instead, the electrons are returned to the Cyt *b6f*.

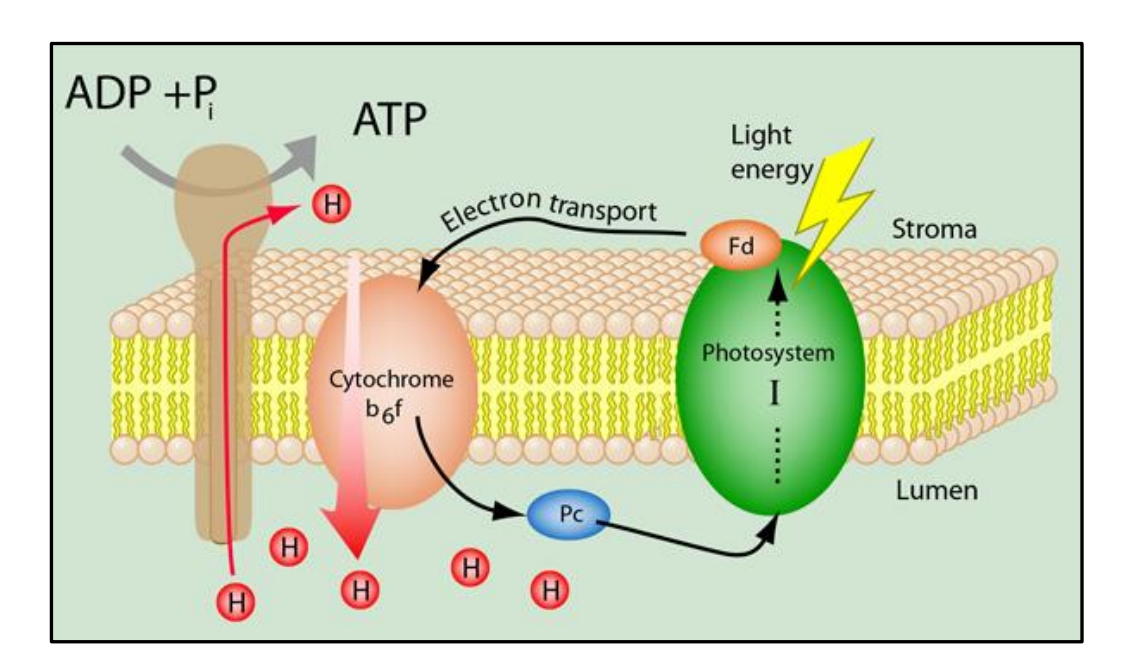


Figure 1.3. Diagram illustrating C. reinhardtii cyclic electron transport. The electron pathway in photosynthesis is illustrated with dotted black arrows in the picture below. The electron is recycled from photosystem I to Fd (Ferredoxin) to PQ (Plastoquinone) complexes, then to PC (Plastocyanin) and back to photosystem I. Image taken from Moore et al (1995).

In CET, Cyt *b6f* utilizes electrons energy from PSI to produce additional ATP as a result of the proton gradient without producing NADPH, hence boosting the ATP/NADPH ratio in the chloroplast. The induction of the energy-dependent quenching (qE) component of non-photochemical quenching (NPQ) of absorbed light is another effect of the transthylakoid pH gradient (Figure 1.3) The carbon assimilation reactions, and eventually all cellular metabolism

(Judge et al., 2020), are powered by ATP and NADPH produced by light-driven electron/proton transport. CET can be mediated by at least two different pathways: the main pathways are proton gradient regulation5 (PGR5) and PGR5- like photosynthetic phenotype (PGRL1) protein whereas the other minor pathway is the chloroplast NDH-like complex-mediated pathway. The molecular machinery involved in this energy transformation cascade, on the other hand, is exceedingly sophisticated and the multisubunit macromolecular structures of PSI and PSII, Cyt *b6f*, light-harvesting complexes (LHCs), and ATP synthase are made up of dozens of integral and peripheral membrane proteins.

1.3 PSI-LHCI and PSII-LHCII supercomplexes organization in microalgae light-harvesting systems

Pigment binding proteins, also known as LHCs, surround photosystem reaction centres and help both photosystems in capturing light energy, establishing charge transfer in the RC and feeding LET and CET. The LHC's pigments capture light for photosynthesis and transfer it to photosystem reaction centres, where solar energy is converted to chemical energy (Barros et al., 2009). Light-harvesting antennas and their organization within photosynthetic supercomplexes have evolved to be more diversified (Drop et al., 2014). LHCs are essential for photosynthetic efficiency, photoprotection, and photoacclimation. *C. reinhardtii* LHCI contains 10 subunits LHCA1- LHCA9 which consist of two LHCA1 subunits (Takahashi et al., 2004), and LHCII trimers consist of 9 genes, LHCBM1 to LHCBM9 (Minagawa and Takahashi, 2004). The most conserved antenna proteins in *C. reinhardtii* are the LHCI subunits, which constitute the PSI peripheral antenna system. The monomeric subunits of the PSII supercomplex, are Lhcb4 (CP29) and Lhcb5 (CP26). Lhcbm genes (Lhcbm1–9) encode trimeric LHCII, the main antennae of *C. reinhardtii* photosynthetic membranes. These LHCII proteins are coupled to both sides of the central dimeric core complex (CP43 and CP47), with the core (D1 and D2) and major LHCII trimers flanked by minor LHCII monomers, according

to single-particle image analysis of electron micrographs (Figure 1.4). However, in *C. reinhardtii*, a double-layered LHCI belt connected to the side of the PsaJ/F/G subunits is formed by nine LHCI proteins encoded by the LHCA1–9 genes (Figure 1.5). The primary antenna LHCII, a 22 kDa polypeptide that binds 14 chlorophylls (Chl) *a* and *b*, as well as 4 xanthophylls (lutein, neoxanthin, violaxanthin, and zeaxanthin), is most well-represented (Dall'Osto et al., 2012). Photoprotective tasks were carried out by (LHC)-like antenna proteins (Rochaix et al., 2019), and they eventually developed into variants capable of either light-harvesting or energy dissipation.

1.3.1 PSII-LHCII supercomplexes

PSII core complex is extremely conserved across every organism and comprises 40 distinct protein subunits. The RC is made up of subunits D1, D2, and Cyt *b559*, and it houses P680, the PSII RC where the main separation of charge occurs (Figure 1.4). P680+ is formed as a result of the light-dependent transfer of reducing equivalents to PQ. The positive charges accumulated by 4 charge separation events drive the water-splitting reaction within the oxygenevolving complex (OEC), which is composed of the extrinsic polypeptides PsbO, PsbQ, PsbP, and PsbR. The light-harvesting supercomplexes potential is increased by the presence of Chl *a* and carotene binding inner antennae (CP43 and CP47).

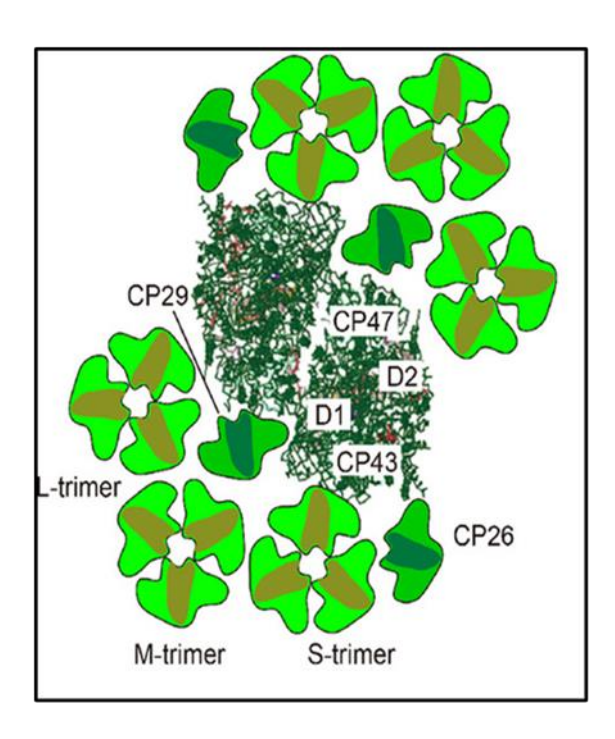


Figure 1.4 Supramolecular organization of PSII-LHCII supercomplex of C. reinhardtii. PSII-LHCII supercomplex of C. reinhardtii structure obtained from the single-particle analysis (Tokutsu et al., 2012).

1.3.2 PSI-LHCI supercomplexes

The PSI-LHCI supercomplex in *C. reinhardtii* was found to be bigger, but less resilient than those seen in the plant kingdom. The antenna composition in PSI-LHCI is diverse (Figure 1.5), because the antenna proteins Lhca1-9 are weakly associated with core complexes. Under anaerobic conditions, a megacomplex containing a Cyt *b6f* interacting with the PSI-LHCI complex is discovered, revealing a mechanism that improves CET in *C. reinhardtii*. (Steinbeck et al., 2018). The PSI-LHCI supercomplex of *C. reinhardtii* demonstrates that up to 10 LHCI are linked to the PSI core (Su et al., 2019).

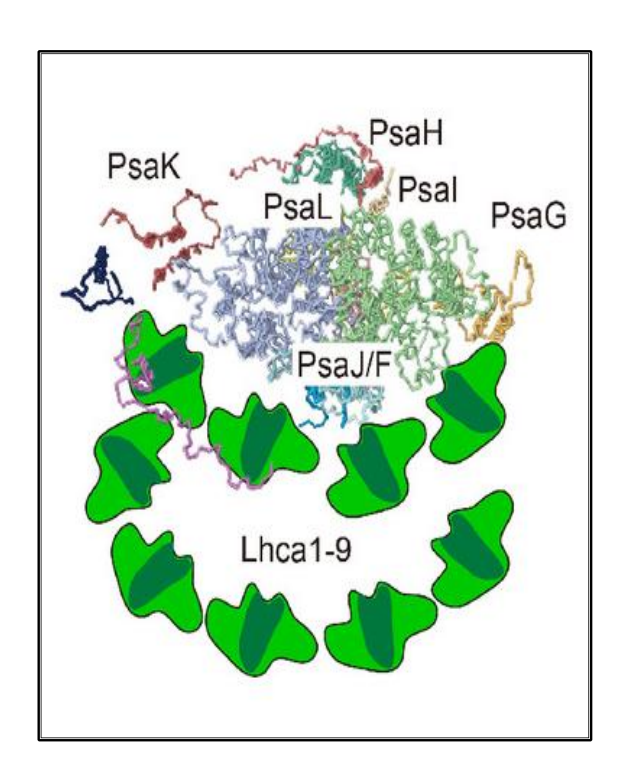


Figure 1.5 Supramolecular organization of PSI-LHCI supercomplex of C. reinhardtii. PSI-LHCI supercomplex (Dekker and Boekema 2005). C. reinhardtii structure was obtained from the single-particle analysis.

1.4 Reactive oxygen species

Photosynthesis functionally houses redox reactions in plants and algae by the transfer of electrons from the donor and an acceptor, and this redox consequently develops reactive oxygen species (ROS). ROS were made by all the living cells as a by-product of metabolism. Other sources of ROS production are chloroplast photosynthesis, mitochondrial respiration, endoplasmic reticulum (ER), and proximal photorespiration (Figure 1.6). Under favourable conditions, ROS is constantly generated at an average level. But they don't cause any damage as antioxidants scavenge them. But under unfavourable conditions or environmental stress conditions like light stress, salt stress, nutrient stress, temperature stress, heavy metal, and pathogen infection, ROS is generated in excess amount and causes damage to cells.

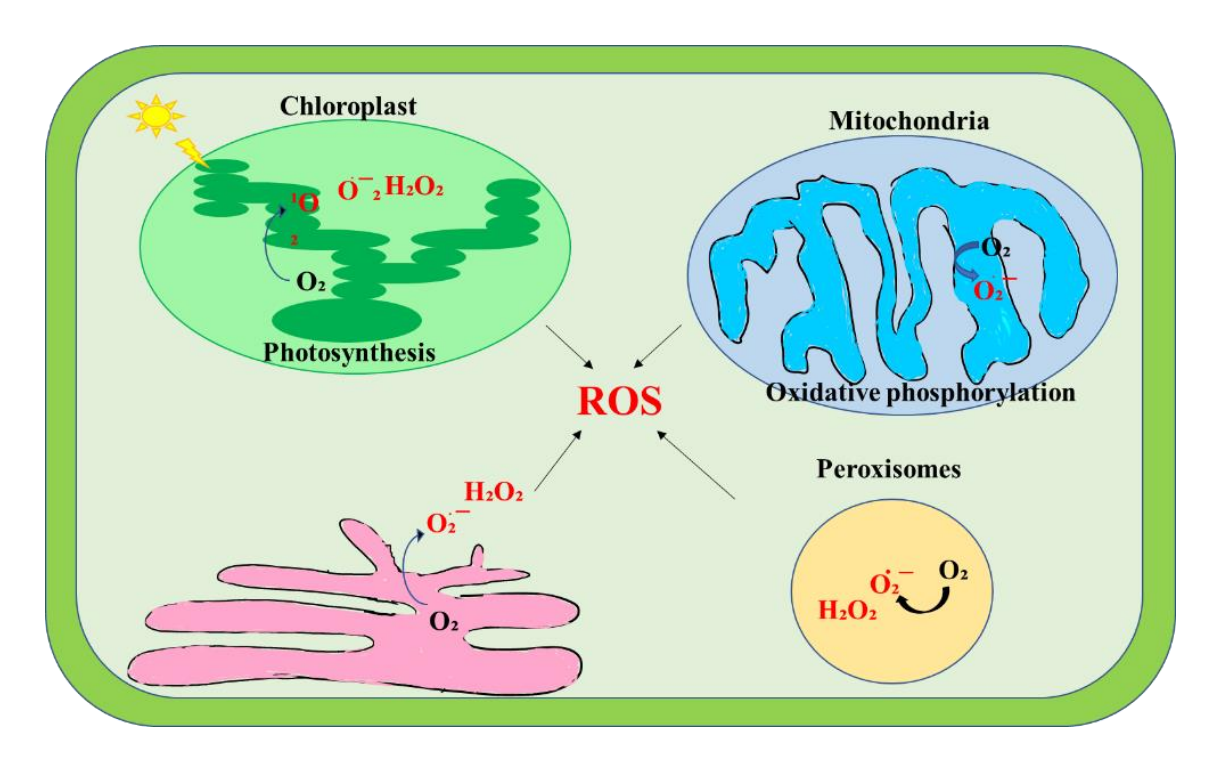


Figure 1.6 Schematic representation of the production of reactive oxygen species (ROS) from different organelles such as photosynthesis, oxidative phosphorylation, endoplasmic reticulum, and peroxisomes in C. reinhardtii. Adapted from Perez- Perez et al.(2012).

The major members of ROS include free radicals like superoxide anion radical (O2⁻), Hydroxyl radical) OH⁺, and non-radicals like hydrogen peroxide (H₂O₂) and singlet oxygen (¹O₂). ¹O₂ is produced due to the interaction of O₂ with the excited Chl i.e. singlet chlorophyll (¹Chl*) or triplet chlorophyll (³Chl*) in the chloroplast. It is a very unstable product and once generated, affects photosynthesis. O⁻₂ maintains the stability of cells but excess O⁻₂ leads to damage to cells. O⁻₂ reacts with hydrogen ions and forms H₂O₂ (Huang et al., 2019). Apart from being an important redox molecule in all organisms, it also controls the development of cells and adaptability to biotic and abiotic challenges. It is well known that H₂O₂ takes part in the cell signaling process but excess of it causes oxidative damage (Sharma et al., 2012). The most energetic antioxidant is OH⁺. It can oxidise cellular polysaccharides, causing cellular membranes disintegration, as well as trigger deoxyribonucleic acid (DNA) single-strand breakage.

Photosynthetic apparatus and PS proteins such as D1 proteins are damaged by ROS, which restricts photosynthetic activity (Yang et al., 2020). D1 protein fragmentation is caused by ROS. LHCII, PSII, and PSI (PSAA/B) are the most common binding sites for chlorophyll. Due to the high amount of Chl in the chloroplast, a significant amount of ³Chl* is formed due to intersystem crossing. Biomolecules such as lipids, proteins, DNA, and normal cellular function can be damaged by an increase in ROS levels. These processes can cause changes in essential membrane properties such as fluidity, membrane permeability, enzymatic loss, protein cross-linking, protein synthesis inhibition, damage of DNA and other factors that can damage the cells.

1.5 Autophagy

Autophagy is a self-degrading system that allows lysosomes to eliminate defective proteins and organelles which are damaged. It regulates a variety of physiological activities, including growth, development, sensitivity to nutritional depletion, oxidative stress, organelle turnover cellular damage, and macromolecule. It is the process where cytoplasmic components are encapsulated within double-membrane vesicles known as autophagosomes that are then transferred to the vacuole/lysosome for oxidatively damaged elements to be degraded and nutrients in need to be recycled (Liu and Bassham, 2012; Mizushima et al., 2011). Autophagy is a degradative mechanism for detoxifying intracellular material that is driven by nutrient deprivation. Autophagy is defined as the development of autophagosomes, which are double-membrane vesicles that swallow cytosolic components. The autophagosome then combines with the vacuole, where cargo is a breakdown by hydrolases in the vacuole. Upon autophagy induction, autophagy involved initiation, formation of autophagosomes, maturation, and degradation as shown in Figure 1.7.

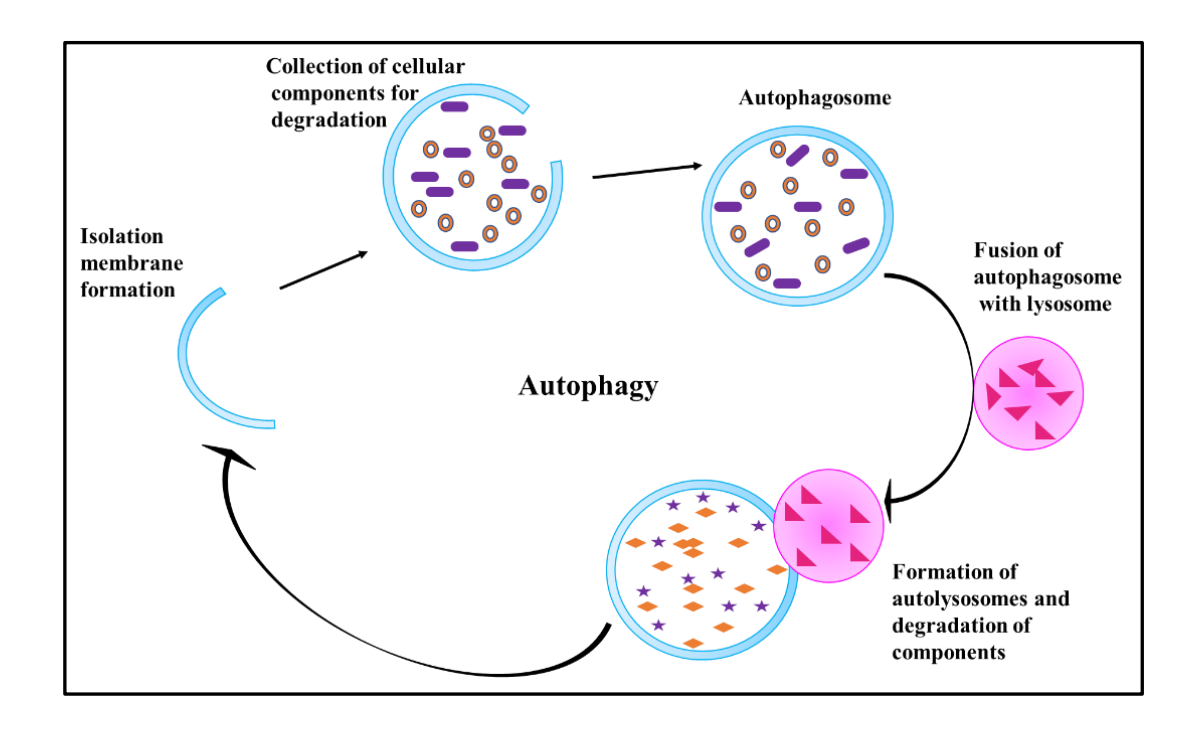


Figure 1.7 The pathway of autophagy in C. reinhardtii

Autophagy-related (ATG) genes are found in all eukaryotes. These genes were first discovered in the budding yeast *Saccharomyces cerevisiae* (Tsukada and Ohsumi, 1993) and 40 ATG homologous genes develop in algae and plants (Meijer et al., 2007; Diaz-Troya et al., 2008). Among these genes, ATG8 is critical in the formation of autophagosomes. ATG8 must be attached to the autophagosome membrane via covalent binding to the membrane lipid phosphatidylethanolamine (PE) to perform its function this process is known as ATG8 conjugation/lipidation (Martens et al., 2020). The detection of lipidated ATG8 (ATG8-PE) is a reliable way to track autophagy. Several studies have proved that nutrient limitation triggers ROS which induces autophagy. ROS generation and photooxidative damage results activation of autophagy (Perez-Perez et al., 2012). Because of the ease of handling cell cultures for physiological and biochemical techniques, as well as the lower complexity of ATG genes in Chlamydomonas compared to higher plants, it has also been advocated as a viable system for studying autophagy in photosynthetic eukaryotes. Autophagy research in Chlamydomonas is

actively assisting in the understanding of the regulation of this degradative process in photosynthetic organisms and has recently identified a crucial role for autophagy in the regulation of lipid metabolism in algae.

1.6 Algal fuels

Algal biofuel is the alternative solution to fossil fuels. Using algae as a biofuel will help in reducing competition with the food resources which is used by the living being. However, algae use a small space, are easy to cultivate and it grows faster. Several companies worldwide working on alternative sources for fossil fuels and mostly on the production of algae biofuel (Ganesan et al., 2020). Food crises and energy crisis has forced scientist to focus on aquaculture for the production of biodiesel and biofuel. Algae uses less land compared to crop plants and can grow in wastewater or saline water without impacting freshwater resources (Demirbas et al., 2009).

1.6.1 Uses of Algae

1.6.1a Algae is a key source in the manufacturing of biodiesel and biofuel

People throughout the world are attempting to increase biofuel production by utilizing algae as a source. Microalgae can produce a significant amount of biomass, which can be utilized to make biofuel. In one year, algae have been known to create 5000 gallons of biodiesel from a single acre.

1.6.1b Algae can function as an energy source

Algae would be a very important feedstock for high-energy transportation fuels like biodiesel, green gasoline, and green jet fuel as it doesn't compete with the food price, and agricultural land and produce large amounts of CO₂ (Bomgardner et al., 2012). Biofuels are one the major sources of renewable energy which include biodiesel, bioethanol, and biogas (Demirbas et al., 2008).

1.6.1c Algae can be used to create vegetable oil

Using microalgae as a source of food oil can save sources of agricultural resources. Microalgae can produce a large amount of oil per unit area. The fatty acid composition of microalgae is the same as oil produced from the plant like C16 and C18 fatty acids. Few microalgae species also have omega-3 polyunsaturated fatty acid which is highly antioxidant and useful in cardiovascular deceases. Because of this reason microalgae, oil has great commercial potential and benefits human health.

1.6.1d Algae is a great human food supplement

Microalgae is rich in higher nutritional values such as calcium, magnesium, iodine, potassium, and iron. Microalgae also contain proteins, lipids, amino acids, carotenoids, vitamins, and also the presence of bioactive components microalgae which is essential for human health benefits. Among bio-active components, pigments are heavily studied because of their antioxidative properties (Koyande et al., 2019). Microalgae is a very diverse group ranging from 200,000 to 800,000. Several species among them were cultivated at a large scale to produce bioactive compounds for human and animal consumption, cosmetics, and the biofuel industry.

1.6.1e Algae is used as fertilizer

Microalgae from long being are used as a fertilizer by several farmers who are staying close to the sea as it contains nutrients and organic matter in abundance. Seaweeds are a very good source of manure. Algae extracts are sprayed on the crops or plants and can be directly deposited on the agricultural land.

1.6.1f Algae use for plastics

Microalgae is biodegradable and environmentally friendly which lets us provide an alternative to oil-based polymers, which have serious environmental consequences. Already companies are making biodegradable plastics water bottles. Algae produce polymers like starch and polyhydroxyalkanoids which have similar properties to polymers that are used to make plastics.

The major properties of the preparation of bioplastics are a high percentage of carbohydrates and low lignin content.

1.7 Biofuels and photosynthesis

Solar energy is a renewable resource that touches the surface of the earth at a rate of about 120,000 TW, more than three orders of magnitude faster than the estimated human energy need. Solar energy can be efficiently stored as a transportable fuel, it will be able to meet future human energy demands (Tuller et al., 2017). Oxidative photosynthesis process or CO₂ reduction by photosynthetic autotrophs (plants and algae) utilizing light and water, the solar energy is collected in the form of reduced carbon molecules at a rate of about 120 TW worldwide (Barber et al., 2009). Microalgae can employ photosynthesis to directly convert water, CO₂, and sunlight into a variety of fuels. As a result, using some of this potential as biofuel by cultivating photosynthetic organisms under controlled conditions can meet a considerable portion of the world's energy needs (Chisti et al., 2008).

The solar energy absorbed by the chromoprotein antenna system is delivered to PSI and PSII, the photosynthetic reaction centers of the thylakoid membrane, as excitation energy. Solar energy is transformed into chemical energy, forming a proton gradient across the membrane and leading to ATP production. NADPH, an electron carrier, is eventually formed in PSI using electrons resulting from the decomposition of water and the release of oxygen, which can result in periodic electron flow. ATP and NADPH are used in photosynthetic light-independent reactions to fix CO₂ to carbohydrates. All cellular activities, such as respiration, biomass yield, and lipid accumulation, rely on solid carbohydrates. Triacylglycerides (TAG) is a type of lipid that is used to produce biofuels. As a result, the conversion of solar energy into lipids determines the efficiency of this process (Wijffels et al., 2010).

1.8 Lipid composition in microalgae

The term "lipid" encompasses a wide range of organic molecules that are insoluble in water but soluble in organic solvents, such as a variety of natural oils, steroids, and waxes each of which serves a specific purpose. Glycerolipids are the most prevalent and well-studied lipid class in microalgae. These are distinguished by a glycerol backbone with one, two, or three fatty acids (FA) groups attached (Klok et al., 2014). FAs compensate for between 5% and 60% of cell dry weight (DW) in microalgae biomass (Ben-Amotz et al., 1985). Lipids are overaccumulated under environmental stress such as temperature, nutrient deficiency, salinity stress, and light stress. Under nitrogen-deficient conditions, for example, C. reinhardtii enhanced lipid synthesis by 93 %, while Acutodesmus dimorphus generated 75 % neutral lipids (Chokshi et al., 2017). Similarly, iron deficiency leads to enhanced lipid accumulation in C. reinhardtii (Devadasu et al., 2021). It's feasible that nitrogen deficiency stimulates lipid production in microalgae by altering other metabolic pathways (Srinuanpan et al., 2018). In Phaeodactylum tricornutum, Nannochloropsis oceanica, and Chlorella protothecoides, strong light intensity was utilised to stimulate the formation of neutral lipids (Krzeminska et al., 2015; Huete-Ortega et al., 2018). Under extreme salinity stress, lipid accumulation increased significantly in *Chlorella vulgaris* and *Dunaliella sp.* by 21.1 and 70 %, respectively (Takagi et al., 2006). Microalgae, Nannochloropsis salina, and Ettlia oleoabundans (Yang et al., 2013; Ma et al., 2016) have been proven to grow faster and produce more total lipids when exposed to high temperatures (Sayegh and Montagnes, 2011). Temperature stress has a bigger impact on lipid composition than total lipid production, particularly in the case of polyunsaturated fatty acids (PUFA) biosynthesis (Guedes et al., 2010; Wagenen et al., 2012). Researchers actively working to improve the algae's economic viability as a biofuel by using current knowledge of algal lipid metabolism to activate the production of beneficial fatty acids and, as a result, increase the lipid content.

Lipids are classified into two groups based on their functions. Non-polar lipids, such as triacylglycerols, with three fatty acids attached to the glycerol structure, which are primarily responsible for energy storage (Alishah et al., 2019), and polar lipids, such as glycerophospholipids, which play an important role in cell structure.

1.8.1 Non-polar lipid

TAG is needed for energy storage in microalgae cells. TAG contains fatty acids which are used to make biofuels for transportation. TAG mainly contains saturated fatty acid (SFA) and monounsaturated fatty acids (MUFA) but PUFA can also be present. Manufacturing of oil includes fatty acid synthesis in the plastid, glycerolipid assembly in the ER, and ultimate packing into the oil bodies. Photosynthesis produces acetyl-CoA, which is used as a precursor for fatty acid synthesis in the chloroplast. The sequential acylation of the glycerol-3-phosphate (GA3P) backbone with three acyl-CoAs mediated by a set of enzymes known as acyltransferases is thought to produce TAG. Its synthesis is carried out in the same way as membrane lipid synthesis until diacylglycerol (DAG) is produced via the Kennedy route (Kennedy et al., 1956).

Through polar and nonpolar lipid pathways, acylation of a glyceraldehyde 3- phosphate (G3P) produces DAG. The final step in TAG formation is the acylation of a DAG molecule to generate TAG. There are two strategies to carry out this acylation reaction: acyl-CoA dependent and acyl-CoA independent. Diacylglycerol acyltransferase (DGAT) and phospholipid: diacylglycerol acyltransferase (PDAT) catalyze the former, whereas PDAT catalyzes the latter. Oil droplet buds from the ER after a considerable number of TAG were accumulated in a specific area of the ER, generating unique cellular organelles (Figure 1.8). Oil bodies and lipid droplets are the names for these subcellular compartments.

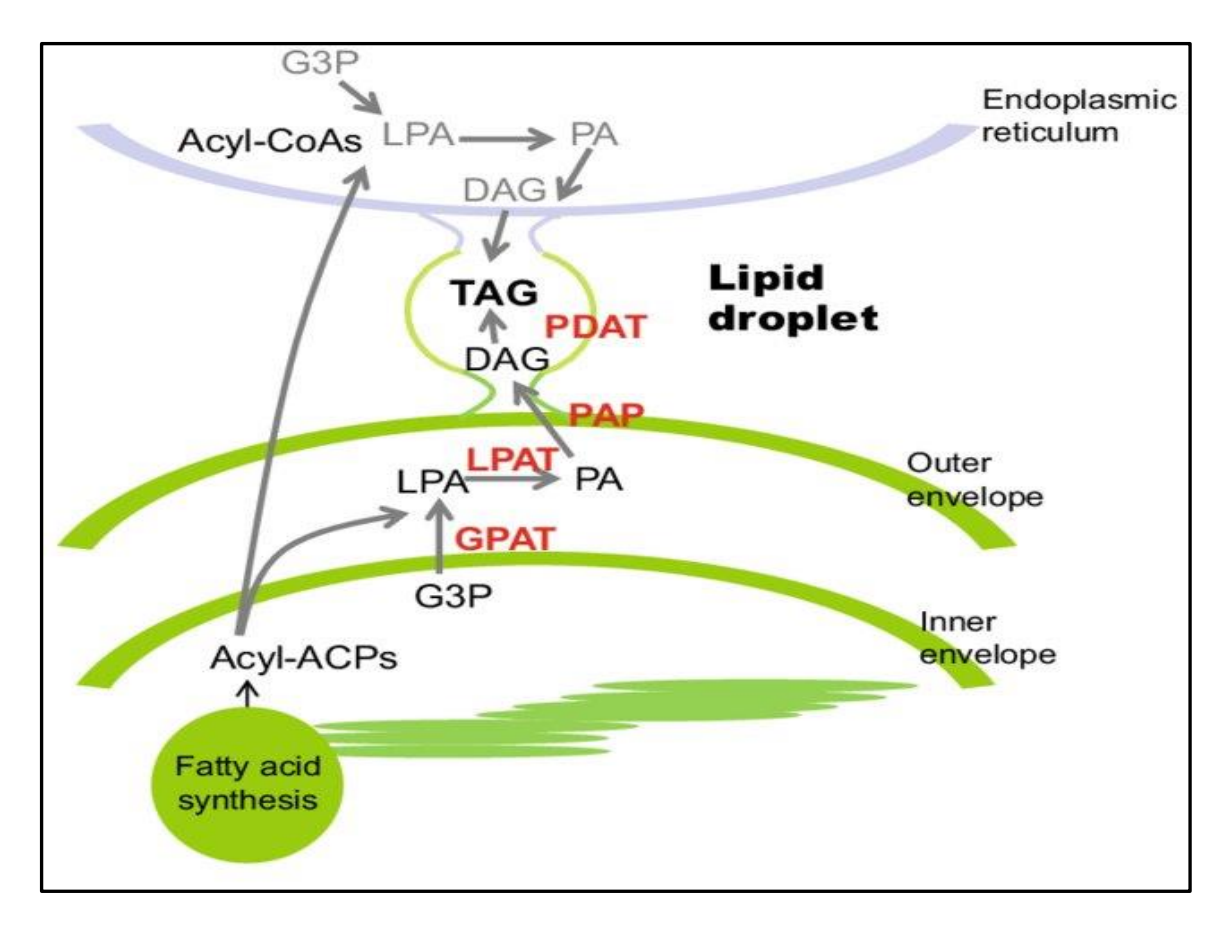


Figure 1.8 Schematic representation of the major TAG biosynthesis pathways in C. reinhardtii. This model is taken from Goold et al. (2014).

1.8.2 Polar lipids

The neutral galactolipids [monogalactosyldiacylglycerol (MGDG) and digalactosyldiacylglycerol (DGDG)] of anionic and two lipids types [sulfoquinovosyldiacylglycerol (SQDG) and phosphoglycerol (PG)] found in chloroplast membranes monogalactosyldiacylglycerol (MGDG) is the most prevalent membrane lipid in the biosphere, accounting for nearly half of the polar lipids of the thylakoid membrane in most organisms with oxygenic photosynthesis (Dormann and Benning, 2002) (Figure 1.9A). Structural lipids (polar lipids) typically contain long chains of fatty acids that can be converted to PUFA. Polar lipids and some sterols form a selectively permeable barrier that protects the cell from the outside environment while also aiding in the separation of various intracellular organelles (Gopalakrishnan and Ramamurthy 2014). Polar lipid synthesis was accomplished by

glycolysis, which led to the formation of GA3P and DAG. DAG is converted to MGDG via MGD1 (monogalactosyldiacylglycerol synthase), and MGDG is transformed to DGDG via DGD1 (Digalactosyldiacylglycerol synthase) as shown in Figure 1.9 B.

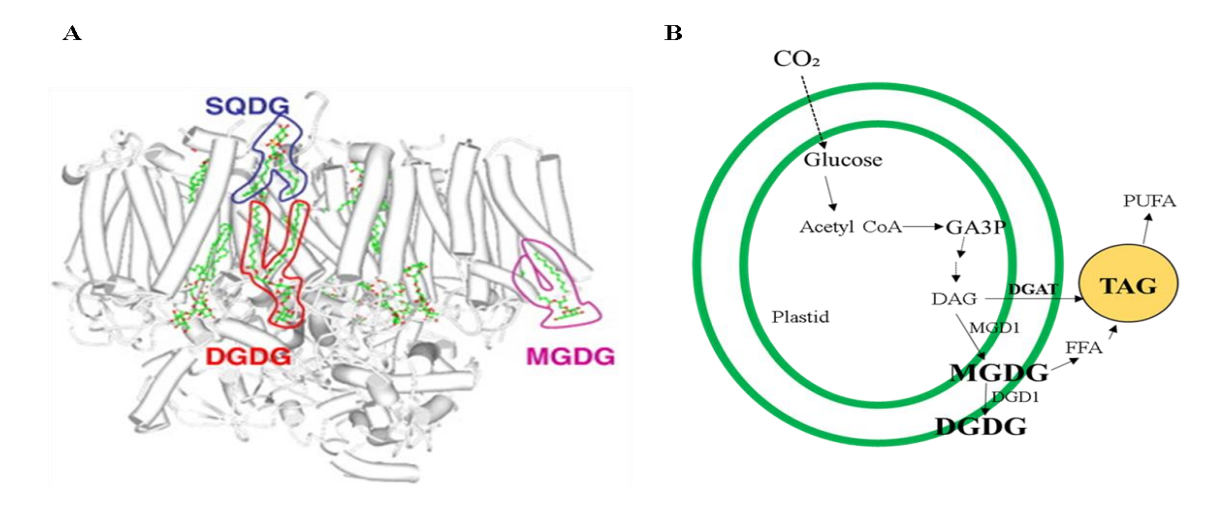


Figure 1.9 Thylakoid lipids association with PSII and pathway of polar lipid synthesis (A) Thylakoid lipids associated with the monomeric form of PSII of cyanobacteria PSII from thermosynechococcum elongate by Guskov et al., 2009. SQDG, sulfoquinovosyldiacylglycerol; MGDG & DGDG, mono, and digalactosyldiacylglycerol are circled. Image Taken from Boudiere et al., 2014. (B) Reactions involved in glycerolipid metabolism in C.reinhardtii. FFA, free fatty acid; GA3P, glycerol 3-phosphate; DAG, diacylglycerol; DGAT, diacylglycerol acyltransferase; MGD1 & DGD1 mono and digalactosyldiacylglycerol synthase; PUFA, polyunsaturated fatty acid.

1.9 Carotenoids and xanthophyll

Carotenoids, like chlorophylls, are crucial components in photosynthesis and photoprotection in photosynthetic organisms, plants, and algae. Singlet–singlet excitation transfer is a process by which carotenoids absorb light energy and transfer it to chlorophylls. Carotenoids, such as α - carotene and β - carotene, are essential phytonutrients. Xanthophyll, which includes lutein and zeaxanthin, is formed when carotenoids are oxidized.

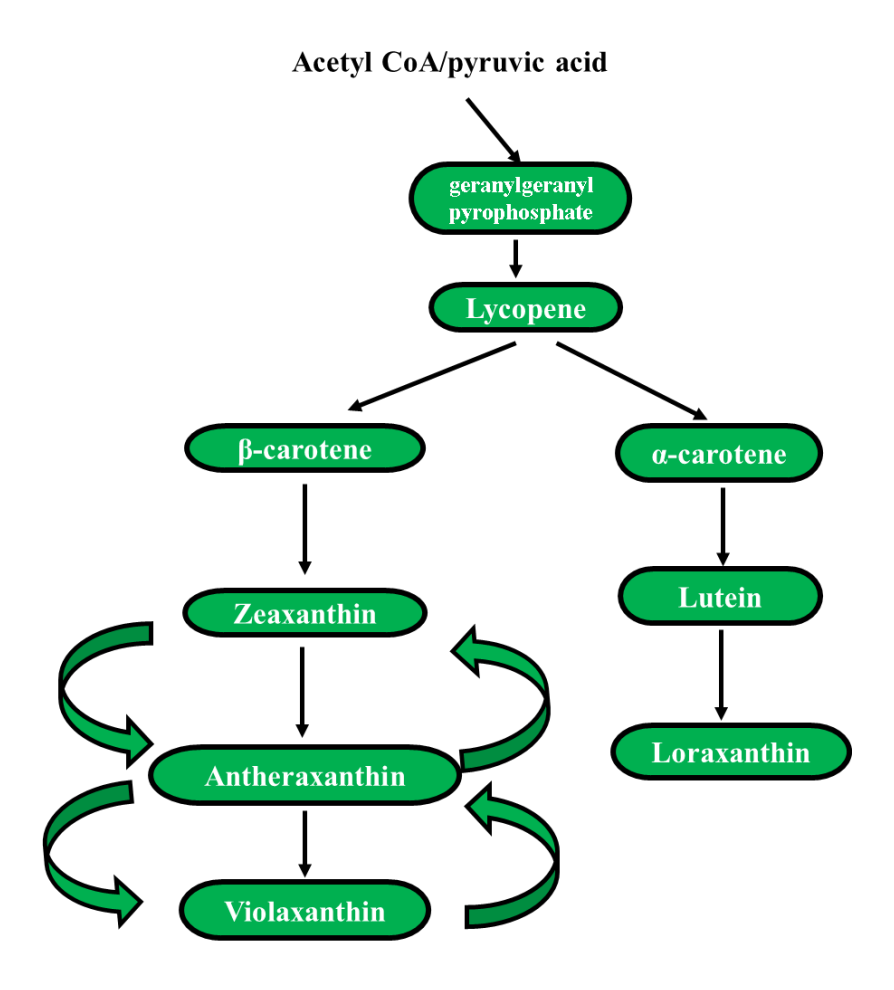


Figure 1.10. Carotenoid biosynthetic pathway in C. reinhardtii

In photosynthetic organisms, xanthophyll and carotenoids fulfil two functions: light-harvesting and energy dissipation as heat. Carotenoids absorb and release excessive energy from chlorophylls via triplet-triplet transfer. The carotenoid biosynthetic pathway was shown in Figure 1.10. The first step of the carotenoid biosynthesis pathway is formed from acetyl Co-A or pyruvic acid. Geranyl pyrophosphate and geranylgeranyl pyrophosphate, phytoene is gradually desaturated and forms lycopene. Carotenoid groups like α -carotene and β -carotene are produced by lycopene cyclase. Enzymatic removal of epoxy groups from xanthophylls (violaxanthin, antheraxanthin, and lutein epoxide) to produce de-epoxy xanthophylls is part of the xanthophyll cycle (zeaxanthin and lutein). During light stress, the intermediate antheraxanthin is transformed into zeaxanthin, which works as a lipid-protective antioxidant and promotes non-photochemical quenching inside light-harvesting proteins. The enzyme

violaxanthin de-epoxidase helps convert violaxanthin to zeaxanthin, whereas zeaxanthin epoxidase helps reverse the process. ROS like ¹O₂ and free radicals are generated during photosynthesis when light and oxygen are combined. Carotenoids with more than eleven conjugated double bonds quench ¹O₂ exceptionally well. When light energy is absorbed in excess, microalgae have a mechanism that works to quench chlorophyll singlet excited state (¹Chl*) in PSII LHCs this phenomenon is called NPQ (Ruban et al., 2016). Rapid activation and relaxation in NPQ are required to deal with frequent changes in natural habitat (Kulheim et al., 2002). An acidic pH in the luminal side of thylakoid under excess light is a recent paradigm in NPQ activation in plants which activates two events activation of light harvesting complex stress- related (LHCSR3) proteins which is essential for NPQ and activation of xanthophyll cycle which causes the synthesis of zeaxanthin and the protonation of a PSII protein. Photoprotection mechanisms are not limited to NPQ, carotenoids, which are tightly linked to LHC proteins, give direct deactivation of ³Chl* and ¹O₂ (Jahn et al., 2012).

1.10 Metabolism

Photosynthesis is separated into two stages: the light stage uses light and water to make energy (ATP and NADPH) and oxygen, while the dark stage incorporates carbon dioxide with the energy obtained. During photosynthesis, GA3P is a three-carbon sugar that is transported to the cytosol. GA3P is a protein that divides glycolysis into two stages: upper and lower.

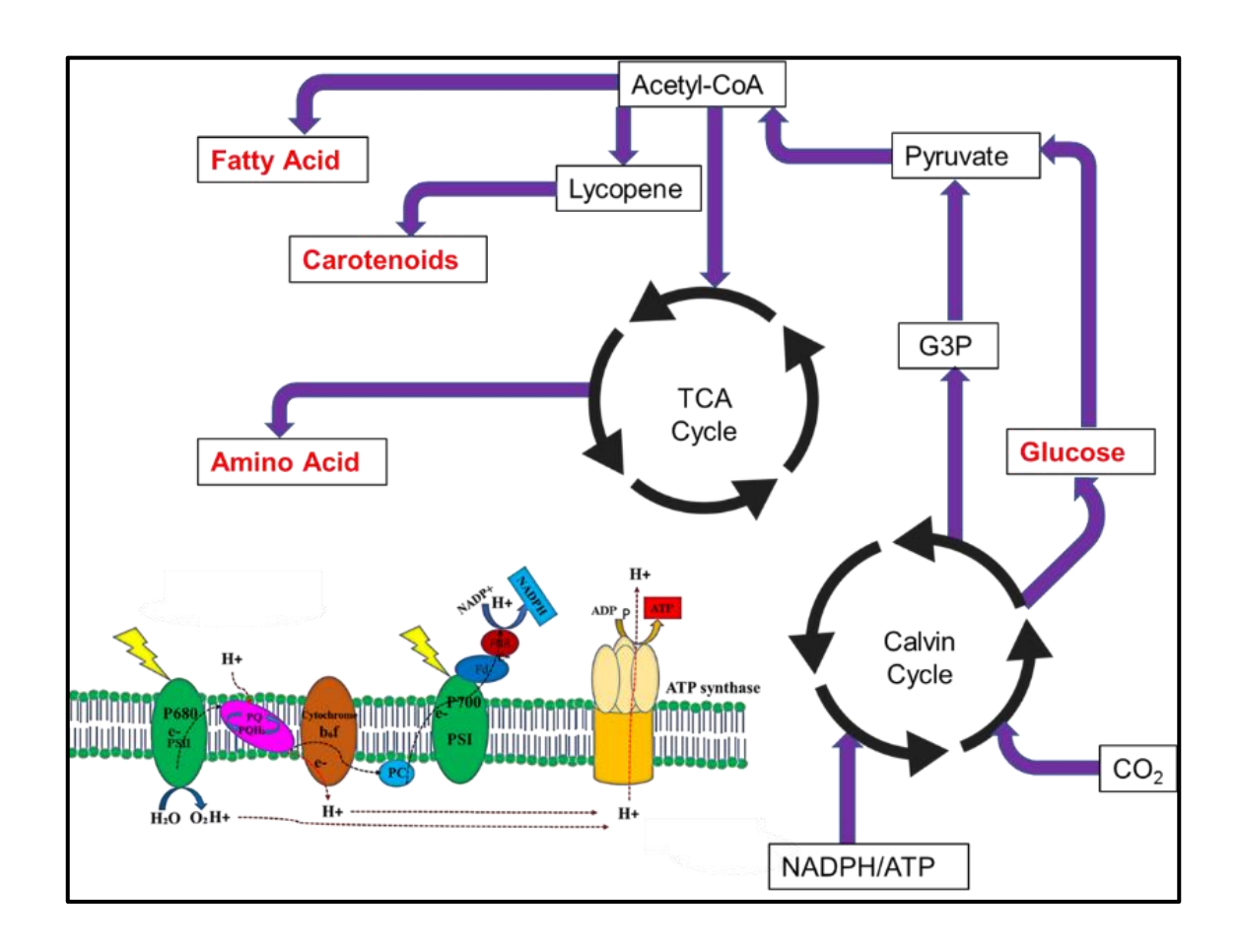


Figure 1.11 Schematic diagram showing the interaction networks of photosynthesis and carbohydrate, lipid, carotenoid, and amino acids metabolism in C. reinhardtii.

Upper glycolysis creates glucose 6-phosphate (G6P), which can be utilized to synthesize carbohydrates or used to produce NADPH in the pentose phosphate pathway. Lower glycolysis produces phosphoenolpyruvate (PEP), followed by the production of acetyl CoA, the first step in the citric acid cycle (CAC). CAC is a link between glycolysis and carbohydrate metabolism. Acetyl CoA is then used in lipid metabolism or the CAC, which generates transitional metabolites for biomass, proteins, ribonucleic acid (RNA), DNA, and chlorophyll synthesis as shown in Figure 1.11. Some algae species grown under stress acquire specialized secondary metabolites (e.g., pigments, vitamins, or lipids), which are high-value bioproducts that can be used in the cosmetic, food, or pharmaceutical industries. Metabolic products, an antioxidant such as carotenoids, vitamins, butylated hydroxytoluene, fatty acid, and their

derivatives, and metabolites with medical properties such as polysaccharides, glycerol, amino acid, glycoprotein, and antibiotics (Skjanes et al., 2013).

1.11 Abiotic stress

Abiotic stress is the negative influence of non-living forces on living organisms in a certain ecosystem. HL, drought, salinity, low or high temperatures, and other environmental extremes are the stresses. Photooxidative damage predominantly affects the PSII supercomplex, which is less stable than PSI and is generated as a result of HL, high or low temperature (Takahashi et al., 2004; Nisshiyama et al., 2007), and high salinity (Ohnishi and Murata 2006). If the organism can't tolerate the over-excitation, it can generate biologically dangerous chemical precursors and by-products, culminating in photo-oxidative disruption photosynthetic reaction centers, PSI and PSI, as well as lipids, proteins, and nucleic acids (Niyogi et al., 1999). As a result, photoinhibition, or a reduction in the maximum efficiency and/or rate of photosynthesis, can occur when excess light is absorbed (Long et al., 1994). PSII photodamage happens at all light intensities, however, under intense light when the degree of impairment exceeds the repair rate it results in a net decrease in photosynthetic activity. HL damages the D1 subunit of the PSII core protein, which is the principal target of photooxidative damage. Previously, it was observed that under HL conditions, Arabidopsis thaliana (Ballottari et al., 2007) LHCII major antenna proteins are substantially reduced, resulting in a smaller PSII antenna. It was also reported under salt stress conditions that PSI-LHCI is damaged due to ROS (Subramanyam et al., 2010). Iron deficiency reduces the number of chlorophyll molecules in C. reinhardtii, prevents the production of large PSI-LHCI supercomplexes, and reduces photosynthetic activity (Yadavalli et al., 2012). To cope with this problem excess energy is released as heat in a process called NPQ which also involves the reorganisation and redistribution of PSII and PSI antenna complexes within the membrane (Horton et al., 2008; Takahashi et al., 2008). According to a previous report, increased light intensity caused a formation of H₂O₂ and O⁻₂,

resulting oxidative damage of PUFA, contributing to an increase of neutral lipid formation with a decrease in polar lipid synthesis (Morales et al., 2021). Microalgae may use light or carbohydrates to generate high-value-added compounds like lipids and carotenoids, and their biosynthesis pathway can be activated by HL stress. Microalgal cells collect lipids as an energy-rich carbon storage battery and synthesize increased levels of carotenoids and other metabolites in response to HL (Sun et al., 2018).

1.12 Strain of C. reinhardtii

C. reinhardtii wild type (WT) strains, CC124 and mutants pgrl1 and pgr5 were chosen as model organisms in this research to study the strategies under high light (HL). PGRL1 and PGR5 are essential for CET and photoprotection (DalCorso et al., 2008). The CET is essential in photoprotection. So the absence of PGRL1 and PGR5 shows a decrease in the CET rate (DalCorso et al., 2008; Yadav et al., 2020). PGR5 is critical in transferring electrons from Fd to the PQ pool. Its function limits the over-reduction of PSI acceptor side, thus preventing photoinhibitions of PSI (Munekage et al., 2002). Proton gradients across the thylakoid membrane was reduced in pgr5, which leads to the defect in CET capacity (Johnson et al., 2014; Yadav et al., 2020). pgrl1 is required for CET and ATP production and for efficient photosynthesis (Tolleter et al., 2011; Leister et al., 2013; Shikanai et al., 2014; Steinbeck et al., 2015,). So the absence of these two mutants leads to acceptor side limitation, leading to stromal redox poise and ROS formation. Photoprotective mechanisms, such as carotenoids, will be activated to guard against ROS. Carotenoids are found in the photosynthetic complexes of the thylakoid membrane and have a variety of roles in photosynthesis and photoprotection. Under Nitrogen deprivation, the CET pathway supplies ATP for the synthesis of lipids in C. reinhardtii. When Nitrogen is scarce, the pgrl1 protein accumulates minimal neutral lipids. There have been several reports of nutrient stress accumulating lipid; however, there is not much research conducted under HL. C. reinhardtii requires sunlight to survive, which converts into chemical energy through the photosynthetic process. At the same time, pgrl1 and pgr5 mutants, which are impaired in CET, are photosensitive and under strong light mutant show an enhancement in stromal redox poise that results in increased lipid production. ROS generated due to light stress is involved in a large number of metabolic changes (Foyer et al., 2009). Therefore, we also initiated the study of metabolomic profiling to see the changes in metabolites. Disturbance in CET network on photosynthesis efficiency and metabolism is not well understood so far. Therefore, we have focused on the effect of HL on biochemical characterization of supercomplexes organization, induction of autophagy due to ROS production, and accumulation of neutral lipid and degradation of membrane lipid and metabolites alteration in pgrl1 and pgr5 mutants. Further, we have checked the enzymes which is responsible for the accumulation of TAG under HL. We also report the mechanism of HL tolerance in pgrl1, and pgr5 mutant at the molecular level using gene expression and metabolomic strategies.

1.13 Objective of the study

Using biochemical and biophysical approaches in *C. reinhardtii* under HL, we investigated alterations in the photosynthetic machinery, lipid accumulation, and membrane lipids. The following objectives have been framed to help us to achieve our goals.

Objectives

- 1. Macromolecular structural changes of supercomplexes of thylakoids in high light from *pgrl1* and *pgr5* mutants of *C. reinhardtii*
- Investigation of autophagy induced lipid accumulation under the high light-grown cells of pgrl1 and pgr5
- Identification and characterization of metabolomics profile from cyclic electron transport mutants

Chapter 2

Materials and methods



2.1 Model organism C. reinhardtii description

The green microalgae *C. reinhardtii* WT strain CC124 is obtained from Chlamydomonas resource centre (University of Minnesota), mutants *pgrl1* and *pgr5* a kind of gift from Prof. Gilles Peltier, (CEA-CNRS- Aix Marseille University, France) and Prof. Michael Hippler, University of Munster.

2.2 Strains and culture conditions

C. reinhardtii (WT, *prgl1*, and *prg5*) was grown photoheterotrophically in Tris-acetate phosphate (TAP) medium at 25 °C with a photon flux density of 50 μmol photons m⁻² s⁻¹ in 250 mL conical flask shaken at 120 rpm in an orbital shaker at 25 °C. The seed cultures of WT, *prgl1*, and *prg5* were harvested at an optical density (OD) of 0.8 (3.0 x 10⁶ cells) and inoculated at OD of 0.2 for all the cultures and cultivated photoheterotrophically at 25 °C for 4 days at a continuous light intensity of 50 μmol photons m⁻² s⁻¹ and 500 μmol photons m⁻² s⁻¹ i.e. is normal light and HL intensity respectively. Later the cultures were collected at 56 h with an OD of 0.8 at 750 nm and experiments were conducted. The intensity of light is calibrated with a photometer (Hansatech, UK).

2.3 Spectrophotometric measurement

2.3.1 Optical density measurement

The spectrophotometer was used to measure the cell density of WT, *pgrl1*, and *pgr5* at an absorbance wavelength of 750 nm which was recorded with UV-Visible Perkin Elmer spectrophotometer lambda 35 (USA).

2.3.2 Total chlorophyll quantification

C. reinhardtii cells were harvested by centrifugation (3000 rpm for 10 mins) after 56 h at a cell density of 3.0 x 10⁶. Cell pellets were resuspended in methanol for extractions of chlorophyll, and the supernatant was used to measure the total chlorophyll according to Porra et al. (Porra

et al., 1989) Absorbance was performed at 645 nm and 663 nm with UV-Visible Perkin Elmer spectrophotometer lambda 35 (USA).

2.4 Biomass determination

To calculate the total biomass of cells (WT, pgrl1 and pgr5), 5 mL of culture was collected after the 3rd day of growth in control and HL by centrifugation at $1,000 \times g$ for 10 min at room temperature (RT), and the supernatant was discarded. The excess media was removed by short centrifugation, and cell pellets were lyophilized at -109 °C for 12 h. The cell pellet was washed with distilled water and transferred into a pre-weighed 15 mL falcon tube. The total DW was later quantified by subtracting the empty tube (Devdasu and Subramanyam, 2021).

$$DW = (w2-w1)/v$$

Where w1 is the empty tube weight, w2 is the dried cell pellet weight, and v is the initial volume of the sample.

2.5 ROS detection by confocal microscopy

The total ROS was detected with 2,7-dichlorodihydrofluorescein diacetate (H₂DCFDA) (Sigma-Aldrich), a fluorescence dye used to identify the ROS in live *C. reinhardtii* cells. 3.0 x 10⁶ cells ml⁻¹ were collected from all the conditions followed by staining with H₂DCFDA staining at 10 μM concentration (Upadhyaya et al., 2020). Further, cells were incubated with dye for 1 h at RT in a continuously rotating shaker under dark. Images were captured using Carl Zeiss NL0 710 Confocal microscope. H₂DCFDA was detected in a 500–530 nm bandpass optical filter with an excitation wavelength of 492 nm and an emission wavelength of 525 nm. Chlorophyll auto-fluorescence was detected using an optical filter of 600 nm. Samples were viewed with a 60× oil immersion lens objective by using the ZEN, 2010 software.

Total ROS produced by *C. reinhardtii* cells was also quantified by spectrophotometer. Logarithmic-phase cells were centrifuged at $1,500 \times g$, 20 °C for 5 min, resuspended in an

equal volume of fresh TAP medium, and then incubated in 5 μ M H₂DCFDA for 1 h in the dark at 25 °C. After dark exposure, the cells were washed twice with TAP to remove excess dye (Devadasu et al., 2019). The fluorescence was measured using a Microplate reader (Tecan M250) at an excitation of 485 nm and an emission of 530 nm. We calculated the total ROS by subtracting the value of fluorescence with dye and without dye.

2.6 Transmission electron microscopy

The cells (3 × 10⁶ cells ml⁻¹) were resuspended in 0.1 M phosphate buffer (pH 7.2). Cells were fixed in a 2 % glutaraldehyde (Sigma-Aldrich, St. Louis, United States) solution for 2 h in the dark. The cells were then washed four times in PBS buffer for 1 h each time before being post-fixed in 2 % aqueous osmium tetraoxide for 3 h, washed six times in deionized distilled water, dehydrated in a series of ethanol solutions (30, 50, 70, and 90 %, and three changes of 100 % for 10 min each), infiltrated, and embedded in araldite resin. Ultra-thin sections (60 nm) were cut with a glass ultramicrotome (Leica Ultra cut UCT-GA-D/E-1/100) and placed on copper grids after incubation at 80°C for 72 h for complete polymerization. The sections were stained with uranyl acetate and counterstained with reynolds lead citrate, with some alterations (Bozzola and Russell, 1998). A hitachi 7500 (Japan) transmission electron microscope was used to take the images.

2.7 Localization of ATG8 from immunofluorescence microscopy

For immunofluorescence, cells (3×10^6 cells mL⁻¹) were fixed in a solution of 4 % paraformaldehyde and 15 % sucrose dissolved in phosphate saline buffer (PBS) for 1 h at RT Later, the cells were washed twice with PBS buffer. First, cells were permeabilized by incubation in 0.01 % Triton X 100 in PBS for 5 min at RT and washed twice in PBS. Next, the samples were transferred to sterile eppendorf tubes and blocked with a 1 % bovine serum albumin (BSA) (w/v) in PBS for 1 h. Samples were incubated with anti- ATG8 diluted (1:1000) in PBS buffer, pH 7.2 containing 1 % BSA overnight at 4 °C on a rotatory shaker. Cells were

then washed twice with PBS for 10 min at 25 °C, followed by incubation in a 1:10000 dilution of the fluorescein Dylight 405 labeled goat anti-rabbit secondary antibody (Sigma) in PBS-BSA for 2 h at 25 °C. Finally, cells were washed three times with PBS for 5 min. Images were captured with Carl Zeiss NL0 710 confocal microscope (Upadhyaya et al., 2020). ATG8 localization was detected with excitation of Dylight at 405 nm and emission at 420 nm by analysing the images with ZEN software.

2.8 Lipid body analysis by nile red staining

We studied the impact of HL on non-polar lipid accumulation with confocal microscopy. Cells $(3 \times 10^6 \text{ cells mL}^{-1})$ were collected after the 3rd-day growth in HL along with control. To stop the mobility of the cells, 5 μ L Iodine solution [0.25 g in ethanol (95 %)] was mixed and kept for 5 min under dark at RT. The cell suspension was then stained with Nile red (NR, 1 μ g mL⁻¹ final concentration, Sigma, Sigma-Aldrich) followed by 20 min incubation in the dark (Devdasu and Subramanyam, 2021). After staining, the samples were placed on a glass slide with a coverslip. Images were captured using Carl Zeiss NL0 710 confocal microscope. A 488 nm scanning laser was used with a 560–615 nm filter to detect neutral lipids. Samples were viewed with a 60× oil immersion lens objective and the ZEN, 2010 software package was used for image analysis.

2.9 Nile red visible light assay for triacylglycerol

The *C. reinhardtii* cultures were diluted to a density of 3.0×10^6 cells mL⁻¹ and placed within 96 well microplate wells. To every well, a 5 μ L aliquot of 50 μ g mL⁻¹ NR; (Sigma; ready in acetone) was added in 200 μ l of equal density cells (3.0×10^6 cells mL⁻¹), and after a thorough mix, the plate was incubated in the dark for 20 min (Devdasu and Subramanyam, 2021). The neutral lipids were then measured by visible light at 485 nm excitation filter and a 595 nm

emission filter employing a plate reader (Tecan infinite M200, Magellan). Quantification was achieved by using a standard curve ready with the lipid Triolein (Sigma T4792).

2.10 Flow cytometry measurements

Flow cytometer Calibur (BD Falcon, United States) was use to quantify neutral lipid stain with NR. Cells were stained with 1 µg mL⁻¹ NR (100 µg mL⁻¹ stock in acetone) in the dark for 30 min before flow cytometry analysis. Measurement of 10,000 cells per sample was analysed and auto-fluorescence was nullified before measuring the NR fluorescence. The fluorescence reading was obtained at a 488 nm excitation filter and a 545 nm emission (Devdasu et al., 2018). The distribution of the cells stained with NR was expressed as a percent of the total neutral lipid.

2.11 Total starch quantification

Cells was quantified by an Anthrone method (plate reader assay). For quantification of starch, cell pellets were resuspended in 50 μ L milliQ water and added 150 μ L of Anthrone chemical agent (0.1 g in 100 mL of conc. H₂SO₄ 98 %) to the 50 μ L algal cells. Initially, plates were incubated at 4 °C for 10 min and then incubated at 100 °C for 20 min. Later on, plates were placed at temperature till colour development. Plates were measured at 620 nm on an assay plate reader (Teccan M250) and total starch was calculated according to Wase et al. (2019).

2.12 Lipid analysis and quantification

For lipid extraction, 5 mg of lyophilized dry biomass was weighed equally from all the conditions. Total lipids were extracted as described by Bligh and Dyer's method (Bligh and Dyer, 1959). Cell powder was resuspended in a mixture of methyl alcohol, chloroform (2:1), and 0.9 % KCl. It was vortexed for 5 min and centrifuged at $3,000 \times g$ for 5 min for phase separation. The organic layer (lower layer phase) was transferred to a clean Eppendorf tube. The solvent was evaporated by purging nitrogen gas. The dried extract was then dissolved in $50 \,\mu$ L chloroform. For standard, TAG (Sigma-Aldrich, St. Louis, United States) was dissolved

in CHCl₃ (1 mg mL⁻¹). Around 0.5 μg of lipid extract was loaded as a spot on 20 cm × 20 cm silica gel TLC plates. For neutral lipids separation, the TLC plate was developed in a mixture of hexane/diethyl ether/acetic acid (17:3:0.2), and polar lipids (membrane lipids) were developed in a mixture of acetone/toluene/water (91:30:8) according to Wang and Benning (2011). Bands were visualized by staining with iodine vapor (Yang and Wittkopp, 2015) and identified the membrane lipids as cited above. For quantitative analysis, individual lipids were extracted from the TLC plates with a razor blade transferred into a glass tube followed by *trans* methylation to fatty acid methyl esters (FAMEs). FAME of the samples were identify quantitatively by GC (gas chromatography) 6,890 fitted with 25 m × 0.2 mm phenylmethyl silicone fused silica capillary. The temperature program ramps from 170 to 270 °C at 5 °C min⁻¹. Following the analysis, a ballistic increase to 300 °C allows cleaning of the column during a hold of 2 min. The amounts of fatty acids were calculated based on the content of fatty acids derived from GC using heptadecanoic acid (Sigma-Aldrich, St. Louis, United States) as an internal standard.

2.13 FAME analysis of total lipids

The 5 mg lyophilized sample was dissolved in 1000 μ L of acetonitrile, 0.1 % formic acid (v/v) and vortexed for 1 h at 900 rpm at RT. The solution was then centrifuged at 13,000 rpm for 10 min at 4 °C. 100 μ L of supernatant was collected and dried the pellet using speed vacuum. The pellet is dissolved in 90 μ L of acetonitrile (ACN) 0.1 % formic acid (v/v) and spiked with 10 μ L of internal standard mixture (Table 2.1). The solution is vortexed for 30 min at 750 rpm at RT and speed vacuumed to dry at 40 °C. The extracted lipids were derivatized with n-Butanol for 20 min at 60 °C, then again speed vacuumed to dry at 60 °C for 15 min (Martin et al., 2014). The dried pellets were dissolved in 100 μ L of ACN 0.1 % FA and vortexed for 5 min at 750 rpm on a thermomixer. The samples were centrifuged at 13,000 rpm for 10 min at RT and the supernatant was taken into HPLC sample vails for further analysis. The 100 μ L extracted lipid

samples were brought to RT and filled into individual HPLC vails with 200 μ L inserts and placed into the autosampler of Nexera X2 UFLC, connected to LC-MS/MS (SHIMADZU 8045) MS system with ESI source (Jouhet et al., 2017). The data was analyzed by Lab solutions software and the concentrations were calculated by measuring the area under the curve respective to the internal standards.

Analyte	Internal			
, and the second	Standard (IS)			
C14:0	² H ₃ C14			
C14:1	² H ₃ C14			
C14:2	² H ₃ C14			
C14:3	$^{2}\text{H}_{3}\text{ C}14$			
C16:0	² H ₃ C16			
C16:1	² H ₃ C16			
C16:2	² H ₃ C16			
C16:3	² H ₃ C16			
C18:0	² H ₃ C18			
C18:1	${}^{2}\text{H}_{3}\text{ C}18$			
C18:2	² H ₃ C18			
C18:3	² H ₃ C18			
C18:4	² H ₃ C18			

Table 2.1 Internal standard mix.

2.14 Isolation of thylakoid membrane

All of the procedures were performed at 4 °C. Pellet was resuspended in 40 mL of solution 1 (0.3M sucrose, 0.5M HEPES, 1M MgCl2 & 0.5 NaF) comprise 1mM PMSF and impeded in a sonicator set to 25 % amplitude for 6 cycles of 15 sec pulse-on and 45 sec pulse-off. For 20 min, the lysate was spun at 10,000 × g. To preserve the membrane vesicles, the supernatant was removed, and the pellet was resuspended in solution 2 (0.3M Sucrose) without starch. Centrifugation at 10,000 × g for 20 min to collect membrane vesicles. In a polycarbonate Beckman tube, the pellet was resuspended in 10 mL of solution 3 (1.8 M Sucrose) and then overlapped with 10 mL of solution 4 (1.3 M Sucrose) accompanied by 15 mL of solution 5 (0.5M) to establish a discontinuous gradient. This was centrifuged at 28,000 × g for 75 min in an SW-Ti 28 swing bucket rotor. Following that, thylakoid membranes settle at the interface

of solutions 4 and 3 were retrieved and diluted 10 times with solution 6. (0.5 M HEPES, 0.5 M EDTA & NaF). This was centrifuged at $10,000 \times g$ for 20 min, the supernatant was discarded, and to the pellet 1 mL of solution 6 was added (Subramanyam et al., 2006). The concentration of chlorophyll was evaluated and optimized to a final concentration of 0.8 mg mL⁻¹ (Chua and Bennoun, 1975; Subramanyam et al., 2006).

2.15 Sucrose density gradient (SDG) ultracentrifugation

Sequential layering of 1.3 M, 1.0 M, 0.7 M, 0.4 M, and 0.1 M sucrose produced discontinuous sucrose density gradients (from bottom to top). Sucrose gradient centrifugation of isolated thylakoid membranes was carried out with some alteration as reported in other studies (Subramanyam et al., 2006; Tokutsu et al., 2012). First, 200 μ g of chlorophyll was mixed thoroughly in 5 mM Hepes (10 mM EDTA, pH 7.5) buffer and solubilized in 1.0 percent n-dodecyl -D-maltoside (β -DM) on ice in the dark for 5 minutes before centrifugation at 5000 rpm for 5 minutes at 4 °C. Supernatant containing solubilized thylakoid membranes was loaded on top of prepared sucrose density gradients and centrifuged for 22 hours at 1,88,000 rpm using Rotor SW41Ti at 4 °C.

2.16 Measurement of circular dichroism spectra

Measurements of circular dichroism (CD) was taken in JASCO 815 Spectropolarimeter. The measurement was recorded within the 400–750 nm wavelength range and a scan speed of 100 nm min⁻¹ with 3 cumulative accumulations. An optical path length was 1 cm, a bandwidth of 2 nm, and a data pitch of 0.5 nm was used. Samples were in 0.1 M sucrose and 10 mM Tricine, pH 8.0. CD secondary structural measurements were made utilizing a quartz cell with a 0.1 cm route length. A buffer (0.1 M sucrose and 10 mM Tricine, pH 8.0) was used to remove the baseline. Three scans were accumulated from the 190–260 nm range at a scan speed of 100 nm min⁻¹, and the bandwidth was kept at 2 nm (Akhtar et al., 2015). Each CD spectrum

ellipticity was measured in millidegrees (mdeg). Measurement was done from the samples obtained from the SDG fractions as we wanted to see the real changes in the bands. We have not used equal Chl or protein because, while equal Chl was used due to solubilizing the thylakoids with β -DM.

2.17 Pigment content determination by HPLC analysis

C. reinhardtii cells (WT, pgrl1, and pgr5) was harvested in the mid-log phase of growth (3.0 $\times 10^6$ cells mL⁻¹). The Chl content of the treated samples was estimated by resuspending them in 1 mL of 100 % methanol. The cells were centrifuged, and the chlorophyll content of the supernatant was calculated using a UV-visible spectrophotometer and the optical absorbance at 652 and 665 nm. For thylakoids and SDG fractions, the pigment was extracted with 100 % methanol. For acetone and methanol (50:50,v/v), the pigment was extracted by centrifuging at 10,000 rpm for 10 min (Tokutsu and Minagawa et al., 2013). The supernatant was filtered using a 0.45 μ m filter before being subjected to HPLC. HPLC (Shimadzu) was used to separate and evaluate pigments on a C-18 column (250 \times 4.6 mm, 5 μ m; Phenomenex) using a 30 min isocratic gradient of methanol: acetonitrile: acetone (70:20:10, v/v/v) as the mobile phase. Carotenoids were also analysed quantitatively using standards, peak areas, and retention time of each compound. Pigments were identified using a UV–Vis detector at 455 nm (SPD 20 A:Shimadzu).

2.18 Immunoblot analysis

Cells were collected by centrifugation. The cell pellet was solubilized in protein extraction buffer (0.1 M DDT, 4 % SDS, and 0.1 M Tris, pH 7.6), and all the samples were kept for heating at 95 °C for 5 min. Cell suspensions were centrifuged at $2,810 \times g$ for 10 min, and the supernatant was collected. Protein concentration was quantified using the Bradford method, and 5 µg of proteins were loaded per well. The individual proteins were separated with 15 % Bis-Tris gels for DGAT2A and PDAT1 proteins and 12 % for ATG8 and Histone3 (H3)

proteins. Separated proteins were then transferred to a nitrocellulose membrane (Towbin et al., 1979). Specific primary antibodies were purchased from Agrisera (Sweden) and used at dilutions of DGAT2A (1:2500), PDAT (1:2500), and ATG8 (1:2500). H3 (1:10,000) was used to see equal loading. SDG fractions are separated by 12 % SDS-PAGE. To quantify the polypeptides of SDG fractions, immunoblotting was performed. Primary antibodies against LHCII, PSII, and PSI complex proteins were purchased from Agrisera. The primary antibodies were used with dilutions as follows: D1, type I, and type II (1:5000), PsaA and PsaF (1:1000), and Lhca6 (1:250). The secondary antibody, anti-IgG raised from goat (1:10,000), was used for identification. Thermo ScientificTM brand chemiluminescence reagents were used to generate the signal on the nitrocellulose membrane. The pictures are taken with a Bio-Rad New Chemi DocTM Touch Imaging System.

2.19 Spectral characterisation of supercomplexes

Absorption spectroscopy of the SDG fractions (F1, F2, and F3) of WT, *pgrl1*, and *pgr5* under normal and HL was recorded with UV-Visible Perkin Elmer spectrophotometer lambda 35 (USA). Samples were suspended in 0.1 M sucrose and 10 mM Tricine, pH 8.0. The measurement was taken in the visible region of 400 – 700 nm with a path length of 1 mm. Low-temperature (77 K) Chl fluorescence emission spectra between 600 and 720 nm were measured in liquid nitrogen with an FP-8500 (Jasco) spectrofluorometer. The excitation wavelength was 440 nm with a path length of 1 mm.

2.20 Observation of aggregation by confocal microscopy

Observation of aggregation of unsolubilized thylakoid membrane was observed by using a confocal microscope (TCS-SP-2-Leica, Heidelberg, Germany). The aggregates are imaged using an excitation range of 530 to 550 nm and an emission range of 590 to 750 nm (Tang et al., 2007). The fluorescence images are taken at 60-fold magnification via a digital camera.

Unsolubilized part of samples (pellet) obtained from solubilization is diluted in 25 mM Tricine medium, pH 8.0, containing 0.05 % DM, and chlorophyll concentration was 4 mg mL⁻¹.

2.21 RNA extraction and cDNA synthesis.

Total RNA was extracted according to the manufacturer's instructions using Trizol reagent (Roche, Mannheim, Germany). 1 mg of total RNA was reverse-transcribed using oligodT and the proto script II first strand cDNA synthesis kit after being treated with DnaseI (New England Biolabs, MA, USA) (New England Biolabs, MA, USA). RNA concentration was calculated at 260 nm with a nanodrop 1000 spectrophotometer. Single-stranded cDNA is synthesized from total RNA by cDNA synthesis kit (Biorad) by priming at 25 °C and reverse transcription at 20 min at 46 °C and followed by inactivation at 1 min at 95 °C in a reaction mixture of 20 µL.

2.22 Quantitative real-time PCR

A total of 33 genes were examined in this study for HL stress-induced expression profile. 11 real-time PCR primers were generated using previously reported primer sequences (Couso et al., 2012). Based on the available gene sequence of *C. reinhardtii* from the Phytozome13 data base, oligo primers for real-time PCR (RT-PCR) were designed for 22 genes (primer list is shown in Table 2.2). Using *C. reinhardtii* cDNA, all of the genes are amplified by primer. 2^{-ΔΔCT} method (the Applied Biosystems User Bulletin No. 2 [P/N 4303859]). (Livak & Schmittgen, 2001) is used which measures accurate gene expression comparison of each primer pair of reference genes and target genes. The guanidine nucleotide-binding protein beta subunit -like (cblp) and glyceraldehyde 3-phosphate dehydrogenase (GAPDH4) were used as reference genes. Real-time PCR was carried out on an Eppendorf Mx3000P Multiplex Quantitative PCR System with the Brilliant SYBR Green QPCR Master Mix (Biorad). Each test was performed in triplicate using cDNA synthesized from total RNA as a template. Cycling conditions for real-time polymerase chain reaction (RT-PCR) were as follows: 3 min initial denaturation at 97 °C followed by 50 sec denaturation at 97 °C and 1 min annealing at 62 °C with 50 sec

extension at 72 °C with a final extension at 72 °C for 10 min followed by the hold at 4 °C substrates.

Oligo name	Seq. 5' to 3'(Fp.)	Seq. 5' to 3' (Rp.)		
PDH-PDC3	CCTGGTTCAACACCATCAA	CCGTTGTTGATGAGGAAGAT		
PDH-DLA2	TCGCAACATGAACGAGAG	CGTTAATCTGGCTGCTGTA		
PDH-DLD1	TGTGAGCAAGTAAGAACGC	GGGAATTGAGCACCTGATAC		
PDH-DLD2	TGACCGAGAAACGTAACCT	GCATCAGCCAACACTCTT		
ACH1	GCCATGCTTCAGTTCATCT	CGTAGTTCTCCAGCACAATC		
ACS1	GGATGCAAGCAGATGTCTAA	GCATCTGTACCCGTGTTATC		
ACS3	TTTGGCTGTCCACACTATG	CATTCGACCCGTTGTAGTT		
SCLB1	GCAAGTACGACCTGAACTAC	CCAAAGATGTTGACCAGGAT		
IDH2	TCTGTGCGTGAGATCTTTG	TTGTAGCCCGGAATGTTG		
IDH3	CAGTACAAGGCCACTGATTT	TGAGGATGGTGTTCTTTGTG		
OGD2	GAACTCTTCTCGCGTCAATC	ACCTTGTCCGTCTCAATCT		
OGD3	TGACGGTGAGTACGAGAA	CCGCCAGGTTAATCAAT		
CIS2	AGTAGCGAGCAAACTTGAC	ATGTTTGCCTGTTCCTACTC		
SDH1	ATCAGATCCAGAGCGAAGTA	GGTTCCTGTCTGCCTTTATC		
SDH2	GGTTCCTGTCTGCCTTTATC	GTCCTGCTCATCCTTGATTT		
SDH3	GATGCGTAGGTAGGATGTTTG	GAGTGCGAACCAAGATGAAT		
FUM1	AGAACTGCATCAAGAAGGTG	GCGACGATTCCTTGACTATT		
MDH1	CTGCTGCTGAAGATGAACA	CGTTGGTGTTGAACAGGT		
MDH2	CCCAACAAATGGCAAACAG	CGCCTCTTGTATGAACAGAA		
MDH3	AAGAAGTAGAGGGCTGAGTAG	CAGGCATCAATCGTCCATTA		
MDH4	CAAACAACCCTGTCTGTGTA	GTGCCAGCAATATCGTAGAG		
MDH5	GTCGTAGTTTGTGGGTACAG	TCCTCCTGCTCTGTGTTAT		

Table 2.2 Primers used for qRT-PCR analysis.

2.23 The extraction method and sample preparation of metabolites

Lyophilized *C. reinhardtii* cells (20 mg) were extracted in 480 L pure methanol, with 20 μ L of 0.2 mg mL⁻¹ ribitol as the internal standard (Kundu et al., 2018). The mixture was continuously shaken for 2 min before being heated at 70 °C for 15 min. Following the addition of equal volumes of water and vigorous shaking, 250 μ L of chloroform was added and shaken vigorously. This mixture was centrifuged at room temperature for 10 min at 2200 x g. The upper aqueous phase was separated and dried in a speed vacuum rotator at 35 °C. The dried fractions were resuspended in 40 μ L (20 mg mL⁻¹ of methoxamine hydrochloride in pyridine) methoxamine hydrochloride and then incubated for 90 min at 3 °C. Add 60 μ L of N-methyl-

N-(trimethylsilyl) trifluoroacetamide (MSTFA) was added and incubated at 37 $^{\circ}$ C for 30 min (Kundu et al., 2018). Then transfer 100 μ L of the derivatized sample in an inert containing GC-MS glass vial and store at -80 $^{\circ}$ C until analysis.

2.24 Mass spectrometry analysis

An Agilent 5860 gas chromatograph with Agilent ChemStation E.02.02.1431 software was used for GC paired with mass spectrometry (GC–MS) analysis (Agilent Technologies, United States). Separation was carried out on a 30 m long 0.25 mm diameter J W HP5MS capillary column (Agilent Technologies, United States) under the following parameters: stationary phase film thickness, 0.1 m; carrier gas, helium; flow rate, 1 mL min⁻¹; evaporator temperature, 340 °C at a flow split ratio of 1: 20. The column thermostat's temperature conditions were an initial temperature of 70 °C and a linear increase rate of 6 °C min⁻¹ to 340 °C. New peaks were measured using an Agilent 5975S mass-specific detector (Agilent Technologies, USA) in cumulative ion current recording mode at 2.5 scans per second. Electron impact ionization was carried out at 70 V and 230 °C for the ion source. The chromatogram recording began 3 min later to remove the solvent and lasted 42 min (Kundu et al., 2008).

2.25 Total protein quantification

Cells were harvested at 0.8 OD. 10 mL of cells were taken and centrifuged at 5000 rpm for 10 min. The supernatant was discarded and the pellet was dissolved in protein extraction buffer (0.1 M Dithio Threitol (DTT), 4 % SDS, 0.1 M Tris HCL (pH 7.6)) and vortex for 30 sec. The sample was heated at 95 °C for 5 min and centrifuge at 14000 x g for 10 min. The supernatant was collected and protein concentration was calculated by the Bradford method using a microplate reader at 495 nm (Bradford et al.,1976).

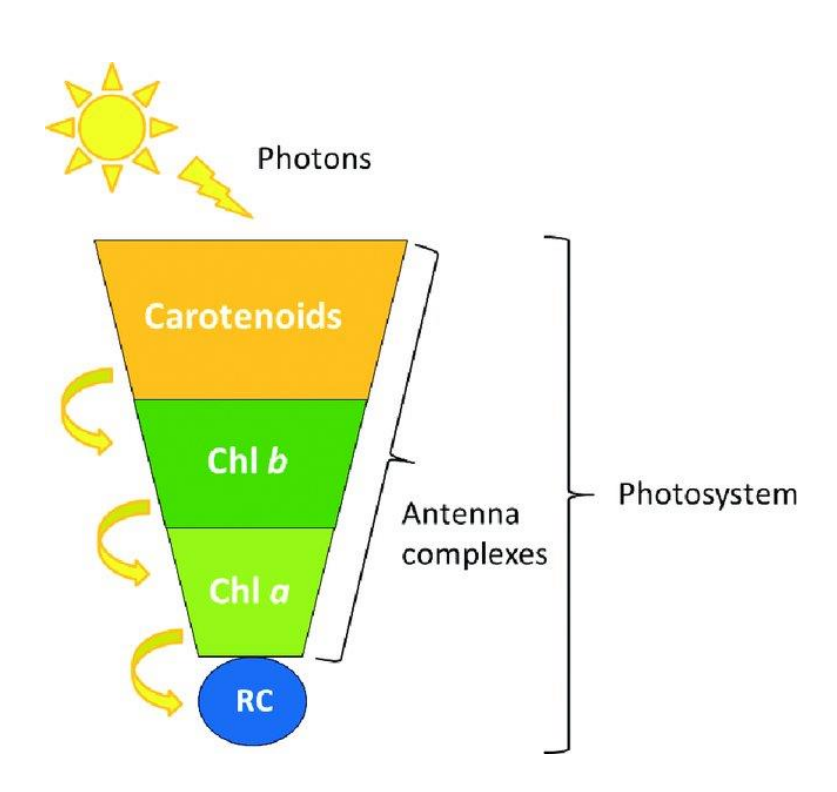
2.26 Statistical analysis

All experiments were done in triplicate, and the data is presented as the mean standard deviation (SD). Sigma plot 14.5 software was used for statistical analysis. Pearson's correlation

coefficient is calculated using the R statistical package to assess the degree of interaction between metabolites (R version 4. 1. 2). Heat maps were created using metabolite correlation values. Metaboanalyst software was used for principal component analysis and metabolic pathway analysis (MetaboAnalyst [V5.0]). The statistical significance difference between WT, pgrl1, and pgr5 was calculated using one-way ANOVA, and the Tukey test was used to analyse the statistical significance at *** p < 0.001, ** p < 0.01 and * p < 0.05.

Chapter 3

Macromolecular structural changes of supercomplexes of thylakoids in high light from pgrl1 and pgr5 mutants of Chlamydomonas reinhardtii



3.1 Introduction

Photosynthesis is the process by which light energy is converted into chemical energy. Photosynthesis requires light as an environmental factor. Excessive light can harm the photosynthetic machinery by creating 1 Chl* and 3 Chl*, which react with the creation of 1 O₂ in the form of molecular oxygen, resulting in photodamage and photoinhibition (Faraloni et al., 2017). Around PSI, plants and algae developed photoprotection systems like CET. Carotenoids played a role in an extra photoprotective mechanism in these species. Carotenoids used the most important photoprotective mechanism: heat dissipation. Excited 3 Chl* and 1 O₂ of the antenna proteins and reaction center were deactivated by tightly bound carotenoids (lutein or carotene). Acetyl CoA to geranylgeranyl diphosphate is converted into phytoene by phytoene synthase enzyme (PSY), the first carotenoid biosynthesis pathway compound. Phytoene leads to the synthesis of lycopene by phytoene desaturase; it is divided into two branches: the synthesis of lutein from α - carotene and the synthesis of violaxanthin from β - carotene by violaxanthin de-epoxidase cycle. Under HL, violaxanthin was modified into zeaxanthin via violaxanthin de-epoxidase (Vde) to eliminate surplus energy from activated chlorophylls (Couso et al., 2012).

Carotenoids perform different photoprotection mechanisms like the change of 3Chl* yield (Dall'Osto et al., 2012), scavenging of ROS (Baroli et al., 2004; Kaushik et al., 2014), and energy dissipation from absorbed light in excess NPQ (Ruban et al., 2016). Xanthophyll is important to safeguard chloroplasts from photooxidative destruction and for light-harvesting (Jahn et al., 2012). Plants and algae regulate photosynthetic light-harvesting and detoxify ROS and free radicals using various antioxidant compounds and enzymes (Foyer et al., 2018), which formed under stress conditions (Sharma et al., 2012; Kaushik et al., 2014).

The majority of algae and plants receive the optimal amount of sunlight. Still, too much light can lead to over-excitation of the photosystem, which is deexcited by thermal energy dissipation called NPQ (Demmig- Adams et al., 2014). The most rapid element of NPQ is qE which is activated when there's a decrease in thylakoid lumen pH. The plant NPQ1 mutant, which is unable to generate zeaxanthin, shows a drop in NPQ (Niyogi et al., 1998). In this process, zeaxanthin synthesis increases the qE and qZ components. In chlorophyte, LHCSR, chlorophyll-binding protein triggered qE and transduced low luminal pH into quenching reactions (Bonente et al., 2011; Pinnola et al., 2013). Microalgae provide carotenoids, liable for light-harvesting in photosynthetic metabolism. Carotenoids are distributed among photosynthetic complex within the thylakoid membrane and have several roles in photosynthesis and photoprotection. Most carotenoids bind majorly to pigment-protein complexes that are membrane-bound like light-harvesting, reaction centers, and Cyt $b_0 f$ (Takaichi et al., 2011). Primary carotenoids like lutein transmit the absorbed energy to chlorophylls, enhancing the light-absorbing spectra of microalgae. The Chl and xanthophyll molecules are arranged in the LHC in such a way that singlet and triplet energy can be transferred between them. The most abundant carotenoids present in PSI (LHCI) and PSII (LHCII) are lutein and violaxanthin. Violaxanthin is present at the peripheral LHC of PSII (Takaichi et al., 2011). The plant pigment-protein complex was assembled into the supercomplex, which contains the core complex and outer antenna. PSI and PSII core possess Chl a and carotenoids, while LHCI and LHCII have Chl a and Chl b and carotenoids.

So far, no reports on the localization of carotene and xanthophylls in the supercomplexes of *C. reinhardtii*. To further understand the nature of these pigments in the macromolecular organization of supercomplexes in thylakoids, we have separated the supercomplexes using the sucrose density gradient of WT, *pgrl1*, and *pgr5* mutants grown under HL (500 µmol photons m⁻²s⁻¹). Also, the carotenoid profile was analyzed by high-

performance liquid chromatography (HPLC). Further, we analyzed the specific genes related to carotenoid biosynthesis by RT-PCR. We also observed the aggregation of core proteins from unsolubilized thylakoids.

3.2 Results

3.2.1 Growth and pigment analysis under HL

The WT, *pgrl1*, and *pgr5* were grown in TAP medium at light intensities of 50 (as a control) and 500 µmol photons m⁻² s⁻² (HL) for 4 days. Under 50 µmol photon m⁻² s⁻² light intensity, all the cultures grew normally (Figure 3.1). The growth of WT cultures increased (Figure 3.1 A), but *pgrl1* and *prg5* mutants exhibited slower growth in HL after 2 days (Figure 3.1 A–C).

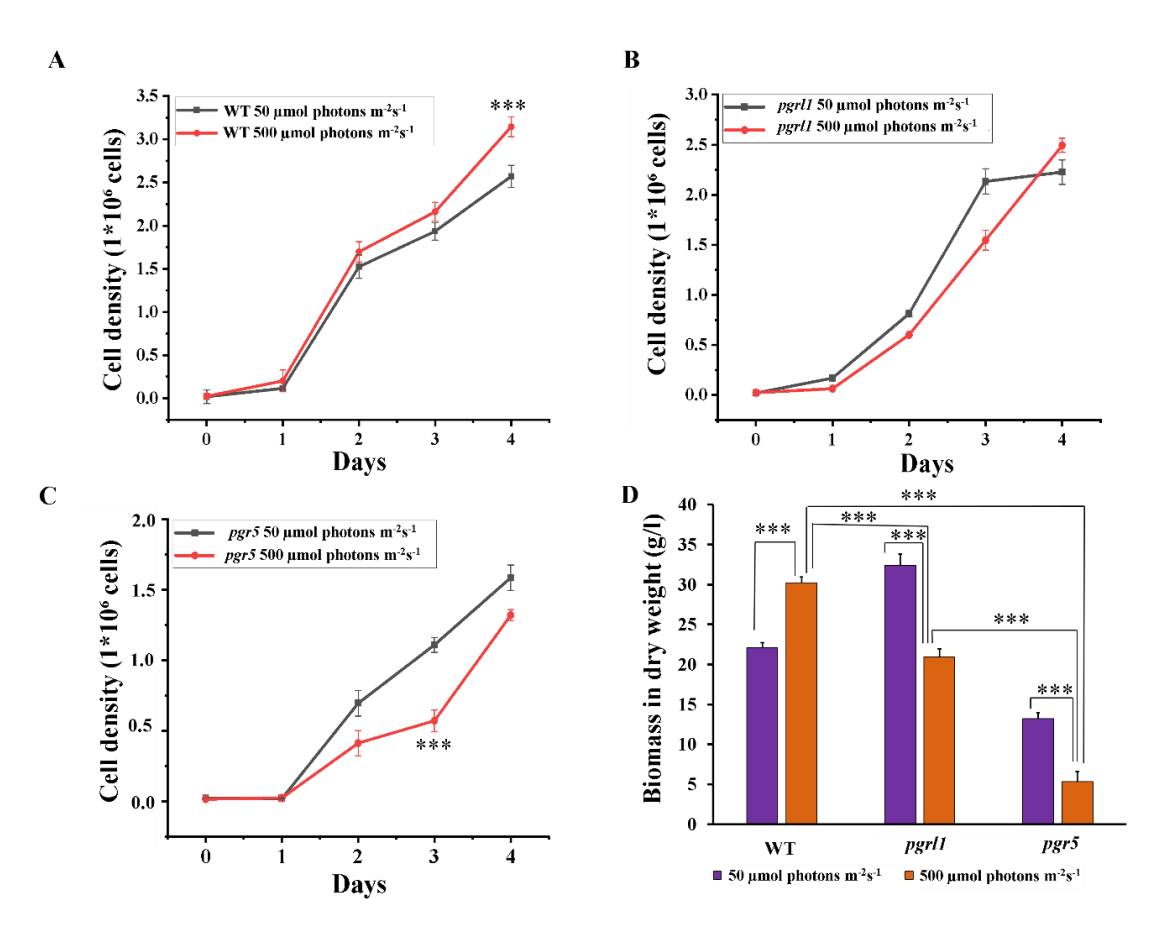


Figure 3.1 Cell growth and dry biomass were monitored from cells grown under normal light and HL conditions. (A–C) Cell growth was analyzed by cell counting by hemacytometer collected for every 24 h of WT, (B), proton gradient regulation 1 (pgrl1), and (C), proton gradient regulation 5 (pgr5) from $50 \, \mu \text{mol}^{-2} \, \text{s}^{-1}$ and $500 \, \mu \text{mol}$ photons $\text{m}^{-2} \, \text{s}^{-1}$ condition. (D) Total biomass in dry weight was calculated after the 3rd day of growth of cells (WT, pgrl1, and, pgr5) grown under light conditions. All the experiments were done three independent times, and error bars represent the mean \pm SD (n = 3).

Statistical comparison was performed using one-way analysis of variance (ANOVA) followed by the Tukey multiple comparison tests, and the p-values obtained are indicated with asterisks (***p < 0.001).

Our results showed that the cell growth pattern of the WT was increased by 30 %, whereas pgrl1 and pgr5 growth were decreased by 21 and 30 % compared to the WT under HL after the 3rd day. Mainly, the pgr5 mutant shows impaired growth, whereas pgrl1 was not affected under the same HL condition after 3rd day of growth (Figure 3.1 B and C). We have studied the effect of light intensity on biomass. The WT shows an increase in biomass yield of 75.5 % in HL, however, it is reduced by 64.6 and 43.6 % in pgrl1 and pgr5, respectively, after the 3rd day (Figure 3.1 D). However, after the 4th day, biomass is almost the same in both mutants when grown in HL.

To determine the effect of HL on the pigment level associated with *C. reinhardtii* photosynthetic complex, we have measured the chlorophyll and carotenoid content from standard and HL-grown cells. Chlorophyll content was significantly reduced in *pgrl1* and *pgr5* mutants, respectively, under HL intensity (Figure 3.2 A). At the same time, we observed a 2-fold increase in carotenoid content in *pgrl1* and *pgr5* under HL (Figure 3.2 B). It is known that increased carotenoid content acts as a protective mechanism against light stress in the *C. reinhardtii* (Li et al., 2009). Carotenoids under HL conditions generally tend to increase to protect PSII from photoinhibition. Data shows that an increase in light intensity results in decreased specific growth rate, increased carotenoid, and reduced biomass production of *pgrl1* and *pgr5*. We assume that reduced growth might be due to ROS production. Our results have elicited us to check further studies and detect the ROS in HL stress.

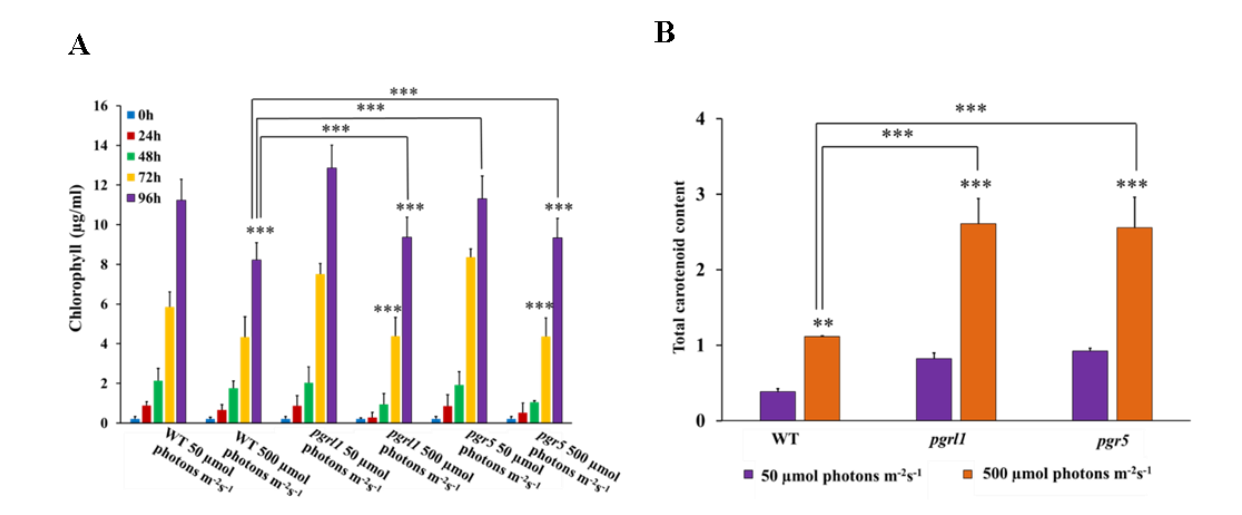


Figure 3.2 Chlorophyll and carotenoid content were quantified from cells grown under normal and HL conditions. (A) Chlorophyll content was quantified from 50 µmol photons $m^{-2}s^{-1}$ and 500 µmol photons $m^{-2}s^{-1}$ condition with different time intervals of 24, 48,72, and 96 h. (B) Total carotenoid content from the cells grown under normal and HL conditions. Carotenoids were calculated from cells grown with control WT and mutant pgrl1 and pgr5 cells grown from normal light (50 µmol photons $m^{-2}S^{-1}$) and HL condition (500 µmol photons $m^{-2}S^{-1}$) measured after 3^{rd} day. Three biological experiments were done n=3. Statistical significance was analyzed using one-way ANOVA with the Tukey test and p-value indicated as (***p < 0.001, **p < 0.01).

3.2.2 ROS induction in HL

To determine the oxidative stress, cells were stained with 2',7 '-dichlorodihydrofluorescein diacetate (H₂DCFDA). ROS was observed using confocal microscopy as well as quantified by spectrophotometry (Figure 3.3 A-C), where an increase in ROS was observed under the HL condition in WT, *prgl1*, and *pgr5* (Figure 3.3). However, this increase was predominant in *pgr5* (Figure 3.3 A-C). The generation of more ROS in *pgr5* could probably explain the reduced growth rate. Further, these results suggest that ROS formation under HL may contribute to autophagy and lipid accumulation. Reports show that ROS may induce multiple metabolic functions like lipid metabolism and autophagy (Shi et al., 2017). HL is one of the factors responsible for ROS formation because of over reduction of the photosynthetic electron transport chain, which might generate ROS that induces autophagy in *C. reinhardtii* (Pérez-Pérez et al., 2012). Based on the above reports, we have conducted experiments related to autophagy caused by HL.

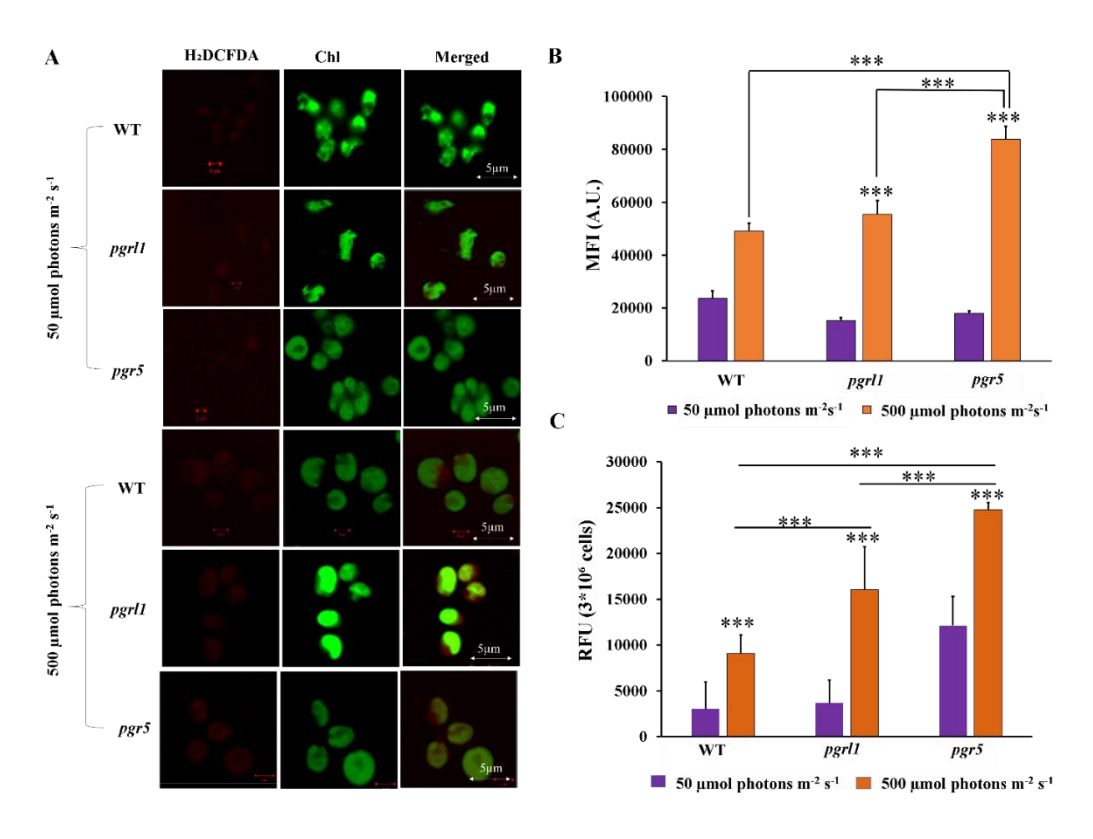


Figure 3.3 Total ROS was measured with H_2DCFDA . (A) C. reinhardtii cells of WT, pgrl1, and pgr5 were collected from the mid-log phase grown under normal (50 µmol photons m^{-2} S^{-1}) and HL (500 µmol photons m^{-2} S^{-1}) for 3^{rd} day. Measured ROS using 2,7dichlorodihydrofluorescein diacetate (H_2DCFDA) (10 µM) staining, and cells were imaged using the Zeiss 510 confocal microscope. The images were collected with three individual measurements for all the conditions (n = 3) and analysed with Zeiss software. Scale bars = 2 µm. (B) Quantification of the fluorescence intensity done by ImageJ. (C) Total ROS was also quantified by spectrophotometry of WT, pgrl1, and pgr5 grown under the light condition on the 3^{rd} day. Three individual measurements were performed for all the conditions (n = 3). Statistical significance was analysed using one-way ANOVA with the Tukey test and the p-value obtained is indicated (***p < 0.001).

3.2.3 Characterization of the supercomplexes isolated from sucrose density gradient

The major pigment-protein complexes were isolated from thylakoid membranes of *C. reinhardtii* WT, *pgrl1*, and *pgr5* cultured in HL by sucrose density gradient (SDG) centrifugation. (Figure 3.4). β-DM solubilized the thylakoid membranes and placed them on top of the SDG with equal chlorophyll (0.8 mgmL⁻¹ Chl). Following centrifugation, three bands are detected in each tube in all conditions (Figure 3.4 A). The separated fractions were called F1 (LHCII), F2 (a small proportion of PSI-LHCI complex with PSII), and F3 (consists

of larger PSI-LHCI-LHCII supercomplexes) (Subramanyam et al., 2010; Ozawa et al., 2010). The density of all of the fractions was measured at 675 nm (Figure 3.4 B). Band intensity of F3 fractions was lowered in the HL condition of WT, *pgrl1*, and *pgr5*. In comparison, the F3 fraction of the *pgr5* mutant was severely affected under HL stress. Suggesting that PSI-LHCI supercomplexes are significantly disturbed in *pgr5* under HL.

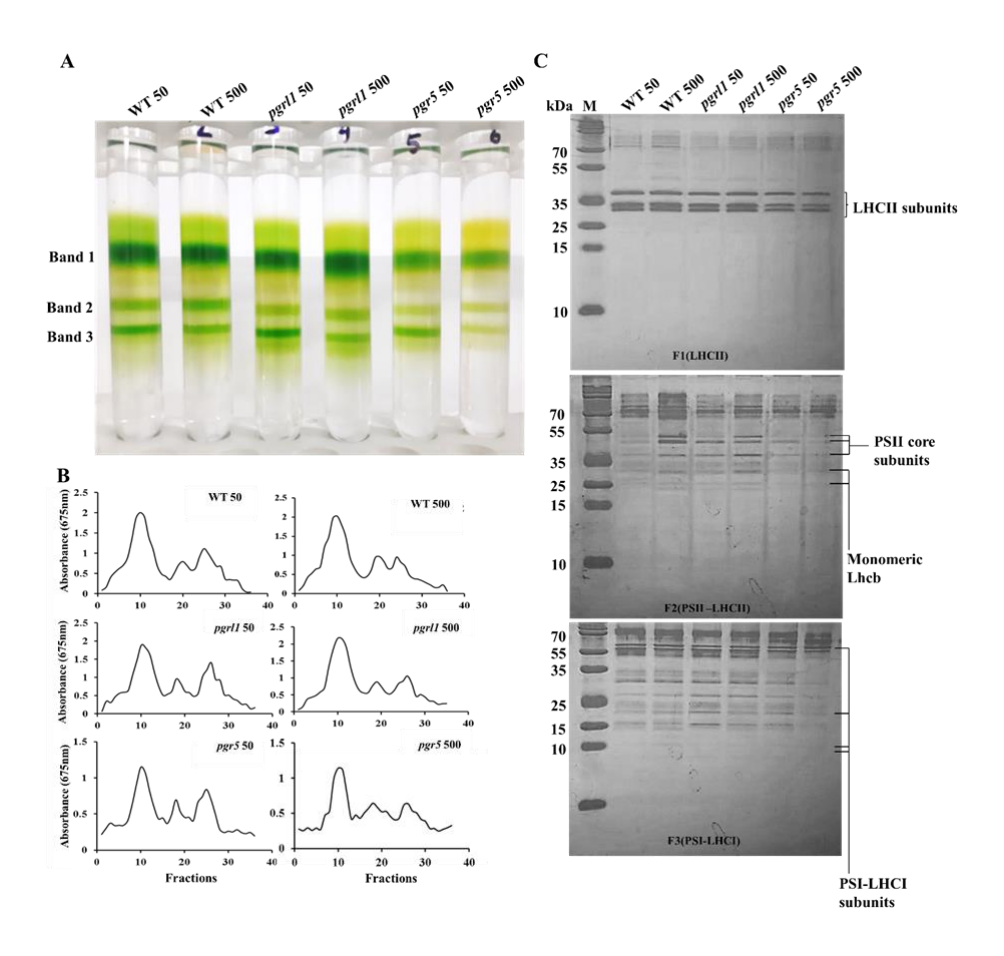


Figure 3.4 Fractionation of major thylakoid membrane complexes of WT, pgrl1, and pgr5 of C. reinhardtii. (A) Isolated thylakoid membranes (0.8 mg/ml of chlorophyll) were solubilized with 0.8 %(w/v) β -DM and equal chlorophyll was loaded on Sucrose density gradient (1.3-0.1 M) of WT, pgrl1, and pgr5 under normal (50 μ mol photons m^2 s^{-1}) and HL (500 μ mol photons m^2 s^{-1}). (B) Absorbance of fractionated complexes following Sucrose density centrifugation at 675 nm recorded from plate reader.(C) Gel electrophoresis of sucrose gradient fractions. SDS-PAGE analyses of gradient bands from Figure 3.4. A. WT, pgrl1 and pgr5 50 and WT, pgrl1 and pgr5 500, represent 50 and 500 μ mol photons m^2 s^{-1} . Each data point represents the mean of the three individual preparations (n=3).

The protein composition of F1, F2, and F3 fractions of all the samples was analyzed via SDS-PAGE (Figure 3.4 C). F1 fractions were characterized by three bands migrating around 27kDa as depicted for LHCII trimers. In F2 fractions, the PSII core proteins CP43,

CP46, D1and D2 were identified based on the molecular weight in agreement with the earlier report (Barera et al., 2012). In F3 fractions (PSI-LHCI), high MW bands around 60-70 kDa are expected to PsaA and PsaB, along with the band at low MW less than 30 kDa was expected to be LHC and other PSI core subunit, which is also in agreement with Subramanyam et al. 2006 (Figure 3.4 C). In most stress conditions, the PSI-LHCI supercomplexes are sensitive, and we also observed under salt and Fe deficiency the complete loss of PSI-LHCI super-complexes (Subramanyam et al., 2010; Yadavalli et al., 2012). These findings suggest that PSI-LHCI supercomplexes are more severely affected under HL stress, especially in *pgr5* than other mutants.

3.2.4 77k fluorescence emission spectra data analysis

The fluorescence emission spectra of the thylakoid membrane of WT, *pgrl1*, and *pgr5* mutant under normal and HL conditions were analyzed. In which a typical 77K fluorescence emission spectrum was obtained with prominent peaks at 680 nm (F680) and 715 nm (F715), originating from LHCII-PSII and PSI, respectively (Subramanyam et al., 2006). Our results show that PSI fluorescence was substantially retarded in *pgr5* of HL compare to normal light (Figure 3.5 F). In addition, when *pgrl1* was grown in HL vs regular light-grown cells, PSI fluorescence was reduced by 1.59-fold (Figure 3.5 D).

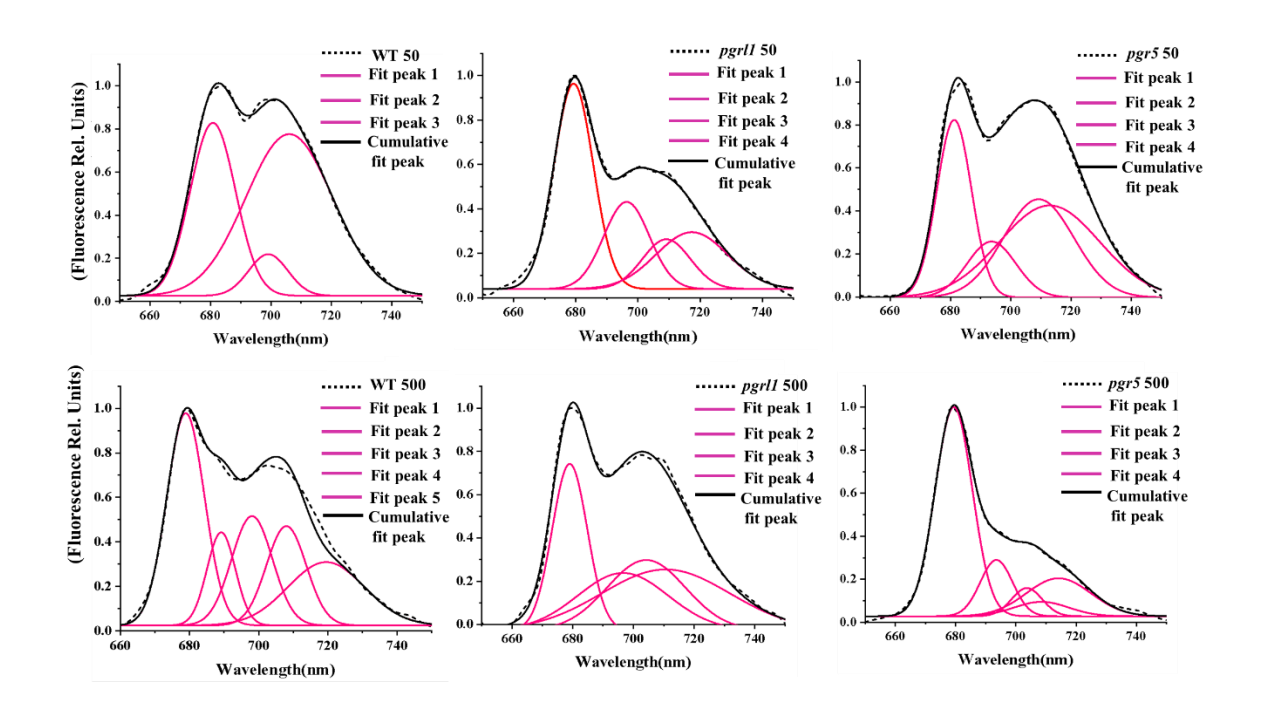


Figure 3.5 77k fluorescence emission spectra. 77k fluorescence emission spectra of thylakoids (A-I) of WT, pgrl1, and pgr5 under normal (50 μ mol photons m⁻² s⁻¹) and HL (500 μ mol photons m⁻² s⁻¹) conditions. WT, pgrl1 and pgr5 50 and WT, pgrl1 and pgr5 500, represent 50 and 500 μ mol photons m⁻² s⁻¹. The values shown are the means of three independent experiments.

We also performed low-temperature fluorescence spectra of fractions pulled out from SDG (Figure 3.6). Band 1 had a large emission peak at 680 nm, which corresponds to fluorescence from LHCII trimers (Krause and Weis 1991). The LHCII trimers showed similar fluorescence spectra in WT, *pgrl1*, and *pgr5*. Band 2 demonstrated an emission peak at 685 nm, agreeing with the PSII core with minor LHCs attributed to PSII. We have seen an additional peak at 700 nm appear in all the strains. The intensity of 700 nm increased in *pgr5* compared to other mutants under HL conditions, which could be aggregated protein (Figure 3.6). In contrast, band 3 exhibited significantly diminished or absent fluorescence associated with PSI-LHCI in HL; Immunoblotting data also confirmed the same. PSI -LHCI complex from WT, *pgrl1*, and *pgr5* isolated from normal light presented two separated peaks; a major peak at 715 nm and a minor peak at 680 nm, emission peak connected with partially dissociated antennae proteins. In PSI-LHCI, the 680 nm peak was more dominant than the 715 nm peak, suggesting a high proportion of detached LHCI subunits under HL. Peak intensity in *pgr5*

mutant was decreased more at 715 nm under HL than *pgrl1*, reflecting the dissociation of mobile LHCII antenna from PSI.

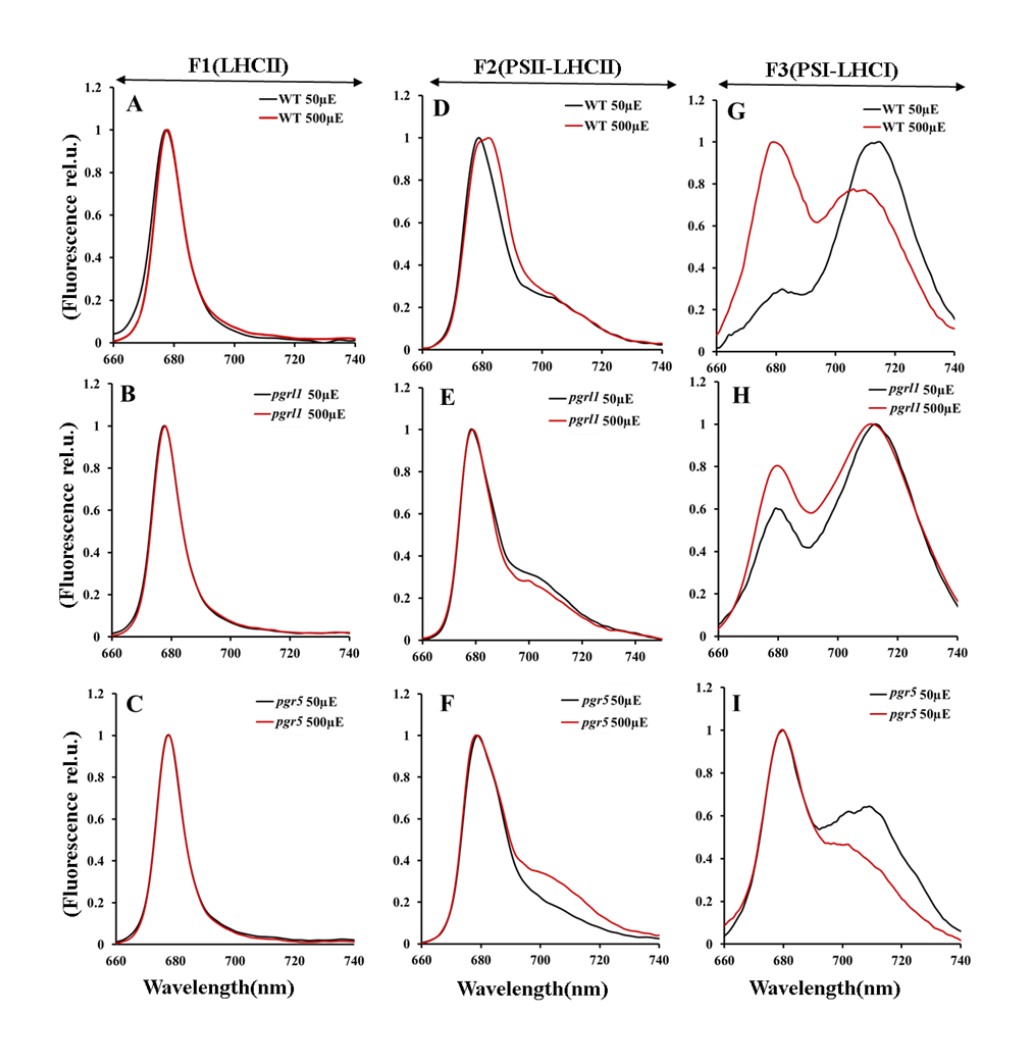


Figure 3.6 77k fluorescence emission spectra. Panel A to I. 77k fluorescence emission spectra of F1(LHCII), F2(PSII-LHCII), and F3(PSI-LHCI) fraction of WT, pgrl1, and pgr5 under normal (50 μ mol photons m^{-2} s^{-1}) and HL (500 μ mol photons m^{-2} s^{-1}). WT, pgrl1 and pgr5 50 and WT, pgrl1 and pgr5 500, represent 50 and 500 μ mol photons m^{-2} s^{-1} . The values shown are the means of three independent experiments.

3.2.5 Absorption spectra analysis of SDG fractions

Absorption cross-section of LHCII, PSII-LHCII-LHCI, and, PSI-LHCI super-complexes under HL conditions of WT, *pgrl1*, and *pgr5*, of three different bands measured to know the pigment-protein interactions. The previous report shows that the F1 band primarily arises from LHCII, F2 from PSII-LHCII, and F3 from PSI-LHCI (Yadavalli et al., 2012). The absorption spectra of the F1 fraction, which have major peaks at 675 nm and 652 nm in the red region and 439

nm and 472 nm in the blue region, originate mainly due to the LHC complex. The major peaks at 675 nm and 652 nm are due to Chl *a* and Chl *b*, respectively, a slight decrease in WT, *pgrl1*, and *pgr5* mutant under HL (Figure 3.7 A). Interestingly, the LHCII accumulation is lesser in *pgr5* than in control.

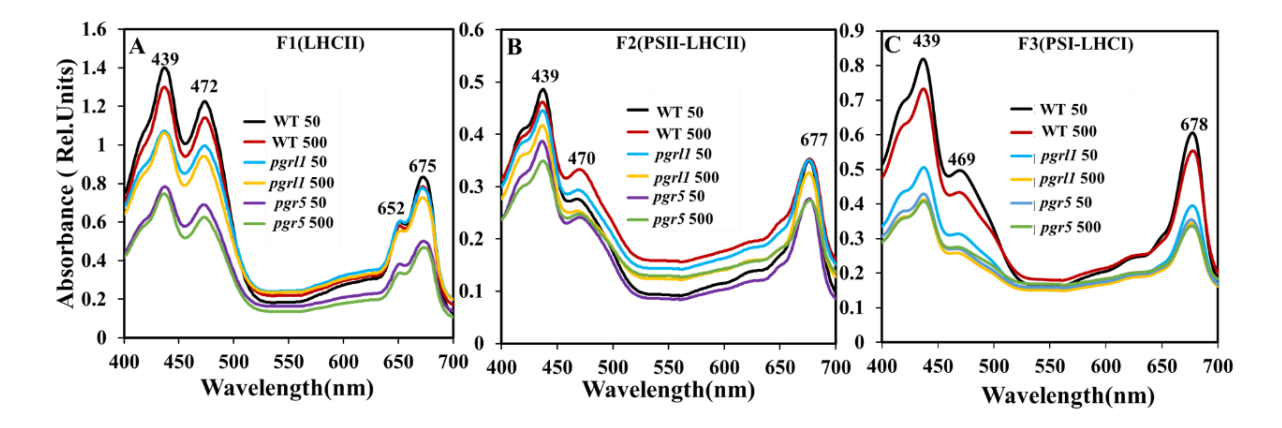


Figure 3.7 Absorbance spectra of pigment binding complexes isolated from C. reinhardtii. Absorption spectra of F1(A), F2(B), and F3(C) fractions of WT, pgrl1, and pgr5 under normal (50 µmol photons m^2 s^{-1}) and HL (500 µmol photons m^2 s^{-1}) of C. reinhardtii cells. WT, pgrl1 and pgr5 50 and WT, pgrl1 and pgr5 500, represent 50 and 500 µmol photons m^2 s^{-1} . Each data point represents the mean of the three individual preparations (n=3).

Similarly, the F2 fraction shows the major peaks at 677 nm and 439 nm and a minor peak at 470 nm corresponding to PSII-LHCII. F2 fractions show the absence of a 650 nm peak (Figure 3.7 B), which corresponds to Chl *b* and give a hint of the presence of PSII core in these fractions (Sugimoto et al., 2003). Absorbance at 470 nm decreased compared to the F1 fraction, also related to Chl *b*. Further, the F3 fractions reveal predominantly Chl *a* with a maximum absorbance in the Qy region at 678 nm and 439 nm (Figure 3.7 C). However, Chl *b* at 469 nm still exists to a lesser degree. F3 fractions were thus likely composed of the PSI-LHCI supercomplex. Differences in the spectra indicate changes in the pigment content and pigment-pigment interaction. F2 and F3 fractions were affected more than F1 fractions of *pgrl1* and *pgr5* due to HL. These results indicate that PSI-LHCI is more prone to HL, especially in *pgr5*.

3.2.6 Pigment-protein interaction studies from visible circular dichroism spectra

The visible CD spectrum is a delicate technique to understand the coupling between pigments and is widely used to determine the pigment organization between complexes. Moreover, it can understand the macromolecular organization among the complexes. The spectra of all three fractions are presented in Figure 3.8 (A-I). LHCII complexes are implicated in the F1 green band observed in the SDG. The band peaks at (-) 653, (+) 669, and (-) 685 nm, which are correlated with the Qy exciton states of Chl *a* and *b*, describing the red region of the spectra: this data correlates with prior studies (Subramanyam et al., 2010; Akhtar et al., 2015). (+) 439, (-) 473, and (-) 493 are the main peaks for the LHCII band (F1) (Figure 3.8 A-C). Because of the prevalence of Chl and carotenoid transitions in the blue area, the spectra have a more complicated structure. The spectra of LHCII trimers are more similar under normal and HL in WT. At the same time, in *pgrl1* and *pgr5*, peak intensity decreased compared to control, suggesting that the LHCII trimers (F1) were significantly affected. However, a decrease in intensity in *pgrl1* and *pgr5* mutant under HL in LHCII trimers leads to a change in the carotenoid organization present in LHCII trimers.

Similarly, Figure 3.8. (D-F) shows PSII-LHCII are critical for the F2 fraction, with CD bands at Qy exciton states of Chl a and b (-) 691, (+) 673, (-) 653 and a blue region with dominant peaks at (-) 465 and (+) 446 (Akhtar et al., 2015). In the spectra of PSII-LHCII (F2), there is a decrease in soret band peak intensity in WT, pgrl1, and pgr5. But a drastic reduction was observed in pgrl1 and pgr5 compared to WT under HL. However, not much difference was observed in the Qy region in WT while we have seen decreased intensity at 653 and 691 nm under HL in pgrl1 and pgr5.

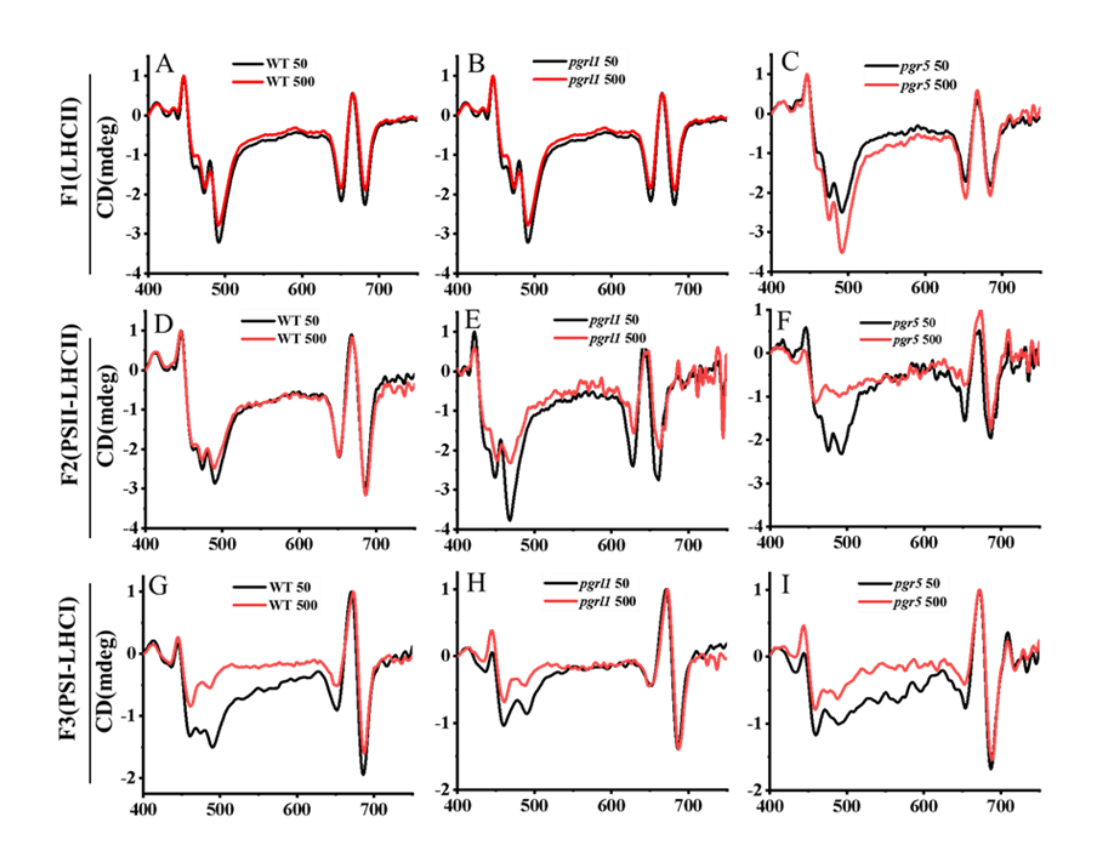


Figure 3.8 Visible circular dichroism spectra of pigment binding complexes isolated from C. reinhardtii. Visible CD of isolated F1(A), F2(B), and F3(C) fractions of WT, pgrl1, and pgr5 under normal (50 μ mol photons m^{-2} s^{-1}) and HL (500 μ mol photons m^{-2} s^{-1}) of C. reinhardtii cells. CD was measured in absorbance units and for comparison, it was normalized to the maximum absorption peak in 600 nm and 700 nm regions. WT, pgrl1 and pgr5 50 and WT, pgrl1 and pgr5 500, represent 50 and 500 μ mol photons m^{-2} s^{-1} . Each data point represents the mean of the three individual experiments (n=3).

PSI-LHCI supercomplexes are also attributed to the F3 fraction (Figure 3.8 G-I) (Akhtar et al., 2015). The excitation states of Chl *a* and *b* (-) 689, (+) 674, and (-) 653, respectively, are shown in the CD peaks, while the main peaks in the blue area are (-) 465 and (+) 446 (Figure 3.8 G-I). The amplitude of the principal peaks at 656 and 672 nm in the visible CD spectra of PSI-LHCI supercomplexes (F3) isolated from *C. reinhardtii* cells cultured at normal and HL indicates a considerable drop in *pgr5*. Under HL, the negative peak at 642 nm show greater amplitude compared to WT and *pgr5*, but no change in *pgr11*. The discrepancies in peak intensity in PSI-LHCI complexes from HL imply significant variances in pigment

interactions. In all complexes, the pigment-pigment or pigment-protein coupling is altered under intense light, especially in pgrl1 and pgr5.

3.2.7 Conformational change in the secondary structure under HL

The "far-UV" CD (190-260 nm) was measured to know the secondary structure of mutant SDG fractions under HL (Figure 3.9 A-C). The F1 fraction, F2 fraction, and F3 fraction of WT, *pgrl1*, and *pgr5* under normal and HL, contain two absorption peaks at 208 and 222 nm, which arise from the protein α- helix. The secondary structure of SDG fractions of WT, *pgrl1*, and *pgr5* was drastically decreased under HL, indicating unstability or unfolding of the protein. Significantly, LHCII complexes was decreased more than the other complexes (PSII-LHCII and PSI-LHCI), indicating that LHCII proteins are more prone to the HL as stress-related protein LHCSR3 was expressed. The findings of CD spectroscopy indicate a variation in supercomplex organization under HL conditions.

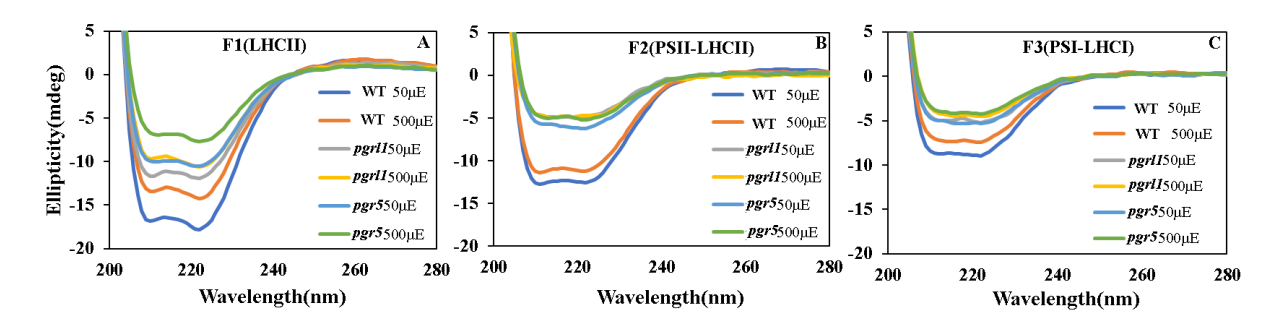


Figure 3.9 Circular dichroism spectra of secondary structure. Circular dichroism spectra of F1(LHCII), F2(PSII-LHCII), and F3(PSI-LHCI) fraction of WT, pgrl1, and pgr5 under normal(50 µmol photons m^{-2} s^{-1}) and HL (500 µmol photons m^{-2} s^{-1}). WT, pgrl1 and pgr5 50 and WT, pgrl1 and pgr5 500, represent 50 and 500 µmol photons m^{-2} s^{-1} . The values shown are the means of three independent experiments.

3.2.8 Carotenoid derivatives change under HL grown cells

Xanthophyll has an essential function in the photosynthetic organism. The primary function of carotenoids in photosynthesis is photoprotection via ³Chl quenching and ¹O₂ scavenging. All plants and microalgae possess the xanthophyll cycle. The plants dissipate excess energy and convert violaxanthin to zeaxanthin under HL. An increase in accumulation of zeaxanthin and

a decrease of violaxanthin are interrelated under HL in WT and pgrl1; however, in pgr5, zeaxanthin presence was insignificant (Table 3.1). Chl a was marginally changed while Chl b was enhanced overall. We have seen a decrease in the Chl a/b ratio in pgr5. At the same time, the Chl a/b ratio was not changed in WT and pgrl1 under intense light. β - carotene and lutein content increased in WT and pgrl1 under HL; however, we haven't seen increased carotenoid and lutein content in pgr5 under HL. This is the possible explanation that in SDG data, the third fraction was decreased in the band's intensity in pgr5 mutant under HL. We have seen conformational changes related to pigment – chlorophyll interaction under stress conditions which is explained here due to not much difference seen in pgr5 under HL. An increase in β -carotenoid and lutein content in pgrl1 mutant under HL suggested the protection of supercomplexes. Chl a/b ratio of pgrl1 mutant was not changed under HL, which means PSII was less affected.

Pigment (mg/g DCW)	Chl a	Chl b	Chl a/b	β-carotene	Violaxanthin	Zeaxanthin	Lutein
WT 50	9.07±0.40	6.22±0.24	1.45±0.05	2.56±0.25	3.56±0.152	0.054±0.003	1.21±0.04
WT 500	7.08 ± 0.17	4.45 ± 0.14	1.59 ± 0.03	3.46 ± 0.194	1.42 ± 0.05	3.02 ± 0.105	2.21 ± 0.01
		1		1	1	T	Ť
pgrl1 50	7.6 ± 0.26	4.24 ± 0.15	1.79 ± 0.07	1.66 ± 0.155	1.37 ± 0.043	0.012 ± 0.010	0.97 ± 0.03
pgrl1 500	6.93 ± 0.16	4.42 ± 0.71	1.59 ± 0.2	3.48 ± 0.433	1.45 ± 0.046	2.13 ± 0.242	1.22 ± 0.06
pgr5 50	6.30 ± 0.49	2.71 ± 0.15	2.32 ± 0.15	1.19 ± 0.170	1.659 ±0.041	0.004 ± 0.0009	0.74 ± 0.03
pgr5 500	6.23 ± 0.21	4.22 ± 0.89	1.52 ± 0.32	1.62 ± 0.28	1.60 ± 0.13	0.006 ± 0.041	0.64 ± 0.48

Table. 3.1 Carotenoid content of C. reinhardtii under normal and HL conditions. WT, pgrl1 and pgr5 50 and WT, pgrl1 and pgr5 500, represent 50 and 500 μ mol photons m^{-2} s^{-1} . The data represents the $\% \pm S.D.$ for n=3.

3.2.9 Carotenoid derivatives in thylakoids

We investigated the changes in carotenoids of WT, pgrl1, and pgr5 under normal and HL conditions. Carotenoids have been shown to increase under HL, salt stress, and nutrientdeficient condition (Quian-Ulloa et al., 2012; Shah et al., 2017; Maltsev et al., 2021). An increase in carotenoids is thought to be a protective mechanism of cells against oxidative stress (Birben et al., 2012). Pigment content (β- carotene, zeaxanthin, violaxanthin, and lutein) was measured by HPLC from isolated thylakoids. Only the level of β- carotene and lutein increase significantly under the HL stress in WT, pgrl1, and pgr5. In particular β- carotene was increased by 50 %, 40 %, and 10 % in WT, pgrl1, and pgr5, respectively, under HL, while lutein content increased by 60 %, 70 %, and 50 % in WT, pgrl1, and pgr5 mutant respectively. Increased levels of β -carotene and lutein content were also observed in HL in npq1 mutant amidst this strain unable to convert violax anthin to zeax anthin. Zeax anthin content was reduced under HL conditions in the *npq1* mutant (Figure 3.10 A). A slight rise in other carotenoids can compensate for the marginal increase of these carotenoids. We have seen a decrease in violaxanthin content in all the strains, which might be converting into zeaxanthin under stress conditions. Zeaxanthin content was enhanced in WT, pgrl1, and pgr5 except in npq1 under HL. But the increase was not significant in the pgr5 mutant; that might be the reason pgr5 showed more ROS accumulations from our previous report.

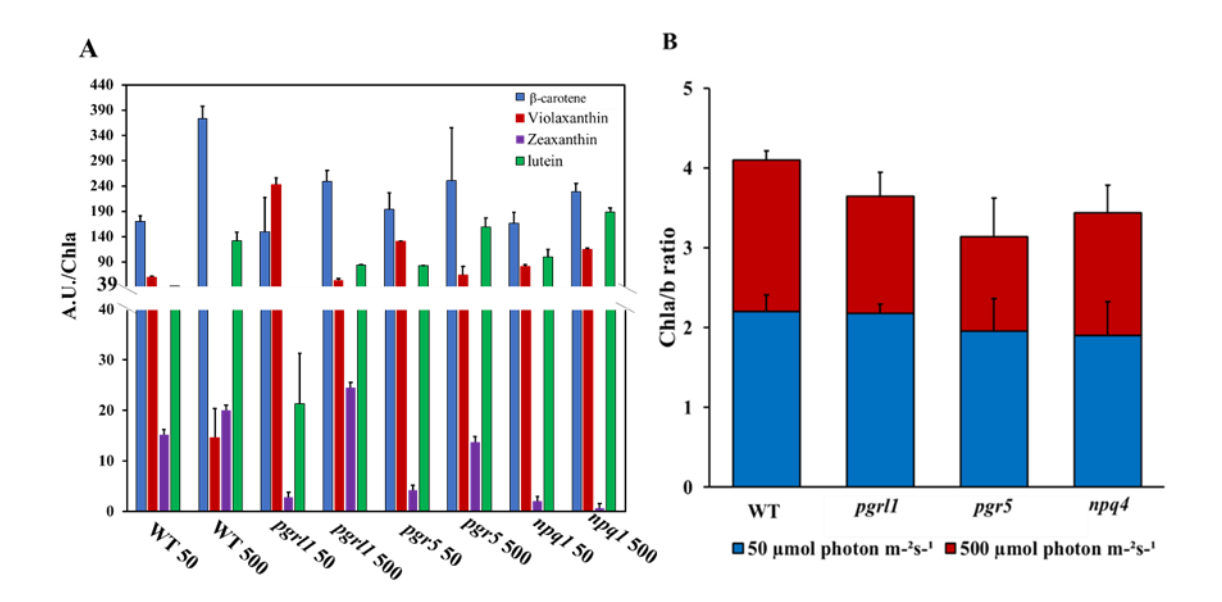


Figure 3.10 Pigment composition of thylakoids and Chlorophyll content of SDG fractions. (A) The relative content of xanthophyll cycle pigment of thylakoids of WT, pgrl1, and pgr5 under normal (50 μmol photons m⁻² s⁻¹) and HL (500 μmol photons m⁻² s⁻¹) of thylakoids membrane. WT, pgrl1 and pgr5 50 and WT, pgrl1 and pgr5 500, represent 50 and 500 μmol photons m⁻² s⁻¹. (B) The relative content of Chla/b ratio of thylakoids of WT, pgrl1, and pgr5 under normal (50 μmol photons m⁻² s⁻¹) and HL (500 μmol photons m⁻² s⁻¹). The values shown are the means of three independent experiments. The error bars represent standard deviations.

3.2.10 Carotenoid associated pigments with LHCII trimers (F1 fractions)

To explore the interactions of chlorophyll-binding proteins and xanthophyll of WT, pgrll, and pgr5, we analyzed the pigments from the fractions obtained from SDG. The obtained three fractions comprised F1(LHCII), F2(PSII-LHCII), and F3(PSI-LHCI) of WT, pgrll, and pgr5 under normal and HL. Each fraction was extracted and analyzed by HPLC to identify protein-bound pigment, particularly xanthophyll cycle pigments. The Chl a/b ratio decreases under HL in WT and pgr5 mutant in all the fractions however Chl a/b ratio of pgrll increases in F1 and F2 fractions (Figure 3.11 A). In the F1 fraction, LHCII trimers, β -carotenoid content of WT and pgr5 was significantly increased under HL (Figure 3.11 B). At the same time, there was a significant decrease in the β -carotenoid in pgrll under HL.

Interestingly, we have observed increased lutein content in all the strains under HL. The F1 fraction is an LHCII complex that requires xanthophyll binding for the correct folding of

antenna protein. Under HL, violaxanthin was increased in WT strains while it was significantly decreased in *pgrl1* due to bleaching of cells. In the *pgr5*, there was no significant difference observed in violaxanthin under HL. Under HL stress, violaxanthin is converted into zeaxanthin. When cells are subjected to HL, their carotenoid content increases because xanthophyll converts to zeaxanthin and lutein, as evidenced by the data presented (Niyogi et al., 1997).

3.2.11 Carotenoid associated pigments of PSII-LHCII supercomplex (F2 fraction)

PSII -LHCII was isolated from the middle layer in a sucrose gradient of WT, pgrl1, and pgr5. The most abundant carotenoid in the PSII was β -carotene whereas xanthophyll level was present in less amount, specially violaxanthin and lutein. Our data shows that PSII-LHCII super-complexes, β -carotenoid content increases significantly under stress conditions in WT compared to pgrl1 and pgr5 which shows the photoprotection of PSII complex from ROS production. We can further confirm from 77 k data and immunoblot data that PSII core protein (D1) was not affected much under HL in WT. While in pgrl1 and pgr5, D1 Protein was decreased under HL conditions. Xanthophyll content of fraction of PSII core complexes increases under HL. Our results show increased lutein and zeaxanthin content in the HL condition in pgrl1 and pgr5 (Figure 3.11C). This could imply that lutein is bound to the PSII core complex, which may be implicated in HL. Our results are in agreement with the previously published data that violaxanthin and lutein coupled with PSII core complexes via the antenna or another pigmented subunit (Bassi et al., 1993; Pineau et al., 2001).

3.2.12 Carotenoid associated pigments of PSI-LHCI supercomplex (F3 fraction)

PSI-LHCI was separated by sedimentation of WT, *pgrl1*, and *pgr5* in a sucrose gradient. According to previous reports, the main xanthophylls linked to the PSI of *C. reinhardtii* are violaxanthin and lutein (Jahns and Holzwarth 2012). Under normal and HL, the xanthophyll content of WT, *pgrl1*, and *pgr5* of PSI-LHCI supercomplexes is shown in Figure 3.11 D. We

found a reduction in xanthophyll content in the F3 fraction compared to the F1 and F2 fractions. Our finding reveals that in the F3 fraction, β - carotenoid reduces significantly under HL conditions in WT and pgrl1, while an increase in β - carotenoid was observed in pgr5. As expected, the violaxanthin content decreases in all the strains under HL. Zeaxanthin level also reduces under low light, although its level was already less in normal light. As reported earlier, the suppression of zeaxanthin increases oxidative stress and photoinhibition under light stress conditions (Kim et al., 2020). We have reported an increased ROS amount recently in pgrl1 and pgr5 mutant under HL because of a decrease in zeaxanthin.

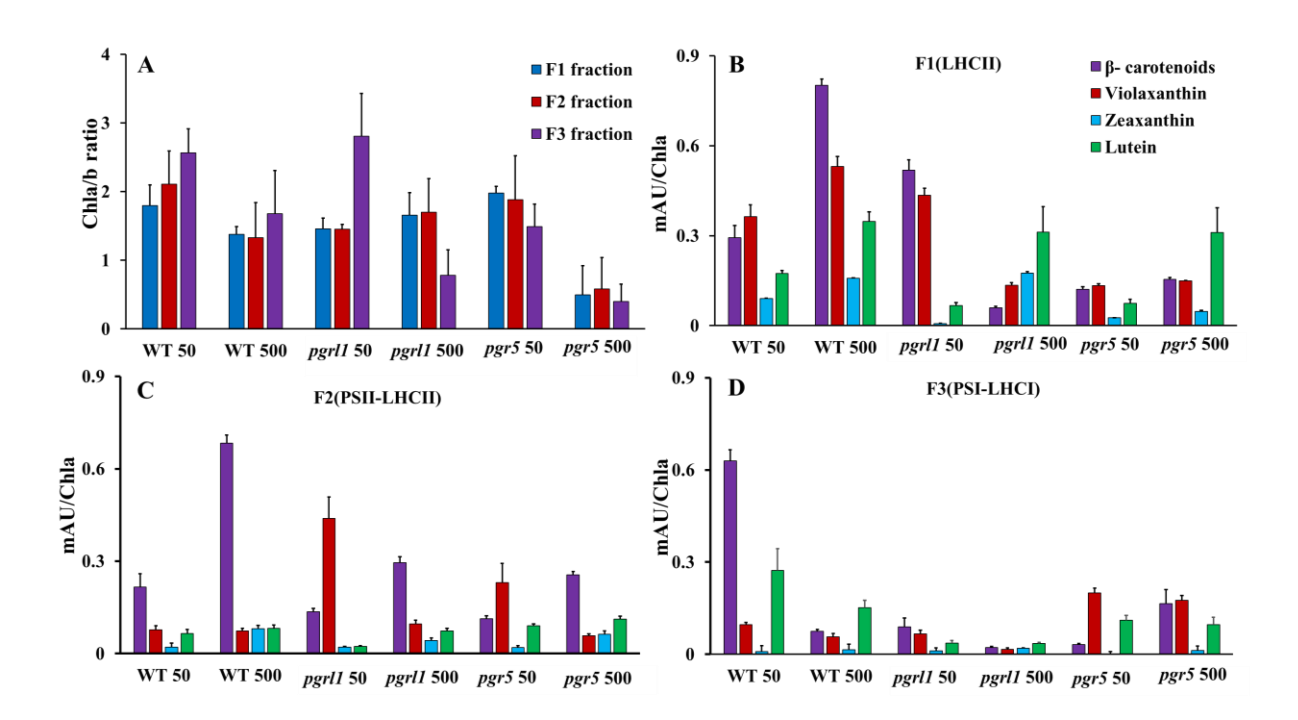


Figure 3.11 Pigment composition of SDG fractions of WT, pgrl1, and pgr5 under normal and HL. (A) The relative content of Chl a/b ratio of isolated F1(A), F2(B), and F3(C) fractions of WT, pgrl1, and pgr5 under normal (50 μ mol photons m^2 s⁻¹) and high light (500 μ mol photons m^2 s⁻¹) of C. reinhardtii cells. Xanthophyll content of the SDG fractions F1(B), F2 (C), and F3 (D)fractions of WT, pgrl1, pgr5 under normal (50 μ mol photons m^2 s⁻¹) and HL (500 μ mol photons m^2 s⁻¹) conditions were analyzed by high-performance liquid chromatography (HPLC). WT, pgrl1 and pgr5 50 and WT, pgrl1 and pgr5 500, represent 50 and 500 μ mol photons m^2 s⁻¹. Each data point represents the mean of the three individual experiments(n=3). The error bars represent standard deviations.

3.2.13 Expression of key genes of the carotenoid biosynthesis pathway under HL

Real-time PCR was performed on WT, pgrl1, and pgr5 under normal and HL to investigate changes in gene expression of carotenoid biosynthesis. Total RNA was isolated from each sample, and the transcript levels of the enzymes that catalyzed the pathway's major stages were analyzed with qPCR. I investigated the major pathway (PSY and PDS), the expression of the genes encoding the enzymes responsible for cyclization of lycopene (LCYE and LCYB), the hydroxylases involved in the production of the xanthophylls, lutein, and zeaxanthin, (CHYB, CYPE, and CYPEB), and zeaxanthin epoxidase (ZEP) (Figure 3.12 A). Thresholds of each transcript were normalized to the housekeeping gene CBLP level and represented relative to the corresponding gene's normalized level at zero time (Figure 3.12 B). Under HL, the genes PSY/PDS were upregulated and increased to 2-fold under HL conditions in WT, pgrl1, and pgr5. LCYE and LCYB are engaged in the cyclization of lycopene to produce α -carotene and β-carotene, LCYE shows upregulation in pgrl1 and pgr5 mutant. At the same time, it offers a slight decrease in WT compared to the mutants. Simultaneously, LCYB is upregulated for WT and pgrl1, and pgr5. We found a decrease in ZEP transcript during HL exposure in pgr5, which catalyzes the formation of violaxanthin and is actively engaged in the xanthophyll cycle. At the same time, it is upregulated in WT and pgrl1. CHYB, which converts β-carotene to zeaxanthin, was progressively induced in WT and pgrl1, while in pgr5, we have observed a slight decrease in the expression of these genes. All the genes were overexpressed in WT, pgrll, and pgr5; however, the expression of these genes was lower in pgr5 under HL. Interestingly, all the transcript data is in agreement with the pigment analysis.

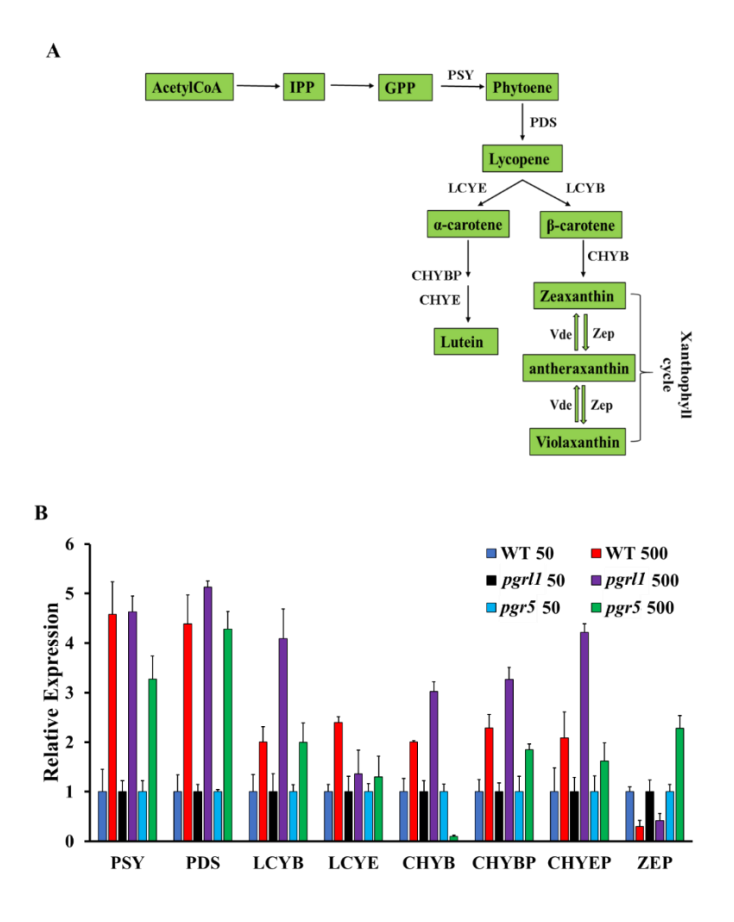


Figure 3.12 Real-time PCR of WT, pgrl1, and pgr5 of C. reinhardtii under normal and HL condition. (A)Xanthophyll biosynthetic pathways of C. reinhardtii. Abbreviations of carotenoid-biosynthetic enzymes: PSY, phytoene synthase; PDS, phytoene desaturase; LCYE, lycopene epsilon-cyclase; LCYB, lycopene beta-cyclase, CHYB, carotenoid β-hydroxylase; CHYBP, beta-carotene 3-hydroxylase; CHYE, carotenoid ε-hydroxylase; ZEP, zeaxanthin epoxidase; VDE, violaxanthin de-epoxidase. (B) The relative content of xanthophyll cycle pigment of cells of WT, pgrl1, and pgr5 mutant under normal(50 μmol photons m⁻² s⁻¹) and HL (500 μmol photons m⁻² s⁻¹). WT, pgrl1 and pgr5 50 and WT, pgrl1 and pgr5 500, represent 50 and 500 μmol photons m⁻² s⁻¹. The values shown are the means of three independent experiments. The error bars represent standard deviations.

3.2.14 Immunoblot analysis of SDG fractions

The protein composition of all the fractions was subsequently investigated by SDS-PAGE (Figure 3.13 A-B). Immunoblotting was used to examine the protein content of specific antibodies. The core protein of PSII, D1, was reduced by only 10 % in *pgrl1* and *pgr5*. While in WT, there was not much change observed in PSII core, D1 protein. The PSI core, PsaA content was decreased in HL; this decrease was predominant in *pgr5*. Light-induced accumulation of LHCSR3 was observed only in the LHCII trimer (F1 band). Though the LHCII

is associated with PSII (F2 band), there is no LHCSR3 present in WT and *pgrl1* in HL. However, no LHCSR3 was present in *pgr5*, showing NPQ defect in *pgr5* mutant because of smaller proton motive force (Johnson 2014; Yadav et al., 2020) The pigment data also supported decreased zeaxanthin content in *pgr5* under HL, while in WT and *pgrl1*, zeaxanthin was accumulated under HL conditions. At the same time, we check PsaF as a loading control which was not changed in all the strains.

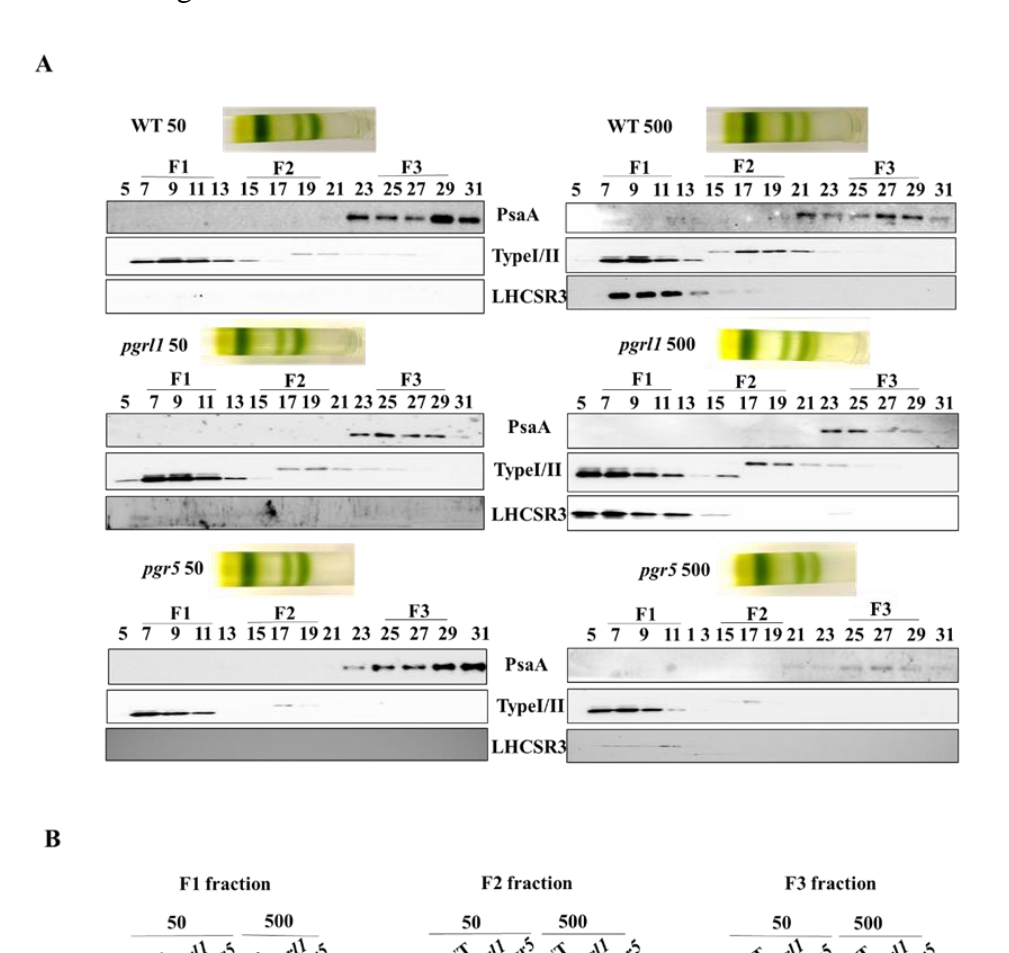


Figure 3.13 Immunoblots of SDG fractions of WT, pgrl1, and pgr5 mutant under normal and HL. (A) Immunoblots of the SDG fractions of PsaA, TypeI/II, and LHCSR3 of WT, pgrl1, and pgr5 under normal(50 μ mol photons m^2 s^{-1}) and HL (500 μ mol photons m^2 s^{-1}) conditions. (B) Immunoblots of the extracted fractions (F1, F2, and F3) of PsaA, D1, Lhca6, and PsaF of WT, pgrl1, and pgr5 under normal(50 μ mol photons m^2 s^{-1}) and HL (500 μ mol photons m^2 s^{-1}) condition. WT, pgrl1, and pgr5 50 and WT, pgrl1, and pgr5 500 represent 50 and 500 μ mol photons m^2 s^{-1} . Data are expressed as n=3.

PsaA

Lhca6

Psaf

D1

Lhca6

D1

PsaA

Lhca6 Psaf

D1

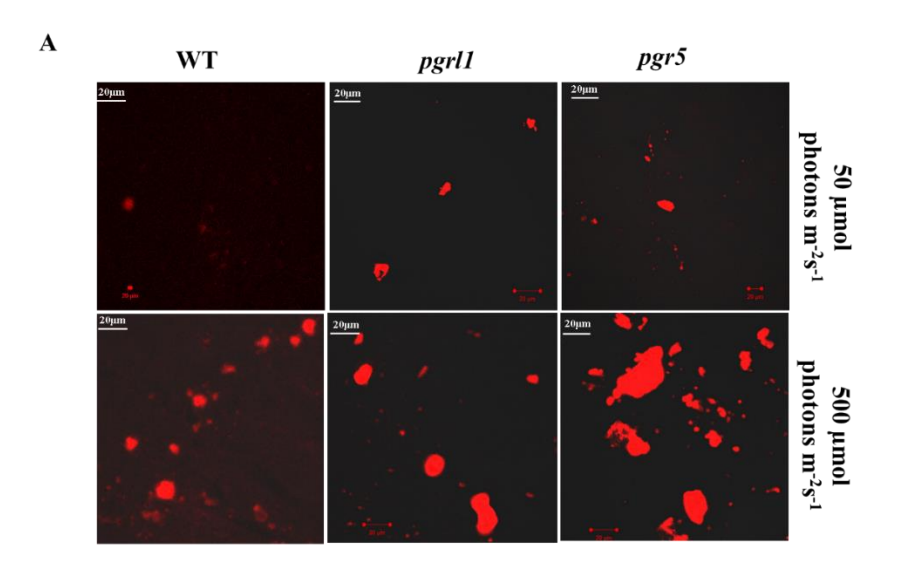
Interestingly, LHCII Type II (LHCBM5), involved in state transitions and energy dissipation (Kim et al., 2020), was not changed under the HL stress in all the strains in the F1 fraction. Surprisingly we have seen an increase in expression of Type II in WT and pgrl1 in the F2 fraction, which might be photo-protected due to an increase in lutein content in F1 fractions. This indicates that lutein and β -carotene play a pivotal role in protecting LHCII trimers in pgrl1 from HL-induced damage.

3.2.15 Confocal image of aggregated cells and immunoblots of unsolubilized thylakoids

When the thylakoids were solubilized with β -DM, the loosely bound or aggregated proteins increased in the pellet. To observe the aggregation caused due to light stress, the confocal microscope was performed on the unsolubilized pellet (Figure 3.14 A). However, no aggregation is observed in WT, pgrl1, and pgr5 under normal light, but under HL moderate aggregation occurred in WT and pgrl1, however, substantial aggregation was observed in pgr5. The aggregates size increased substantially with an increased in light stress in pgr5 (Figure 3.14 A).

We further confirm the aggregated protein with a western blot to observe the specific proteins in unsoluble fractions. Interestingly, core protein PsaA and D1 and Lhca6 protein accumulated in WT, pgrl1, and pgr5 under stress conditions (Figure 3.14 B). Thus, unsoluble proteins aggregates during HL stress in all the strains. But PsaA accumulated more in pgrl1 and pgr5 mutant than in WT. Aggregation of the D1 Protein was detected during photoinhibition of PSII and heat-inhibition (Yamamoto et al., 2008). A similar report has been observed from Chlamydomonas cells under Fe deficiency (Devadasu et al., 2021). When protein aggregate, the change in protein conformation happens due to misfolded form, and because of that, cells are unable to perform regular photosynthesis. These results support the

previous reports that aggregated proteins in various stress reduced photosynthesis (Yamamoto et al., 2008; Devadasu et al., 2021).



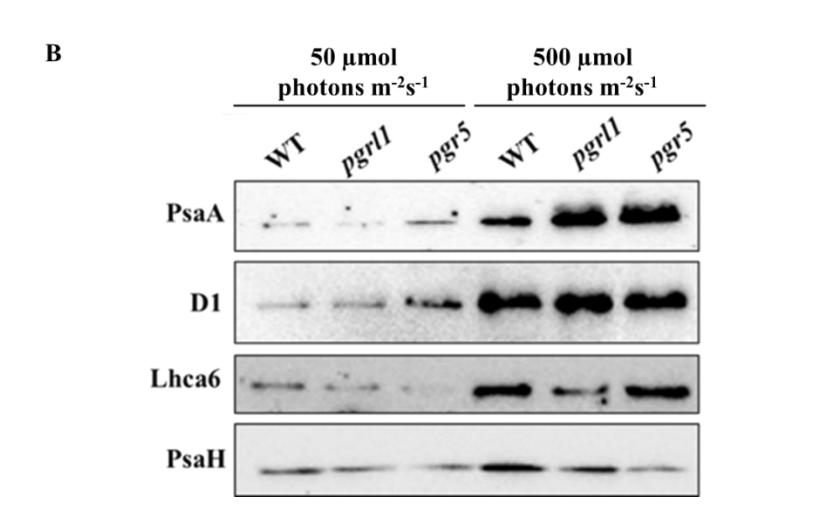


Figure 3.14 Confocal image of aggregated cells and Immunoblots of unsolubilized cells. (A) Confocal images of aggregated cells of WT, pgrl1, and pgr5 mutant under normal (50 μmol photons m^{-2} s^{-1}) and HL (500 μmol photons m^{-2} s^{-1}). Scale bar = 20 μm. (B) Immunoblots of PsaA, D1, and Lhca6 from unsolubilized cells of WT, pgrl1, and pgr5 mutant under normal (50 μmol photons m^{-2} s^{-1}) after solubilization with 0.8 % β-DM. Each data point represents the mean of the three individual experiments (n=3).

3.3 Discussion

Too much light is deleterious to photosynthetic organisms. However, our recent report shows that C. reinhardtii can acclimatize to the HL up to 500 µmol photons m⁻²s⁻¹ in cyclic electron transport mutants (PGRL1 and PGR5) (Yadav et al., 2020). Also, we have reported that NPQ induction is lower, especially in PGR5; therefore, the cyclic electron transport plays a major role in photoprotection. Further, when the WT cells were grown in 1000 µmol photon m⁻²s⁻¹, the efficiency of photosynthesis and their related proteins were significantly changed (Nama et al., 2019). However, the macromolecular level changes of supercomplexes (LHCII, PSII-LHCII, and PSI-LHCI) were not attempted so far in these mutants under HL conditions. Also, the abundance of photoprotective pigments in these macromolecular complexes' organization under HL has not been addressed. Therefore, we have attempted to address the relationship of the photoprotective pigments (carotene and xanthophylls) in macromolecular complexes (LHCII, PSII-LHCII, and PSI-LHCI) isolated from thylakoids of C. reinhardtii (WT, pgrl1, and pgr5) grown under HL. Our recent results addressed that ROS is increased in WT, pgrl1, and pgr5; however, it significantly increases in pgr5. ROS formation trigger over-accumulation of β- carotenoids in the cytosol in *Heamatococus pulvalies* under HL (Mascia et al., 2017). βcarotenoids, lutein, and zeaxanthin accumulated in the excess light condition in many photosynthetic organisms and upregulated the photoprotective mechanism, including NPQ (Kaushik et al., 2014; Nama et al., 2019). Scavenging of ROS and ³Chl yield (Dall'Osto et al., 2012) induced reorganization of the thylakoid membrane and helped increase resistance to excess light conditions.

Xanthophyll is located in light-harvesting antenna complexes in almost all algae and higher plants. It plays a significant role in the photoprotection of light-harvesting in LHC assembly (Jahns and Holzwarth 2012). Under extreme light conditions, zeaxanthin was induced to bind to LHCII by replacing violaxanthin and performing a photoprotective function by

inducing NPQ (Goss et al., 2015). To see the changes in pigment -pigment and pigment-protein interaction, we study pgrl1 and pgr5 mutant at the complexes level, demonstrating HL-induced destabilization of the PSI- LHCI super-complexes compared to other supercomplexes, especially in pgr5 (Figure 3.8). In the case of PSI-LHCI, HL acclimation caused a destabilization of the interaction between peripheral antenna complexes and the PSI core, as demonstrated by 77k (Figure 3.6). Most carotenoids are located in thylakoids and cytoplasmic membranes (Zhang et al., 2015). Carotenoids are found close to the reaction center of PSII and quenches the triplet state of chlorophyll to prevent the formation of free radicals and ROS, which is produced from PSII during the transfer of excitation energy under HL conditions. The photochemical quenching of LHCI proteins decreases due to reduced energy connection between antenna proteins and the PSI reaction center, exposing them to a higher risk of photooxidations (Mascia et al., 2017). In this work, we demonstrated that HL conditions induce destabilization of both PSI-LHCI and PSII-LHCII in WT, pgrl1, and pgr5, which might be due to loss of carotenoids content (Figure 3.11 B-C). HPLC data of cells (Table 3) and thylakoid (Figure 3.10) confirms that Chl b is degraded in WT to inhibit overexcitation of PS, which leads to photoinhibition leading to increasing in Chl a/b ratio (Kouril et al., 2015). However, in pgrl1 and pgr5, there was a decrease in Chl a/b ratio. The amount of β -carotene, lutein, and zeaxanthin increases under HL in WT, which may be responsible for the dissipation of excess energy absorbed by Chls through Chl-Car interactions (Ruban et al., 2012). We reported recently that HL induces NPQ in WT but is reduced in these mutants where the NO was increased (Yadav et al., 2020). Therefore, increased β-carotene, lutein, and zeaxanthin emphasize that the WT can acclimatize to the HL through the NPQ mechanism. Our HPLC data of the cells (Table 3.3) and thylakoids (Figure 3.10) show a similar expression trend of carotenoids/xanthophyll pigment compositions. The carotenoid content was high in WT and pgrl1 under HL; however, there was not much effect observed in the pgr5. These carotenoids

might be compensated by a slight increase of other carotenoids that were not measured; instead, they decreased under HL conditions except for lutein which increased. Also, genes responsible for converting α -carotene to lutein and β - carotene to zeaxanthin were also transcriptionally enhanced under light stress in WT, pgrl1, and pgr5, but in pgr5 mutant β - carotene to zeaxanthin was downregulated under light stress (Figure 3.12). This supports our pigment content data where zeaxanthin was downregulated. In thylakoids, we have seen almost the same xanthophyll pigments in WT and pgrl1, but the trend is slightly different in the pgr5 mutant, which increases lutein content (Figure 3.10). This could be the reason the pgr5 is more sensitive to HL, where usually one of the carotenoids pigments increases to protect against HL.

Pigment binding properties of different isolated fractions LHCII(F1), PSII-LHCII(F2), and PSI-LHCI (F3) show that zeaxanthin was present in all the fractions as it was already said zeaxanthin was present in LHC proteins (Bassi et al., 1993). Comparing the zeaxanthin distribution among WT and mutant with HL samples, we have observed enrichment in LHCII and PSII-LHCII fractions (Figure 3.11). We followed the zeaxanthin enrichment level in the F1 fraction compared to other fractions (F1>F2>F3). Our immunoblot data of the fraction (Figure 3.13 A) was enriched in LHCSR3 protein under HL in WT and pgrl1 mutant. The zeaxanthin expression was not prominent in pgr5 mutant under stress conditions, thus suggesting zeaxanthin might be a ligand for LHCSR as previously reported (Pinnola et al., 2013). An increase in lutein content in pgr5 might be the reason for protecting LHCII from photodamage in pgr5 (Figure 3.11B). Since pgr5 does not have LHCSR3 expression, therefore, no zeaxanthin expression was observed in pgr5.

In PSII, carotenoid plays an essential role in deactivating 3 Chl* and 1 O₂ and reducing ROS formation due to thermal dissipation of excess light energy. Activation of β -carotene was triggered by oxidative stress and ROS accumulation in the chloroplast, followed by export into the cytosol. Rapid turnover of the PSII core subunits, D1 is likely to be the reason for the rapid

destabilization observed for F2 fractions in pgrl1 and pgr5. In the PSII core complex, β -carotene is in close contact with Chl and is required for quenching of 3 Chl* and 1 O₂; therefore, depletion of β -carotene will produce photooxidation of PSII and PSI core complexes (Pineau et al., 2001; Cazzaniga et al., 2012). CD data witnessed drastically decreased intensity at 400 to 500 nm wavelength under intense light (Figure 3.8), indicating pigment-protein interaction changes. The 77 k emission spectra data confirm that PSI was damaged under HL conditions in pgr5 (Figure 3.5 & 3.6). Lutein content decrease under HL in WT strains. PSI-LHCI is far more sensitive in pgrl1 and pgr5 under HL, as reported (Yadav et al., 2020). Thus, the HL effect on PSI-LHCI might be due to a reduced amount of carotenoid associated with the supercomplex, which leads to less quenching of 3 Chl.

ROS are responsible for the photoinactivation of PSII (Nishiyama et al., 2005) and light-induced damage to the D1 protein during acceptor-side photoinhibition (Jegerschoeld et al., 1990). We also observed ROS accumulation under HL in all the strains; however, significant accumulation was observed in *pgr5*. The accumulation of ROS may lead to the aggregation of both PSII and PSI proteins (Figure 3.14 A-B). In higher plants, it was also observed that the PSII proteins were aggregated due to ROS (Yamamoto et al., 2008). Usually, misfolded proteins are cross-linked with the surrounding proteins, which reduces their expression, as shown in immunoblot of SDG fractions (Figure 3.13 A-B).

Consequently, protein aggregation is one of the primary processes to indulge the photochemical reactions. As a result, a change in energy transfer and thylakoid organization was observed in *pgrl1* and *pgr5* under HL. This destabilization of the supercomplex occurs due to protein aggregation under HL conditions. Therefore, protein misfolding leads to several changes like alteration of macro-aggregation, photosynthesis efficiency, macromolecular structure, etc., in photosynthetic complexes.

3.4 Conclusion

Here, we reported the differential components of carotene and xanthophylls present in various organizations of thylakoids supercomplexes/mega complexes of C. reinhardtii WT, pgrl1, and pgr5 mutant under HL. Carotenes (β-Carotene) and xanthophylls (violaxanthin and lutein) are structural elements of the photosynthetic apparatus and contribute to increasing both the lightharvesting and photoprotective capacity of the PS. β-Carotene is present in both the core and light-harvesting complexes (LHCII and LHCI), while xanthophylls, lutein, and violaxanthin bind exclusively to its antenna moiety; another xanthophyll, zeaxanthin, which protects chloroplasts against photooxidative damage, binds to the LHC complexes under HL stress. The β-carotene, lutein, and zeaxanthin increased in WT and pgrl1 under HL, whereas the zeaxanthin content is decreased in pgr5. The increased zeaxanthin corresponds to the dissipation of excess energy absorbed by Chls through Chl-Car interactions responsible for high NPQ. As expected, the amount of zeaxanthin and LHCSR3 protein content was more abundant in LHCII complexes than in two other supercomplexes (PSII-LHCII and PSI-LHCI) from WT and pgrl1. Further, the β - carotenoid reduces significantly in WT and pgrl1, whereas an increase in β- carotenoid was noticed in pgr5 from PSI-LHCI complexes; however, more accumulation of lutein was observed in PSII-LHCII complexes. Similarly, the genes involved in carotenoids biosynthesis and their respective genes' expression are in line with the pigment content.

The pigment-pigment and pigment-protein interactions were changed due to the differential expression of pigments with supercomplexes. Since an increase in zeaxanthin could lead to a change in protein conformation, it is evident that LHCII trimer conformation is significantly modified than other supercomplexes. Furthermore, we also observed that protein aggregation of core proteins, especially in pgr5, could change the differential expression of pigments in HL conditions. Therefore, the lack of zeaxanthin/LHCSR3 content and differential

expressions of other pigments (lutein and violaxanthin) induced change in the macromolecular organization of thylakoid supercomplexes, which ultimately involved in photoprotection.

Chapter 4

Investigation of autophagy induced lipid accumulation under the high light-grown cells of *pgrl1* and *pgr5*



4.1 Introduction

Light is vital for microalgae for efficient photosynthesis. CO₂ fixation by the CBB cycle occurs through photosynthesis that primarily synthesizes carbohydrates, leading to the synthesis of lipid stored as TAG (Mondal et al., 2017). Microalgal species do not accumulate increased amounts of neutral lipids under normal growth conditions. Neutral lipid is accumulated under unfavorable conditions like nutrient, light, salt, and temperature stresses. Under normal light conditions, the rate of light absorbed is equal to the pace of photosynthesis, but when light intensity increases, the system cannot tolerate over-excitation. In this condition, the primary by-product of photosynthesis formed as ROS, which regulate the autophagy mechanism. Autophagy is a stress-responsive mechanism that can induce organelle deterioration (Liu and Bassham, 2012). This mechanism in C. reinhardtii regulates the degradative process in photosynthetic organisms. Autophagy plays a divulged role in the control of lipid metabolism. Inhibition of Target of Rapamycin (TOR) kinase by treatment of C. reinhardtii cells with rapamycin resulted in increased ATG8 lipidation (Pérez-Pérez et al., 2010a) and vacuolization (Pérez-Pérez et al., 2010b). Previous results have proven that ROS is an inducer of autophagy in algae (Pérez-Pérez et al., 2010a). HL stress induces photo-oxidative damage due to ROS production, leading to autophagy activation in C. reinhardtii (Pérez-Pérez et al., 2010b). A recent report has shown that a starchless mutant of C. reinhardtii induces oxidative stress, triggering autophagy, and leading to TAG accumulation under nitrogen starvation (Pérez-Pérez et al., 2012). In a group of ATG (autophagy-related) proteins, the accumulation of ATG8 and ATG3 increased in a conditional repression line of a chloroplast protease (ClpP1), suggesting the chloroplast proteolysis systems and autophagy partially complement each other in C. reinhardtii (Ramundo et al., 2014). Additionally, these proteins were shown a similar function to that of other organisms (Pérez- Pérez et al., 2010; Pérez- Pérez et al., 2016). Loss of cytoplasmic structure with a significant increase in the volume occupied by lytic vacuoles and

discharge of vacuole hydrolases can be assigned as autophagic cell death markers (Van Doorn, 2011). However, the mechanism of autophagy caused by HL stress in C. reinhardtii is poorly understood. Additionally, it can achieve neutral lipid accumulation by exposing the cells to unfavorable conditions, such as removing the nutrients like nitrogen, sulfur, iron, or phosphate, or changing salinity and temperature (Alishah Aratboni et al., 2019). Most of the knowledge on TAG metabolism in C. reinhardtii has been gained from the N starvation (Siaut et al., 2011; Abida et al., 2015). Recent studies showed that cells exposed to small chemically active compounds could also accumulate TAG in C. reinhardtii (Wase et al., 2019). However, an increase in light intensity influences the microalgal lipid production in Scenedesmus at 6,000 lux (Mandotra et al., 2016), as well as *Nannochloropsis sp* at 700 µE m⁻² s⁻¹ (Pal et al., 2011) and Botryococcus sp. at 6,000 lux (Yeesang and Cheirsilp, 2011). Further, Haematococcus pluvialis (Zhekisheva et al., 2002), Tichocarpus crinitus (Khotimchenko and Yakovleva, 2005), and Synechocystis sp. (Cuellar-Bermudez et al., 2015) also showed an increased neutral lipid content under HL conditions. Lipid bodies are synthesized in algal chloroplast by fatty acid synthase complex. These newly synthesized free fatty acids are translocated to the ER, where they convert G3P to DAG through various enzymes. DAG is converted to triacylglycerol by the DGAT enzyme. So, the enzyme is considered to reinforce the assembly of lipids in microalgae. DGAT enzyme catalyzes the ultimate step of TAG synthesis pathway's, and PDAT also helps accumulate TAG. However, it does not hook into the acyl CoA pathway. Here, PDAT transfers carboxylic acid moiety from a phospholipid to DAG to make TAG (Sorger and Daum, 2002; Shockey et al., 2006). A recent report from our group shows that a significant accumulation of TAG was observed under severe iron deficiency, and this could have been obtained from degraded chloroplast lipids through the DGAT enzyme (Devadasu et al., 2021).

Few studies have focused on increased fatty acid content, decreased photosynthetic activity, and retarded biomass, ultimately inhibiting microalgae growth in nutrient limitation.

A pgrl1 is required for efficient CET and ATP supply for efficient photosynthesis (Tolleter et al., 2011; Leister and Shikanai, 2013; Shikanai, 2014; Steinbeck et al., 2015). A pgr5 mutant has been characterized in C. reinhardtii (Johnson et al., 2014), which revealed that pgr5 deficiency results in a diminished proton gradient across the thylakoid membrane accompanied by less effective CET capacity. The CET pathway has been suggested to provide ATP for lipid production during N starvation in C. reinhardtii mutants impaired in pgrl1, which accumulates significantly fewer neutral lipids. However, under the HL condition, there is an increase in oil content after the 3rd day. So far, the accumulation of lipids has been well characterized by nutrient stress; however, not many studies are available under HL conditions. In C. reinhardtii (WT) the solar light is transformed into chemical energy using linear electron transport. However, pgrl1 and pgr5 may show an increase in stromal redox poise that would cause an increase in lipid production under strong light. In this study model, algae C. reinhardtii was propagated with different light conditions (50 and 500 µmol photons m⁻²s⁻¹) to realize insights into the autophagy and lipid accumulation response to HL. We propose that C. reinhardtii cell's exposure to HL resulted in ROS accumulation, which induced autophagy and lipid accumulation in pgr5.

4.2 Results

4.2.1 Cellular localization of ATG8

We have used an anti-ATG8 antibody to examine this protein's cellular localization in immunofluorescence microscopy (Figure 4.1A). Autophagy (ATG)8 proteins localize as small red dots in the cytoplasm under the normal light condition in WT, pgrl1, and pgr5. However, under HL conditions, the number of spots significantly increased in pgr5 (40%), which shows activation of autophagy and formation of autophagosomes in close agreement with the high accumulation of ATG8 [phosphatidylethanolamine (PE) modified ATG8] detected by western

blotting. The autophagy-related protein ATG8-PE was significantly expressed in *pgr5* in HL conditions (Figure 4.1 B &C). Upon autophagy activation, ATG8 binds to the autophagosome membrane through phospholipid PE to form ATG8-PE in a process called lipidation.

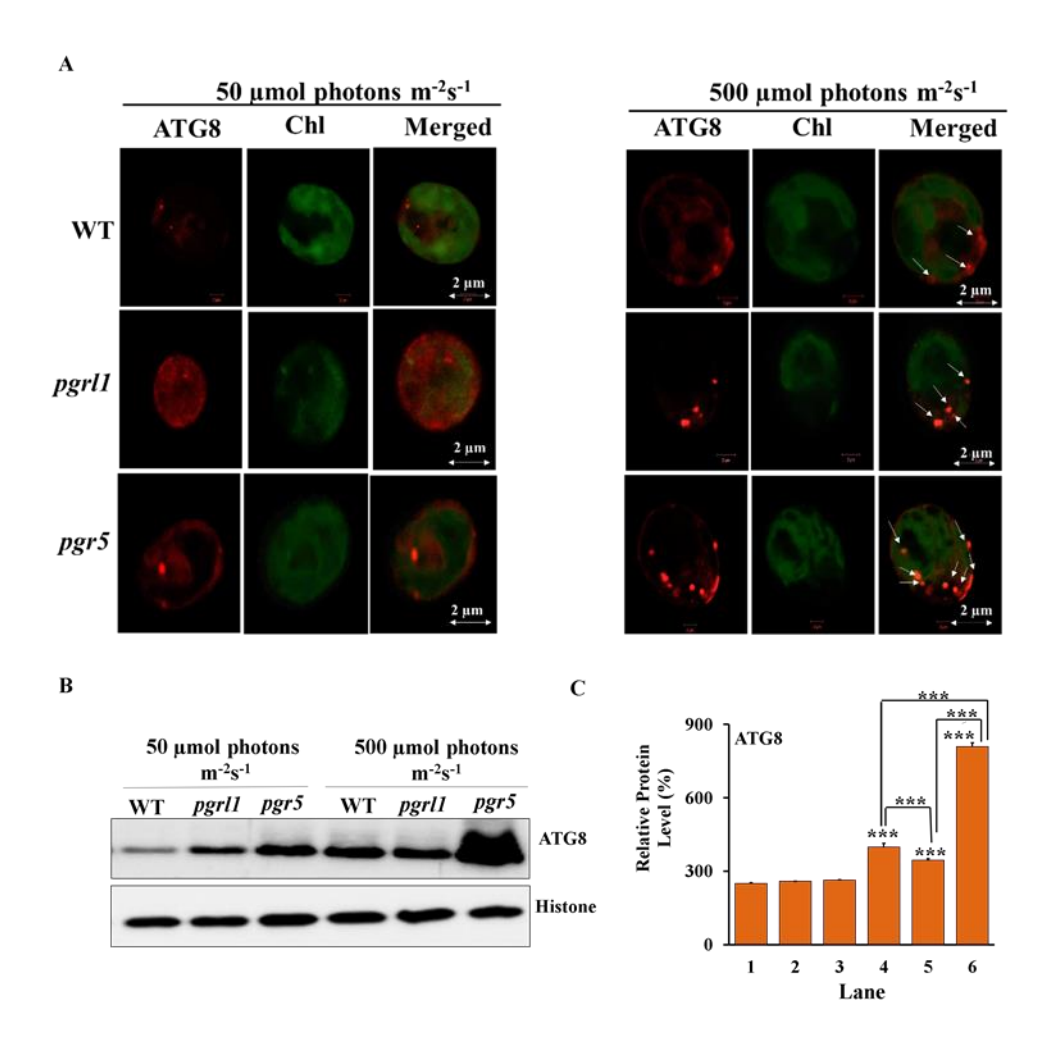


Figure 4.1 Autophagy (ATG)8 accumulation in C. reinhardtii cells under high light conditions. (A) Autophagy induction in C. reinhardtii cells collected at phase cells (3.0×10^6 cells) grown in tris-acetate phosphate (TAP) medium under continuous light of 50 and 500 µmol photons m² s⁻¹. Samples were collected after 3rd day and immunoassay with anti-ATG8 antibody (in red). Chloroplasts were visualized by auto-fluorescence (in green). The images were collected with three individual measurements for all the conditions (n = 3). The image was taken using a Zeiss confocal microscope. Scale bars = 2 µm. (B) Protein identification by western blot. Western blot analysis of ATG8 evaluated from 3rd-day cells under the normal ($50 \text{ }\mu$ mol photons m⁻² s⁻¹) and HL ($500 \text{ }\mu$ mol photons m⁻² s⁻¹) condition, and in each lane 5 µg protein were loaded. Autophagy (ATG)8-PE protein was resolved on 15% Bis-Tris gel in denaturing conditions. Histone (H3) was used as a loading control. All the blots were conducted in three independent experiments (n = 3) and obtained similar results. (C) Quantification of the immunoblots was done by ImageJ. The measurements were repeated with three individual cultures, and error bars represented the mean \pm SD (n = 3). Statistical significance was analyzed using one-way ANOVA with the Tukey test and the p-value obtained is indicated (***p < 0.001).

Hence autophagy may play a significant role in the accumulation of lipids in HL in *pgr5*. Therefore, in line with autophagy, the accumulation of lipids is lower in WT and *pgrl1*. However, the ATG8 expression is predominant in *pgr5* under HL. These results suggested that induction of ROS due to HL may induce autophagy in *pgr5* than WT and *pgrl1* (Pérez-Pérez et al., 2012; Perez-Martin et al., 2014). Therefore, it may trigger the lipid metabolism in *C. reinhardtii* cells.

4.2.2 Lipid droplet analysis from confocal microscopy

We have stained the cells with NR for lipid studies, which binds explicitly to lipid bodies in the cell and gives a characteristic yellow-orange fluorescence. Our results clearly show the overall increase of lipid droplets under HL in WT, pgrl1, and pgr5 (Figure 4.2 A & B). When we measure the fluorescence intensity from the confocal images, the number of lipid spots is higher in HL-grown cells, but it is more significant in pgr5 (Figure 4.2 C). However, autofluorescence due to chlorophyll was less in pgrl1 and pgr5 than in control, indicating decreased chlorophyll content under HL, even though cells had a significant accumulation of lipid bodies (Figure 4.2 A). Lipid accumulation was observed in all strains under HL conditions (Goold et al., 2016). However, lipid accumulation is more significant in pgr5 (60 %) than in other strains under HL. We have tested NR fluorescence from fluorescent activated cell sorter (FACS) to assess the lipid accumulation in HL conditions. We obtained 2-fold higher mean fluorescence intensity from all the strains with HL than in normal growth conditions (Figure 4.2 D).

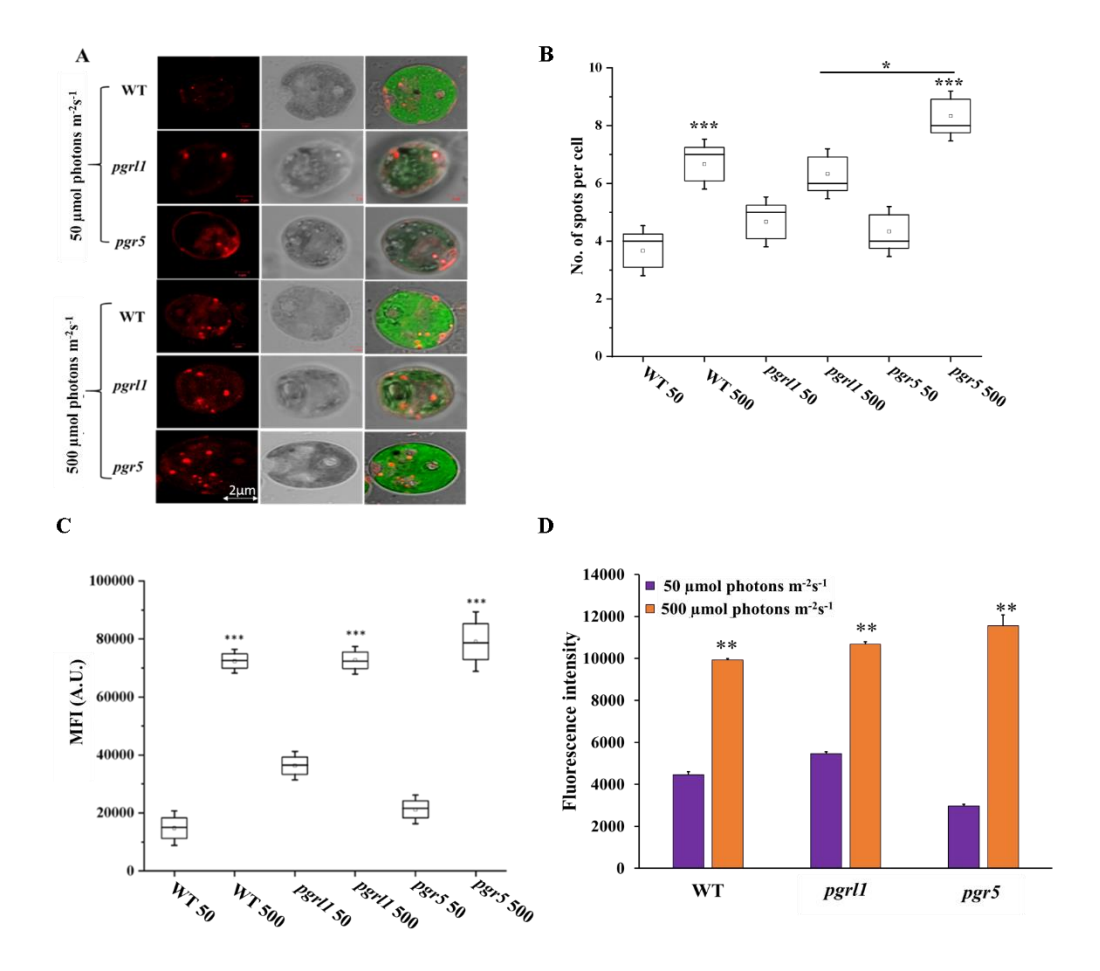


Figure.4.2 Lipid droplets were identified through confocal microscopy and FACS analysis. (A) Cells were grown under normal (50 μ mol photons m⁻² s⁻¹) and HL (500 μ mol photons m⁻² s⁻¹)conditions and were stained with Nile Red (5 μM/mL) for lipid droplets in C. reinhardtii strains, WT, pgrl1, and pgr5. The images were collected with three individual measurements for all the conditions. Bars = 2 μm. (B) Quantification of number (quantification was performed from a single cell with three individual cultures) and (C) fluorescence intensity of lipid droplets as shown. Box plots indicate the medians, means, and quartiles. Statistical significance was analyzed using one-way ANOVA with the Tukey test, and the p-value obtained is indicated (***p < 0.001, *p < 0.05). Bars = 2 μ m. (D) Fluorescent activated cell sorter (FACS) analysis was carried out for lipid accumulation with BD Fortessa, United States. WT, pgrl1 and pgr5 50; WT, pgrl1 and pgr5 500, represent 50 and 500 µmol photons m⁻²s⁻¹. All the measurements were done with the PE-A filter. The analysis showed mean fluorescence values to compare light conditions of normal (50 μmol photons m⁻² s⁻¹) and HL (500 μmol photons m⁻² s⁻¹). An unstained condition was kept to minimize the chlorophyll autofluorescence from cells. Cells were stained with Nile Red (NR), and measurements were done after incubated for 20 min under dark at room temperature (RT). The measurements were repeated with three individual cultures, and error bars represented the mean \pm SD (n = 3). Statistical significance was analyzed using one-way ANOVA with the Tukey test and the p-value obtained are indicated (***p < 0.001, **p < 0.05). Bars = 2

4.2.3 Neutral lipid identification by NR fluorescence

The neutral lipids were semi-quantified by using NR fluorescence from an equal number of cells. NR fluorescence results show that the neutral lipid level was increased with equal cell density. NR fluorescence of *C. reinhardtii* cells WT, *pgrl1*, and *pgr5* were calculated every 24 h while growing them in light at 50 and 500 µmol photon m⁻² s⁻¹ (Figure 4.3). After 24 h, cells did not cause any change in total lipid content. However, after 48 h of HL growth, there was an increase in NR fluorescence. In contrast, there is an increase in signal at 750 nm. Overall, HL-grown cells exhibit a relative 2-fold increase in neutral lipid content over 3–4 days. However, this accumulation of neutral lipids is predominantly more in the *pgr5* mutant when compared to other strains. Therefore, our results indicate that an increase in light intensity facilitates the production of neutral lipids in *C. reinhardtii*. Further, we have performed electron microscopic studies to determine whether HL induces lipid accumulation in the cells.

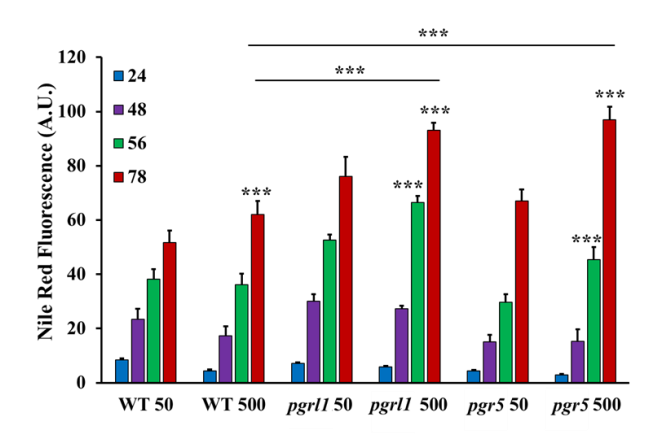


Figure 4.3 Neutral lipid content is quantified from the cells grown under normal and HL. Neutral lipid content was qualitatively measured with NR fluorescence from the cells WT, pgrl1, and pgr5 grown with normal (50 μ mol photons m⁻² S⁻¹) and HL (500 μ mol photons m⁻² S⁻¹) conditions stained with NR on days 1–4. The measurements have been done with a microplate reader. Three biological experiments were done (n = 3). In 'x-axis WT, pgrl1 and pgr5 50; WT, pgrl1 and pgr5 500, represents 50 and 500 μ mol photons m⁻² s⁻¹. Statistical significance was analyzed using one-way ANOVA, and subsequent Tukey's post hoc t-test and p-value obtained are indicated (****p < 0.001).

4.2.4 Neutral lipid and membrane lipid analysis by thin layer chromatography

To observe the overall change in lipid content caused by HL, we prepared a neutral lipid extract from equal DW of WT, *pgrl1*, and *pgr5* cells under normal and HL. Further, the TAG was separated on thin-layer chromatography (TLC) plates from the 3rd day of culture showed an accumulation of TAG content that was increased significantly under HL conditions, especially in *pgr5* (Figure 4.4 A). There is more TAG accumulation in the *pgr5* mutant, which could have been obtained from the reduced membrane lipids. This supports the electron microscopic data that the stacks of thylakoids disturbed, which could be a change in membrane lipids. It is already proven that a decrease in MGDG usually accelerates TAG under stress conditions (Figure 4.4 B). A drastic decrease in MGDG content occurs during freezing or ozone treatment (Li et al., 2008). Our group recently reported that TAG accumulation originated from the degradation of MGDG under Fe deficiency from C. *reinhardtii* (Devadasu et al., 2019, Devadasu and Subramanayam, 2021).

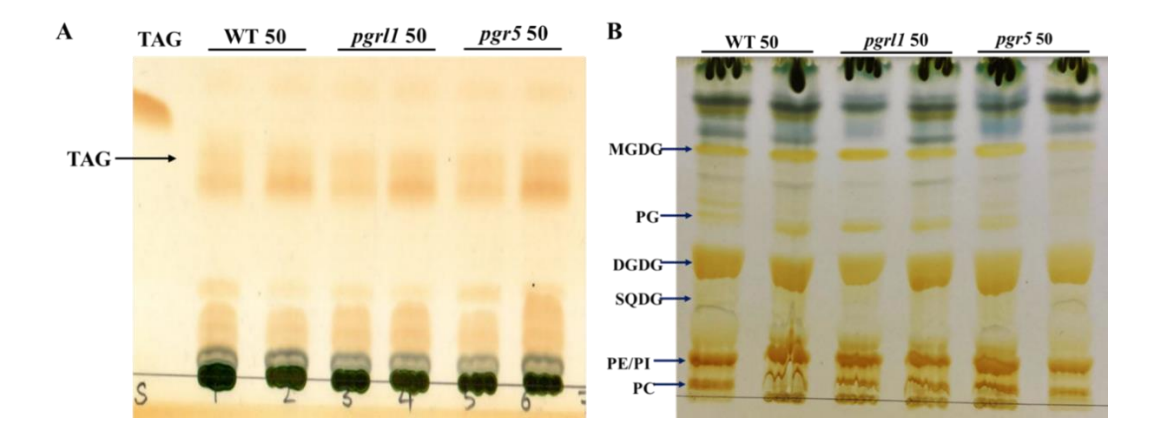


Figure 4.4 Alteration of membrane lipid and TAG in C. reinhardtii cells grown under normal and HL conditions. (A) TLC analysis showing TAG accumulation of C. reinhardtii cells WT and mutants pgrl1 and pgr5 under 50 μ mol photons m^{-2} s⁻¹ and 500 μ mol photons m^{-2} s⁻¹. Three independent experiments were conducted for all samples (n=3). (B) Separation of polar lipids by TLC from C. reinhardtii strains WT, pgrl1, and pgr5 under 50 μ mol photons m^{-2} s⁻¹ and 500 μ mol photons m^{-2} s⁻¹. Polar lipids and TAG was visualized by iodine staining. Three independent experiments were conducted for all samples (n=3). WT, pgrl1 and pgr5 50, WT, pgrl1, and pgr5 500, represent 50 and 500 μ mol photons m^{-2} s⁻¹. TAG, triacylglycerol. DGDG, digalactosyldiacylglycerol; MGDG, monogalactosyldiacylglycerol; PC, phosphatidylcholine; PE, phosphatidylethanolamine; PG, phosphatidylglycerol; PI, phosphatidylinositol; SQDG, sulfoquinovosyldiacylglycerol.

We detected TAG accumulation in *C. reinhardtii* under HL, accompanied by substantial chloroplast membrane lipid degradation in *pgrl1* and *pgr5*. Thus fatty acids from the chloroplasts and other intracellular membrane systems may have converted into TAG. Further, we have performed electron microscopic studies to determine whether HL induces lipid accumulation in the cells.

4.2.5 Transmission electron microscopy studies

To see the clear lipid vacuoles in the cell, we have carried out transmission electron microscopy (TEM). It reveals that *pgrl1* and *pgr5* exhibit a large cytoplasmic vesicle under HL-grown cells (Figure 4.5). It showed that the membrane structure is aberrant under HL, especially in the *pgrl1* and *pgr5*. The majority of the thylakoid membranes were loosened in HL-grown cells. While in the WT cells, the thylakoid membranes are arranged as layers (stacked) in the chloroplast, with some membrane appressed.

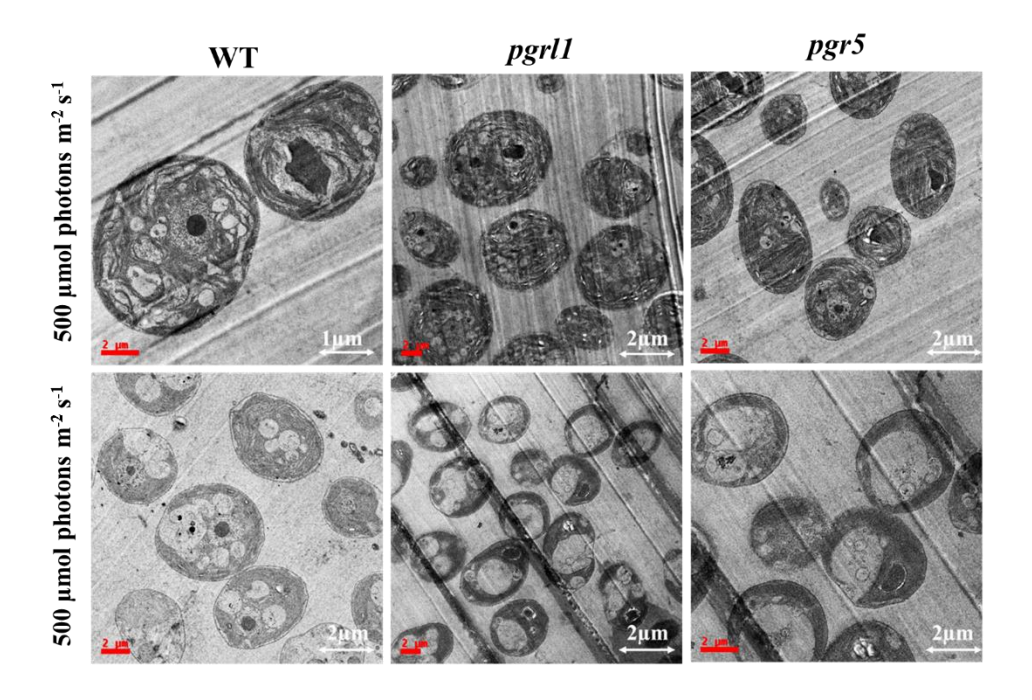


Figure 4.5. Ultrastructure analysis of C. reinhardtii cells during normal (50 μ mol photons m^{-2} s⁻¹) and HL (500 μ mol photons m^{-2} s⁻¹). Transmission electron micrographs of C. reinhardtii cells WT and mutants pgrl1 and pgr5 grown under photoheterotrophic conditions under 50 μ mol photons m^{-2} s⁻¹ and 500 μ mol photons m^{-2} s⁻¹. Representative images were taken after the 3rd day of growth. Three independent experiments were conducted from each sample (n=3).

Recently we reported that photosynthetic efficiency is reduced under the HL condition in WT, pgrl1, and pgr5, which may be due to a change in chloroplast structure (Yadav et al., 2020). Such phenotype raised the question that mutant strains are defective in generating the functional membrane under HL conditions. The earlier report emphasized that autophagic bodies accumulate in plant cell vacuoles under concanamycin A treatment since vacuolar hydrolase cannot act (Thompson et al., 2005). However, in our case, under HL conditions, we have observed a high degree of vacuolization and an increase in vacuole size in mutants (Figure 4.6). It was also reported that vacuole lytic function is needed to synthesize TAG and lipid bodies in *C. reinhardtii* cells when subjected to light stress (Couso et al., 2018).

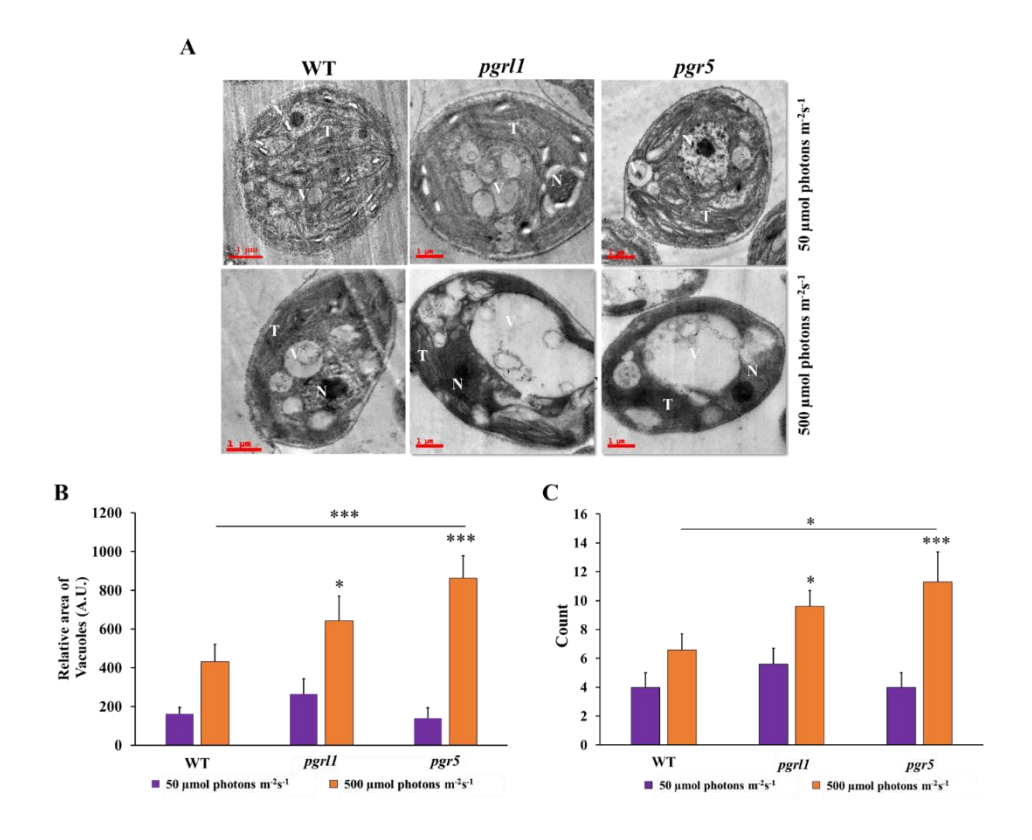


Figure 4.6 Ultrastructure analysis of Chlamydomonas cells during normal (50 μ mol photons m^{-2} s^{-1}) and HL (500 μ mol photons m^{-2} s^{-1}). (A) Transmission electron micrographs of C. reinhardtii cells WT and mutants pgrl1 and pgr5 grown under photoheterotrophic conditions under normal (50 μ mol photons m^{-2} s^{-1}) and HL (500 μ mol photons m^{-2} s^{-1}). Representative images for the cells sampled after the 3^{rd} day, N-nucleus; O, T-thylakoid membranes; V-vacuole. Three independent experiments were conducted from each sample (n = 3). Scale bar = 1 μ m. (B) Quantification of area vacuoles. (C) The number of vacuoles. Quantification and number of vacuoles were performed from a single cell with three independent cultures. Statistical significance was analyzed using one-way ANOVA with the Tukey test and the p-value obtained is indicated (***p < 0.001, *p < 0.05).

4.2.6 Carbohydrate assay

Carbohydrate is a polysaccharide, and it is the storage form of sugars and starch in plants/algae. We quantified the carbohydrate content in WT, pgrl1, and pgr5 in normal and HL conditions. The carbohydrate content of WT and pgrl1 was increased significantly under the HL condition. The carbohydrate content was cross-checked with a starchless mutant (sta6) under normal light and HL. It shows about 8 μ g of carbohydrate/10⁶ cells in normal and HL conditions (Figure 4.7) as measured with the anthrone reagent, which estimates starch and soluble sugars. Overall, our reports indicate that carbohydrate content has increased under the HL condition in WT and pgrl1. However, it reduced in pgr5 mutant under HL. Microalgae change their metabolism and convert excess energy into an energy-rich products such as lipid, starch, carbohydrate, or proteins under unfavorable conditions (Heredia-Arroyo et al., 2010).

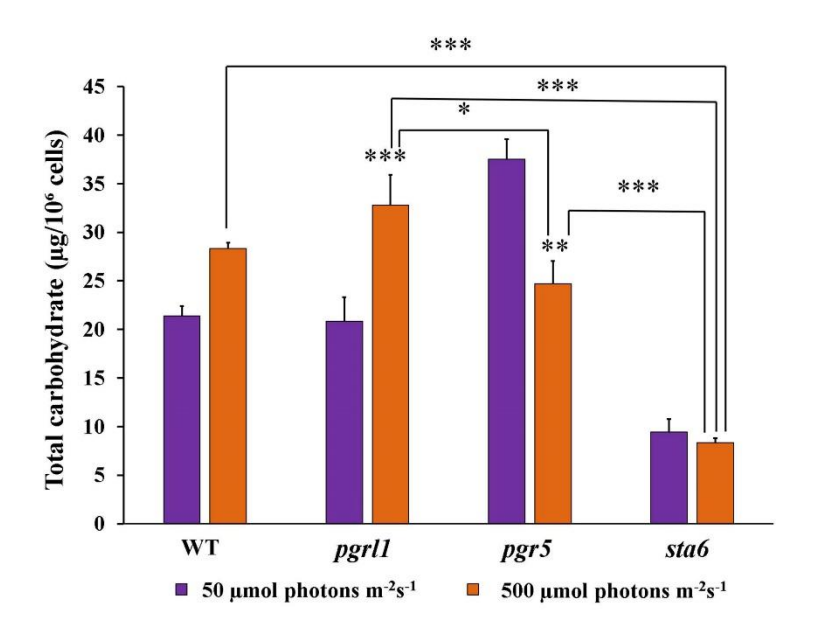


Figure 4.7 Total carbohydrate content was quantified by the Anthrone method from the cells grown under normal to high light conditions. Cells were collected at the mid-log phase from normal (50 μ mol photons m-2 s-1) and HL (500 μ mol photons m-2 s-1) conditions. The color was measured with spectrophotometry at 620 nm. Three biological experiments were done (n = 3), and error bars represent the mean \pm SD (n = 4). Statistical significance was analyzed using one-way ANOVA with the Tukey test and the p-value obtained are indicated (***p < 0.001, **p < 0.01, *p < 0.05).

However, *pgr5* may have an altered NADPH and ATP ratio during photosynthesis, switching metabolic pathways that lead to lipid accumulation. These results indicate that HL induces the lipid pathways due to more energy equivalents in the *pgr5* mutant. Further, we have tested the protein/enzyme of the lipid pathway under all the conditions.

4.2.7 Protein analysis by immunoblot

We have focused on the enzymes involved in the TAG synthesis known as the Kennedy pathway. This pathway is mainly catalyzed by the acylation of DAGs by DGAT, in which acyl-CoA is a substrate to form TAG. Acylation of DAGs by PDAT1 enzyme is the acyl-CoA independent pathway in the ER. To determine the involvement of PDAT and DGAT in HL response in *C. reinhardtii* and their protein level regulation was calculated (Figures 4.8A–C). The PDAT and DGAT were transiently upregulated in response to HL conditions. Protein expression was increased after the 3rd day, specifically in pgr5 expression of PDAT compared to pgrl1 (Figure 4.8). Our results confirm an increase in TAG in pgrl1 and pgr5 due to the enhanced content of PDAT and DGAT enzymes. Further, we have focused on the enzymes involved in the TAG synthesis known as the Kennedy pathway. This pathway is mainly catalyzed by the acylation of DAGs by DGAT, in which acyl-CoA is a substrate to form TAG. Acylation of DAGs by PDAT1 enzyme is the acyl-CoA independent pathway in the ER. To determine the involvement of PDAT and DGAT in HL response in C. reinhardtii and their protein level regulation was calculated (Figure 4.8 C&D). The PDAT and DGAT were transiently upregulated in response to HL conditions. Protein expression was increased after the 3rd day, specifically in pgr5 expression of PDAT compared to pgrl1 (Figure 4.8 B). Our results confirm an increase in TAG in pgrl1 and pgr5 due to the increase of PDAT and DGAT enzymes.

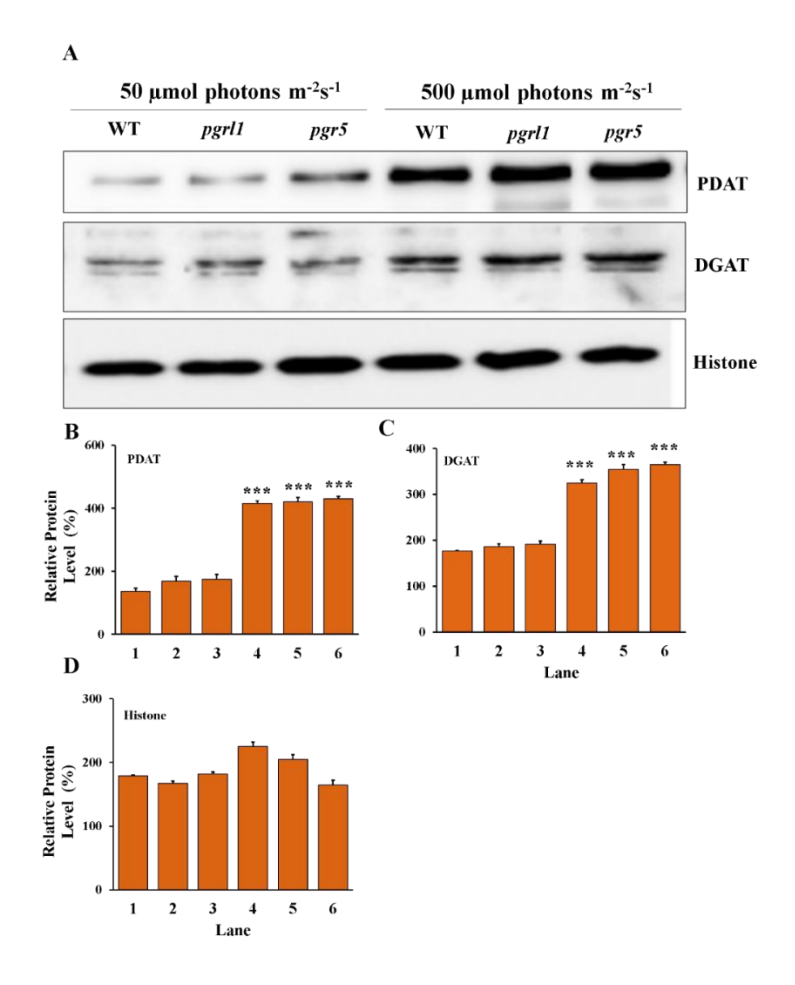


Figure 4.8 Protein identification from western blot analysis. (A) The proteins were separated by denaturing gel electrophoresis, transferred to nitrocellulose membranes, and probed for the indicated proteins. Western blot analysis of Acyl-CoA: diacylglycerol acyltransferase (DGAT2A) and phospholipid diacylglycerol acyl-transference (PDAT1) evaluated from 3rd-day cells under the normal (50 μ mol photons m^{-2} s⁻¹) and HL (500 μ mol photons m^{-2} s⁻¹) condition, and each lane (5 μ g) protein were loaded on to 10% Bis-Tris gel in denaturing condition. Histone (H3) was used as a loading control. All the blots were in three independent times (n = 3) and obtained similar results. (B) Quantification of the immunoblots of PDAT, (C) DGAT, and (D) histone. Data are expressed as mean \pm SD of 3 replicates. Statistical significance was analyzed using one-way ANOVA with Tukey test and p-value obtained are indicated (***p < 0.001).

4.2.8 Fatty acid composition under HL condition

Liquid chromatography/mass spectrometry (LC/MS) was used to analyze the fatty acids transesterification and the resultant fatty acid methyl esters (FAMEs) from WT, *pgrl1*, and *pgr5* under normal and HL (Table 4.1). Different compositions of fatty acids are observed in the HL grown *C. reinhardtii*. There was an increase in C16:1, C16:2 C16:3, C18:0, C18:1, and C18:3 in *pgrl1* and *pgr5* mutant under HL. We recently observed increasing total fatty acids in severe Fe deficiency from *C. reinhardtii* (Devadasu et al., 2019; Devadasu and Subramanyam,

2021). In our case also the total fatty acid content is significantly increased in pgrl1 and pgr5 mutant

Fatty acid	WT (50 μmol	WT (500 μmol	pgri1 (50 μmol	pgri1 (500μmol	pg r5 (50 μmol	pgr5 (500 μmol
	photonm ⁻² s ⁻¹)					
	% ± S.D.	% ± S.D.	% ± S.D.	%±S.D.	% ± S.D.	% ± S.D.
C14:0	0.237 ± 0.003	0.546 ± 0.004	0.185 ± 0.001	0.176 ± 0.001	0.594 ± 0.003	0.609 ±0.003
C14:1	0.182 ± 0.002	0.589 ± 0.005	0.42 3 ± 0.002	0.154 ± 0.001	0.329 ± 0.002	0.508 ± 0.003
C14:2	0.296 ± 0.003	0.767 ± 0.003	0.423 ±.0002	0.132 ± 0.001	0.632 ± 0.003	0.406 ± 0.002
C14:3	0.123 ± 0.002	0.412 ±. 0003	0.318 ± 0.002	0.64 ± 0.003	0.228 ± 0.001	0.216 ± 0.001
C16:0	1.182 ± 0.002	1.412 ± 0.003	2.123 ± 0.007	3.415 ± 0.007	3.45 ± 0.005	7.132 ± 0.006
C16:1	1.070 ± 0.006	2.391 ± 0.021	1.874 ± 0.004	4.178 ± 0.006	2.212 ± 0.003	4.398 ± 0.001
C16:2	0.192 ± 0.002	1.764 ± 0.004	0.36 ± 0.002	2.544 ± 0.003	0.573 ± 0.003	5.027 ± 0.005
C16:3	1.213 ± 0.019	4.76 ± 0.008	1.816 ± 0.009	2.78 ± 0.014	2.1 ± 0.010	3.13 ± 0.016
C18:0	0.499 ± 0.002	1.12 ± 0.004	1.659 ± 0.008	2.061 ± 0.012	1.025 ± 0.005	3.752 ± 0.007
C18:1	0.168 ± 0.001	0.942 ± 0.003	0.439 ± 0.002	1.998 ± 0.004	0.826 ± 0.004	5.46 ± 0.012
C18:2	0.427 ± 0.002	0.200 ± 0.001	0.651 ± 0.003	0.212 ± 0.001	0.199 ± 0.003	1.15 ± 0.003
C18:3	3.124 ± 0.018	7.200 ± 0.029	2.725 ± 0.029	5.895 ± 0.014	5.738 ± 0.109	7.266 ± 0.046
C18:4	1.21 ± 0.005	2.56 ± 0.019	2.114 ± 0.011	1.23 ± 0.006	3.161 ± 0.04	3.395 ± 0.017
MUFA	1.42 ± 0.007	3.92± 0.008	2.736 ± 0.027	5.33 ± 0.019	3.367 ±.011	10.366 ± 0.025
PUFAb	4.192 ± 0.051	17.46 ± 0.059	8.407 ± 0.203	12.43 ± 0.072	12.631 ± 0.042	20.59 ± 0.09
TFAc	7.53 ±0.079	24.45 ± 0.091	15.11± 0.252	25.415 ±0.101	21.067 ± 0.073	42.449± 0.131

Table 4.1 Fatty acid content of *C. reinhardtii* under normal and HL conditions. The data represents the $\% \pm S.D.$ for n=3.

Overall saturated fatty acid increases from 6 to 10 %, 13 to 18 %, and 12 to 37 % in WT, *pgrl1*, and *pgr5* mutant, respectively, and monounsaturated fatty acid increases from 5 to 15 %, 10 to 20 %, and 12 % to 38 % in WT, *pgrl1*, and *pgr5*, respectively. However, there are also changes in total polyunsaturated fatty acids from 6 to 23 %, 11 to 16 %, and 17 to 27 %. This result implies that HL increases SFA and MUFA in WT, *pgrl1*, and *pgr5* mutant, but specifically, the SFA and MUFA increased significantly in *pgr5*.

4.2.9 Neutral lipid and membrane lipid analysis

To examine the fatty acid formed under HL, we studied the changes in neutral lipid, especially TAG and membrane lipid content and composition. We prepared neutral lipid extract from equal DW of WT, pgrl1, and pgr5 cells under normal and HL. Further, the extracted lipids were separated on TLC plates from the 3rd day of culture. This was stained with iodine, and results revealed that accumulation of more TAG was observed in pgr5 compared to pgrl1 and WT (Figure 4.9 A). To quantify the TAG, the TLC bands were recovered, and FAMES quantifies TAG content through GC (Figure 4.9). TAG concentration in WT and pgrl1 increased from 9 to 18 %; however, pgr5 significantly increased from 11 to 34 % (Figure 4.9 D). The fatty acid composition of TAG bands, 16:0, was raised in all strains under HL. However, the level of 18:0 was increased significantly in pgrl1 and pgr5 mutants. Further, 18:1ω9c majorly increased in pgr5 mutant under HL (Figure 4.9 A&D). The accumulation of a significant amount of TAG in pgrl1 and pgr5 under HL may suggest the role of membrane lipid in TAG synthesis (Fan et al., 2011). To assess all the membrane lipids of C. reinhardtii, TLC is carried out. In WT, we observed not much change in chloroplast specific lipid MGDG, but chloroplast lipid DGDG was marginally increased. However, in pgr5 mutant, MGDG and DGDG content reduced significantly under HL conditions.

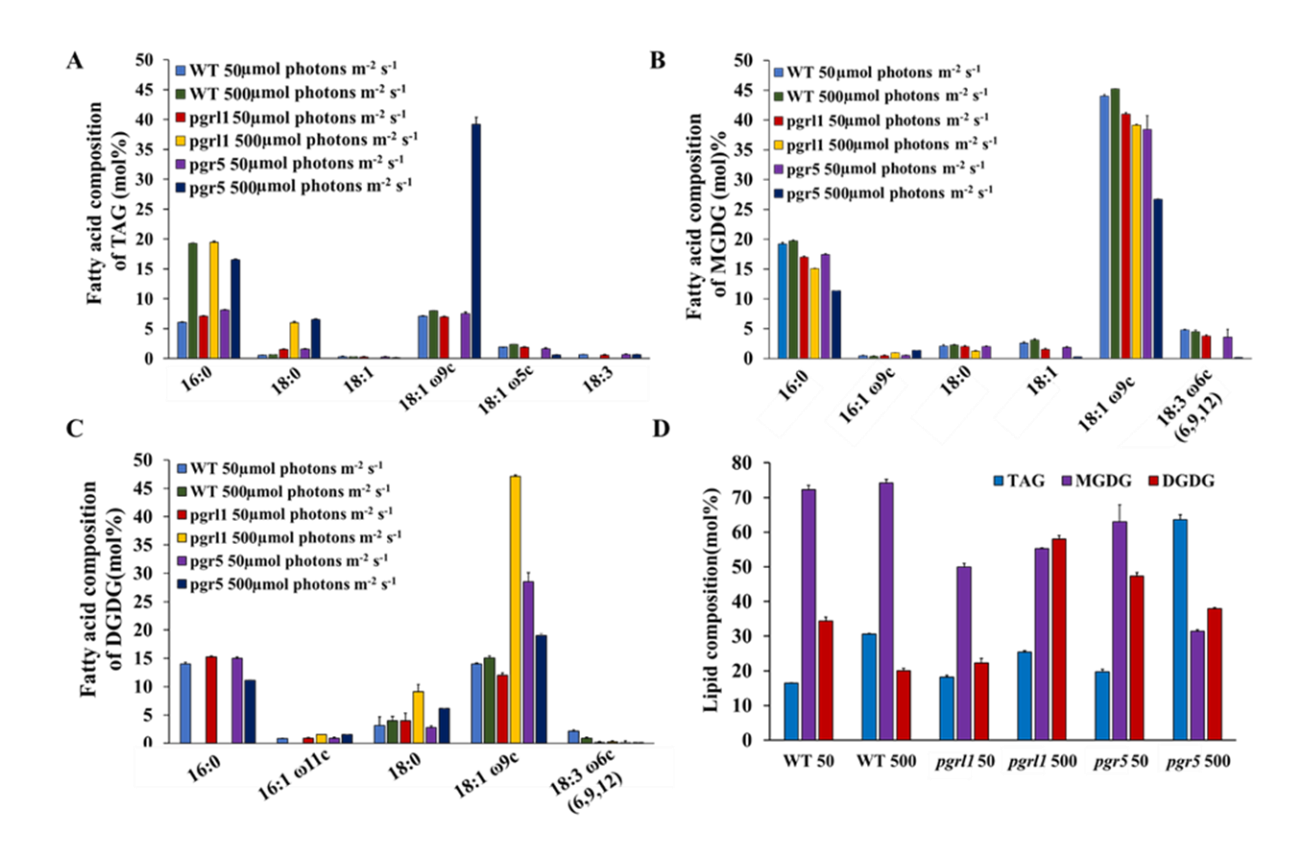


Figure 4.9 Changes in lipid composition of C. reinhardtii cells grown under HL conditions. (A) Fatty acid composition of the TAG of WT, pgrl1, and pgr5 under normal (50 μmol photons m⁻² s⁻¹) and HL (500 μmol photons m⁻² s⁻¹). Fatty acids are represented as the total carbon number followed by the number of double bonds. The position of specific double bonds is indicated from the methyl end 'ω.' (B) Fatty acid composition of MGDG. (C) Fatty acid composition of DGDG. (D) Changes in major lipid class in WT, pgrl1, and pgr5 under HL (500 μmol photons m-2 s-1). In the 'x-axis of (D), WT, pgrl1 and pgr5 50, WT, pgrl1 and pgr5 500, represents 50 and 500 μmol photons m⁻² s⁻¹. Averages from two independent experiments and their standard deviations are shown. TAG, triacylglycerol; PG, phosphoglyceride; DGTS, diacylglycerol-trimethyl homoserine; MGDG, monogalactosyldiacylglycerol; and DGDG, digalactosyldiacylglycerol. Averages from two replicate experiments and their standard deviations are shown.

Further GC quantification confirmed that the MGDG and DGDG were significantly decreased in HL (Figure 4.9 B&D). The fatty acid composition shows that DGDG 18:1 and 18:1 ω 9c increased in pgrl1 while decreased in pgr5; however, not much change was observed in WT (Figure 4.9 C&D). Further, the MGDG is enriched with C16:0, C18:1 ω 9c, C18:3, and C18:0. Not much change was seen in the fatty acid composition of MGDG in WT and pgrl1 but significantly decreased in pgr5 under HL (Figure 4.9 B&D). We assume that the reduced amounts of MGDG and DGDG are metabolized to TAG synthesis in pgr5, and a similar report was also observed in other studies (Li et al., 2008; Devadasu and Subramanyam, 2021). The

TLC and the GC data of membrane lipids support the electron microscopic data that the stacks of thylakoids were disturbed because of change in membrane lipids. Thus fatty acids from the chloroplasts and other intracellular membrane systems may have converted into TAG.

4.3 Discussion

CET around PSI requires the functions of PGRL1 and PGR5 to generate a proton gradient over the thylakoid membrane. PGR5 plays a regulatory role in cyclic electron flow around the PSI. It indirectly protects the PSI by enhancing photosynthetic control, a pH-dependent downregulation of electron transfer at the Cyt b6f (Buchert et al., 2020). Less proton motive force across the thylakoid membrane and reduced CET around PSI suggest these proteins' pivotal role in photosynthesis to protect it from HL (Yadav et al., 2020). Therefore, the CET is diminished in these mutants. It is known that CET plays a significant role in protecting plants in light stress. Recently, we reported that the photosynthetic activity was severely affected in pgrl1 and pgr5 of C. reinhardtii when the cells were grown in HL (Yadav et al., 2020). We have also observed that non-photochemical quenching is substantially reduced in pgr5, which is supposed to protect the algae from HL that could harmlessly dissipate excess excitation energy as heat (Nama et al., 2019). When they grow in photoautotrophic conditions, the pgr5 cells were much more sensitive to HL. To our knowledge, in pgrl1 and pgr5, the autophagyinduced lipid accumulation has not been explored in HL conditions despite being well characterized in the photosynthesis. This study shows that autophagy induces lipid accumulation under high light in pgrl1 and pgr5 mutants.

4.3.1 HL induces the reactive oxygen species and autophagy in C. reinhardtii

On the other hand, when microalgal cells were grown in high light, PSII undergoes severe damage. Hence photosynthetic electron transport chain induces ROS (Li et al., 2009). Antioxidants usually accumulate in cells such as carotenoids to repair the damage caused by

ROS (Perez-Martin et al., 2014). Interestingly, the ROS generation was much higher in pgr5 because the lack of this gene led to acceptor side limitations as PGR5 is involved in protecting PSI (Figure 3.3). Thus, PSI acceptor side is limited in pgr5. Because of the acceptor side limitation, one could expect more ROS generation at the PSI acceptor side (Tiwari et al., 2016), suggesting that lipid synthesis could serve as a receptor to excess electrons to acclimatize to the abiotic stress. As already reported, oxidative stress causes lipid accumulation under nitrogen stress in microalgae (Yilancioglu et al., 2014). TEM images of C. reinhardtii showed a pronounced increase in vacuoles' size under HL intensity, particularly in mutant strains (Figure 4.6). Accumulated autophagy bodies can play an essential role in lipid metabolism. A similar report was observed in nutrient limitations like nitrogen limiting conditions in C. reinhardtii (Couso et al., 2016). It has been reported that in stress conditions (like oxidative stress, rapamycin stress, and ER stress), the ATG8 gene was expressed in C. reinhardtii (Perez-Martin et al., 2014). In agreement with this hypothesis, we reported that significant expression of ATG8-PE protein was observed under HL conditions by immunofluorescence microscopy. It indicates that ATG8 is a pivotal protein to induce the autophagy process in C. reinhardtii (Figure 4.1). An abundance of ATG8-PE protein was increased in mutants due to HL, especially in pgr5. It seems to an increase in stromal redox poise, induces autophagy, thereby leading to TAG accumulation. HL stress leads to ROS formation, which activates the autophagy mechanism. Increased ROS was seen in HL conditions; however, this was more prevalent in pgr5 mutant when grown in HL, indicating that HL increases oxidative stress and autophagy, which accompanies increased lipid content in the cell. The autophagy of C. reinhardtii contains numerous autophagy-related proteins. Among various ATG proteins, ATG8-PE protein is essential for forming autophagosomes (Pérez-Pérez et al., 2016). In this study, we measured the expression level of ATG8-PE protein to evaluate the autophagy role in WT, pgrl1, and pgr5 (Figure 4.1). ATG8 appeared as a faint band in the WT and mutants (pgrl1 and *pgr5*) grown under optimal conditions and it was increased when cells were exposed to HL . However, lipidated form ATG8-PE was detected in the *pgr5* mutant. Further, TEM confirmed several lytic vacuoles and small vesicles inside the vacuoles in HL treated cells (Figure 4.6). Under HL vacuoles size was markedly increased abundantly. This supports our hypothesis that light stress causes ROS production, especially in the *pgr5* mutant. In turn, ROS induces autophagy, as reported earlier, leading to an increase in lipid production. Confocal and FACS data also suggested an increase in lipid droplet formation under HL in *pgr5* mutant (Figure 4.2 A&D). Continuous light exposure leads to the accumulation of biomass and the cellular over reduction and formation of ROS, which induces autophagy and lipids in microalgae (Shi et al., 2017). Our previous results indicate that PSI and PSII were damaged when cells were grown in HL (Nama et al., 2019; Yadav et al., 2020). Based on this result, we interpret that lipid accumulation in mutant strains could be explained by PSII or PSI being over-reduced, leading to high ROS production. These increased ROS levels act as an autophagy inducer (Heredia-Martinez et al., 2018).

4.3.2 HL induces a high amount of lipids in C. reinhardtii

In microalgae, lipids and carbohydrates are the primary energy storage forms and share the common carbon precursors for biosynthesis. Carbon partitioning is essential for the development of biofuels and chemicals. Most carbohydrates are stored as starch and sugars in microalgae. In several algal species, carbohydrate and lipid accumulate, while in some species, carbohydrate level decreases, and TAG increases, suggesting that lipids may be synthesized from carbohydrate degradation. Our results showed that both lipid and carbohydrate content increased in WT and *pgrl1*. However, lipid accumulation precedes carbohydrate accumulation (Figure 4.2&4.7), consistent with the previous studies in the microalga, *Pseudochlorococcum*, under nitrogen stress conditions (Li et al., 2011). However, the carbohydrate content was reduced in *pgr5* mutant under HL growth, explaining that carbohydrate degradation would

have been converted to lipids in pgr5. Therefore more lipid accumulation was observed. Complex metabolic regulations in the cell may control the accumulation of lipid droplets. The pgr5 prevents the proton gradient and PSI dependant CET; therefore, the altered NADPH and ATP ratio may switch the metabolic pathways during the photosynthesis process. Some of the metabolic alterations would have converted to lipids, which is necessary to acclimatize to the HL in pgr5. Carbohydrate is the dominant sink for carbon storage in C. reinhardtii mutant, which lacks cell walls, so lipid synthesis occurs only when the carbon supply exceeds carbohydrate synthesis (Fan et al., 2012). Under saturating light, the C. reinhardtii culture induces lipid droplets formation without disrupting growth, while N starvation leads to the significantly lower level (Goold et al., 2016). In our case, a significant accumulation of TAG was observed in HL conditions and the accumulation of TAG is more in pgr5 (Figure 4.2). In, Arabidopsis thaliana and C. reinhardtii TAG synthesis originated from multiple types of acyltransferases. The final step of TAG biosynthesis was catalyzed by DGAT and PDAT both involved in seed oil accumulation (Zhang et al., 2009). In the present study, we find the regulation of PDAT and DGAT at the protein level. Both the enzymes are accumulated under HL intensity, supporting these enzymes in the synthesis of TAG (Figure 4.8). Thus, the accumulation of TAG would be either through DGAT or PDAT routes.

Interestingly, the TLC results show that the membrane lipids have been decreased, which indicates that the degradation of these lipids could have converted to TAG, especially on *pgr5*. Similar reports were observed suggesting the recycling of membrane lipids, MGDG, and DGDG into TAG accumulation in *C. reinhardtii* (Abida et al., 2015, Devadasu and Subramanyam, 2021). Therefore, we assume that fatty acids are dissociated from glycolipids, which are involved in the Kennedy pathway to synthesize the TAGs through the DGAT enzyme (Yoon et al., 2012).

4.3.3 HL alters the fatty acid composition in C. reinhardtii

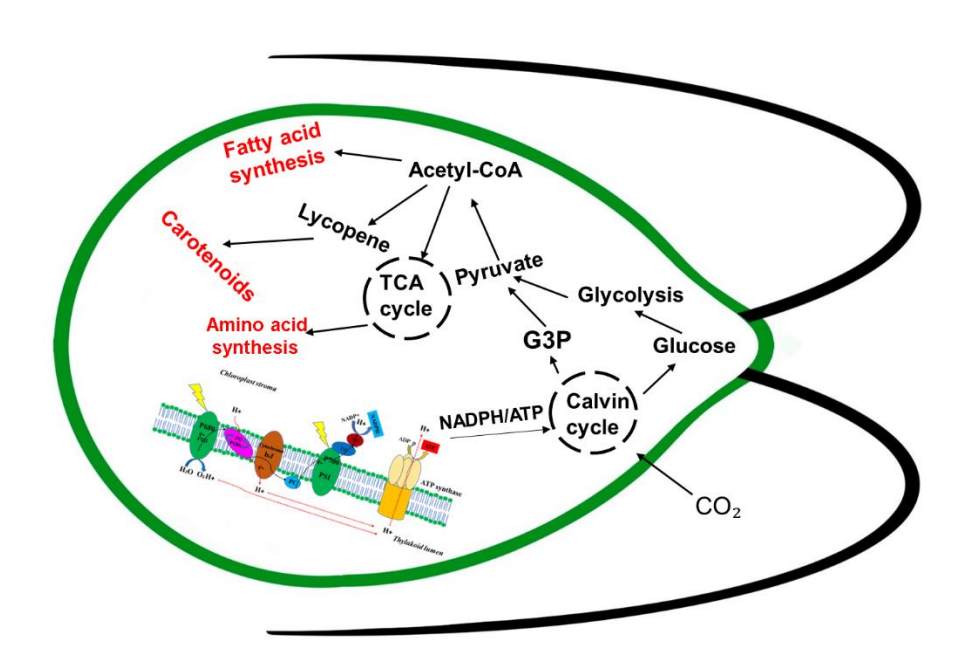
The fatty acid composition also plays a significant role in biofuel production. The results of total fatty acids show that the composition and content of fatty acids were different in WT, pgrl1, and pgr5 under normal and HL. The pgrl1 and pgr5 have a higher percentage of SFA and MUFA under HL, as shown in Table 4. Palmitic (C16:0), stearic acid (C18:0), oleic acid content (C18:1), and palmitoleic (C16:1) increased in WT, pgrl1, and pgr5 under HL. This result implies HL stress conditions increase SFA and MUFA content in WT, pgrl1, and pgr5 because the excess fatty acids could provide energy sink to the cells. The increase in the polar lipids was probably due to the remodeling of membrane lipids in response to HL stress (Han et al., 2017). The relative abundance of SFAs, MUFAs, and PUFAs is critical in determining the feasibility of using a microorganism as a source for algal lipid, biofuel feedstock, biomaterial synthesis, or high-value nutrient supplement.

4.4 Conclusion

Our results provided complete evidence that the two mutants, *pgrl1* and *pgr5*, of *C. reinhardtii*, accumulate fatty acid and induced autophagy under HL conditions. The correlation between stress and TAG accumulation in the photosynthesis of algae has been known for a century. Under HL conditions, these mutant's fatty acid compositions may be an important study for biotechnological applications. It suggests that one possible reason for the increase in lipid content may be the unbalanced redox state of the cells, leading to the generation of ROS. Therefore, the increased ROS levels in *pgr5* cells could play a dual role as signals to activate lipid biosynthesis and autophagy inducers to start recycling cellular components to fuel lipid production in this mutant (Tran et al., 2019). Therefore, *pgrl1* and *pgr5* of *C. reinhardtii* would be appropriate for producing high yield lipids (Lipids/TAG). Hence, our study could offer an essential value: microalgae-based lipid production can be promoted by applying various feedstocks to biodiesel and animal feed.

Chapter 5

Identification and characterization of metabolomics profile from cyclic electron transport mutants



5.1 Introduction

C. reinhardtii is a microalgae and model organism for photosynthetic process that can generate biomass quickly from solar energy, CO₂, and nutrients. Sugar, proteins, and lipids found in algal biomass can be transformed into products of significant values like living being feeds, vehicle fuel, chemical products, and medication via metabolic pathways (Larkum et al., 2011; Scranton et al., 2015). Microalgae metabolism reacts to changes in environmental stress by stimulating the biosynthesis of specific compounds to acclimatize to the environmental stress. In response to excessive irradiation, microalgae trigger defense mechanisms to safeguard the photosynthetic system from oxidative species (Rastogi et al., 2020). HL stimulates the formation of ROS in pgr5 and pgr11, according to the prior research. ROS are produced due to light stress and are engaged in a variety of metabolic processes (Foyer et al., 2009). Changes in metabolic pathways including nitrogen and carbon can impact the redox level in the cells. It was reported in A. thaliana that under HL several metabolites increase (Wulff-Zottele et al., 2010). Plants such as *Thalassiosira weisflogii* (Post et al., 1985) and microalgae such as C. reinhardtii (Davis et al., 2013) showed an increase in carbohydrate content under HL. The radiolabeled carbon studies suggested that the ingested radiolabeled carbon into the CBB cycle, is channeled into carbohydrate synthesis, which can serve as an energy sink (Kolling et al., 2013). Alterations in protein content have also been documented during shortterm HL exposure, implying that alterations in nitrogen and carbon metabolism plays a role in the photoacclimation in cells to achieve equilibrium (Post et al., 1985). The photosynthetic reductants such as ferredoxin and NADPH and along with ATP generate sugar, amino acid, and many other metabolites (Geigenberger et al., 2014). Additional stresses namely anaerobic conditions (Doebbe et al., 2010), nutritional scarcity (Bölling and Fiehn 2005), and CO₂ deceleration (Renberg et al., 2010), have shown changes in amino acid abundances, demonstrating that they are metabolically flexible during stress. The plants or algae use mechanisms such as endowment in ROS species detoxification and chemical or protein adaptability during stressful conditions (Hayat et al., 2012). The level of free amino acids was increased under the HL condition and decreases in low light conditions as reported earlier in Chlamydomonas (Davis et al., 2013).

In the present study, metabolites are measured using gas chromatography coupled with the dynamic networks of metabolites are affected by HL stress, which enhances our understanding of the regulatory processes during photosynthesis. Mass spectrometry (GC-MS) is a subset of omics technologies used to discover the differential expression in a metabolic pathways or regulatory components (Gargouri et al., 2015; Wase et al., 2017). Only a few metabolomic investigations using the Chlamydomonas system have been done so far (Timmins et al., 2009; Renberg et al., 2010). ROS generated due to light stress is involved in a large number of metabolic changes (Foyer et al., 2009). Similarly, our previous reports showed HL stimulates the formation of ROS in pgr5 and pgr11, as well as the accumulation of TAG. Therefore, we initiated the study of metabolome profiling of WT, cyclic electron-deficient mutant (pgrl1 and pgr5) grown under control light and HL to see the changes in metabolites. For effective CET, PGRL1 is essential in Chlamydomonas and is assumed to be a vital part of the CET supercomplex (Tolleter et al., 2011; Terashima et al., 2012). PGR5 deficiency causes a reduced proton gradient throughout the thylakoid membrane, as well as a reduced CET potential in pgr5 mutant (Johnson et al., 2014; Yadav et al., 2021). Under control light conditions, the lack of CET is compensated by a coordinated action of various mechanisms, including mitochondrial respiration and oxygen photoreduction (Dang et al., 2014). However, under HL, both pgrl1 and pgr5 mutants adopt alternate defense mechanisms as compared to WT. Further, nitrogen metabolism in pgr5 is drastically influenced by HL, which could be an effort to improve the chloroplast's redox level and also to sustain the greater cell division and translation rates. We report the mechanism of HL tolerance in WT, pgrl1, and pgr5 using

metabolomics and gene expression techniques on a molecular scale. The goal of this study was to use GC-MS, mapping, and contemporary methodologies involving metaboanalyst to illustrate the profile of metabolite in WT, *pgrl1*, and *pgr5* under control and HL. Also, to understand the role of the key metabolic genes, we analyzed mRNA expression levels by real-time polymerase chain reaction (RT-PCR).

5.2 Results

5.2.1 Metabolite profiling and PCA analysis

The levels of metabolites in WT, pgr11, and pgr5 under control and HL were quantified by using GC-MS analysis. A total of 55 metabolites were identified and arranged as follows 12 metabolites grouped into 12 amino acids, 3 carbohydrates, 8 carboxylic acids, 3 fatty acids, 3 glycerol, 2 ions, 3 nucleotide, 4 TCA cycle, 4 secondary, and 9 other metabolites. The relative abundance of each metabolite in WT, pgr11, and pgr5 was represented in the form of a heat map (the order and abbreviations of metabolites are listed in Table 5.1–5.6 (Figure 5.1). To study the interaction between the metabolites in each sample of WT, pgr11, and pgr5, a correlation matrix is performed via Pearson's correlation values. The metabolite-metabolite interaction network in WT, pgr11, and pgr5 was also deduced based on Pearson's correlation coefficient (r) values with p > 0.05.

5.2.1a Amino acid and TCA cycle metabolism

Amino acids such as glycine (Gly), L-alanine (L-Ala), N-acetyl-L-aspartic acid (NALA), glutamate (Glu), isoleucine (Ile), phenylalanine (Phe), threonine (Thr), L-valine (L-Val), serine (Ser), and proline (Pro) increased by 2.5-fold in *pgr5* under HL with respect to control light conditions. However, no significant change was observed in amino acids including urea, Glu, Ile, Phe, and L-Val in WT and *pgrl1* under HL. Similarly, HL did not affect the L-Ala and Ser levels in *pgrl1* as well as N-Acetyl-beta-alanine (NAA) and Gly levels in WT. NAA, urea, and Phe levels showed no change in *pgrl1* under HL. Further, TCA cycle intermediates including

fumaric acid (FA), (Tricarboxylic acid) TCA and malic acid (MA) were upregulated by 2.5-fold in *pgr5*, but these levels were downregulated by 1.5-fold in WT and *pgrl1* under HL with respect to control light.

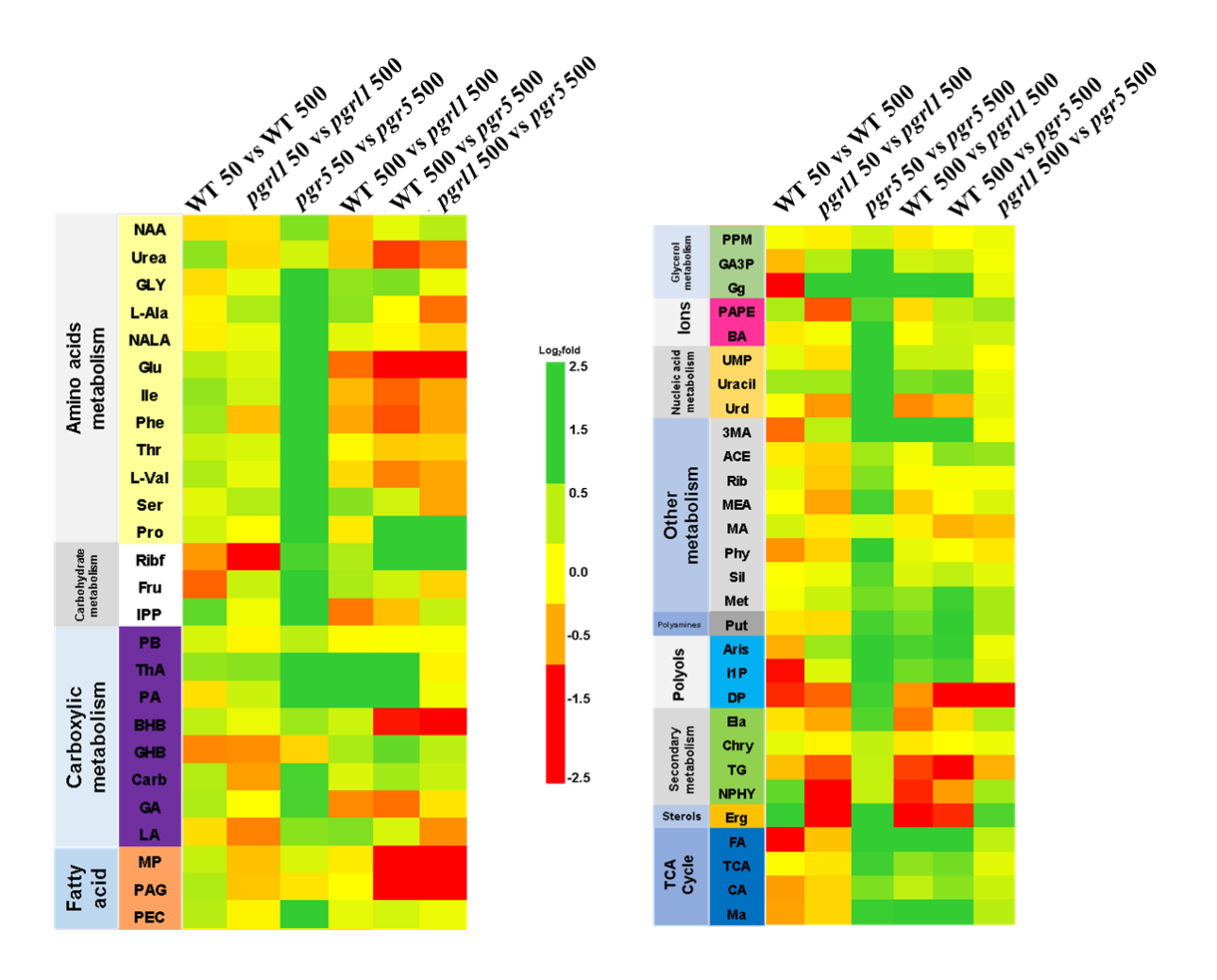


Figure 5.1 A heat map showing the significantly changing metabolites. In WT, pgrl1, and pgr5 under HL treatments, relative alterations in metabolite abundance were observed. According to the colour scale shown, each biological replicate is represented by a colour-based metabolite profile, red colour is downregulation and green colour is upregulation. The scale indicated a log² fold change from 2.5 to -2.5 (upregulation to downregulation). WT, pgrl1 and pgr5 50, and WT, pgrl1 and pgr5 500, represent 50 and 500 μmol photons m⁻² s⁻¹.

5.2.1b Carbohydrate metabolism

Carbohydrate metabolites like Ribofuranose (Ribf), fructose (Fru), inositol pentaphosphate (IPP), aristeromycin (Aris), D-myo-Inositol-1-monophosphate (I1P), and D-pinitol (DP) were induced by 2.5-fold in *pgr5* under HL compared to control light. Only IPP was increased by

2.5-fold in WT, but its level did not change in *pgrl1* under HL. Aris was unaffected by HL, whereas I1P and DP were downregulated by 2.5-fold in WT. Similarly, Aris and I1p were upregulated by 2.5-fold in *pgr5* under HL with respect to control light. We did not observe a significant change in Fru level in *pgrl1*, whereas Ribf and Fru levels were reduced by 1.5-fold in WT under HL.

5.2.1c Carboxylic acid and fatty acid metabolism

Under HL, carboxylic acids including threonic acid (ThA) and propionic acid (PA) were increased by 2.5-fold in *pgr5* compared to WT and *pgrl1*. Similarly, palmitic acid (PEC) level was enhanced by 2.5-fold in *pgr5*, while the metabolite level did not change significantly in WT and *pgrl1* under HL in comparison to control light. The level of glycerol 3-phosphate (GA3P) elevated by 2.5-fold in *pgr5*, but the metabolite levels remained unchanged in *pgrl1* under HL. Similarly, glyceryl-glycoside (Gg) was upregulated by 2.5-fold in both mutants, whereas downregulated by 2.5-fold in WT under HL. Ions namely phosphoric acid propyl ester (PAPE) and boric acid (BA) levels were enhanced by 2.5-fold in *pgr5*, however, these metabolites did not change in WT and *pgrl1* under HL.

5.2.1d Nucleotide metabolism and other metabolites

Nucleotide metabolism, mainly uridine-5'-monophosphate (UMP), uracil, and uridine (Urd) was induced 2.5-fold in *pgr5*, but unaffected in WT and *pgrl1* under HL. Putrescine (Put) level was enhanced significantly by 2.5-fold in *pgr5*, whereas the metabolite level in *pgrl1* and WT did not change under HL. Further, Neophytadiene (NPHY) level was upregulated by 2.5-fold in *pgr5* and *pgrl1*, but chrysanthemol alcohol (Chry) and trigallic acid (TG) levels were unaffected in *pgrl1* under HL. Other metabolites such as methoxyamphetamine (3MA), ethanolamine (MEA), phytol (Phy), and silanol (Sil) were increased significantly by 2.5-fold in *pgr5* under HL.

We also compared the metabolites among the strains under HL. Carboxylic acids namely ThA and PA, as well as the TCA cycle intermediates (FA and MA) were upregulated by 2.5-fold in *pgrl1* and *pgr5* under HL. Similarly, polyols (Aris and I1P) and glycerol (Gg) were significantly enhanced by 2.5-fold in *pgrl1* and *pgr5* compared to WT under HL. Interestingly, a 2.5-fold rise of Pro and Put levels was observed in *pgr5*, but no change was observed in *pgr11* and WT under HL.

The principal component analysis (PCA) was performed on each sample data set to determine the impact of HL on WT, *pgrl1*, and *pgr5* (Figure 5.2). We observed that WT50 vs WT500, *pgrl1*50 vs *pgrl1*500, and *pgr5*50 vs *pgr5*500 showed 68.9%, 66.4%, and 91.8% variation among the sample data sets respectively (Fig. 5.2 A-C). The biplot between *pgr5*50 and *pgr5*500 was the highest PCA score (91.8%). The PCA analysis explained that 74.6%, 89.6%, and 80.8% of the variation in WT500 vs *pgr11*500, WT500 vs *pgr5*500 and *pgr11500* vs *pgr5*500 respectively (Figure 5.2 D-F). PCA scores were high for *pgr5*50 vs *pgr5*500 (91.8%), *pgr11*500 vs *pgr5*500 (66.4%), and WT500 vs *pgr5*500 (68.9%). PCA score showed the overall metabolic changes amongst samples in each group, including the degree of diversity across samples within each group.

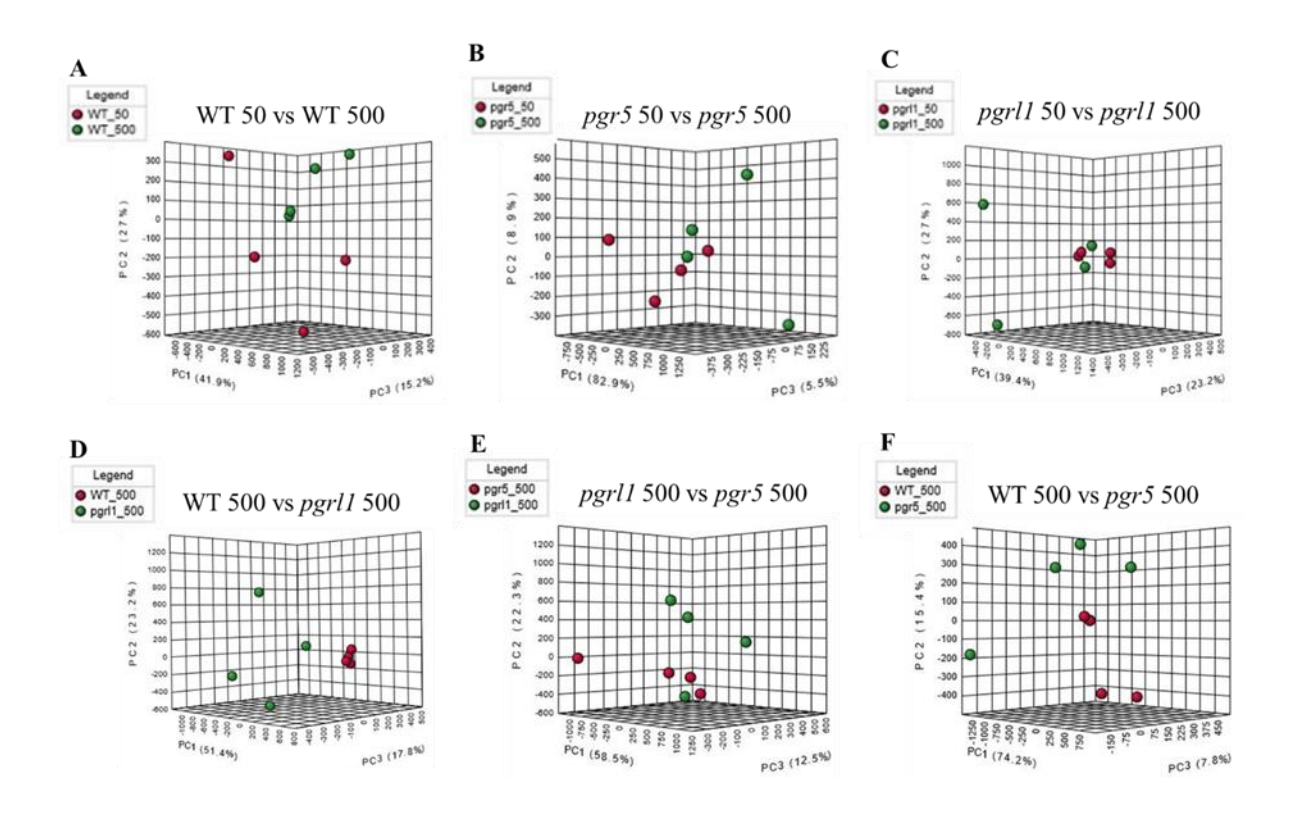


Figure 5.2 Principle component analysis (PCA plot) of the gas chromatography of (A)WT50 vs WT500, (B) pgrl150 VS pgrl1500, (C) pgr5 50 VS pgr5 500, (D)WT 500 VS pgrl1 500, (E) pgrl1 500 VS pgr5 500, and (F)WT500 VS pgr5 500. Principal component (PC) 1 is given on the x-axis, while PC2 is given on the y-axis of each plot. The per cent of variance explained by each PC is given below each PCA plot. WT, pgrl1 and pgr5 50 and WT, pgrl1 and pgr5 500, represents 50 and 500 μmol photons m⁻² s⁻¹.

5.2.2 The pathway enrichment analysis under HL

A KEGG pathway enrichment analysis was performed to examine the induction of biological processes at the metabolic pathway level in WT, *pgrl1*, and *pgr5* under HL. Our metabolite data was connected with the KEGG database to elucidate the possible metabolic pathways, which were altered under HL. Figure 5.3 & 5.4 showed an interactive representation of enrichment analysis. Glycerophospholipid and terpenoid backbone synthesis pathways were the most prevalent routes in WT50 vs WT500 (Figure 5.3 A). In *pgrl150* vs *pgrl15*00, pathways related to linoleic acid, unsaturated fatty acid, alanine, aspartate and glutamate, phenylalanine, tyrosine, phenylalanine, tryptophan, and sphingolipid metabolism were elevated considerably (Figure 5.3 B). Furthermore, pathways related to the biosynthesis of pantothenate and co-

enzyme, valine, isoleucine, leucine, pyrimidine, and arginine biosynthesis were enhanced dramatically in pgr550 vs pgr5500 (Figure 5.3 C).

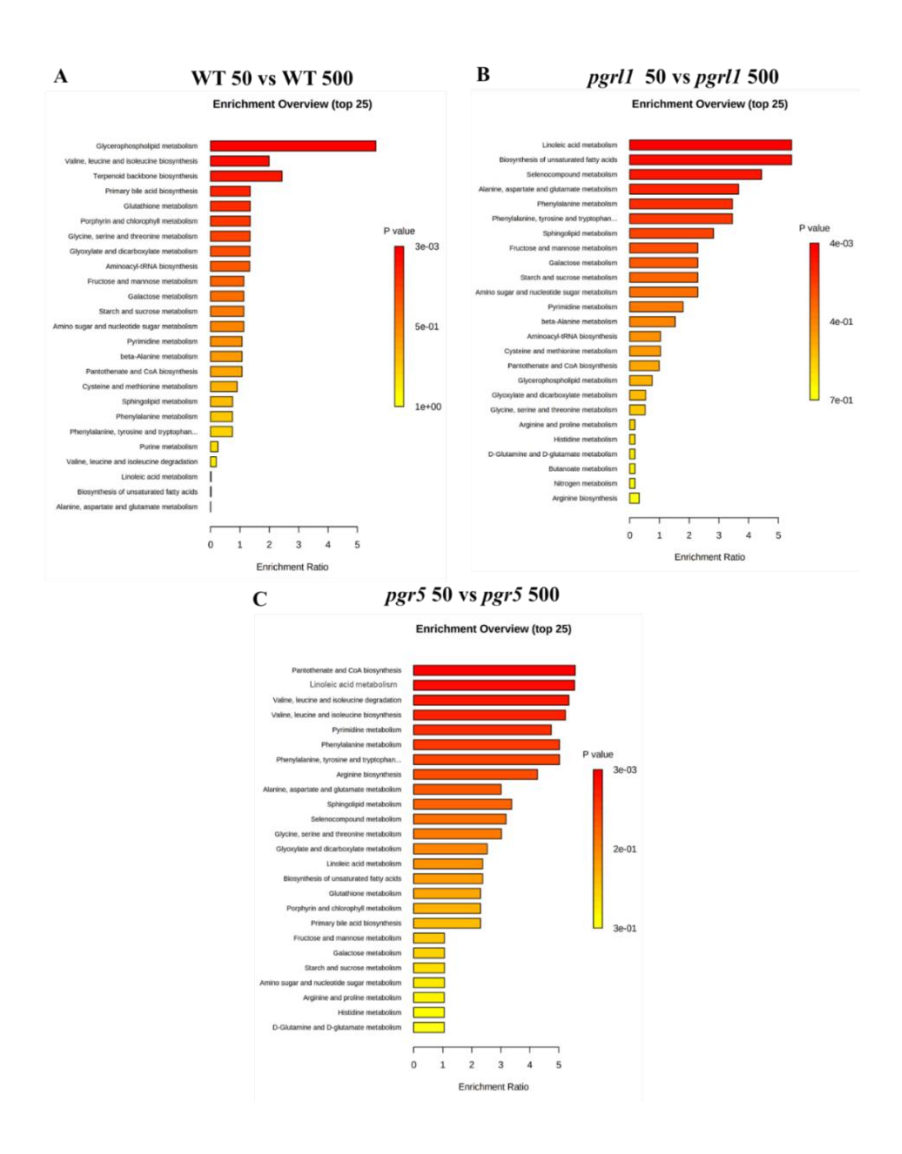


Figure 5.3 Analysis of metabolic pathways of WT, pgrl1, and pgr5 under control and HL. Results were obtained from the Metaboanalyst 5.0 software. Every bar represents a metabolic pathway with a p-value < 0.05 and were determined to have significant changes. (A) WT 50 vs WT 500 (b) pgrl1 50 vs pgrl1 500 (c) pgr5 50 vs pgr5. WT, pgrl1 and pgr5 50, and WT, pgrl1 and pgr5 500, represent 50 and 500 μ mol photons m^{-2} s⁻¹.

We also performed enrichment analysis among the strains under HL between WT500 vs pgr1500, WT500 vs pgr5500, and pgr1500 vs pgr5500 as shown in Figure 5.4 A-C. Cysteine and methionine biosynthesis, as well as glycerophospholipid, pyrimidine, pantothenate, and CoA biosynthesis were increased considerably in WT500 vs pgr5500 and pgr1500 vs

pgr5500. Under HL, fatty acid, amino acid, and glucose metabolite pathways were accelerated in pgr11 and pgr5 compared to WT. Furthermore, pantothenate and CoA biosynthesis pathways were exclusively enhanced in pgr5 under HL.

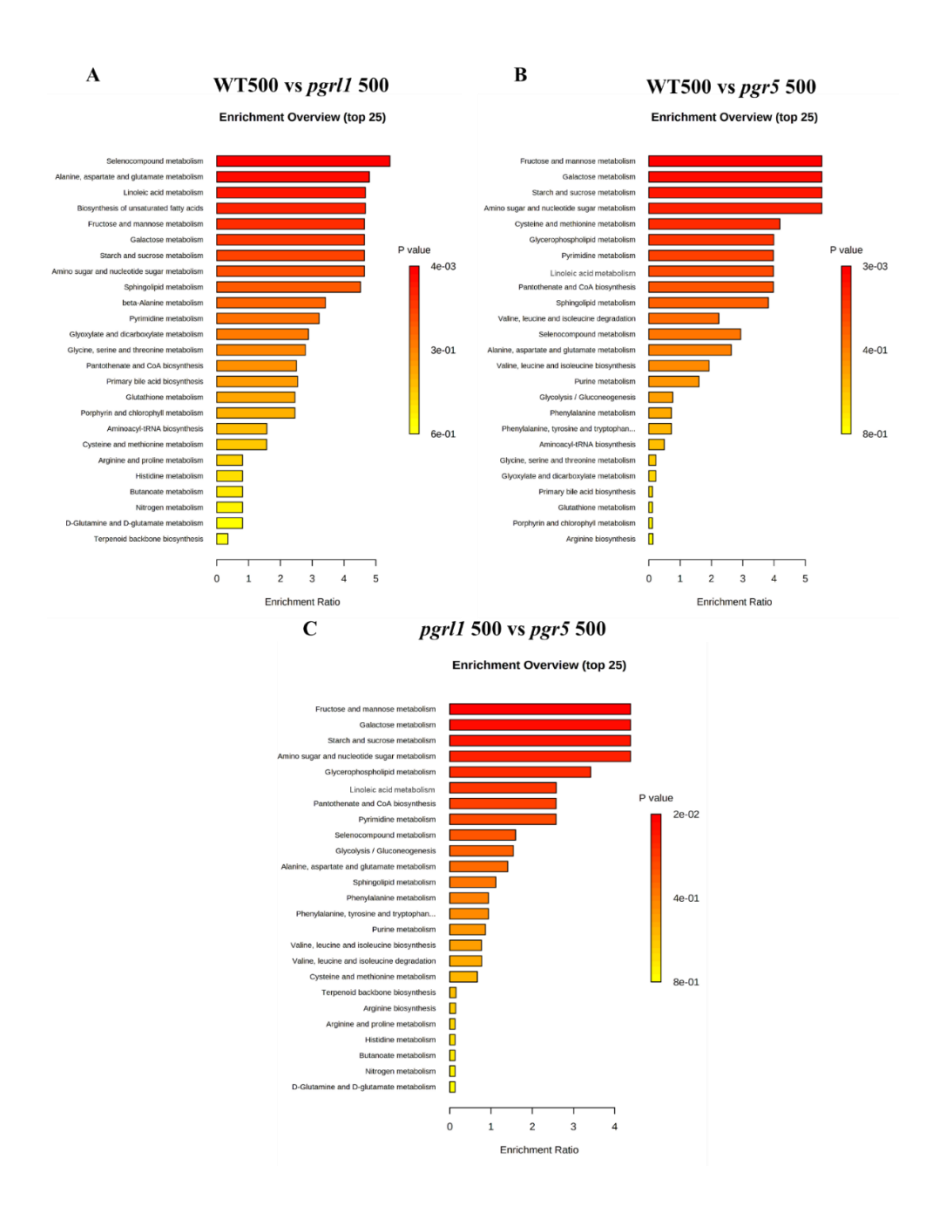


Figure 5.4 Analysis of metabolic pathways of WT, pgrl1, and pgr5 under HL. Results were obtained from the analysis using the Metaboanalyst 5.0 software. Every bar represents a metabolic pathway the pathways with a p-value < 0.05 were determined to have significant changes. (A) WT 500 vs pgrl1 500 (b) WT 500 vs pgr5 500 (c) pgrl1 500 vs pgr5 500. WT, pgrl1 and pgr5 50, and WT, pgrl1 and pgr5 500, represent 50 and 500 μ mol photons m^{-2} s⁻¹.

5.2.3 Correlation-based clustering among the metabolites in *C. reinhardtii*

To explore the interaction between the metabolites, a matrix of correlation is created based on Pearson's correlation value. Hierarchical cluster (HAC) analysis was conducted on a total of 55 metabolites of WT, pgrl1, and pgr5 under control and HL as shown in Figure 5.5 & 5.6. Our results were divided into 6 groups: 1st group: WT50 vs WT500, 2nd group: pgrl150 vs pgrl1500, 3rd group: pgr550 vs pgr5500, 4th group: WT500 vs pgrl1500, 5th group: WT500 vs pgr5500, 6th group: pgr11500 vs. pgr5500. To make it simple, only a strong correlation (r > 0.6) was shown separately. The order and abbreviations of metabolites were given in Table 5.1–5.6. In WT50 vs WT500, there was a strong association among the group of the amino acid (L-Val: Ilu: Phe: Ser: Thr: Glu: Pro) (Figure 5.5 A). Furthermore, a strong link within the carboxylic acid category (LA: PA: PB: Carb: GA) was detected. Amino acid group (L-Val: Ilu: Phe: Ser: Thr: Glu: Pro) showed strong interaction with fatty acid (PEC), carboxylic group (BHB), and carbohydrate group (IPP), and TCA cycle (MA). A strong interaction was also observed among other metabolites, such as uracil, Urd, PEC, Sil, MA, BHB, IPP, and NPHY. Polyol groups (IIP: DP: Aris) showed a significant interaction within themselves. Furthermore, a positive correlation among TCA cycle (CA: MA: FA), polyamines (Put), carbohydrate (Ribf: Fru), and secondary metabolites (Ela: TG) was recorded.

Amino acids such as NAGA, Gly, and urea were substantially associated with *pgrl150* vs *pgrl1500*. The carboxylic acid group was strongly correlated with the metabolites of PPM, PB, Chry, PEC, Put, and DAHP. The TCA cycle group (CA: FA: MA) shows a positive correlation with amino acids (Phe), fatty acids (MP: PAG), and secondary metabolites (EA). Amino acids (Ser: Ilu: Thr: Val: urea: Glu: L-Ala) showed a strong interaction with metabolites such as PA, Sil, Ma, Fru, EA, Phy, D-myo, IIP, NAA, carb, and MEA. Other metabolites namely LA, PAPE, GHB, Urd, Erg, NPHY, TG, and DP showed a significant interaction with each other. BHB, Aris, G3P, and Gg also have a substantial connection. Amino acids including

Gly, Ser, Val, Thr, Ilu, Pro, and Phe were positively associated in the *pgr550* vs *pgr5500*. TCA cycle intermediates namely TCA, MA, and CA showed a strong interaction with amino acids (Gly: Ser: Val: Thr: Ilu: Pro: Phe). Furthermore, amino acids (Glu) and fatty acids (PEP) exhibited a significant interaction with one another. In addition, metabolites such as carbohydrate (Fru: Ribf), amino acids (NALA: Phe: L-Ala), polyols (Aris: Ilp), TCA cycle intermediate (FA), and polyamines (Put) were found to be strongly connected. Other metabolites including Ga, G3P, LA, Rib, ACE, L-Met, IPP, Gg, and BHB interacted positively with one another. EA, PPM, MA Chry, MP, and PB were significantly correlated with each other.

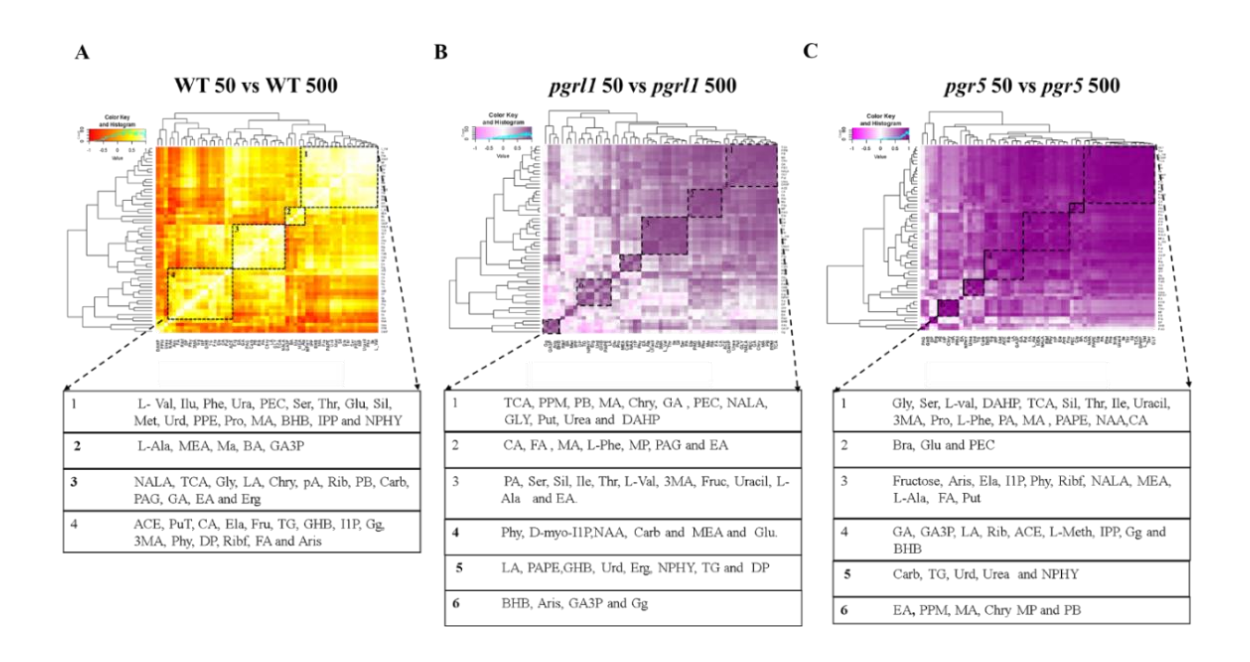


Figure 5.5 Metabolites – metabolites correlation heat map hierarchical clustering of WT, pgrl1, and pgr5. (A) WT50 vs WT500,(B) pgrl150 vs pgrl1500, (C) pgr550 vs pgr5500. Each correlation value (based on the Pearson correlation coefficient) corresponds to an average of four biological replicates. WT, pgrl1 and pgr5 50, and WT, pgrl1 and pgr5 500, represent 50 and 500 μ mol photons m^{-2} s⁻¹.

We also compared the correlation between WT500 and *pgrl1*500, WT500 vs *pgr5*500 and *pgrl1*500 vs *pgr5*500 (Figure 5.6 A-C). In WT500 vs *pgrl1500*, amino acids such as L-Ala, Thr, L-Val, Phe, and Pro are positively correlated with each other. Strong interaction was observed within the TCA cycle group (TCA: LA: MA: FA). We also observed a positive

correlation among the metabolites such as amino acid (Ser), nucleotide (uracil), carbohydrate (Fru), fatty acid (MP: PAG: PEC), and carboxylic acid metabolism (Rib: PB). Similarly, the amino acid group (L-Ala: Thr: L-Val: Phe: Pro), showed a strong correlation with other metabolites (Urd: Chry). Carboxylic acid (GA: IPP), secondary metabolites (Ela: TG), and amino acids (Ile: Glu) were also significantly correlated with each other. Additionally, a significant correlation is observed between carboxylic acid (PA: GHB), polyamines (Put), and the TCA cycle (TCA: LA: MA: FA).

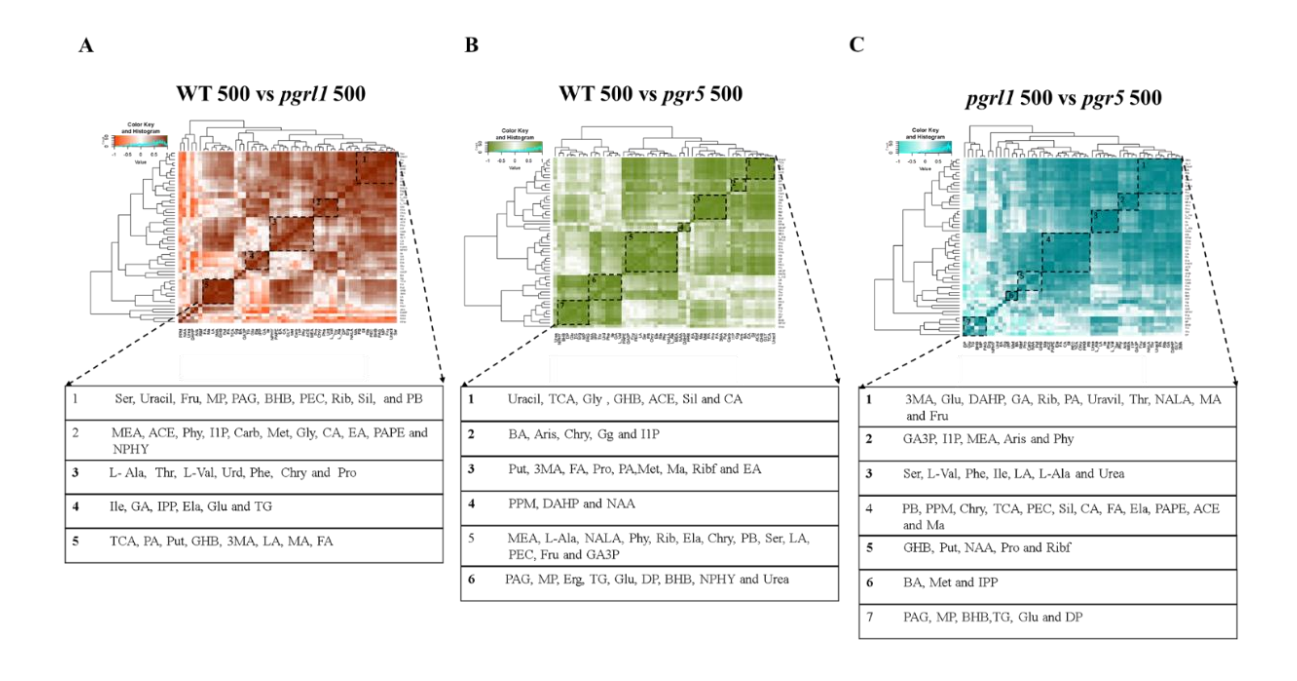


Figure 5.6 Metabolite – metabolites correlation heat map hierarchical clustering of WT, pgrl1, and pgr5. (A) WT500 vs pgrl1500,(B) pgrl1500 vs pgr5500, and (C) WT500 vs pgr5500. Each correlation value (based on Pearson correlation coefficient) corresponds to an average of 4 biological replicates. WT, pgrl1 and pgr5 50 and WT, pgrl1 and pgr5 500, represent 50 and 500 μmol photons m⁻² s⁻¹.

In WT500 vs *pgr*5500, a strong correlation is observed between amino acids and other metabolites such as nucleotides (Uracil), carboxylic acids (GHB), TCA cycle (TCA: CA), and other metabolites (ACE: Sil). Polyamines (Put), TCA cycle (FA: TCA), amino acid (Pro: Met) carboxylic acid (PA), and carbohydrate (Ribf) showed significant interaction with each other. Strong interaction was observed between amino acid group (L-Ala: NALA: Phe: Ser),

carbohydrate group (Fru: Rib), carboxylic acid group (PB: LA), fatty acid (PEC), secondary metabolites (Ela: Chry), and glycerol metabolites (GA3P). Similarly, strong interaction between fatty acid (PAG: MP), sterols (Erg), amino acid (Glu: urea), polyols (DP), and secondary metabolites (TG: NPHY). In addition, several metabolites (BA: Aris: Chry: Gg: I1P) were associated with each other.

In *pgrl15*00 vs *pgr55*00, amino acid groups (Ser: L-Val: Phe: Ile: L-Ala: urea) were positively correlated among themselves. The amino acids (Glu: Thr: NALA), carbohydrate (Rib: Fru), TCA cycle (MA), and nucleotide (Uracil) revealed a high correlation. GA3P showed a strong interaction with other metabolites namely MEA, Aris, and Phy. Secondary metabolites (Ela: Chry), the TCA cycle (TCA: MA: CA: FA), fatty acid (PEC), and carboxylic acid (PB) were found to be substantially associated with each other. Other metabolites (GHB: Put: NAA: Proline: Ribf) were also significantly associated with each other. Furthermore, fatty acids (PAG: MP), amino acids (GLU), and carboxylic acids (BHB: BA: Met: IPP) interacted strongly. Our findings revealed a strong interaction of metabolites between polyamine, amino acid, carbohydrate, fatty acid, and carboxylic acid metabolism in *pgr11* as compared to WT under HL.

5.2.4 Network analysis of C. reinhardtii under HL

To elucidate the metabolite-metabolite interaction network, we performed Pearson's correlation coefficient (r) at selected fold values p > 0.05. Each data point was considered as a node in the correlation network (circle represents a node) and a total of 55 nodes (each node representing single metabolites) formed 350 edges (neighbouring interactions), on average. A total of six networks were constructed by correlation-based network modelling of WT50 vs WT500, pgr1150 vs pgr11500, pgr550 vs pgr5500, WT500 vs pgr11500, WT500 vs pgr11500. Interestingly, we observed a high degree of correlation (size 90) in pgr5500 compared to pgr550 (Figure 5.7 C). Almost all the metabolites showed a huge network with

the neighbouring nodes containing an average of 22 interactions, which corresponds to carboxylic metabolites, TCA cycle intermediates, nucleotide, glycerol, fatty acid, and other metabolisms. TCA cycle intermediates and fatty acid metabolites showed a huge network with 7 interacting partners namely Ilu, Thr, Gly, Rib, Fru, Chry, and uracil with an average sharing network of 22. In *pgrl1* under HL important metabolites include carboxylic acid metabolism (EA, BHB, and PB), carbohydrate metabolism (Ribf and Fru), and nucleotide metabolism (Uracil, Erg, and Urd) showed significant interaction with neighbouring nodes (Figure 5.7 B). In WT under HL, amino acids namely Phe, Met, Ser, Thr, Ilu, L-Val, Pro, and Glu, as well as fatty acids notably PEC, PAG, and MP, showed a strong interaction with adjacent nodes.

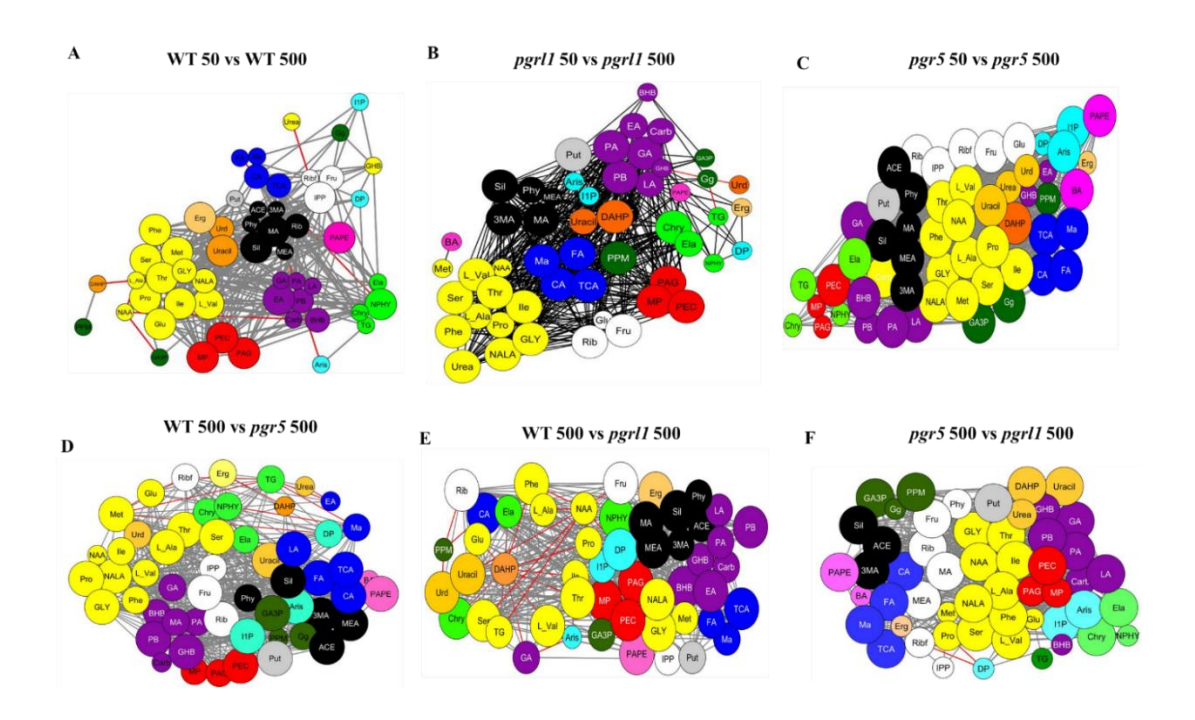


Figure 5.7 Correlation network of metabolites based on Pearson's coefficient with a probability threshold of P>0.05. Metabolites are shown in colours and represented as nodes: yellow (amino acid metabolites), white (carbohydrate metabolites), red colour (fatty acid metabolites), blue colour (TCA cycle intermediate), orange colour (nucleotide metabolism), green colour (glycerol metabolites), sky blue (polyols), pink (ions), black (other metabolites) and parrot green (secondary metabolites). Three different circle sizes (based on the degree of interaction), including 50 (the smallest size), 70 (medium-sized circle), and 90 (the biggest circle), to determine which one is the most interactive among the others. Smaller circles represent 50 and 10 interacting partners with 1, 2, or 3... 10 sharing networks. Medium-sized circles represent 70 and 4 interacting partners, with 12, 13, and 15 sharing networks. The bigger size circles represent 90 and 7 interacting partners with 16, 17, and 22 sharing networks. In the network, the grey line showed positive interaction, and the red line showed negative interaction. The stroke represents interactions with other metabolites.

Under HL, amino acids (NALA, Gly, L-Val, Thr, Ser, and Phe), fatty acids (PEC, PAG, and MP), carbohydrates (Ribf and Fru), nucleotides (uracil, Erg, and Urd), and carboxylic acids (EA, BHB, and PB) revealed a substantial interaction in *pgrl1* compare to WT (Figure 5.7 D). Amino acids including Pro, Gly, Met, NALA, L-Ala, and Ser, as well as TCA cycle components such as FA, TCA, and CA, showed strong interaction. Carbohydrates (Fru and Ribf), fatty acids (PEC), carboxylic acids (PB and GHB), polyols (Aris and I1P), and nucleotides (uracil) were showed significant interaction (Figure 5.7 E). Under HL, *pgr5* showed a high degree of interaction with the neighbouring metabolites as compared to *pgrl1* (Figure 5.7 F). The interaction results showed that under HL, the degree of interaction with other metabolites was significantly increased in *pgr5* compared to WT and *pgrl1*.

5.2.5 Differential expression of genes associated with TCA cycle under HL in *C. reinhardtii*

To evaluate our metabolomic data with the experimental analysis, we have performed some specific key genes of the TCA cycle. We examined the relative mRNA expression of TCA cycle genes, citrate synthase (CIS2), which was significantly upregulated by 6-fold in *pgr5* and downregulated by 1.5-fold in WT, while its expression remained unchanged in *pgrl1* under HL (Figure 5.8). Furthermore, in *pgr5* aconitase (ACS1 and ACS3) gene expression was increased by 1.2-fold under HL (Figure 5.8). Interestingly, the expression of gene 2-oxoglutarate dehydrogenase (OGD2 and OGD3) was induced in all strains under HL. Acetyl-CoA hydrolase (ACH1) expression was enhanced by 3.9-fold in *pgr5* and the 6-fold increase was observed in *pgr11* when compared to WT. Further succinate dehydrogenase (SDH1 and SDH2) levels were upregulated 3-fold and 1.5-fold in WT and *pgr11* respectively, while these levels were unaffected in *pgr5*. Interestingly, fumarate hydratase (FUM1) expression was induced by 5.9-fold in *pgr5*, while its expression was decreased by -1-fold in WT but not changed in *pgr11*.

The expression of malate dehydrogenase 1 (MDH1) was reduced by -2-fold in WT and -1.8 in *pgrl1* under HL but significantly enhanced by 4-fold in *pgr5*. Under HL, malate dehydrogenase 2 (MDH2) increased by 2.3-fold, and MDH5 was enhanced 1.8-fold in *pgrl1*, however, it was unchanged in WT.

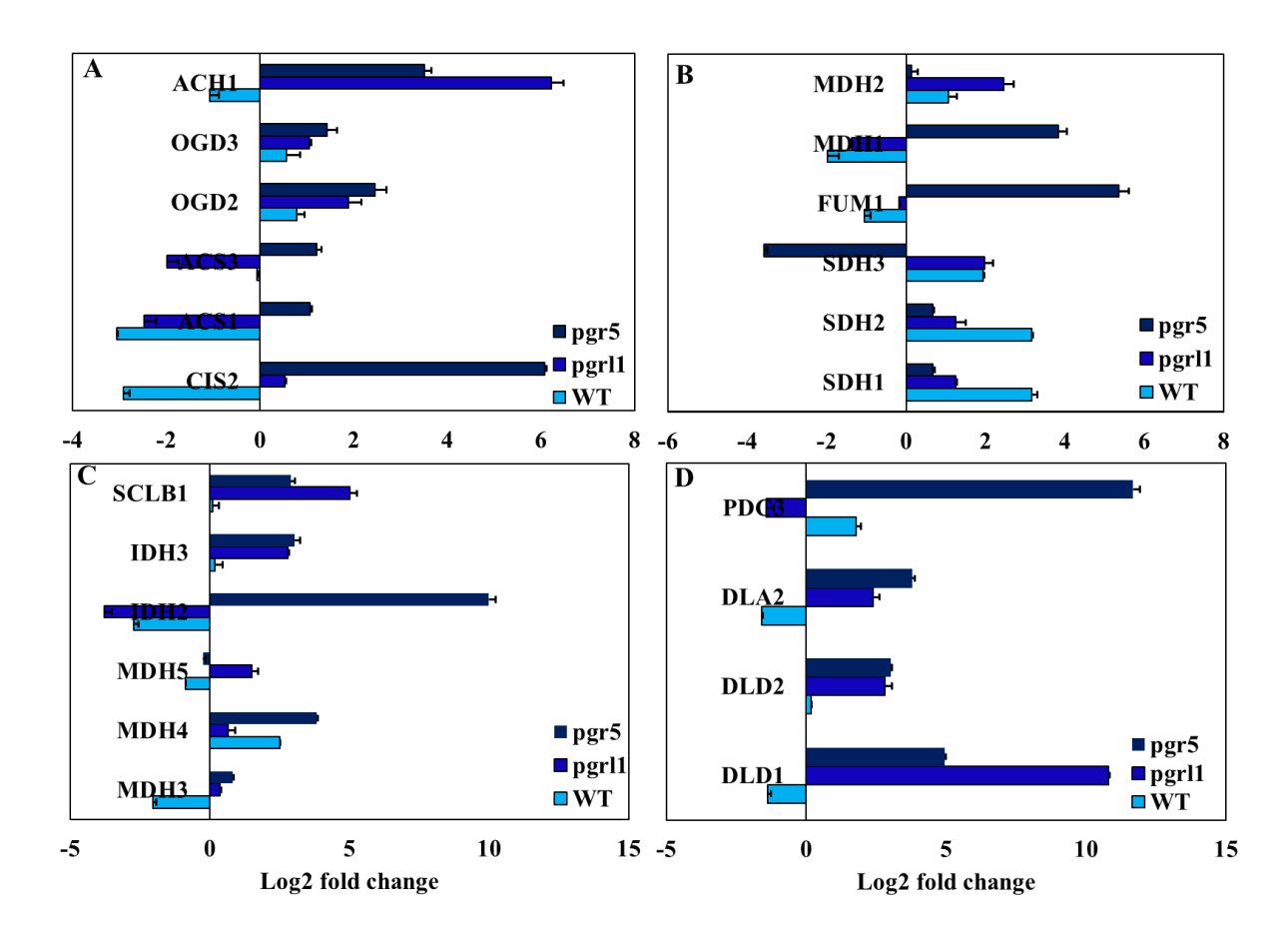


Figure 5.8 The relative content of the TCA cycle intermediate of cells of WT, pgrl1, and pgr5 under control (50 μmol photons m⁻² s⁻¹) and HL (500 μmol photons m⁻² s⁻¹). WT, pgrl1 and pgr5 50 and WT, pgrl1 and pgr5 500, represent 50 and 500 μmol photons m⁻² s⁻¹. The values shown are the means of three independent experiments. The error bars represent standard deviations. Citrate synthase (CIS2), aconitase (ACS1 and ACS3) 2-oxoglutarate (OGD2 and OGD3) acetyl-CoA hydrolase (ACH1) fumarate (FUM1), malate dehydrogenase (MDH1), isocitrate dehydrogenase (IDH3), isocitrate dehydrogenase (IDH2), SCLB1 pyruvate dehydrogenase complexes (PDC3), D-lactate dehydrogenase (DLD1).

Under HL conditions, the expression of isocitrate dehydrogenase (IDH3) was increased by 3-fold in *pgrl1* and *pgr5*, while it was unaltered in WT. Furthermore, the expression of isocitrate dehydrogenase (IDH2) was significantly increased by 10-fold in *pgr5* under HL. The succinyl-CoA ligase (SCLB1) levels were upregulated by 5-fold in *pgr5* and by 3-fold in *pgr11*, but these

levels were unchanged in WT under HL. Interestingly, pyruvate dehydrogenase complexes (PDC3) showed a 12-fold rise in *pgr5* under HL. Conversely, PDC3 was downregulated in *pgrl1* by -2-fold under HL and was raised by 1.9-fold in WT. D-lactate dehydrogenase (DLD1) expression was upregulated by 10.7-fold in *pgrl1* and 5-fold in *pgr5*. DLD2 expression was increased by 3-fold in both *pgrl1* and *pgr5*. DLA2 expression elevated by 4-fold in *pgr5* and by 3.3-fold in *pgrl1*, whereas it was reduced in WT under HL.

5.3 Discussion

HL intensity causes impairment of growth and shows a detrimental effect on algal biomass of pgrl1 and pgr5 mutants (Yadav et al., 2020). The reduced biomass could be due to the limitation of photosynthesis and oxidative stress. In the present study, we used metabolite profiling to investigate the adaptive mechanisms of pgrl1 and pgr5 under HL conditions. Our previous study in chapter 3 shows that HL induces ROS production, leads to autophagy, and generation of neutral lipids in pgrl1 and pgr5. The current study also elucidates the regulatory insights of primary metabolites in pgrl1 and pgr5 under HL.

5.3.1 Alternation of nitrogen metabolism under HL

Amino acids serve as a precursor of many metabolites including pyrimidines, nucleotides, polyamines, glutathione, etc. The major metabolic change observed under HL is the variation of amino acid metabolism (Figure 5.1, Figure 5.9). HL-adapted cells induce a great variety of amino acids due to the activation of increased protein degradation or *de novo* amino acid production caused by photodamage of photosynthetic apparatus (McKim & Durnford, 2006; Chen et al., 2017; Wang et al., 2018). Under HL, increased amino acid levels provide dietary support for plant growth (Ufaz et al., 2008). A decrease in protein content in *pgrl1* and *pgr5* suggests the degradation of proteins into free amino acids which might utilize as an alternative substrate for mitochondrial ATP generation (Huang and Jander, 2017; Hildebrandt et al., 2018). The levels of aromatic amino acids (Phe) and branched-chain amino acids (Val and Ile) were

increased in *pgr5* as a result of increased protein catabolism under HL. Similarly, the increased Glu levels in *pgr5* compared to WT and *pgrl1* strongly suggests that glutamate has a significant impact on reducing oxidative stress, i.e. ROS, produced under HL stress (Qiu et al., 2020). Glu is also known as an essential amino acid for photosynthesis because it serves as a precursor for chlorophyll synthesis (Wettstein et al., 1995; Forde et al., 2007) and it also acts as a donor in the production of major N-containing molecules such as amino acids, nucleotides, chlorophyll, and polyamines (Ireland and Lea, 1999).

We also noticed a 2.5-fold increase in photorespiration metabolites such as glycine and serine in pgr5, which serve a role in preserving the photosynthetic apparatus (Voss et al., 2013; Timm et al., 2013; Hossain et al., 2017;). This result provides a link between CET-PSI and photorespiration. PGR5 under HL might be involved in the alternative pathways which is helping in the energy balancing mechanism. Under HL photorespiration enable to use of the reducing power operation as a photoprotective mechanism to prevent photoinhibition (Takahashi and Badger, 2011). Ser is essential for cell proliferation and involved in the biosynthesis of numerous metabolites such as amino acids, phospholipids, and sphingolipids (Kalhan & Hanson, 2012) and is also implicated in signaling cascades (Chaneton et al., 2012).

5.3.2 Enhancement of carbohydrate, fatty acids, and organic acids under HL

Carbohydrates are the primary products of photosynthesis (Blechschmidt-Schneider et al., 1989) (Figure 5.1). The increased availability of Fru upon HL treatment is more pronounced in pgr5 as compared to WT, accumulation of Fru in pgr5 in the form of carbon might be channel towards the formation of fatty acid as reported earlier. However, Fru levels were not changed significantly in pgr11. An increase in Fru in pgr5 under HL could allow for the use of alternative carbon sources as previously reported in Pgr11 Helianthus tuberosus, which can be utilized as a renewable biomass resource for bioenergy because it can withstand more severe circumstances

than most crop production (Rossini et al., 2019). Ribofuranose levels in pgr5 rise under HL proves an increase in TCA cycle intermediate pathway. Previously it was reported that electron acceptors in redox reactions such as NAD, FAD, and NAPD, and containing D-ribofuranose moiety as a functional component, are involved in several metabolic pathways such as glycolysis, the CAC, and the electron transport chain (Wulf et al., 1997). We observed Urd and uracil levels were enhanced along with Ribf induction in the pgr5 under HL in agreement with the earlier report (Lee et al., 2012). This demonstrates that the metabolism of amino acids and amines which prove a source of nitrogen is essential in photoacclimation to increased light intensities (Davis et al., 2013). Polyols (Aris, I1P, and DP), linked to osmotic stress response, were significantly increased in pgr5 under HL, to eliminate excess oxidizing counterparts and bring the cell's redox state into equilibrium, which might help pgr5 to tolerate the light stress. PEC, representing one of the major fatty acids in triacylglycerols for biodiesel production was significantly increased in the pgr5 mutant under HL (Chen et al., 2016). Also, we found a significant increase of metabolites linked to glycerol metabolism (Gg and GA3P) in *pgr5* under HL, which provides osmotic adjustment (He et al., 2009). GA3P is very important for DAG and TAG synthesis through the Kennedy pathway and acts as a major link for carbon transfer between carbohydrate metabolism and lipid metabolism (Johnson and Aldric, 2013). Because TAGs have a glycerol backbone and fatty acids, glycerol is a necessary component for their production (FAs). This data supports our recent report that under HL, GA3P levels rise, resulting in an increase in lipid content production in the pgr5 mutant. As a result, it indicates that increased GA3P and neutral lipid synthesis are necessary for lipid accumulation in C. reinhardtii.

5.3.3 Alternative defense metabolites are activated under HL

Proline is a stress biomarker that has been produced in response to light stress in *Vigna* radiata (Arora et al., 2002) and salt stress in *C. reinhardtii* (Bazzani et al., 2021; Meena et al.,

2019). Increased Pro content in pgr5 might help to minimize the amount of ROS produced in HL circumstances (Hayat et al., 2012) (Figure 5.1). Pro also protects PSII from the adverse effects of oxidative stress (Nishiyama et al., 2004) and helps in maintaining membrane integrity or osmotic balance, protecting membranes to minimize electrolyte leakage (Hayat et al., 2012). Polyamines regulate key functions such as cell division, differentiation, membrane stability, reproduction, and senescence (Galston and Sawhney, 1990). Furthermore, polyamines regulate key functions such as cell division, differentiation, membrane stability, reproduction, and senescence (Galston and Sawhney, 1990). It was involved in the production of chlorophyll and photosynthetic membrane complexes, as well as antioxidant enzyme activity and oxidative stress management (Navakoudis et al., 2007). We found increased Put content in the pgr5 under HL due to an increase in ROS content in pgr5. However, the Put level was down-regulated in the pgrl1 mutant and did not change in the WT. Polyamine interacts with negatively charged macromolecules such as proteins and nucleic acids to stabilize their structure, implying that downregulation of Put under HL in pgrl1 aids in cell structure stabilization under HL. Polyamines have been found to have the ability to convert unsaturated fatty acids to saturated fatty acids, which aids in the protection of membrane stability and permeability. However, in the case of the pgr5 mutant, the increase in Put concentration indicates that Put could not bind to the phospholipid of the thylakoid membrane, and therefore the membrane stability deteriorated, contributing to the degradation of membrane lipid to TAG biosynthesis. Increased Put content may result in increased antioxidant enzyme activity and ROS scavenging capabilities, allowing the pgr5 mutant to tolerate stress better than the pgrl1 (Wu et al., 2017). As a result, a surge in ROS production in the stress-tolerant pgr5 mutant is typically accompanied by an increase in antioxidant metabolites like Put and proline to attenuate ROS produce due to light stress. Therefore, Pro functions as an osmolyte for osmotic adjustment and also aids in the maintenance of subcellular structures, and the scavenging of oxidative stress. Consequently increasing Put levels also stimulate catabolism, leading to an increase in ROS and antioxidant systems as well as binding to the phospholipids of the thylakoid membrane. Thus Put can alter the membrane stability and also help in the structure and function of photosynthetic apparatus under stress conditions.

5.3.4 The study of metabolite correlations yields new insights

KEGG enrichment analysis was performed on metabolites, revealing the top 25 most enriched pathways (Figure 5.3& 5.4). Under HL, in *pgr5*, pantothenate CoA biosynthesis and linoleic acid metabolism were markedly enhanced. Pantothenate is a necessary precursor for the synthesis of CoA, a ubiquitous and important cofactor involved in phospholipid formation, lipid metabolism and degradation, and the tricarboxylic acid cycle (Leonardi and Jackowski, 2007). The de novo synthesis of linoleic acids is estimated to result from acetate fragments created during carbohydrate catabolism. The ultimate metabolites of fatty acid production in plants are usually linolenic acids. Metabolites related to glycolysis, TCA cycle, and pyruvate metabolism were upregulated in WT, *pgr11*, and *pgr5* but increased significantly in *pgr5* under HL, resulting in the funneling of carbon sources towards lipid metabolism which is in agreement with previous reports.

Correlation analysis was used to compare the metabolite profiles of WT, *pgrl1*, and *pgr5* under light stress (Figure 5.7). The TCA cycle is indeed the main and intermediate step of the metabolite pathway. TCA intermediates are used for the biosynthesis of glucose, amino acids, and fatty acids. An increase in the interaction of amino acids with the TCA cycle stimulates acetyl-CoA for *de novo* synthesis of fatty acids in *pgrl1* and *pgr5* under HL. The strong correlation between amino acid, nucleotide, and carboxylic acid suggests essential roles associated with photosynthesis, respiration, and growth and development in *pgr5* under HL. Amino acid catabolism (Ala, Leu, and Glu) might lead to TAG metabolism by providing

carbon resources and ATP, especially in *pgr5* under HL which is in agreement with the earlier report (Liang *et al.* 2019). Under HL in *pgrl1* and *pgr5*, carbohydrates, polyols, amino acids, and the TCA cycle provide a rapid carbon energy source also in biological cell adaptation.

5.3.5 HL induced changes in expression of the gene of TCA cycle and TCA metabolites

Increased TCA cycle intermediates (TCA, FA, MA, and CA) in pgr5 confirm real-time PCR findings were MDH, IDH, FUM, and CIS transcripts significantly upregulated (Figure 5.8). We also observed an increase in DLA2, a subunit of the chloroplast pyruvate dehydrogenase complex, that produces acetyl-CoA during fatty acid biosynthesis in pgrl1 and pgr5 under HL. The increased TCA cycle intermediates might be due to an increase in carbon flow from glycolysis into the TCA cycle, which leads to an increase in the generation of reducing powers of NADH, ATP, and FADH2. Increase PDC, ACS1, and ACS3 transcripts enhance FA synthesis in pgr5 under HL (Shtaida et al., 2015). Further acetyl-CoA can be utilized to boost gluconeogenesis and other anabolic processes in the glyoxylate cycle, or it can be used to generate NADH for the respiratory chain and ATP in the Krebs cycle (Plancke et al., 2014). This result demonstrates that an increase in TCA cycle intermediate (MDH1, CIS2, FUM, and IDH2) in pgr5 which were the essential intermediate metabolic pathway connecting carbohydrates, fatty acids, and amino acid metabolism, is accelerated in pgr5 under HL, while they are downregulated in pgrl1 mutant that might be the reason fatty acid accumulation was less in pgrl1 compare to pgr5 under HL. ACH, OGD3, OGD2, SCLB1, and IDH3 few TCA cycle intermediates upregulated in both pgrl1 and pgr5 under HL suggesting algae enhancing respiration to produce the energy needed for the production of defense compounds to deal counteract oxidative stress caused under light stress. Thus our study shows that the TCA cycle can maintain the cell's oxidative and energy levels and also provide precursors for amino acid synthesis through the activation of malate, Fumarate, and citrate channels.

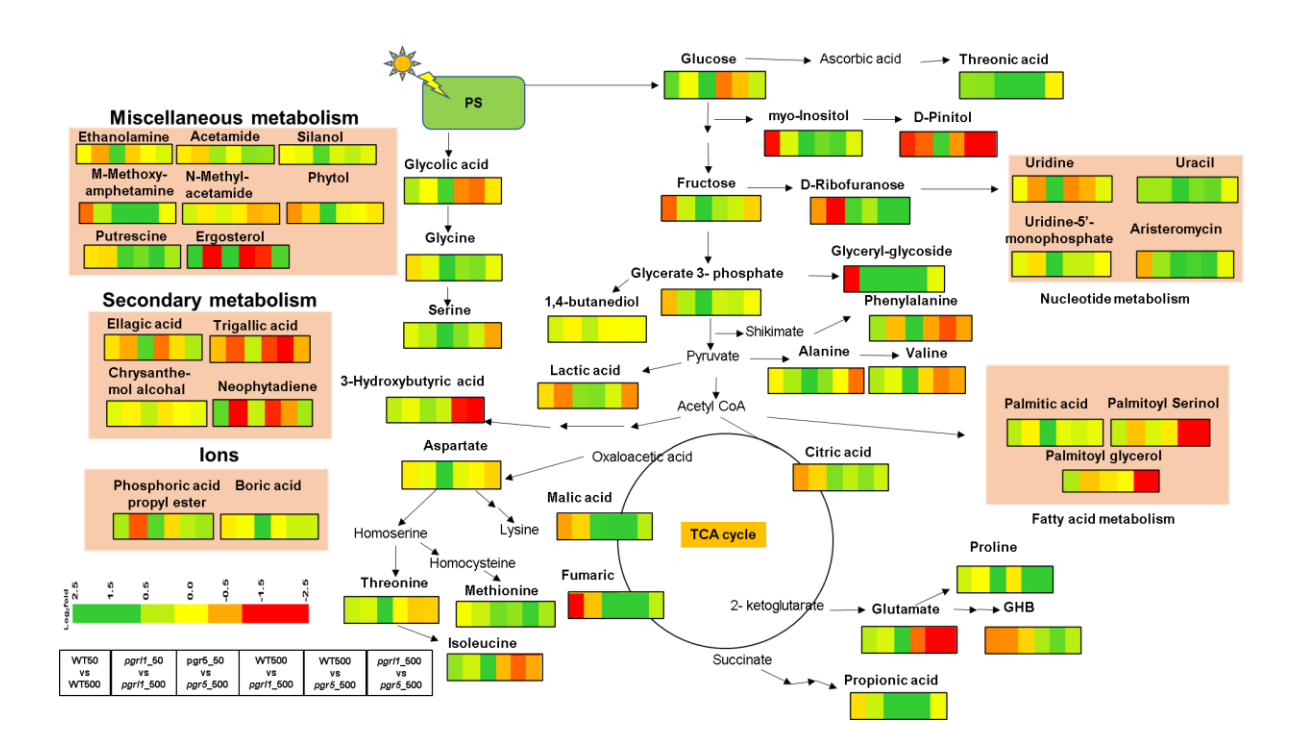


Figure 5.9 An overview of the proposed metabolite change in C. reinhardtii under high light conditions. The scale indicated a log 2 ratio of relative fold change from 2.5 to -2.5 (upregulation to downregulation), represented as a single horizontal box: WT50 vs WT500, pgrl50 vs pgrl1500, pgr50 vs pgr5 500, W500 vs pgrl1 500, W500 vs pgr5500, pgrl1500 vs pgr5500. Each metabolite value is an average of four biological replicates. WT, pgrl1 and pgr5 50, and WT, pgrl1 and pgr5 500, represent 50 and 500 μ mol photons m^{-2} s⁻¹.

5. 4 Conclusion

Changes in metabolites (amino acid metabolism, carbohydrate metabolism, fatty acid metabolism, carboxylic metabolism, nucleic acid metabolism) of *C. reinhardtii* in (cyclic electron-deficient mutant) *pgrl1* and *pgr5* under HL (500 mol photon m⁻² s⁻¹) are demonstrated. The fact that WT, *pgrl1*, and *pgr5* metabolites have a positive correlation showed that mutants are involved in a variety of metabolic pathways including amino acids, fatty acids, nucleotides, TCA, antioxidants, photosynthesis, photorespiration, and antioxidants. Also in the cyclic electron-deficient mutant, the production of metabolites such as amino acids, polyamines, and sugars ensures a steady supply of nutrients under HL stress. *pgr5* triggers a variety of alternate defense mechanisms, including Pro and Put synthesis, to help survive

stressful situations. Under HL, a considerable increase in polyamine (Put) implies that *pgr5* is protected from oxidative stress. Further, the TCA cycle, which connects fatty acids, carbohydrates, and protein metabolism, was enhanced in *pgrl1* and *pgr5* under HL. This discovery demonstrated that the TCA cycle, which is the major intermediate metabolic process that links carbohydrates, amino acid, and fatty acids metabolism, was enhanced substantially in *pgr5* compared to *pgrl1* under HL. Hence we conclude that the HL condition in *pgr5* induces metabolic disturbances, rerouting the energy acquired by photosynthesis for the formation of several metabolites of TCA, amino acids, and fatty acids.

Table 5.1 Relative concentration and fold changes of major metabolites in WT under normal and high light in *C. reinhardtii*.

Metabolites	Abbreviation	Annotation	WT_50	stdev	WT_500	stdev	p-values	Significance	fold change	log2fold change
N-Acetyl-beta- alanine	NAA	amino acid metabolism	1412.759	655.737	1227.694	507.3843	0.32497	ns	0.869004	-0.20256
Urea	Urea	amino acid metabolism	2558.865	717.581	4551.914	1215.981	0.32596	ns	1.77888	0.830969
Aristeromycin	Aris	polyols	6687.28	3081.847	4814.721	1439.689	0.316276	ns	0.719982	-0.47397
2-Phenyl-1,3- propanediol monocarbamate	PPM	glycerol metabolism	3882.188	447.3136	4057.386	831.6361	0.325367	ns	1.045129	0.063681
1-(3-Pyridinyl)-1,4- butanediol	PB	carboxylic acid metabolism	830.1163	340.4102	1036.627	241.3893	0.324604	ns	1.248773	0.320511
Monopalmitoyl serinol	MP	fatty acid metabolism	8359.333	3937.938	11256.68	5068.711	0.323692	ns	1.3466	0.429321
Uridine5- monophosphate	UMP	nucleic acid metabolism	1743.313	364.5676	2009.037	1092.387	0.309644	ns	1.152425	0.204673
Threonic acid	ThA	carboxylic acid metabolism	873.4948	198.6555	1507.369	631.8105	0.308485	ns	1.725676	0.787162
Ellagic acid	Ela	secondary metabolism	2819.879	1509.604	2523.966	655.8851	0.30559	ns	0.895062	-0.15994
Fumaric acid	FA	TCA cycle	450.2498	63.91332	126.7559	30.88636	0.307094	ns	0.281523	-1.82867
Palmitoyl Serinol	PAG	fatty acid metabolism	447.3825	201.8082	675.3794	401.9633	0.308739	ns	1.509624	0.594189
Propionic acid	PA	carboxylic acid metabolism	1801.513	946.2163	1587.248	702.2712	0.307781	ns	0.881064	-0.18268
3-Hydroxybutyrate	ВНВ	carboxylic acid metabolism	436.4675	217.845	606.0106	219.4734	0.308923	ns	1.388444	0.473469
methoxyamphetamine	3MA	other metabolism	16836.1	12631.91	9264.81	3927.672	0.308253	ns	0.550294	-0.86172
Gama- hydroxybutyrate	GHB	carboxylic acid metabolism	320.937	123.9121	198.1013	81.72834	0.344181	ns	0.617259	-0.69605
Acetamide	ACE	other metabolism	33527.04	21575.13	31214.31	11745.72	0.344965	ns	0.931019	-0.10312
Ribitol	Rib	other metabolism	21254.43	8893.364	24368.34	9233.004	0.356909	ns	1.146506	0.197244
Tri-carboxylic acid	TCA	TCA cycle	10795.91	3990.04	10683.7	4108.033	0.340874	ns	0.989607	-0.01507
Carbamic acid	Carb	carboxylic acid metabolism	21791.88	13193.05	32304.51	17074.07	0.341627	ns	1.48241	0.567945
Chrysanthemol alcohal	Chry	secondary metabolism	1832.376	851.9357	2110.404	339.5783	0.288372	ns	1.151731	0.203804
Citric acid	CA	TCA cycle	2833.025	1504.15	1908.653	1121.055	0.287282	ns	0.673716	-0.56979
Ribofuranose	Ribf	carbohydrate metabolism	201.269	35.48173	131.9855	26.47664	0.2917	ns	0.655767	-0.60875
Fructose	Fru	carbohydrate metabolism	3378.07	1310.543	1798.512	786.5212	0.292229	ns	0.532408	-0.9094
Inositol pentaphosphate	IPP	carbohydrate metabolism	7900.459	3216.868	17789.23	9013.517	0.299751	ns	2.25167	1.170995
D-myo-Inositol-1- monophosphate (I1P)	I1P	polyols	24834.52	10505.44	9183.697	4326.374	0.253378	ns	0.369796	-1.4352
D-pinitol	DP	polyols	21529.32	20589.29	8988.41	4038.034	0.319447	ns	0.417496	-1.26017
Ergosterol	Erg	sterol metabolism	2300.806	1170.829	6451.88	3582.644	0.381921	ns	2.804183	1.48758
Ethanolamine	MEA	other metabolism	25653.85	12647.83	26174.28	12250.71	0.359029	ns	1.020287	0.028975
Trigallic acid	TG	secondary metabolism	5851.553	1981.71	4490.414	995.4244	0.356578	ns	0.767388	-0.38197
Glycerol 3 phosphate	GA3P	glycerol metabolism	93080.6	56182.34	70747.81	26184.68	0.36427	ns	0.76007	-0.3958
glyceryl-glycoside	Gg	glycerol metabolism	104687.7	91135.99	11223	8563.911	0.485654	ns	0.107205	-3.22156
Glycine	GLY	amino acid metabolism	11457.29	6890.968	10007.78	4025.279	0.025026	*	0.873486	-0.19514
Glycolic acid	GA	carboxylic acid metabolism	821.2211	400.1924	1239.851	445.1266	0.016105	*	1.509765	0.594324
Lactic acid	LA	carboxylic acid metabolism	18030.59	5729.973	15702.57	5405.797	0.017771	*	0.870885	-0.19945

L- alanine	L_Ala	amino acid metabolism	8494.832	2202.515	8138.991	3335.44	0.007352	**	0.958111	-0.06174
N-acetyl-L-aspartic acid	NALA	amino acid metabolism	6817.078	3287.347	6392.984	2929.644	0.006311	**	0.937789	-0.09266
Glutamate	Glu	amino acid metabolism	3543.071	1748.796	5040.573	2130.141	0.005208	**	1.422656	0.508587
L-Isoleucine	Ile	amino acid metabolism	3819.323	2026.922	6646.84	2956.085	0.007785	**	1.740319	0.799352
L-Phenylalanine	Phe	amino acid metabolism	3799.843	2164.108	6178.569	2856.24	0.014528	**	1.626006	0.701333
Threonine	Thr	amino acid metabolism	7021.133	4373.898	9240.276	4096.609	0.024751	*	1.316066	0.396232
L-Valine	L_Val	amino acid metabolism	4770.277	2136.973	7233.463	3129.793	0.040096	*	1.516361	0.600613
Neophytadiene	NPHY	secondary metabolism	3340.506	1488.413	7520.548	2600.367	0.065677	ns	2.25132	1.170771
N-methyl-acetamide	MA	other metabolism	3625.514	1561.409	4575.377	1015.02	0.12508	ns	1.261994	0.335705
Palmitic acid	PEC	fatty acid metabolism	7005.617	3905.613	10127.15	3243.921	0.152569	ns	1.445576	0.531644
Phosphoric acid propyl ester	PAPE	ions	9094.687	4729.816	13888.76	6304.84	0.251223	ns	1.527129	0.610822
Phytol	Phy	other metabolism	2063.918	1284.575	1334.472	676.7728	0.468135	ns	0.646572	-0.62912
Putrescine	Put	polyamine metabolism	20992.86	9113.896	18910.1	6858.979	0.412881	ns	0.900787	-0.15074
Serine	Ser	amino acid metabolism	4934.894	2388.466	5715.411	2595.833	0.252747	ns	1.158163	0.211838
Silanol	Sil	other metabolism	120281	44403.55	121435.3	29492.85	0.30448	ns	1.009597	0.01378
Trisaminol	Met	metabolism	139587.1	57990.84	146210	26679.96	0.388863	ns	1.047446	0.066876
Uracil	Uracil	nucleic acid metabolism	1986.222	1028.212	3239.618	1488.524	0.991932	ns	1.631045	0.705796
Uridine	Urd	nucleic acid metabolism	2823.672	2163.355	2900.089	1606.902	0.581462	ns	1.027063	0.038525
Proline	Pro	amino acid metabolism	2149.198	1109.311	2708.008	1398.072	0.588597	ns	1.260009	0.333434
Boric acid	BA	ions	1642.322	221.8338	1517.184	412.2144	0.45421	ns	0.923804	-0.11434
Malic acid	Ma	TCA cycle	5484.682	1760.769	3747.878	845.6073	0.1	ns	0.683336	-0.54933

Table 5.2 Relative concentration and fold changes of major metabolites in *pgrl1* under normal and high light in *C. reinhardtii*.

Metabolites	abbreviation	annotation	pgrl1_50	stdev	pgrl1_500	stdev	p-values	Significance	fold change	log2fold change
N-Acetyl-beta-alanine	NAA	amino acid metabolism	1105.937	767.0471	979.5129	712.4857	0.332402	ns	0.885686	-0.17513
Urea	Urea	amino acid metabolism	4123.581	1282.627	3552.385	2204.805	0.331888	ns	0.861481	-0.21511
Aristromycin	Aris	polyols	7270.034	728.9842	12088.95	6030.23	0.329273	ns	1.662847	0.733655
2-Phenyl-1,3- propanediol monocarbamate	PPM	glycerol metabolism	3953.088	144.4052	3722.426	1150.389	0.35204	ns	0.94165	-0.08674
1-(3-Pyridinyl)-1,4- butanediol	PB	carboxylic acid metabolism	1059.791	54.00173	1025.271	298.1529	0.351005	ns	0.967427	-0.04777
Monopalmitoyl serinol	MP	fatty acid metabolism	13272.5	2587.002	10379.86	5545.825	0.350939	ns	0.782058	-0.35465
Uridine5- monophosphate	UMP	nucleic acid metabolism	3065.538	652.7455	2698.35	1320.91	0.33685	ns	0.880221	-0.18406
Threonic acid	ThA	carboxylic acid metabolism	2574.946	675.0715	4691.107	2523.992	0.335202	ns	1.821827	0.865386
Ellagic acid	Ela	secondary metabolism	2043.806	429.4105	1443.102	698.5203	0.345404	ns	0.706086	-0.50209
Fumaric acid	FA	TCA cycle	1115.695	77.86108	870.6557	405.3824	0.342605	ns	0.78037	-0.35777
Palmitoyl serinol	PAG	fatty acid metabolism	847.1671	201.5164	670.4631	379.9121	0.341545	ns	0.791418	-0.33749
Propionic acid	PA	carboxylic acid metabolism	3697.595	648.2185	4824.314	2899.878	0.340823	ns	1.304717	0.383736
3-Hydroxybutyrate	ВНВ	carboxylic acid metabolism	711.97	59.37177	789.3315	375.776	0.346389	ns	1.108658	0.148815
methoxyamphetamine	3MA	other metabolism	24685.61	2626.578	34607.76	18299.62	0.34691	ns	1.401941	0.487425
Gama- hydroxybutyrate	GHB	carboxylic acid metabolism	482.3631	114.7591	305.7194	125.2603	0.395317	ns	0.633795	-0.65791
Acetamide	ACE	other metabolism	40210.14	7932.219	33226.95	13250.94	0.394552	ns	0.826333	-0.27521
Ribitol	Rib	other metabolism	29912.87	1361.598	24074.99	11433.67	0.357752	ns	0.804837	-0.31323
Tri-carboxylic acid	TCA	TCA cycle	20897.21	889.1993	18936.93	7549.099	0.32871	ns	0.906194	-0.14211
Carbamic aicd	Carb	carboxylic acid metabolism	57284.72	24315.35	38845.87	27713.8	0.31957	ns	0.678119	-0.56039
Chrysanthemol alcohol	Chry	secondary metabolism	1985.773	165.1971	1914.078	592.6515	0.233281	ns	0.963896	-0.05305
Citric acid	CA	TCA cycle	3151.391	160.0721	2648.457	989.6349	0.233153	ns	0.840409	-0.25084
Ribofuranose	Ribf	carbohydrate metabolism	831.4595	1171.15	199.1759	64.68101	0.231367	ns	0.23955	-2.0616
Fructose	Fru	carbohydrate metabolism	2088.199	482.9398	2775.426	1451.709	0.2291	ns	1.329101	0.41045
Inositol pentaphosphate	IPP	carbohydrate metabolism	9602.634	7937.257	10308.68	7100.635	0.2319	ns	1.073527	0.102358
D-myo-Inositol-1- monophosphate (I1P)	I1P	polyols	15858.25	5585.754	18948.41	17353.29	0.23481	ns	1.194861	0.256843
D-pinitol	DP	polyols	11029.34	4017.603	5866.662	562.3184	0.247022	ns	0.531914	-0.91074
Ergosterol	Erg	sterol metabolism	5509.661	2352.157	1106.662	905.0203	0.22643	ns	0.200858	-2.31575
Ethanolamine	MEA	other metabolism	30700.09	6453.488	21425.63	13242.48	0.209872	ns	0.697901	-0.51891
Trigallic acid	TG	secondary metabolism	4139.836	1089.799	2062.072	673.2749	0.17645	ns	0.498105	-1.00548
Glycerol 3 phosphate	GA3P	glycerol metabolism	61653.17	21415.72	90662.9	44926.31	0.169915	ns	1.470531	0.556337
glyceryl-glycoside	Gg	glycerol metabolism	17772.76	24520.93	88324.89	92403.56	0.258504	ns	4.969678	2.313152
Glycine	GLY	amino acid metabolism	15402.5	1130.885	17467.37	12499.59	0.548241	ns	1.13406	0.181498
Glycolic acid	GA	carboxylic acid metabolism	766.8506	50.9397	770.0196	356.5025	0.56872	ns	1.004133	0.00595
Lactic acid	LA	carboxylic acid metabolism	50201.85	6553.524	30223.08	12290.98	0.569293	ns	0.602031	-0.73209

L- alanine	L_Ala	amino acid metabolism	9677.422	3279.823	14718.99	7142.746	0.36758	ns	1.520961	0.604984
N-acetyl-L-aspartic acid	NALA	amino acid metabolism	6533.119	1904.367	7380.779	5739.546	0.409546	ns	1.129748	0.176001
Glutamate	Glu	amino acid metabolism	2315.208	1501.202	2790.592	1540.295	0.417724	ns	1.205331	0.26943
Isoleucine	Ile	amino acid metabolism	3931.032	363.818	5032.305	2698.24	0.422779	ns	1.280149	0.356311
Phenylalanine	Phe	amino acid metabolism	5594.863	1003.081	4316.922	2757.683	0.433526	ns	0.771587	-0.3741
Threonine	Thr	amino acid metabolism	7436.781	370.2696	9030.877	5645.115	0.423082	ns	1.214353	0.280188
L-Valine	L_Val	amino acid metabolism	5459.035	468.931	6232.522	3814.899	0.438466	ns	1.141689	0.19117
Neophytadiene	NPHY	secondary metabolism	10351.25	3366.255	3112.783	556.9384	0.446884	ns	0.300716	-1.73353
N-methyl-acetamide	MA	other metabolism	4641.344	441.9163	4297.688	1534.31	0.381787	ns	0.925958	-0.11098
Palmitic acid	PEC	fatty acid metabolism	12063.85	766.6871	11559.81	3332.772	0.380744	ns	0.958219	-0.06157
Phosphoric acid propyl ester	PAPE	ions	23835.64	7736.007	12011.83	6064.6	0.378703	ns	0.503944	-0.98866
Phytol	Phy	other metabolism	1809.484	564.2554	1513.8	1211.046	0.279372	ns	0.836592	-0.2574
Putrescine	Put	polyamine metabolism	44172.99	9728.619	38235.22	28408.26	0.279868	ns	0.865579	-0.20826
Serine	Ser	amino acid metabolism	7145.098	1185.26	10567.3	6332.784	0.2387	ns	1.478958	0.564581
Silanol	Sil	other metabolism	132483.8	4900.819	146611.9	48158.6	0.265828	ns	1.10664	0.146186
Trisaminol	Met	other metabolism	193815.7	25569.12	254295.9	126760	0.371987	ns	1.31205	0.391823
Uracil	Uracil	nucleic acid metabolism	3913.476	859.9467	6330.976	4015.335	0.832098	ns	1.617737	0.693977
Uridine	Urd	nucleic acid metabolism	2751.308	446.4903	1821.299	950.0505	0.253867	ns	0.661976	-0.59515
Proline	Pro	amino acid metabolism	2490.594	877.2425	2491.973	1175.558	0.43971	ns	1.000554	0.000799
Boric acid	BA	ions	1475.063	265.3594	1545.301	548.0824	0.518197	ns	1.047617	0.067111
Malic acid	Ma	TCA cycle	15938.51	1119.37	13481.93	6250.996	#DIV/0!	ns	0.845871	-0.24149

Table 5.3 Relative concentration and fold changes of major metabolites in *pgr5* under normal and high light in *C. reinhardtii*.

Metabolites	abbreviation	annotation	pgr5_50	stdev	pgr5_500	stdev	p-values	Significance	fold change	log2fold change
N-Acetyl-beta-alanine	NAA	amino acid metabolism	742.0933	153.6656	1415.271	481.9932	0.002179	**	1.907134	0.931406
Urea	Urea	amino acid metabolism	1616.784	207.8133	2047.98	865.3264	0.002187	**	1.266699	0.341074
Aristromycin	Aris	polyols	3571.031	3009.313	13351.55	12650.89	0.002186	**	3.738849	1.902594
2-Phenyl-1,3- propanediol monocarbamate	PPM	glycerol metabolism	3165.954	2638.005	4095.076	1962.707	0.002483	**	1.293473	0.37125
1-(3-Pyridinyl)-1,4- butanediol	PB	carboxylic acid metabolism	746.4474	534.8214	1057.824	504.5044	0.0025	**	1.417145	0.502988
Monopalmitoyl serinol	MP	fatty acid metabolism	1776.491	1112.933	2143.318	864.869	0.002494	**	1.20649	0.270816
Uridine5- monophosphate	UMP	nucleic acid metabolism	953.5602	422.8425	2711.399	1267.578	0.00249	**	2.843448	1.507641
Threonic acid	ThA	carboxylic acid metabolism	1141.949	630.0338	4469.809	1708.181	0.002535	**	3.914194	1.968715
Ellagic aicd	Ela	secondary metabolism	911.8017	47.81695	2209.95	1852.85	0.002637	**	2.423717	1.277221
Fumaric acid	FA	TCA cycle	341.5663	192.0791	1203.062	755.0979	0.002666	**	3.522193	1.816474
Palmitoyl serinol	PAG	fatty acid metabolism	212.2166	112.6758	191.5105	58.22633	0.002677	**	0.902429	-0.14811
Propionic acid	PA	carboxylic acid metabolism	1518.598	1171.386	5162.374	1889.513	0.002653	**	3.399433	1.765294
3-Hydroxybutyrate	ВНВ	carboxylic acid metabolism	141.2345	71.10831	234.0058	114.7507	0.00277	**	1.65686	0.728451
methoxyamphetamine	3MA	other metabolism	7929.965	4887.541	36733.7	15312.59	0.002748	**	4.632265	2.211718
Gama- hydroxybutyrate	GHB	carboxylic acid metabolism	513.91	281.7993	432.9492	204.4289	0.003866	**	0.842461	-0.24732
Acetamide	ACE	other metabolism	35263	20019.72	56995.47	16691	0.003827	**	1.616297	0.692692
Ribitol	Rib	other metabolism	13290.15	7377.964	25301.98	8077.504	0.004975	**	1.903814	0.928892
Tri-carboxylic acid	TCA	TCA cycle	8263.585	4673.316	22003.02	9888.567	0.005764	**	2.662648	1.412862
Carbamic aicd	Carb	carboxylic acid metabolism	20266.83	10908.67	51631.81	26547.55	0.006803	**	2.547602	1.34914
chrysanthemol alcohol	Chry	secondary metabolism	1526.472	1144.291	2103.027	724.5221	0.009577	**	1.377704	0.462266
Citric acid	CA	TCA cycle	1788.784	1261.695	3472.012	1313.516	0.009585	**	1.94099	0.956793
Ribofuranose	Ribf	carbohydrate metabolism	253.9643	103.5246	636.5509	268.388	0.009728	**	2.506458	1.32565
Fructose	Fru	carbohydrate metabolism	498.9556	349.1634	2321.858	2030.26	0.009705	**	4.653436	2.218296
Inositol pentaphosphate	IPP	carbohydrate metabolism	4638.377	2672.938	13787.1	10432.19	0.009859	**	2.972398	1.571627
D-myo-Inositol-1- monophosphate (I1P)	I1P	polyols	3813.78	2944.593	22426.48	18120.04	0.010963	**	5.880382	2.55591
D-pinitol	DP	polyols	467.1167	189.9706	1232.686	737.0885	0.013519	**	2.638924	1.39995
Ergosterol	Erg	sterol metabolism	899.2669	35.35925	2715.748	994.545	0.013548	**	3.019957	1.594528
Ethanolamine	MEA	other metabolism	10283.03	5795.552	26012.53	18775.19	0.01375	**	2.529656	1.338941
Trigallic acid	TG	secondary metabolism	1099.594	155.3031	1506.274	525.1614	0.016391	*	1.369846	0.454014
Glycerol 3 phosphate	GA3P	glycerol metabolism	32725.15	32327.03	96104.79	50963.25	0.01634	*	2.936726	1.554209
glyceryl-glycoside	Gg	glycerol metabolism	11837.56	19709.53	99494.21	133101.4	0.02815	*	8.40496	3.071241

Glycine	GLY	amino acid metabolism	5472.106	3158.746	19325.36	9105.234	0.05246	ns	3.531612	1.820327
Glycolic acid	GA	carboxylic acid metabolism	274.1875	141.8121	694.288	355.8792	0.060463	ns	2.532165	1.340371
Lactic acid	LA	carboxylic acid metabolism	10554.52	6121.985	19195.38	11092.73	0.060633	ns	1.818687	0.862897
L- alanine	L_Ala	amino acid metabolism	1692.315	679.5881	8236.38	4911.734	0.066253	ns	4.866932	2.283013
N-acetyl-L-aspartic acid	NALA	amino acid metabolism	2140.606	1471.218	6173.282	4461.508	0.070821	ns	2.883894	1.528018
Glutamate	Glu	amino acid metabolism	99.14632	66.77145	339.7139	102.7318	0.073766	ns	3.426389	1.776689
Isoluecine	Ile	amino acid metabolism	743.559	497.0597	3541.572	1515.136	0.073846	ns	4.763001	2.251871
Phenyalaine	Phe	amino acid metabolism	524.1996	432.6568	3018.087	1250.027	0.075934	ns	5.757515	2.525446
Threonine	Thr	amino acid metabolism	1619.056	1010.235	7466.153	3334.644	0.077828	ns	4.611423	2.205212
L-Valine	L_Val	amino acid metabolism	1009.475	551.9279	4352.925	1996.04	0.082566	ns	4.31207	2.10838
Neophytadiene	NPHY	secondary metabolism	3759.235	1829.872	5048.344	1333.554	0.085371	ns	1.342918	0.425371
N-methyl-acetamide	MA	other metabolism	2783.202	2047.734	3343.436	1460.825	0.086399	ns	1.201291	0.264586
Palmitic acid	PEC	fatty acid metabolism	4448.275	2854.087	12675.7	3806.704	0.086739	ns	2.849576	1.510747
Phosphoric acid propyl ester	PAPE	ions	8430.179	5979.908	19578.74	5618.785	0.094303	ns	2.322459	1.215653
Phytol	Phy	other metabolism	433.0912	240.4247	1377.711	839.7588	0.105499	ns	3.18111	1.66953
Putrescine	Put	polyamine metabolism	23183.31	13778.08	59513.64	27894.49	0.1065	ns	2.567089	1.360133
Serine	Ser	amino acid metabolism	1764.382	1190.54	7327.661	3853.79	0.147801	ns	4.153104	2.05419
Silanol	Sil	other metabolism	72223.29	34856.03	169967.8	49110.37	0.157172	ns	2.353366	1.234726
Trisaminol	Met	other metabolism	193637.2	135752.4	394684.8	79997.91	0.29525	ns	2.03827	1.027345
Uracil	Uracil	nucleic acid metabolism	1191.46	733.1408	7109.518	3569.108	0.050897	ns	5.967064	2.577021
Uridine	Urd	nucleic acid metabolism	639.106	548.2075	2119.13	1058.206	0.126182	ns	3.315773	1.729345
Proline	Pro	amino acid metabolism	1324.459	980.8869	8034.176	3484.042	0.164593	ns	6.066006	2.600747
Boric acid	BA	ions	661.1197	262.7718	2006.205	683.5511	0.430402	ns	3.034556	1.601486
Malic acid	Ma	TCA cycle	7017.662	3832.345	19272.23	5343.708	#DIV/0!	ns	2.746247	1.457461

Table 5.4 Relative concentration and fold changes of major metabolites in WT and pgrl1 under high light in C. reinhardtii.

Metabolites	abbreviation	annotation	WT_500	stdev	pgrl1_500	stdev	p-values	Significance	fold change	log2fold change
N-Acetyl-beta-alanine	NAA	amino acid metabolism	1227.694	507.3843	979.5129	712.4857	0.02193	*	0.797848	-0.32581
Urea	Urea	amino acid metabolism	4551.914	1215.981	3552.385	2204.805	0.021796	*	0.780416	-0.35769
Aristromycin	Aris	polyols	4814.721	1439.689	12088.95	6030.23	0.021341	*	2.510831	1.328165
2-Phenyl-1,3- propanediol monocarbamate	PPM	glycerol metabolism	4057.386	831.6361	3722.426	1150.389	0.024355	*	0.917444	-0.12431
1-(3-Pyridinyl)-1,4- butanediol	PB	carboxylic acid metabolism	1036.627	241.3893	1025.271	298.1529	0.024167	*	0.989045	-0.01589
Monopalmitoyl serinol	MP	fatty acid metabolism	11256.68	5068.711	10379.86	5545.825	0.024128	*	0.922107	-0.11699
Uridine5- monophosphate	UMP	nucleic acid metabolism	2009.037	1092.387	2698.35	1320.91	0.023685	*	1.343106	0.425573
Threonic acid	ThA	carboxylic acid metabolism	1507.369	631.8105	4691.107	2523.992	0.023966	*	3.112116	1.637896
Ellagic aicd	Ela	secondary metabolism	2523.966	655.8851	1443.102	698.5203	0.025413	*	0.57176	-0.80652
Fumaric acid	FA	TCA cycle	126.7559	30.88636	870.6557	405.3824	0.024844	*	6.86876	2.78005
Palmitoyl serinol	PAG	fatty acid metabolism	675.3794	401.9633	670.4631	379.9121	0.025162	*	0.992721	-0.01054
Propionic acid	PA	carboxylic acid metabolism	1587.248	702.2712	4824.314	2899.878	0.025117	*	3.03942	1.603796
3-Hydroxybutyrate	ВНВ	carboxylic acid metabolism	606.0106	219.4734	789.3315	375.776	0.026652	*	1.302504	0.381288
methoxyamphetamine	3MA	other metabolism	9264.81	3927.672	34607.76	18299.62	0.026699	*	3.735399	1.901262
Gama- hydroxybutyrate	GHB	carboxylic acid metabolism	198.1013	81.72834	305.7194	125.2603	0.03925	*	1.543248	0.625969
Acetamide	ACE	other metabolism	31214.31	11745.72	33226.95	13250.94	0.039283	*	1.064478	0.090146
Ribitol	Rib	other metabolism	24368.34	9233.004	24074.99	11433.67	0.04069	*	0.987962	-0.01747
Tri-carboxylic acid	TCA	TCA cycle	10683.7	4108.033	18936.93	7549.099	0.040423	*	1.772506	0.82579
Carbamic aicd	Carb	carboxylic acid metabolism	32304.51	17074.07	38845.87	27713.8	0.046485	*	1.20249	0.266025
chrysanthemol alcohol	Chry	secondary metabolism	2110.404	339.5783	1914.078	592.6515	0.051886	ns	0.906972	-0.14087
Citric acid	CA	TCA cycle	1908.653	1121.055	2648.457	989.6349	0.05166	ns	1.387605	0.472597
Ribofuranose	Ribf	carbohydrate metabolism	131.9855	26.47664	199.1759	64.68101	0.052285	ns	1.509074	0.593664
Fructose	Fru	carbohydrate metabolism	1798.512	786.5212	2775.426	1451.709	0.052295	ns	1.543179	0.625905
Inositol pentaphosphate	IPP	carbohydrate metabolism	17789.23	9013.517	10308.68	7100.635	0.053143	ns	0.57949	-0.78714
D-myo-Inositol-1- monophosphate (I1P)	I1P	polyols	9183.697	4326.374	18948.41	17353.29	0.046085	*	2.063266	1.04493
D-pinitol	DP	polyols	8988.41	4038.034	5866.662	562.3184	0.054208	ns	0.652692	-0.61553
Ergosterol	Erg	sterol metabolism	6451.88	3582.644	1106.662	905.0203	0.051139	ns	0.171525	-2.54351
Ethanolamine	MEA	other metabolism	26174.28	12250.71	21425.63	13242.48	0.046144	*	0.818576	-0.28881
Trigallic acid	TG	secondary metabolism	4490.414	995.4244	2062.072	673.2749	0.042008	*	0.459216	-1.12275
Glycerol 3 phosphate	GA3P	glycerol metabolism	70747.81	26184.68	90662.9	44926.31	0.039969	*	1.281494	0.357827
glyceryl-glycoside	Gg	glycerol metabolism	11223	8563.911	88324.89	92403.56	0.054884	ns	7.869988	2.976361

Glycine	GLY	amino acid metabolism	10007.78	4025.279	17467.37	12499.59	0.105816	ns	1.74538	0.803541
Glycolic acid	GA	carboxylic acid metabolism	1239.851	445.1266	770.0196	356.5025	0.120677	ns	0.621058	-0.6872
Lactic acid	LA	carboxylic acid metabolism	15702.57	5405.797	30223.08	12290.98	0.11973	ns	1.924722	0.94465
L- alanine	L_Ala	amino acid metabolism	8138.991	3335.44	14718.99	7142.746	0.151417	ns	1.808453	0.854756
N-acetyl-L-aspartic acid	NALA	amino acid metabolism	6392.984	2929.644	7380.779	5739.546	0.168875	ns	1.154512	0.207284
Glutamate	Glu	amino acid metabolism	5040.573	2130.141	2790.592	1540.295	0.171989	ns	0.553626	-0.85302
Isoluecine	Ile	amino acid metabolism	6646.84	2956.085	5032.305	2698.24	0.165824	ns	0.757097	-0.40145
Phenyalaine	Phe	amino acid metabolism	6178.569	2856.24	4316.922	2757.683	0.16161	ns	0.698693	-0.51727
Threonine	Thr	amino acid metabolism	9240.276	4096.609	9030.877	5645.115	0.156789	ns	0.977338	-0.03307
L-Valine	L_Val	amino acid metabolism	7233.463	3129.793	6232.522	3814.899	0.156613	ns	0.861624	-0.21487
Neophytadiene	NPHY	secondary metabolism	7520.548	2600.367	3112.783	556.9384	0.1543	ns	0.413904	-1.27263
N-methyl-acetamide	MA	other metabolism	4575.377	1015.02	4297.688	1534.31	0.142649	ns	0.939308	-0.09033
Palmitic acid	PEC	fatty acid metabolism	10127.15	3243.921	11559.81	3332.772	0.142371	ns	1.141468	0.19089
Phosphoric acid propyl ester	PAPE	ions	13888.76	6304.84	12011.83	6064.6	0.146696	ns	0.86486	-0.20946
Phytol	Phy	other metabolism	1334.472	676.7728	1513.8	1211.046	0.142202	ns	1.134381	0.181905
Putrescine	Put	polyamine metabolism	18910.1	6858.979	38235.22	28408.26	0.143388	ns	2.021947	1.015745
Serine	Ser	amino acid metabolism	5715.411	2595.833	10567.3	6332.784	0.19702	ns	1.848914	0.886678
Silanol	Sil	other metabolism	121435.3	29492.85	146611.9	48158.6	0.216507	ns	1.207325	0.271814
Trisaminol	Met	other metabolism	146210	26679.96	254295.9	126760	0.311142	ns	1.739251	0.798466
Uracil	Uracil	nucleic acid metabolism	3239.618	1488.524	6330.976	4015.335	0.308886	ns	1.954235	0.966604
Uridine	Urd	nucleic acid metabolism	2900.089	1606.902	1821.299	950.0505	0.467376	ns	0.628015	-0.67113
Proline	Pro	amino acid metabolism	2708.008	1398.072	2491.973	1175.558	0.433937	ns	0.920224	-0.11994
Boric acid	BA	ions	1517.184	412.2144	1545.301	548.0824	0.498161	ns	1.018533	0.026492
Malic acid	Ma	TCA cycle	3747.878	845.6073	13481.93	6250.996	0.42	ns	3.597217	1.846881

Table 5.5 Relative concentration and fold changes of major metabolites of WT and pgr5 under high light in *C. reinhardtii*.

Metabolites	Abbreviation	annotation	WT_500	stdev	pgr5_500	stdev	p-values	Significance	fold change	log2fold change
N-Acetyl-beta-alanine	NAA	amino acid metabolism	1227.694	507.3843	1415.271	481.9932	0.040675	*	1.152788	0.205128
Urea	Urea	amino acid metabolism	4551.914	1215.981	2047.98	865.3264	0.040722	*	0.449916	-1.15227
Aristromycin	Aris	polyols	4814.721	1439.689	13351.55	12650.89	0.039769	*	2.773067	1.471483
2-Phenyl-1,3- propanediol monocarbamate	PPM	glycerol metabolism	4057.386	831.6361	4095.076	1962.707	0.042852	*	1.009289	0.01334
1-(3-Pyridinyl)-1,4- butanediol	PB	carboxylic acid metabolism	1036.627	241.3893	1057.824	504.5044	0.042841	*	1.020449	0.029204
Monopalmitoyl serinol	MP	fatty acid metabolism	11256.68	5068.711	2143.318	864.869	0.042823	*	0.190404	-2.39286
Uridine5- monophosphate	UMP	nucleic acid metabolism	2009.037	1092.387	2711.399	1267.578	0.039264	*	1.349601	0.432533
Threonic acid	ThA	carboxylic acid metabolism	1507.369	631.8105	4469.809	1708.181	0.039488	*	2.965305	1.56818
Ellagic acid	Ela	secondary metabolism	2523.966	655.8851	2209.95	1852.85	0.040536	*	0.875586	-0.19168
Fumaric acid	FA	TCA cycle	126.7559	30.88636	1203.062	755.0979	0.040386	*	9.491177	3.246587
Palmitoyl serinol	PAG	fatty acid metabolism	675.3794	401.9633	191.5105	58.22633	0.040753	*	0.28356	-1.81827
Propionic acid	PA	carboxylic acid metabolism	1587.248	702.2712	5162.374	1889.513	0.040535	*	3.252405	1.701507
3-Hydroxybutyrate	ВНВ	carboxylic acid metabolism	606.0106	219.4734	234.0058	114.7507	0.041836	*	0.386141	-1.3728
methoxyamphetamine	3MA	other metabolism	9264.81	3927.672	36733.7	15312.59	0.041654	*	3.964862	1.987271
Gama- hydroxybutyrate	GHB	carboxylic acid metabolism	198.1013	81.72834	432.9492	204.4289	0.052071	ns	2.185494	1.127959
Acetamide	ACE	other metabolism	31214.31	11745.72	56995.47	16691	0.052145	ns	1.82594	0.86864
Ribitol	Rib	other metabolism	24368.34	9233.004	25301.98	8077.504	0.063992	ns	1.038314	0.054243
Tri-carboxylic acid	TCA	TCA cycle	10683.7	4108.033	22003.02	9888.567	0.064478	ns	2.059493	1.04229
Carbamic acid	Carb	carboxylic acid metabolism	32304.51	17074.07	51631.81	26547.55	0.070712	ns	1.598285	0.676525
Chrysanthemol alcohol	Chry	secondary metabolism	2110.404	339.5783	2103.027	724.5221	0.082185	ns	0.996504	-0.00505
Citric acid	CA	TCA cycle	1908.653	1121.055	3472.012	1313.516	0.082171	ns	1.81909	0.863217
Ribofuranose	Ribf	carbohydrate metabolism	131.9855	26.47664	636.5509	268.388	0.083216	ns	4.822885	2.269897
Fructose	Fru	carbohydrate metabolism	1798.512	786.5212	2321.858	2030.26	0.083551	ns	1.290988	0.368476
Inositol pentaphosphate	IPP	carbohydrate metabolism	17789.23	9013.517	13787.1	10432.19	0.0839	ns	0.775025	-0.36768
D-myo-Inositol-1- monophosphate (I1P)	I1P	polyols	9183.697	4326.374	22426.48	18120.04	0.081133	ns	2.441988	1.288056
D-pinitol	DP	polyols	8988.41	4038.034	1232.686	737.0885	0.090012	ns	0.137142	-2.86626
Ergosterol	Erg	sterol metabolism	6451.88	3582.644	2715.748	994.545	0.084346	ns	0.420923	-1.24837
Ethanolamine	MEA	other metabolism	26174.28	12250.71	26012.53	18775.19	0.081729	ns	0.99382	-0.00894
Trigallic acid	TG	secondary metabolism	4490.414	995.4244	1506.274	525.1614	0.081598	ns	0.335442	-1.57586
Glycerol 3 phosphate	GA3P	glycerol metabolism	70747.81	26184.68	96104.79	50963.25	0.079537	ns	1.358414	0.441923
glyceryl-glycoside	Gg	glycerol metabolism	11223	8563.911	99494.21	133101.4	0.096435	ns	8.865205	3.148154
Glycine	GLY	amino acid metabolism	10007.78	4025.279	19325.36	9105.234	0.160709	ns	1.931034	0.949374
Glycolic acid	GA	carboxylic acid metabolism	1239.851	445.1266	694.288	355.8792	0.17208	ns	0.559977	-0.83656
Lactic acid	LA	carboxylic acid metabolism	15702.57	5405.797	19195.38	11092.73	0.171626	ns	1.222435	0.289758

L- alanine	L_Ala	amino acid	8138.991	3335.44	8236.38	4911.734	0.176296	ns	1.011966	0.01716
N-acetyl-L-aspartic	NALA	metabolism amino acid	6392.984	2929.644	6173.282	4461.508	0.176718	ns	0.965634	-0.05045
acid Glutamate	Glu	metabolism amino acid metabolism	5040.573	2130.141	339.7139	102.7318	0.176763	ns	0.067396	-3.8912
Isoluecine	Ile	amino acid metabolism	6646.84	2956.085	3541.572	1515.136	0.171017	ns	0.53282	-0.90828
Phenyalaine	Phe	amino acid metabolism	6178.569	2856.24	3018.087	1250.027	0.16744	ns	0.488477	-1.03364
Threonine	Thr	amino acid metabolism	9240.276	4096.609	7466.153	3334.644	0.163863	ns	0.808001	-0.30757
L-Valine	L_Val	amino acid metabolism	7233.463	3129.793	4352.925	1996.04	0.16209	ns	0.601776	-0.7327
Neophytadiene	NPHY	secondary metabolism	7520.548	2600.367	5048.344	1333.554	0.158991	ns	0.671273	-0.57503
N-methyl-acetamide	MA	other metabolism	4575.377	1015.02	3343.436	1460.825	0.156466	ns	0.730745	-0.45256
Palmitic acid	PEC	fatty acid metabolism	10127.15	3243.921	12675.7	3806.704	0.15554	ns	1.251655	0.323837
Phosphoric acid propyl ester	PAPE	ions	13888.76	6304.84	19578.74	5618.785	0.159378	ns	1.409683	0.49537
Phytol	Phy	other metabolism	1334.472	676.7728	1377.711	839.7588	0.167471	ns	1.032401	0.046004
Putrescine	Put	polyamine metabolism	18910.1	6858.979	59513.64	27894.49	0.168691	ns	3.147188	1.654063
Serine	Ser	amino acid metabolism	5715.411	2595.833	7327.661	3853.79	0.224067	ns	1.282088	0.358496
Silanol	Sil	other metabolism	121435.3	29492.85	169967.8	49110.37	0.230002	ns	1.399657	0.485074
Trisaminol	Met	other metabolism	146210	26679.96	394684.8	79997.91	0.314204	ns	2.699438	1.432659
Uracil	Uracil	nucleic acid metabolism	3239.618	1488.524	7109.518	3569.108	0.165007	ns	2.194555	1.133928
Uridine	Urd	nucleic acid metabolism	2900.089	1606.902	2119.13	1058.206	0.259279	ns	0.730712	-0.45262
Proline	Pro	amino acid metabolism	2708.008	1398.072	8034.176	3484.042	0.249667	ns	2.966821	1.568918
Boric acid	BA	ions	1517.184	412.2144	2006.205	683.5511	0.479953	ns	1.322322	0.403073
Malic acid	Ma	TCA cycle	3747.878	845.6073	19272.23	5343.708	#DIV/0!	ns	5.142171	2.362377

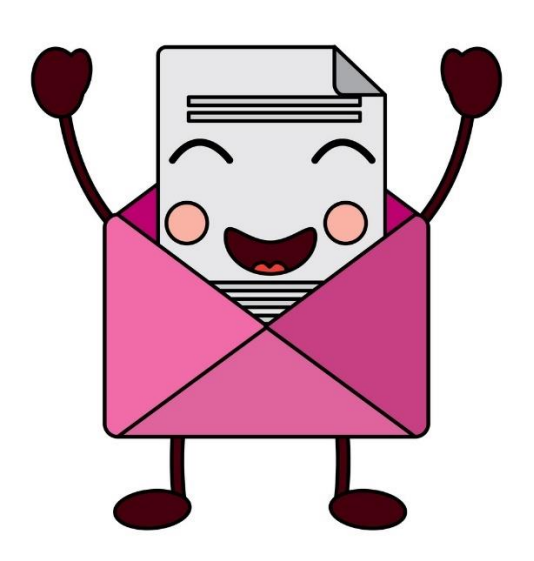
Table 5.6 Relative concentration and fold changes of major metabolites of *pgrl1* and *pgr5* under high light in *C. reinhardtii*.

Metabolites	abbreviation	annotation	pgrl1_500	stdev	pgr5_500	stdev	p-values	Significance	fold change	log2fold change
N-Acetyl-beta-alanine	NAA	amino acid metabolism	979.5129	712.4857	1415.271	481.9932	0.107128	ns	1.444872	0.530942
Urea	Urea	amino acid metabolism	3552.385	2204.805	2047.98	865.3264	0.107792	ns	0.576508	-0.79459
Aristromycin	Aris	polyols	12088.95	6030.23	13351.55	12650.89	0.105534	ns	1.104442	0.143318
2-Phenyl-1,3- propanediol monocarbamate	PPM	glycerol metabolism	3722.426	1150.389	4095.076	1962.707	0.107419	ns	1.10011	0.137647
1-(3-Pyridinyl)-1,4- butanediol	PB	carboxylic acid metabolism	1025.271	298.1529	1057.824	504.5044	0.107992	ns	1.031751	0.045095
Monopalmitoyl serinol	MP	fatty acid metabolism	10379.86	5545.825	2143.318	864.869	0.108054	ns	0.206488	-2.27587
Uridine5- monophosphate	UMP	nucleic acid metabolism	2698.35	1320.91	2711.399	1267.578	0.095607	ns	1.004836	0.00696
Threonic acid	ThA	carboxylic acid metabolism	4691.107	2523.992	4469.809	1708.181	0.09563	ns	0.952826	-0.06972
Ellagic acid	Ela	secondary metabolism	1443.102	698.5203	2209.95	1852.85	0.09533	ns	1.531389	0.61484
Fumaric acid	FA	TCA cycle	870.6557	405.3824	1203.062	755.0979	0.096393	ns	1.381789	0.466537
Palmitoyl serinol	PAG	fatty acid metabolism	670.4631	379.9121	191.5105	58.22633	0.096863	ns	0.285639	-1.80773
Propionic acid	PA	carboxylic acid metabolism	4824.314	2899.878	5162.374	1889.513	0.0962	ns	1.070074	0.097711
3-Hydroxybutyrate	ВНВ	carboxylic acid metabolism	789.3315	375.776	234.0058	114.7507	0.096677	ns	0.296461	-1.75409
methoxyamphetamine	3MA	other metabolism	34607.76	18299.62	36733.7	15312.59	0.095907	ns	1.061429	0.086009
Gama- hydroxybutyrate	GHB	carboxylic acid metabolism	305.7194	125.2603	432.9492	204.4289	0.098873	ns	1.416165	0.50199
Acetamide	ACE	other metabolism	33226.95	13250.94	56995.47	16691	0.099064	ns	1.715339	0.778493
Ribitol	Rib	other metabolism	24074.99	11433.67	25301.98	8077.504	0.132509	ns	1.050965	0.071715
Tri-carboxylic acid	TCA	TCA cycle	18936.93	7549.099	22003.02	9888.567	0.13477	ns	1.161911	0.216499
Carbamic acid	Carb	carboxylic acid metabolism	38845.87	27713.8	51631.81	26547.55	0.140429	ns	1.329146	0.410499
Chrysanthemol alcohol	Chry	secondary metabolism	1914.078	592.6515	2103.027	724.5221	0.164525	ns	1.098715	0.135818
Citric acid	CA	TCA cycle	2648.457	989.6349	3472.012	1313.516	0.165015	ns	1.310957	0.39062
Ribofuranose	Ribf	carbohydrate metabolism	199.1759	64.68101	636.5509	268.388	0.166867	ns	3.195923	1.676233
Fructose	Fru	carbohydrate metabolism	2775.426	1451.709	2321.858	2030.26	0.16791	ns	0.836577	-0.25743
Inositol pentaphosphate	IPP	carbohydrate metabolism	10308.68	7100.635	13787.1	10432.19	0.167037	ns	1.337426	0.419459
D-myo-Inositol-1- monophosphate (I1P)	I1P	polyols	18948.41	17353.29	22426.48	18120.04	0.174656	ns	1.183555	0.243126
D-pinitol	DP	polyols	5866.662	562.3184	1232.686	737.0885	0.182542	ns	0.210117	-2.25074
Ergosterol	Erg	sterol metabolism	1106.662	905.0203	2715.748	994.545	0.172011	ns	2.454	1.295135
Ethanolamine	MEA	other metabolism	21425.63	13242.48	26012.53	18775.19	0.175718	ns	1.214085	0.279869
Trigallic acid	TG	secondary metabolism	2062.072	673.2749	1506.274	525.1614	0.186187	ns	0.730466	-0.45311
Glycerol 3 phosphate	GA3P	glycerol metabolism	90662.9	44926.31	96104.79	50963.25	0.185079	ns	1.060023	0.084096
glyceryl-glycoside	Gg	glycerol metabolism	88324.89	92403.56	99494.21	133101.4	0.197994	ns	1.126457	0.171792

Glycine	GLY	amino acid metabolism	17467.37	12499.59	19325.36	9105.234	0.225544	ns	1.106369	0.145833
Glycolic acid	GA	carboxylic acid metabolism	770.0196	356.5025	694.288	355.8792	0.230868	ns	0.90165	-0.14936
Lactic acid	LA	carboxylic acid metabolism	30223.08	12290.98	19195.38	11092.73	0.231031	ns	0.635123	-0.65489
L- alanine	L_Ala	amino acid metabolism	14718.99	7142.746	8236.38	4911.734	0.201149	ns	0.559575	-0.8376
N-acetyl-L-aspartic acid	NALA	amino acid metabolism	7380.779	5739.546	6173.282	4461.508	0.185223	ns	0.8364	-0.25774
Glutamate	Glu	amino acid metabolism	2790.592	1540.295	339.7139	102.7318	0.182704	ns	0.121735	-3.03818
Isoleucine	Ile	amino acid metabolism	5032.305	2698.24	3541.572	1515.136	0.177291	ns	0.703767	-0.50683
Phenylalanine	Phe	amino acid metabolism	4316.922	2757.683	3018.087	1250.027	0.174233	ns	0.699129	-0.51637
Threonine	Thr	amino acid metabolism	9030.877	5645.115	7466.153	3334.644	0.171682	ns	0.826736	-0.2745
L-Valine	L_Val	amino acid metabolism	6232.522	3814.899	4352.925	1996.04	0.168582	ns	0.698421	-0.51783
Neophytadiene	NPHY	secondary metabolism	3112.783	556.9384	5048.344	1333.554	0.164836	ns	1.621811	0.697606
N-methyl-acetamide	MA	other metabolism	4297.688	1534.31	3343.436	1460.825	0.169781	ns	0.777961	-0.36223
Palmitic acid	PEC	fatty acid metabolism	11559.81	3332.772	12675.7	3806.704	0.168291	ns	1.096531	0.132947
Phosphoric acid propyl ester	PAPE	ions	12011.83	6064.6	19578.74	5618.785	0.171709	ns	1.629956	0.704833
Phytol	Phy	other metabolism	1513.8	1211.046	1377.711	839.7588	0.190624	ns	0.910101	-0.1359
Putrescine	Put	polyamine metabolism	38235.22	28408.26	59513.64	27894.49	0.191824	ns	1.556514	0.638318
Serine	Ser	amino acid metabolism	10567.3	6332.784	7327.661	3853.79	0.248126	ns	0.693428	-0.52818
Silanol	Sil	other metabolism	146611.9	48158.6	169967.8	49110.37	0.241873	ns	1.159305	0.21326
Trisaminol	Met	other metabolism	254295.9	126760	394684.8	79997.91	0.317141	ns	1.552069	0.634193
Uracil	Uracil	nucleic acid metabolism	6330.976	4015.335	7109.518	3569.108	0.111689	ns	1.122973	0.167324
Uridine	Urd	nucleic acid metabolism	1821.299	950.0505	2119.13	1058.206	0.142187	ns	1.163527	0.218505
Proline	Pro	amino acid metabolism	2491.973	1175.558	8034.176	3484.042	0.1519	ns	3.224021	1.688861
Boric acid	BA	ions	1545.301	548.0824	2006.205	683.5511	0.449432	ns	1.298262	0.376581
Malic acid	Ma	TCA cycle	13481.93	6250.996	19272.23	5343.708	#DIV/0!	ns	1.429486	0.515496

Chapter 6

Summary



Summary

The thesis has emphasized the effect of HL on cell growth, biochemical characterization of photosynthetic supercomplexes, lipid content, carotenoid content, composition of fatty acid, and changes in metabolite content in the WT as well as *pgrl1* and *pgr5 mutants of C. reinhardtii*.

The first objective aimed at the localization of carotenoids and macromolecular organization of thylakoid supercomplexes. Cells were grown photoheterotrophically under HL, where pgr5 mutant had retarded growth due to an increase in ROS. The thylakoids is solubilized by β-DM to separate macromolecular supercomplexes (PSII-LHCII, LHCII trimer and PSI-LHCI) to check for pigments, protein composition, and pigment-protein interactions. LHCII trimer's abundance and pigment-pigment interaction were not changed under HL in all the strains. However, a drastic change was seen in PSI-LHCI complexes than in PSII complexes, especially in pgrl1 and pgr5 mutants. The amount of lutein and β - carotene was increased under HL in LHCII trimers compared to other supercomplexes, indicating that these pigments protected the LHCII trimers against HL. However, xanthophylls, lutein, and βcarotene content were less in PSI-LHCI, indicating that pigment-protein complexes was altered in HL. Even the real-time PCR data showed that pgr5 mutant does not accumulate zeaxanthin dependant genes under HL, which indicated that violaxanthin was not converted to zeaxanthin under HL in pgr5. Also, the protein data confirms that the LHCSR3 expression is absent in PSI-LHCI and PSII complexes and some of the core proteins were aggregated in pgr5 under HL.

The second objective was to investigate autophagy-induced lipid accumulation in pgrl1 and pgr5 mutant. From our reports, in pgr5 under HL, concentration of lipid enhanced while concentration of carbohydrate decline. Further, electron microscopy also showed the formation of large vacuoles in HL in all strains. We also reported a rise in ROS level, which

we believe leads to autophagy. In addition, *pgr5* showed an enhanced accumulation of ATG8 and identification of ATG8-PE protein. Interestingly, the TAG level increases because of DGAT and PDAT enzymes' expression, majorly in *pgr5*. Here, the formation of TAG hypothesized from the degradation of membrane lipid. Furthermore in HL, mono, polyunsaturated, and saturated fatty acids showed significant enhancement. Hence increased light generate ROS, which activate autophagy and TAG formation, according to our findings.

The third objective describes the metabolomic changes that allow the cells to cope with the stress conditions. A total of 55 metabolites were detected using GC-MS analysis. Under HL, pgr5 accumulated several metabolites related to amino acid metabolisms such as Gly, L-Ala, Glu, Ilu, Phe, Thr, L-val, Ser, and Prol, which were upregulated by 2.5-fold under HL. Further, we have recorded an increase of 0.5-fold in L-Ala, Ilu, and Ser in pgrl1. pgr5 showed an enhancement in carbohydrate, polyamines, and polyol metabolism by 2.5-fold under HL. Metabolites, which are associated with glycerol pathways such as GA3P and Gg were increased significantly by 2.5-fold under HL in pgr5. Both correlation network studies and KEGG pathway enrichment analysis revealed that the metabolites affiliated to several biological pathways namely carbohydrate, TCA cycle, fatty acid, and amino acid were positively correlated with each other in pgrl1 and pgr5 under HL stress conditions. The relative mRNA expression of gene related to TCA cycle including ACH1, OGD2, OGD3, IDH3, and MDH4 were significantly upregulated in pgrl1 and pgr5 under HL. In pgr5, IDH2 and PDC3 increased by 10-fold, while CIS2 and FUM1 increased 6-fold. An increase in proline and putrescine content in pgr5 shows activation of the defense mechanism. Our results support that the role of energy metabolism, particularly the TCA cycle, in the supply of ATP and other metabolites which are required for growth and development and also induction of several alternative defense pathways enable pgrl1 and pgr5 to thrive under HL conditions.

This study could be important from the point of view that under the minimal operation of cyclic electron transport, the algae was acclimated to HL by overproduction of several biomolecules including lipids. As a result, the increased buildup of TAGs can be employed as a biodiesel feedstock.

Bibliography

References

- Akhtar, P., Dorogi, M., Pawlak, K., Kovács, L., Bóta, A., Kiss, T., Garab, G., Lambrev, P.H. (2015) Pigment interactions in light-harvesting complex II in different molecular environments. *J. Biol. Chem.* 290, 4877-4886.
- Abida, H., Dolch, L.J., Meï, C., Villanova, V., Conte, M., Block, M.A., Finazzi, G., Bastien, O., Tirichine, L., Bowler, C., Rébeillé, F., Petroutsos, D., Jouhet, J., Maréchal, E. (2015) Membrane glycerolipid remodeling triggered by nitrogen and phosphorus starvation in *Phaeodactylum tricornutum. Plant Physiol.* 167, 118-136.
- Alishah Aratboni, H., Rafiei, N., Garcia-Granados, R. (2019) Biomass and lipid induction strategies in microalgae for biofuel production and other applications. *Microb. Cell Fact.* 18, 178.
- Arora, A., Sairam, R.K., Srivastava, G. (2002) Oxidative stress and antioxidative system in plants. *Curr. Sci.* 82, 1227-1238.
- Ballottari, M., Girardon, J., Dall'Osto, L., Bassi, R. (2012) Evolution and functional properties of Photosystem II light harvesting complexes in eukaryotes. *Biochim. Biophys. Acta Bioenerg.* 1817, 143-157.
- Barber, J. (2009) Photosynthetic energy conversion: natural and artificial. *Chem. Soc. Rev.* 38, 185-196.
- Barros, T., Kuhlbrandt, W. (2009) Crystallisation, structure and function of plant light-harvesting Complex II. *Biochim. Biophys. Acta Bioenerg.* 1787, 753-772.
- Baroli, I., Gutman, B.I., Ledford, H.K., Shin, J.W., Chin, B.L., Havaux, M., Niyogi, K.K. (2004) Photooxidative stress in a xanthophyll-deficient mutant of Chlamydomonas. *J. Biol. Chem.* 279, 6337-6344.
- Barera, S., Pagliano, C., Pape, T., Saracco, G., Barber, J. (2012) Characterization of PSII– LHCII supercomplexes isolated from pea thylakoid membrane by one-step treatment

- with α and β-dodecyl-D-maltoside. *Phil. Trans. R. Soc. B.* 367, 3389-3399.
- Bassi, R., Pineau, B., Dainese, P., Marquardt, J. (1993) Carotenoid-binding proteins of photosystem II. *Eur. J. Biochem.* 212, 297-303.
- Bazzani, E., Lauritano, C., Mangoni, O., Bolinesi, F., Saggiomo, M. (2021) Chlamydomonas Responses to salinity stress and possible biotechnological exploitation. *J. Mar. Sci. Eng.* 9, 1242.
- Ben-Amotz, A., Gressel, J., Avron, M. (1987) Massive accumulation of phytoene induced by norflurazon in *Dunaliella bardawil* (Chlorophyceae) prevents recovery from photoinhibition. *J. Phycol.* 23, 176-181.
- Birben, E., Sahiner, U.M., Sackesen, C., Erzurum, S., Kalayci, O. (2012) Oxidative stress and antioxidant defense. *World Allergy Organ J.* 5, 9-19.
- Blankenship, R.E. (2010) Early evolution of photosynthesis. *Plant Physiol.* 154, 434-438.
- Blechschmidt-Schneider, S., Ferrar, P., Osmond, C.B. (1989) Control of photosynthesis by the carbohydrate level in leaves of the C₄ plant *Amaranthus edulis L. Planta*. 177, 515-525.
- Bligh, E.G., Dyer, W.J. (1959) A rapid method for total lipid extraction and purification.

 Can. J. Biochem. Physiol. 37, 911-917.
- Bradford, M.M. (1976) A rapid and sensitive method for the quantitation of microgram quantities of protein utilizing the principle of protein-dye binding. *Anal. Biochem.*72, 248-254.
- Bölling, C., Fiehn, O. (2005) Metabolite profiling of *Chlamydomonas reinhardtii* under nutrient deprivation. *Plant Physiol*. 139, 1995-2005.
- Bomgardner, M.M. (2012) Flying the green skies with biofuels: with test flights behind them, airlines push for more production of biobased jet fuel. *Chem. Eng. News.* 90, 18–21.
- Bonente, G., Ballottari, M., Truong, T.B., Morosinotto, T., Ahn, T.K. (2011) Analysis of LhcSR3, a protein essential for feedback de-excitation in the green algae

- Chlamydomonas reinhardtii. PLoS Biol. 9, e1000577.
- Boudiere, L., Michaud, M., Petroutsos, D., Rébeillé, F., Falconet, D., Bastien, O., Roy, S., Finazzi, G., Rolland, N., Jouhet, J., Block, M.A., Maréchal, E. (2014) Glycerolipids in photosynthesis: composition, synthesis and trafficking. *Biochim. Biophys. Acta Bioenerg.* 1837, 470-480.
- Bozzola, J.J., Russell, L.D. (1998) Electron microscopy: principles and techniques for biologists, 2nd Ed. Sudbury, MA: Jones and Barlett publishers, 4, 19-144.
- Buchert, F., Mosebach, L., Gäbelein, P., Hippler, M. (2020) PGR5 is required for efficient Q cycle in the cytochrome *b6f* complex during cyclic electron flow. *Biochem. J.* 477, 1631-1650.
- Casero, R.A. Jr., Woster, P.M. (2009) Recent advances in the development of polyamine analogues as antitumor agents. *J. Med. Chem.* 52, 4551-4573.
- Cazzaniga, S., Li, Z., Niyogi, K.K., Bassi, R., Dall'Osto, L. (2012) The Arabidopsis szl1 mutant reveals a critical role of β-carotene in photosystem I photoprotection. *Plant Physiol.* 159, 1745-1758.
- Chen, H., Zheng, Y., Zhan, J., He, C., Wang, Q. (2017) Comparative metabolic profiling of the lipid- producing green microalga Chlorella reveals that nitrogen and carbon metabolic pathways contribute to lipid metabolism. *Biotechnol. Biofuels.* 10, 153.
- Chen, Y.P., Tsai, C.W., Shen, C.Y., Day, C.H., Yeh, Y.L., Chen, R.J., Ho, T.J., Padma, V.V., Kuo, W.W., Huang, C.Y. (2016) Palmitic acid interferes with energy metabolism balance by adversely switching the SIRT1-CD36-fatty acid pathway to the PKC zeta- GLUT4- glucose pathway in cardiomyoblasts. *J. Nutr. Biochem.* 31, 137-149.
- Chaneton, B., Hillmann, P., Zheng, L., Martin, A.C.L., Maddocks, O.D.K., Chokkathukalam, A., Coyle, J.E., Jankevics, A., Holding, F.P., Vousden, K.H., Frezza, C., O'Reilly, M., Gottlieb, E. (2012) Serine is a natural ligand and allosteric activator of pyruvate

- kinase M2. Nature. 491, 458-462.
- Chisti, Y. (2008) Biodiesel from microalgae beats bioethanol. *Trends Biotechnol*. 26, 126-131.
- Chokshi, K., Pancha, I., Ghosh, A. (2017) Nitrogen starvation-induced cellular crosstalk of ROS-scavenging antioxidants and phytohormone enhanced the biofuel potential of green microalga *Acutodesmus dimorphus*. *Biotechnol*. *Biofuels*. 10, 60.
- Chua, N.H., Bennoun, P. (1975) Thylakoid membrane polypeptides of *Chlamydomonas* reinhardtii: wild-type and mutant strains deficient in photosystem II reaction center. *Proc. Natl. Acad. Sci. U S A.* 72, 2175-1279.
- Couso, I., Vila, M., Vigara, J., Cordero, B.F., Vargas, M.A., Rodriguez, H., Leon, R. (2012)

 Synthesis of carotenoids and regulation of the carotenoid biosynthesis pathway in response to high light stress in the unicellular microalga *Chlamydomonas reinhardtii*.

 Eur. J. Phycol. 47, 223-232.
- Couso, I., Evans, B.S., Li, J., Liu, Y., Ma, F., Diamond, S., Allen, D.K., Umen, J.G. (2016)

 Synergism between inositol polyphosphates and TOR kinase signaling in nutrient sensing, growth control and lipid metabolism in Chlamydomonas. *Plant Cell.* 28, 2026-2042.
- Couso, I., Pérez-Pérez, M.E., Martínez-Force, E., Kim, H.S., He, Y., Umen, J.G., Crespo, J.L. (2018) Autophagic flux is required for the synthesis of triacylglycerols and ribosomal protein turnover in Chlamydomonas. *J. Exp. Bot.* 69, 1355-1367.
- Cuellar-Bermudez, S.P., Romero-Ogawa, M.A., Vannela, R., Lai, Y.S., Rittmann, B.E., Parra-Saldivar, R. (2015) Effects of light intensity and carbon dioxide on lipids and fatty acid produced by *Synechocystis* sp. PCC6803 during continuous flow. *Algal Res.* 12, 10-16.
- DalCorso, G., Pesaresi, P., Masiero, S., Aseeva, E., Schünemann, D., Finazzi, G., Joliot, P., Barbato, R., Leister, D. (2008) A complex containing PGRL1 and PGR5 is involved in

- the switch between linear and cyclic electron flow in Arabidopsis. Cell, 132, 273-285.
- Dall'Osto, L., Holt, N.E., Kaligotla, S., Fuciman, M., Cazzaniga, S., Carbonera, D., Frank,
 H.A., Alric, J., Bassi, R. (2012) Zeaxanthin protects plant photosynthesis by
 modulating chlorophyll triplet yield in specific light-harvesting antenna subunits. *J. Biol. Chem.* 287, 41820-41834.
- Davis, MC., Fiehn, O., Durnford, D.G. (2013) Metabolic acclimation to excess light intensity in *Chlamydomonas reinhardtii*. *Plant Cell Environ*. 36, 1391-1405.
- Dang, K.V., Plet, J., Tolleter, D., Jokel, M., Cuiné, S., Carrier, P., Auroy, P., Pierre, R., Johnson, X., Alric, J., Allahverdiyeva, Y., Peltier, G. (2014) Combined increases in mitochondrial cooperation and oxygen photoreduction compensate for deficiency in cyclic electron flow in *Chlamydomonas reinhardtii*. *Plant Cell*. 26, 3036–3050.
- Dekker, J.P., Boekema, E.J. (2005) Supramolecular organization of thylakoid membrane proteins in green plants. *Biochim. Biophys. Acta.* 1706, 12-39.
- Devadasu, E., Pandey, J., Dhokne, K., Subramanyam, R. (2021) Restoration of photosynthetic activity and super complexes from severe iron starvation in *Chlamydomonas reinhardtii. Biochim. Biophys. Acta.* 1862, 148331.
- Diaz-Troya, S., Pérez-Pérez, M.E., Florencio, F.J., Crespo, J.L. (2008) The role of TOR in autophagy regulation from yeast to plants and mammals. *Autophagy*. 4, 851-865.
- Demirbas, A. (2009) Progress and recent trends in biodiesel fuels. *Energy Convers. Manag.* 50, 14-34.
- Demirbas, A. (2008) Biofuels sources, biofuel policy, biofuel economy and global biofuel projections. *Energy Convers. Manag.* 49, 2106-2116.
- Demmig-Adams, B., Garab, G., Adams, W., Govindjee. (2014) Non-Photochemical quenching and energy dissipation in plants, algae and cyanobacteria. Dordrecht, The Netherlands: *Springer*.

- Devadasu, E., Chinthapalli, D.K., Chouhan, N., Madireddi, S.K., Rasineni, G.K., Sripadi, P., Subramanyam, R. (2019) Changes in the photosynthetic apparatus and lipid droplet formation in *Chlamydomonas reinhardtii* under iron deficiency. *Photosynth Res.* 139, 253-266.
- Devadasu, E., Subramanayam, R. (2021) Enhanced lipid production in *Chlamydomonas* reinhardtii caused by severe iron deficiency. *Front. Sci.* 12, 615577.
- Doebbe, A., Keck, M., La, R.M., Mussgnug, J.H., Hankamer, B., Tekce, E., Niehaus, K., Kruse, O. (2010) The interplay of proton, electron, and metabolite supply for photosynthetic H₂ production in *Chlamydomonas reinhardtii*. *J. Biol. Chem.* 285, 30247-30260.
- Dormann, P., Benning, C. (2002) Galactolipids rule in seed plants. *Trends Plant Sci.* 7, 112-118.
- Drop, B., Webber-birungi, M., Yadav, S.K.N., Filipowicz-Szymanska, A. Fusetti, F., Boekema, E.J., Croce, R. (2014) Light-harvesting complex II (LHCII) and its supramolecular organization in *Chlamydomonas reinhardtii*. *Biochim. Biophy. Acta. Bioenerg.* 1837, 63-72.
- Fan, J., Yan, C., Andre, C., Shanklin, J., Schwender, J., Xu, C. (2012) Oil accumulation is controlled by carbon precursor supply for fatty acid synthesis in *Chlamydomonas* reinhardtii. Plant Cell Physiol. 53, 1380-1390.
- Faraloni, C., Torzillo, G. (2017) Synthesis of antioxidant carotenoids in microalgae in response to physiological stress. In D.J. Cvetkovic, & G. S. Nikolic (Ed.), Carotenoids. *IntechOpen*.
- Forde, B.G., Lea, P.J. (2007) Glutamate in plants: metabolism, regulation, and signalling. *J. Exp. Botany*. 58, 2339-2358.

- Foyer, C.H. (2018) Reactive oxygen species, oxidative signalling and the regulation of photosynthesis. *Envir. Exp. Botany.* 154, 134-142.
- Foyer, C.H., Noctor, G. (2009) Redox regulation in photosynthetic organisms: signalling, acclimation, and practical implications. *Antioxid. Redox Signal.* 11, 861-905.
- Galston, A.W., Sawhney. R.K. (1990) Polyamines in plant physiology. *Plant Physiol*. 94, 406–410.
- Gargouri, M., Park, J.J., Holguin, F.O. (2015) Identification of regulatory network hubs that control lipid metabolism in *Chlamydomonas reinhardtii*. *J. Exp. Bot*. 66, 4551-4566.
- Ganesan, R., Manigandan, S., Samuel, M.S., Shanmuganathan, R., Brindhadevi, K., Chi, N.T.L., Duc, P.A., Pugazhendhi, A. (2020) A review on prospective production of biofuel from microalgae. *Biotechnol. Rep.* 27, e00509.
- Geigenberger, P., Fernie, A.R. (2014) Metabolic control of redox and redox control of metabolism in plants. *Antioxid. Redox Signal.* 21, 1389-1421.
- Goold, H., Beisson, F., Peltier, G., Li-Beisson, Y. (2015) Microalgal lipid droplets: composition, diversity, biogenesis and functions. *Plant Cell Rep.* 34, 545-555.
- Goold, H.D., Cuiné, S., Légeret, B. (2016) Saturating light induces sustained accumulation of oil in plastidal lipid droplets in *Chlamydomonas reinhardtii*. *Plant Physiol*. 171, 2406-2417.
- Gopalakrishnan, V., Ramamurthy, D. (2014) Dyeing industry effluent system as lipid production medium of *Neochloris* sp. for biodiesel feedstock preparation. *Biomed Res. Int.* 2014, 529560.
- Goss, R., Lepetit, B. (2015) Biodiversity of NPQ. J. Plant Physiol. 172, 13-32.
- Guskov, A., Kern, J., Gabdulkhakov, A., Broser, M., Zouni, A., Saenger, W. (2009)

 Cyanobacterial photosystem II at 2.9-A resolution and the role of quinones, lipids,

- channels and chloride. Nat. Struct. Mol. Biol. 16, 334-340.
- Guedes, A., Meireles, L.A., Amaro, H., Malcata, F. (2010) Changes in lipid class and fatty acid composition of cultures of *Pavlova lutheri*, in response to light intensity. *J. Oil Fat Industries*. 87, 791-801.
- Shah, S.H., Houborg, R., Matthew, F., McCabe, M.F. (2017) Response of chlorophyll, carotenoid and SPAD-502 measurement to salinity and nutrient stress in wheat (*Triticum aestivum L.*). *Agronomy*. 7, 61.
- Havaux, M., Dall'osto, L., Bassi, R. (2007) Zeaxanthin has enhanced antioxidant capacity with respect to all other xanthophylls in Arabidopsis leaves and functions independent of binding to PSII antennae. *Plant Physiol.* 145, 1506-1520.
- Hayat, S., Hayat, Q., Alyemeni, M.N., Wani, A.S., Pichtel, J., Ahmad, A. (2012) Role of proline under changing environments: a review. *Plant Signal Behav.* 7, 1456-1466.
- He, Y., Meng, X., Fan, Q., Sun, X., Xu, Z., Song, R. (2009) Cloning and characterization of two novel chloroplastic glycerol-3-phosphate dehydrogenases from *Dunaliella* viridis. Plant Mol. Biol. 71, 193–205.
- Heredia-Arroyo, T., Wei, W., Hu, B. (2010) Oil accumulation via heterotrophic/mixotrophic Chlorella protothecoides. Appl. Biochem. Biotechnol. 162, 1978-1995.
- Heredia-Martinez, L.G., Andres-Garrido, A., Martinez-Force, E., Perez-Perez, M.E., Crespo, J.L. (2018) Chloroplast damage induced by the inhibition of fatty acid synthesis triggers autophagy in Chlamydomonas. *Plant Physiol.* 178, 1112-1129.
- Hildebrandt, T.M. (2018) Synthesis versus degradation: directions of amino acid metabolism during Arabidopsis abiotic stress response. *Plant Mol. Biol.* 98, 121-135.
- Han, D., Jia, J., Li, J., Sommerfeld, M., Xu, J., Hu, Q. (2017) Metabolic remodelling of membrane glycerolipids in the microalga *Nannochloropsis oceanica* under nitrogen

- deprivation. Front. Mar. Sci. 4, e00242.
- Huang, H., Farhan, U., Dao-Xiu, Z., Yi. M., Zhao, Y. (2019) Mechanisms of ROS regulation of plant development and stress responses. *Front. Plant Sci.* 10, 3389.
- Huang, T., Jander, G. (2017) Abscisic acid-regulated protein degradation causes osmotic stress- induced accumulation of branched-chain amino acids in *Arabidopsis* thaliana. Planta. 246, 737-747.
- Huete-Ortega, M., Okurowska, K., Kapoore, R.V. (2018) Effect of ammonium and high light intensity on the accumulation of lipids in *Nannochloropsis oceanica* (CCAP 849/10) and *Phaeodactylum tricornutum* (CCAP1055/1). *Biotechnol. Biofuels*. 11, 60.
- Hossain, M.S., Persicke, M., Ismail, A., Sayed, E., Kalinowski, J., Dietz, K.J. (2017)

 Metabolite profiling at the cellular and subcellular level reveals metabolites associated with salinity tolerance in sugar beet. *J. Exp. Bot.* 68, 5961-5976.
- Ireland, R.J., Lea, P.J. (1999) The enzymes of glutamine, glutamate, asparagine and aspartate metabolism. In B. Singh (Ed.), *Plant Amino Acids: Biochem. Biotechnol.*Marcel Dekker Inc, 49-109.
- Jahns, P., Holzwarth, A.R. (2012) The role of the xanthophyll cycle and of lutein in photoprotection of photosystem II. *Biochim. Biophy. Acta Bioenerg.* 1817, 182-193.
- Jegerschoeld, C., Virgin, I., Styring, S. (1990) Light-dependent degradation of the D1 protein in photosystem II is accelerated after inhibition of the water splitting reaction.

 *Biochemistry. 29, 6179-6186.
- Johnson, X., Alric, J. (2013) Central carbon metabolism and electron transport in *Chlamydomonas reinhardtii*: metabolic constraints for carbon partitioning between oil and starch. *Eukaryot. Cell.* 12, 776-793.

- Johnson, X., Steinbeck, J., Dent, R.M., Takahashi, H., Richaud, P., Ozawa, S.I. (2014)

 Proton gradient regulation 5-mediated cyclic electron flow under ATP- or redoxlimited conditions: a study of ΔATpase pgr5 and ΔrbcL pgr5 mutants in the
 green alga *Chlamydomonas reinhardtii*. *Plant Physiol*. 165, 438-452.
- Jouhet, J., Lupette, J., Clerc, O., Magneschi, L., Bedhomme, M., Collin, S., Roy, S., Maréchal, E., Rébeillé, F. (2017) LC-MS/MS versus TLC plus GC methods: consistency of glycerolipid and fatty acid profiles in microalgae and higher plant cells and effect of a nitrogen starvation. *PloS One*. 12, e0182423.
- Judge, A., Dodd, M.S. (2020) Metabolism. Essays Biochem. 64, 607-647.
- Kaushik, D., Aryadeep, R. (2014) Reactive oxygen species (ROS) and response of antioxidants as ROS-scavengers during environmental stress in plants. *Front. Env. Sci.* 2, 53.
- Kalhan, SC., Hanson, R.W. (2012) Resurgence of serine: an often neglected but indispensable amino acid. *J. Biol. Chem.* 287, 19786-19791.
- Khotimchenko, S.V., Yakovleva, I.M. (2005). Lipid composition of the red alga *Tichocarpus* crinitus exposed to different levels of photon irradiance. *Phytochem.* 66, 73-79.
- Klok, A., Lamers, P., Martens, D., Draaisma, R., Wijffels, R. (2014) Edible oils from microalgae: insights in TAG accumulation. *Trends Biotechnol.* 32, 521-528.
- Kolling, K., Müller, A., Flütsch, P. (2013) A device for single leaf labelling with CO₂ isotopes to study carbon allocation and partitioning in *Arabidopsis thaliana*. *Plant Methods*. 9, 45.
- Kouril, R., Wientjes, E., Bultema, J.B., Croce, R., Boekema, E.J. (2013) High-light vs. low-light: effect of light acclimation on photosystem II composition and organization in *Arabidopsis thaliana*, *Biochim. Biophys. Acta. Bioenerg*.1827, 411-419.
- Kim, E., Kawakami, K., Sato, R., Ishii, A., Minagawa, J. (2020) Photoprotective capabilities

- of light-harvesting complex II trimers in the green alga *Chlamydomonas* reinhardtii. J. Phys. Chem. Lett. 11, 7755-7761.
- Krause, G.H., Weis, E. (1991) Chlorophyll fluorescence and photosynthesis: the basics. *Ann. Rev. Plant Physiol. Plant. Mol. Biol.* 42, 313-349.
- Krzeminska, I., Piasecka, A., Nosalewicz, A., Simionato, D., Wawrzykowski, J. (2015)

 Alterations of the lipid content and fatty acid profile of *Chlorella protothecoides*under different light intensities. *Bioresource Tech.* 196, 72-77.
- Koyande, A.K., Chew, K.W., Rambabu, K., Tao, Y., Chu, D.T., Show, P.L. (2019)

 Microalgae: a potential alternative to health supplementation for humans. *Food Sci. Hum. Wellness.* 8, 16-24.
- Kennedy, E.P., Weiss, S.B. (1956) The function of cytidine coenzymes in the biosynthesis of phospholipids. *J. Biol. Chem.* 222, 193-214.
- Kulheim, C., Agren, J., Jansson, S. (2002) Rapid regulation of light harvesting and plant fitness in the field. *Science*. 297, 91-93.
- Kundu, A., Mishra, S., Vadassery, J. (2018) Spodoptera litura-mediated chemical defense is differentially modulated in older and younger systemic leaves of *Solanum lycopersicum*. *Planta*. 248, 981-997.
- Larkum, A.W.D., Ross, I.L., Kruse, O., Hankamer, B. (2011) Selection, breeding and engineering of microalgae for bioenergy and biofuel production. *Trends Biotechnol*. 30, 198-205.
- Lee, D.Y., Park, J.J., Barupal, D.K., Fiehn, O. (2012) System response of metabolic networks in *Chlamydomonas reinhardtii* to total available ammonium. *Mol. Cell. Proteomics.* 11, 973-988.
- Leonardi, R., Jackowski, S. (2007) Biosynthesis of pantothenic acid and coenzyme A. *Eco. Sal. Plus.* 2, 1128.

- Leister, D., Shikanai, T. (2013) Complexities and protein complexes in the antimycin Asensitive pathway of cyclic electron flow in plants. *Front. Plant Sci.* 4, 161.
- Livak, K.J., Schmittgen, T.D. (2001) Analysis of relative gene expression data using real-time quantitative PCR and the 2 (-Delta Delta C (T)). *Method*. 25, 402-408.
- Liang, Y., Kong, F., Torres-Romero, I., Burlacot, A., Cuine, S., Légeret, B., Billon, E.,
 Brotman, Y., Alseekh, S., Fernie, A.R., Beisson, F., Peltier, G., Li-Beisson, Y.
 (2019) Branched-chain amino acid catabolism impacts triacylglycerol
 homeostasis in *Chlamydomonas reinhardtii*. *Plant Physiol*. 179, 1502-1514.
- Li, Y., Horsman, M., Wang, B., Wu, N., Lan, C.Q. (2008) Effects of nitrogen sources on cell growth and lipid accumulation of green alga *Neochloris oleoabundans*. *Appl. Microbiol. Biotechnol.* 81, 629-636.
- Li, Y., Han, D., Sommerfeld, M., Hu, Q. (2011) Photosynthetic carbon partitioning and lipid production in the oleaginous microalga *Pseudochlorococcum* sp. (Chlorophyceae) under nitrogen-limited conditions. *Bioresour. Technol.* 102, 123-129.
- Li, Z., Wakao, S., Fischer, B.B., Niyogi, K.K. (2009) Sensing and responding to excess light. *Ann. Rev. Plant Biol.* 60, 239-260.
- Liu, Y., Bassham, D.C. (2012) Autophagy: pathways for self-eating in plant cells. *Ann. Rev. Plant Biol.* 63, 215-237.
- Long, S.P., Humphries, S., Falkowski, P.G. (1994) Photoinhibition of photosynthesis in nature. Ann. Rev. Plant Biol.45, 633-662.
- Mandotra, S.K., Kumar, P., Suseela, M.R., Nayaka, S., Ramteke, P.W. (2016) Evaluation of fatty acid profile and biodiesel properties of microalga *Scenedesmus abundans* under the influence of phosphorus, pH, and light intensities. *Bioresour. Technol.* 201, 222-229.
- Martens, S., Fracchiolla, D. (2020) Activation and targeting of ATG8 protein lipidation. Cell

- Discov. 6, 23.
- Martin, G. J., Hill, D. R., Olmstead, I. L., Bergamin, A., Shears, M. J., Dias, D. A., et al. (2014). Lipid profile remodeling in response to nitrogen deprivation in the microalgae *Chlorella* sp. (Trebouxiophyceae) and *Nannochloropsis* sp. (Eustigmatophyceae). *PLoS One* 9:e103389.
- Ma, X.N., Chen, T.P., Yang, B., Liu, J., Chen, F. (2016) Lipid Production from Nannochloropsis. *Mar. drugs.* 14, 61.
- Maltsev, Y., Maltseva, K., Kulikovskiy, M., Maltseva, S. (2021) Influence of light condition on microalgae growth and content of lipids, carotenoids, and fatty acid composition. *Biology.* 10, 1060.
- Mascia, F., Girolomoni, L., Alcocer, M.J.P. (2017) Functional analysis of photosynthetic pigment binding complexes in the green alga *Haematococcus pluvialis* reveals distribution of astaxanthin in photosystems. *Sci. Rep.* 7, 16319.
- McKim, S., Durnford, D.G. (2006) Translational regulation of light-harvesting complex expression during photoacclimation to high-light in *Chlamydomonas reinhardtii*. *Plant Physiol. Biochem.* 44, 857-865.
- Meena, M., Divyanshu, K., Kumar, S., Swapnil, P., Zehra, A., Shukla, V., Yadav, M., Upadhyay, R.S. (2019) Regulation of L-proline biosynthesis, signal transduction, transport, accumulation and its vital role in plants during variable environmental conditions. *Heliyon.* 5, e02952.
- Meijer, W.H., Van Der Klei, I.J., Veenhuis, M., Kiel, J.A. (2007) ATG genes involved in non-selective autophagy are conserved from yeast to man, but the selective Cvt and autophagy pathways also require organism-specific genes. *Autophagy*. 3, 106-116.
- Minagawa, J., Takahashi, Y. (2004) Structure, function and assembly of photosystem II and its light-harvesting proteins. *Photosynth. Res.* 82, 241-263.

- Mizushima, N., Yoshimori, T., Ohsumi, Y. (2011) The role of Atg proteins in autophagosome formation. *Annu. Rev. Cell Dev. Biol.* 27, 107-132.
- Mondal, M., Goswami, S., Ghosh, A., Oinam, G., Tiwari, O.N., Das, P., Gayen, K., Mandal, M.K. Halder, G.N. (2017) Production of biodiesel from microalgae through biological carbon capture. *Biotech*. 7, 99.
- Morales, M., Aflalo, C., Bernard, O. (2021) Microalgal lipids: a review of lipids potential and quantification for 95 phytoplankton species. *Biomass Bioenergy*. 150, 106108.
- Moore, R., Clark, W.D., Kingsley, R.S., Vodopich, D. (1995) Electron transport in photosynthesis. Botany. Wm. C. Brown Pub., Dubuque, Iowa.
- Munekage, Y., Hojo, M., Meurer, J., Endo, T., Tasaka, M., Shikanai, T. (2002) PGR5 is involved in cyclic electron flow around photosystem I and is essential for photoprotection in *Arabidopsis thaliana*. *Cell*. 110, 361-371.
- Nama, S., Madireddi, S.K., Yadav, R.M., Subramanyam, R. (2019) Non-photochemical quenching- dependent acclimation and thylakoid organization of *Chlamydomonas* reinhardtii to high light stress. *Photosynth. Res.* 139, 387-400.
- Navakoudis, E., Vrentzou, K., Kotzabasis, K. (2007) A polyamine- and LHCII protease activity base mechanism regulates the plasticity and adaptation status of the photosynthetic apparatus. *Biochim. Biophys. Acta.* 1767, 261-271.
- Niyogi, K.K., Bjorkman, O., Grossman, A.R. (1997) Chlamydomonas xanthophyll cycle mutants identified by video imaging of chlorophyll fluorescence quenching. *Plant Cell.* 9, 1369-1380.
- Nishiyama, Y., Allakhverdiev, S.I., Murata, N. (2005) Inhibition of the repair of photosystem

 II by oxidative stress in cyanobacteria. *Photosynth. Res.* 84, 1-7.
- Nishiyama, Y., Allakhverdiev, S.I., Murata, N. (2006) A new paradigm for the action of reactive oxygen species in the photoinhibition of photosystem II. *Biochim. Biophys*.

- Acta. 1757, 742-749.
- Niyogi, K.K., Grossman, A.R., Björkman, O. (1998) Arabidopsis mutants define a central role for the xanthophyll cycle in the regulation of photosynthetic energy conversion.

 *Plant Cell.10, 1121-1134.
- Ohnishi, N., Murata, N. (2006) Glycine betaine counteracts the inhibitory effects of salt stress on the degradation and synthesis of D1 protein during photoinhibition in *Synechococcus* sp. PCC 7942. *Plant Physiol*. 141, 758-765.
- Ozawa, S.I. Onishi, T. Takahashi, Y. (2010) Identification and characterization of an assembly intermediate subcomplex of photosystem I in the green algae *Chlamydomonas reinhardtii. J. Biol. Chem.* 285, 20072-20079.
- Pal, D., Khozin-Goldberg, I., Cohen, Z., Boussiba, S. (2011) The effect of light, salinity, and nitrogen availability on lipid production by Nannochloropsis sp. *Appl. Microbiol. Biotechnol.* 90, 1429-1441.
- Plancke, C., Vigeolas, H., Höhner, R., Roberty, S., Emonds-Alt, B., Larosa, V., Willamme, R., Duby, F., Onga Dhali, D., Thonart, P., Hiligsmann, S., Franck, F., Eppe, G., Cardol, P., Hippler, M., Remacle, C. (2014) Lack of isocitrate lyase in Chlamydomonas leads to changes in carbon metabolism and in the response to oxidative stress under mixotrophic growth. *Plant J.* 77, 404-417.
- Perez-Martin, M., Perez-Perez, M.E., Lemaire, S.D., Crespo, J.L. (2014) Oxidative stress contributes to autophagy induction in response to endoplasmic reticulum stress in Chlamydomonas. *Plant Physiol.* 166, 997-1008.
- Pérez-Pérez, M.E., Lemaire, S.D., Crespo, J.L. (2012) Reactive oxygen species and autophagy in plants and algae. *Plant Physiol*. 160, 156-64.
- Perez-Perez, M.E., Florencio, F.J., Crespo, J.L. (2010a) Inhibition of target of rapamycin signaling and stress activate autophagy in *Chlamydomonas reinhardtii*. *Plant*

- Physiol. 152, 1874-1888.
- Perez-Perez, M.E., Florencio, F.J., Crespo, J.L. (2010b) Inhibition of target of rapamycin signaling and stress activate autophagy in *Chlamydomonas reinhardtii*. *Plant Physiol*. 152, 874-888.
- Pérez-Pérez, M.E., Lemaire, S.D., Crespo, J.L. (2016) Control of autophagy in Chlamydomonas is mediated through redox-dependent inactivation of the ATG4 protease. *Plant Physiol.* 172, 2219-2234.
- Pineau, B., Gérard-Hirne, C., Selve, C. (2001) Carotenoid binding to photosystems I and II of *Chlamydomonas reinhardtii* cells grown under weak light or exposed to intense light. *Plant Physiol. Biochem.* 39, 73–85.
- Pinnola, A., Dall'Osto, L., Gerotto, C., Morosinotto, T., Bassi, R., Alboresia, A. (2013)

 Zeaxanthin binds to light-harvesting complex stress-related protein to enhance
 nonphotochemical quenching in *Physcomitrella patens*. *Plant Cell*. 25, 3519-3534.
- Porra, R.J., Thompson, W.A., Kriedemann, P.E. (1989) Determination of accurate extinction coefficients and simultaneous equations for assaying chlorophylls a and b extracted with four different solvents: verifying the concentration of chlorophyll standards by atomic absorption spectroscopy. *Biochim. Biophys. Acta. Bioenerg.* 975, 384-394.
- Post, W., Pastor, J., Zinke, P. (1985) Global patterns of soil nitrogen storage. *Nature*. 317, 613-616.
- Quian-Ulloa, R., Stange, C. (2021) Carotenoid biosynthesis and plastid development in plants: the Role of light. *Int. J. Mol. Sci.* 22, 1184.
- Ramundo, S., Casero, D., Mühlhaus, T., Hemme, D., Sommer, F., Crèvecoeur, M. (2014)

 Conditional depletion of the *Chlamydomonas* chloroplast ClpP protease activates

 nuclear genes involved in autophagy and plastid protein quality control. *Plant Cell*.

 26, 2201-2222.

- Rastogi, R.P., Madamwar, D., Nakamoto, H., Incharoensakdi, A. (2020) Resilience and self-regulation processes of microalgae under UV radiation stress. *J. Photochem. Photobio Photobiol. C: Photochem. Rev.* 43, 100322.
- Renberg, L., Johansson, A.I., Shutova, T., Stenlund, H., Aksmann, A., Raven, J.A., Gardeström, P., Moritz, T., Samuelsson, G. (2010) A metabolomic approach to study major metabolite changes during acclimation to limiting CO₂ in *Chlamydomonas reinhardtii. Plant Physiol.* 154, 187-196.
- Rochaix, J.D., Bassi, R. (2019) LHC -like protein involved in stress response and biogenesis/repair of photosynthetic apparatus. *Biochem. J.* 476, 581-593.
- Rossini, F., Provenzano, M.E., Kuzmanović, L., Ruggeri, R. (2019) Jerusalem artichoke (*Helianthus tuberosus* L.): a versatile and sustainable crop for renewable energy production in europe. *Agronomy*. 9, 528.
- Ruban, A.V. Johnson, M.P. Duffy, C.D.P. (2012) The photoprotective molecular switch in the photosystem II antenna. *Biochim. Biophys. Acta. Bioenerg.* 1817, 167-181.
- Ruban, A.V. (2016) Nonphotochemical chlorophyll fluorescence quenching: mechanism and effectiveness in protecting plants from photodamage. *Plant physiol.* 4, 1903-1916.
- Sasso, S., Stibor, H., Mittag, M., Grossman, A.R. (2018) The Natural history of model organisms: from molecular manipulation of domesticated *Chlamydomonas* reinhardtii to survival in nature. *eLife*. 7, e39233.
- Sayegh, F.A., Montagnes, D.J. (2011) Temperature shifts induce intraspecific variation in microalgal production and biochemical composition. *Bioresour. Technol.* 102, 3007-3013.
- Sharma, P., Jha, A.B., Dubey, R.S., Pessarakli, M. (2012) Reactive oxygen species, oxidative damage, and antioxidative defense mechanism in plants under stressful

- conditions. J. Botany. 7, 1-26.
- Srinuanpan, S., Cheirsilp, B., Prasertsan, P., Kato, Y., Asano, Y. (2018) Photoautotrophic cultivation of oleaginous microalgae and co-palletisation with filamentous fungi for cost-effective harvesting process and improved lipid yield. *Aquac. Int.* 26, 1493-1509.
- Scranton, M.A., Ostrand, J.T., Fields, F.J., Mayfield, S.P. (2015) Chlamydomonas as a model for biofuels and bio-products production. *Plant J.* 82, 523–531.
- Shi, K., Gao, Z., Shi, T.Q., Song, P., Ren, L.J., Huang, H., Ji, X.J. (2017) Reactive oxygen species-mediated cellular stress response and lipid accumulation in oleaginous microorganisms: the state of the art and future perspectives. *Front. Mirobiol.* 8, 793.
- Siaut, M., Cuiné, S., Cagnon, C., Fessler, B., Nguyen, M., Carrier, P., Beyly, A., Beisson, F., Triantaphylidès, C., Li-Beisson, Y., Peltier, G. (2011) Oil accumulation in the model green alga *Chlamydomonas reinhardtii*: characterization, variability between common laboratory strains, and relationship with starch reserves. *BMC Biotechnol*. 11, 7.
- Shikanai, T. (2014) Central role of cyclic electron transport around photosystem I in the regulation of photosynthesis. *Curr. Opin. Biotechnol.* 26, 25-30.
- Shtaida, N., Khozin-Goldberg, I., Boussiba, S. (2015) The role of pyruvate hub enzymes in supplying carbon precursors for fatty acid synthesis in photosynthetic microalgae. *Photosynth. Res.* 125, 407-422.
- Simkin, A.J., López-Calcagno, P.E., Raines, C.A. (2019) Feeding the world: improving photosynthetic efficiency for sustainable crop production. *J. Exp. Bot.* 70, 1119-1140.
- Skjanes, K., Rebours, C., Lindblad, P. (2013) Potential for green microalgae to produce hydrogen, pharmaceuticals and other high value products in a combined process.

- Crit. Rev. Biotechnol. 33, 172-215.
- Sorger, D., Daum, G. (2002) Synthesis of triacylglycerols by the acyl-coenzyme A:diacyl-glycerol acyltransferase Dga1p in lipid particles of the yeast *Saccharomyces* cerevisiae. *J. Bacteriol.* 184, 519-524.
- Steinbeck, J., Ross, I.L., Rothnagel, R., Gäbelein, P., Schulze, S., Giles, N., Ali, R., Drysdale,
 R., Sierecki, E., Gambin, Y., Stahlberg, H., Takahashi, Y., Hippler, M., Hankamer,
 B. (2018) Structure of a PSI-LHCI Cyt b₆f supercomplex in *Chlamydomonas*reinhardtii promoting cyclic electron flow under anaerobic conditions. *Proc. Natl.*Acad. Sci. U S A. 115, 10517-10522.
- Su, X., Ma, J., Pan, X., Zhao, X., Chang, W., Liu, Z., Zhang, X., Li, M. (2019) Antenna arrangement and energy transfer pathways of a green algal photosystem I–LHCI supercomplex. *Nat. Plants.* 5, 273-281.
- Subramanyam, R., Jolley, C., Thangaraj, B., Nellaepalli, S., Webber, A.N., Fromme, P. (2010) Structural and functional changes of PSI-LHCI supercomplexes of *Chlamydomonas reinhardtii* cells grown under high salt conditions. *Planta*. 231, 913 -922.
- Subramanyam, R., Jolley, C., Brune, D.C., Fromme, P., Webber, A.N. (2006)

 Characterization of a novel photosystem I–LHCI supercomplex isolated from

 Chlamydomonas reinhardtii under anaerobic (state II) conditions. FEBS Lett. 580,
 233-238.
- Sun, X.M., Ren, L.J., Zhao, Q.Y. (2018) Microalgae for the production of lipid and carotenoids: a review with focus on stress regulation and adaptation. *Biotechnol. Biofuels*.11, 272.
- Tang, Y., Wen, X., Lu, Q., Yang, Z., Cheng, Z., Lu, C. (2007) Heat stress induces an aggregation of the light -harvesting complex of photosystem II in spinach plant.

- Plant Physiol. 143, 629-638.
- Takaichi, S. (2011) Carotenoids in algae: distributions, biosynthesis and functions. *Mar. Drugs*. 9, 1101-1118.
- Takagi, M., Karseno, K., Yoshida, T. (2006) Effect of salt concentration on intracellular accumulation of lipids and triacylglyceride in marine microalgae Dunaliella cells. *J. Biosci. Bioeng.* 101, 223-226.
- Takahashi, Y., Yasui, T., Stauber, E.J., Hippler, M. (2004) Comparison of the subunit compositions of the PSI-LHCI supercomplex and the LHCI in the green alga *Chlamydomonas reinhardtii. Biochemistry.* 43, 7816-7823.
- Takahashi, S., Badger, M.R. (2011) Photoprotection in plants: a new light on photosystem II damage. *Trends Plant Sci.* 16, 53-60.
- Thompson, A.R., Doelling, J.H., Suttangkakul, A., Vierstra, R.D. (2005) Autophagic nutrient recycling in arabidopsis directed by the ATG8 and ATG12 conjugation pathways.

 *Plant Physiol. 138, 2097-2110.
- Tiwari, A., Mamedov, F., Grieco, M., Suorsa, M., Jajoo, A., Styring, S., (2016) Photodamage of iron-sulphur clusters in photosystem I induces non-photochemical energy dissipation. *Nat. Plants.* 2, 16035.
- Timmins, M., Thomas-Hall, S.R., Darling, A., Zhang, E., Hankamer, B., Marx U.C., Schenk, P.M. (2009) The metabolome of *Chlamydomonas reinhardtii* following induction of anaerobic H₂ production by sulfur depletion. *J. Exp. Bot.* 60, 1691–1702.
- Timm, S., Florian, A., Wittmiß, M., Jahnke, K., Hagemann, M., Fernie, A.R., Bauwe, H. (2013) Serine acts as a metabolic signal for the transcriptional control of photorespiration-related genes in Arabidopsis. *Plant physiol.* 162, 379–389.
- Tran, Q.G., Cho, K., Park, S.B., Kim, U., Lee, Y.J., Kim, H.S. (2019) Impairment of starch

- biosynthesis results in elevated oxidative stress and autophagy activity in *Chlamydomonas reinhardtii*. *Sci. Rep.* 9, 9856.
- Tsukada, M., Ohsumi, Y. (1993) Isolation and characterization of autophagy-defective mutants of *Saccharomyces cerevisiae*. *FEBS Lett.* 333, 169-174.
- Tokutsu, R., Kato, N., Bui, K.H., Ishikawa, T., Minagawa, J. (2012) Revisiting the supramolecular organization of photosystem II in *Chlamydomonas reinhardtii*. *J. Biol. Chem.* 287, 31574-31581.
- Tolleter, D., Ghysels, B., Alric, J., Petroutsos, D., Tolstygina, I., Krawietz, D., Happe, T.,
 Auroy, P., Adriano, J.M., Beyly, A., Cuiné, S., Plet, J., Reiter, I.M., Genty, B.,
 Cournac, L., Hippler, M., Peltier, G. (2011). Control of hydrogen photoproduction
 by the proton gradient generated by cyclic electron flow *in Chlamydomonas reinhardtii. Plant Cell.* 23, 2619-2630.
- Terashima, M., Petroutsos, D., Hüdig, M., Tolstygina, I., Trompelt, K., Gäbelein, P. (2012)

 Calcium-dependent regulation of cyclic photosynthetic electron transfer by a CAS,

 ANR1, and PGRL1 complex. *Proc. Natl. Acad. Sci. U.S.A.* 109, 17717-17722.
- Towbin, H., Staehelin, T., Gordon, J. (1979) Electrophoretic transfer of proteins from polyacrylamide gels to nitrocellulose sheets: procedure and some applications. *Proc.*Natl. Acad. Sci. USA. 76, 4350-4354.
- Tuller, H.L. (2017) Solar to fuels conversion technologies: a perspective. *Mater. Renew. Sustain. Energy.* 6, 3.
- Ufaz, S., Galili, G. (2008) Improving the content of essential amino acids in crop plants: goals and opportunities. *Plant Physiol*. 147, 954-961.
- Upadhyaya, S., Agrawal, S., Gorakshakar, A., Rao, B.J. (2020) TOR kinase activity in *Chlamydomonas reinhardtii* is modulated by cellular metabolic states. *FEBS Lett*. 594, 3122-3141.

- Van Doorn, W.G. (2011) Classes of programmed cell death in plants, compared to those in animals. *J. Exp. Bot.* 62, 4749-4761.
- Voss, I., Sunil, B., Scheibe, R., Raghavendra, A.S. (2013) Emerging concept for the role of photorespiration as an important part of abiotic stress response. *Plant Biol.* 15, 713-722.
- Wase, N., Tu, B., Rasineni, G.K., Cerny, R., Grove, R., Adamec, J., Black, P.N., DiRusso,
 C.C. (2019) Remodeling of Chlamydomonas metabolism using synthetic inducers
 results in lipid storage during growth. *Plant Physiol.* 181, 1029-1049.
- Wagenen, J.V., Miller, T.W., Hobbs, S., Hook, P., Crowe, B., Huesemann, M. (2012) Effects of light and temperature on fatty acid production in *Nannochloropsis Salina*. *Energies.* 5, 731-740.
- Wijffels, R.H., Barbosa, M.J. (2010) An outlook on microalgal biofuels. *Science*. 13, 796-799.
- Wang, Z., Benning, C. (2011) *Arabidopsis thaliana* polar glycerolipid profiling by thin layer chromatography (TLC) coupled with gas-liquid chromatography (GLC). *J. Vis. Exp.* 49, 2518.
- Wang, H. Zhang, Y., Zhou, W., Noppol, L., Liu, T. (2018) Mechanism and enhancement of lipid accumulation in filamentous oleaginous microalgae *Tribonema minus* under heterotrophic condition. *Biotechnol. Biofuels.* 1, 328.
- Wettstein, D.V., Gough, S., Kannangara, C.G. (1995) Chlorophyll Biosynthesis. *Plant Cell.* 7, 1039 -1057.
- Wu, H.H., Zou, Y.N., Rahman, M. (2017) Mycorrhizas alter sucrose and proline metabolism in trifoliate orange exposed to drought stress. *Sci. Rep.* 7, 42389.
- Wulf, P., Vandamme, E.J. (1997) Microbial synthesis of D-ribose: metabolic deregulation and fermentation process. *Adv. Appl. Microbiol.* 44, 167-214.

- Wulff-Zottele, C., Gatzke, N., Kopka, J., Orellana, A., Hoefgen, R., Fisahn, J., Hesse, H.(2010) Photosynthesis and metabolism interact during acclimation of *Arabidopsis* thaliana to high irradiance and sulphur depletion. *Plant Cell Environ*. 33, 1974-1988.
- Qiu, X.M., Sun, Y.Y., Ye, X.Y., Li, Z.G. (2020) Signaling role of glutamate in plants. *Front. Plant Sci.* 10, 1743.
- Yadav, R.M., Aslam, S.M., Madireddi, S.K. (2020) Role of cyclic electron transport mutations *pgrl1* and *pgr5* in acclimation process to high light in *Chlamydomonas* reinhardtii. Photosynth. Res. 146, 247-258.
- Yadavalli, V., Jolley, C.C., Malleda, C., Thangaraj, B., Fromme, P., Subramanyam, R. (2012)

 Alteration of proteins and pigments influence the function of photosystem I under iron deficiency from *Chlamydomonas reinhardtii*. PLoS One. 7, e35084.
- Yamamoto, Y., Aminaka, R., Yoshioka, M., Khatoon, M., Komayama, K., Takenaka, D., Yamashita, A., Nijo, N., Inagawa, K., Morita, N., Sasaki, T., Yamamoto, Y. (2008)

 Quality control of photosystem II: impact of light and heat stresses. *Photosynth. Res.* 98, 589-608.
- Yang, W., Wang, F., Liu, L.N., Sui, N. (2020) Responses of membranes and the photosynthetic apparatus to salt stress in Cyanobacteria. *Front. Plant Sci.* 11, 00713.
- Yang, Y., Mininberg, B., Tarbet, A., Weathers, P. (2013) At high temperature lipid production in *Ettlia oleoabundans* occurs before nitrate depletion. *Adv. Appl. Microbiol.* 97, 2263-2273.
- Yang, W., Wittkopp, T.M., Li, X., Warakanont, J., Dubini, A., Catalanotti, C., Kim, R.G.,
 Nowack, E.C., Mackinder, L.C., Aksoy, M., Page, M.D., D'Adamo, S., Saroussi,
 S., Heinnickel, M., Johnson, X., Richaud, P., Alric, J., Boehm, M., Jonikas, M.C.,

- Benning, C., Grossman, A.R. (2015) Critical role of *Chlamydomonas reinhardtii* ferredoxin-5 in maintaining membrane structure and dark metabolism. *Proc. Natl. Acad. Sci. U.S.A.* 112, 14978-14983.
- Yilancioglu, K., Cokol, M., Pastirmaci, I., Erman, B., Cetiner, S. (2014) Oxidative stress is a mediator for increased lipid accumulation in a newly isolated *Dunaliella* salina strain. *PLoS One*. 9, e91957.
- Yeesang, C., Cheirsilp, B. (2011) Effect of nitrogen, salt, and iron content in the growth medium and light intensity on lipid production by microalgae isolated from freshwater sources in Thailand. *Bioresour. Technol.* 102, 3034-3040.
- Yoon, K., Han, D., Li, Y., Sommerfeld, M., Hu, Q. (2012) Phospholipid:diacylglycerol acyltransferase is a multifunctional enzyme involved in membrane lipid turnover and degradation while synthesizing triacylglycerol in the unicellular green microalga *Chlamydomonas reinhardtii*. *Plant Cell*. 24, 3708-3724.
- Zhang, L., Selao, T.T., Selstam, E., Norling, B. (2015) Subcellular localization of carotenoid biosynthesis in *Synechocystis* sp. PCC 6803. *PLoS One*. 10, e0130904.
- Zhang, M., Fan, J., Taylor, D.C., Ohlrogge, J.B. (2009) DGAT1 and PDAT1 acyltransferases have overlapping functions in Arabidopsis triacylglycerol biosynthesis and are essential for normal pollen and seed development. *Plant Cell.* 21, 3885-3901.
- Zhekisheva, M., Boussiba, S., Khozin-Goldberg, I., Zarka, A., Cohen, Z. (2002)

 Accumulation of triacylglycerols in *Haematococcus Pluvialis* is correlated with that of astaxanthin esters. *J. Phycol.* 38, 40-41.

Publications

- 1 **Chouhan, N**., Devadasu E., Yadav, R., Subramanyam R. Autophagy Induced Accumulation of Lipids in *pgrl1* and *pgr5* of *Chlamydomonas reinhardtii* Under High Light . *Frontiers in Plant Science*, 12, 2022.
- 2 Devadasu, E., Chinthapalli, DK., Chouhan, N., Madireddi, SK., Rasineni, GK., Sripadi, P., Subramanyam, R.(2019) Changes in the photosynthetic apparatus and lipid droplet formation in *Chlamydomonas reinhardti*i under iron deficiency. *Photosynth Res.* 2019 Mar;139(1-3):253-266.
- 3 Yadav, RM., Aslam, SM., Madireddi, SK., **Chouhan, N.**, Subramanyam, R. Role of cyclic electron transport mutations pgrl1 and pgr5 in acclimation process to high light in *Chlamydomonas reinhardtii*. *Photosynth Res.* 2020 Dec;146(1-3):247-258.
- 4 **Chouhan, N.,** Yadav, RM., Pandey, J., Subramanyam, R. Macromolecular structural changes in thylakoid supercomplexes of cyclic electron transport mutants of *C. reinhardtii* under high light. submitted in BBA (under review).
- 5 Yadav. RM., **Chouhan, N.**, Madireddi, SK., Subramanyam, R. PGR5 dependent cyclic electron transport pathway is independent of LHCSR3 in high light from *C.reinhardtii* (under review).
- 6 **Chouhan, N.,** Marriboina, S., Subramanyam, R., Metabolomic response of *pgrl1* and *pgr5* mutants of *C.reinhardtii* under high light(under review).

High light induced changes in metabolites, lipids and thylakoid supercomplexes organisation of cyclic electron transport deficeint mutant of Chlamydomonas reinhardtii

by Nisha Chouhan

Submission date: 17-May-2022 03:16PM (UTC+0530)

Submission ID: 1838261684

File name: Nisha_Chouhan.pdf (503.83K)

Word count: 26695 Character count: 142695 High light induced changes in metabolites, lipids and thylakoid supercomplexes organisation of cyclic electron transport deficeint mutant of Chlamydomonas reinhardtii

ORIGINALITY REPORT STUDENT PAPERS PUBLICATIONS INTERNET SOURCES SIMILARITY INDEX PRIMARY SOURCES www.frontiersin.org Internet Source University of Hyderab Nisha Chouhan, Elsinraju Devadasu, Ranay Mohan Yadav, Rajagopal Subramanyam. "Autophagy Induced Accumulation of Lipids in pgrl1 and pgr5 of Chlamydomonas reinhardtii Under High Light", Frontiers in Plant Science, 2022 Publication www.biorxiv.org Internet Source Elsinraju Devadasu, Jayendra Pandey, Kunal Dhokne, Rajagopal Subramanyam. "Restoration of photosynthetic activity and supercomplexes from severe iron starvation in Chlamydomonas reinhardtii", Biochimica et Biophysica Acta (BBA) - Bioenergetics, 2021

www.mdpi.com

Publication

5	Internet Source	1 %
6	Submitted to University of Hyderabad, Hyderabad Student Paper	<1%
7	link.springer.com Internet Source	<1%
8	www.ncbi.nlm.nih.gov Internet Source	<1%
9	www.tandfonline.com Internet Source	<1%
10	hdl.handle.net Internet Source	<1%
11	R. K. Puzanskiy, A. L. Shavarda, E. R. Tarakhovskaya, M. F. Shishova. "Analysis of metabolic profile of Chlamydomonas reinhardtii cultivated under autotrophic conditions", Applied Biochemistry and Microbiology, 2014 Publication	<1%
12	www.plantphysiol.org Internet Source	<1%
13	idus.us.es Internet Source	<1%

14	"Chlamydomonas: Molecular Genetics and Physiology", Springer Science and Business Media LLC, 2017 Publication	<1%
15	www.thaiscience.info Internet Source	<1%
16	Submitted to Jawaharlal Nehru University (JNU) Student Paper	<1%
17	Janani Manochkumar, C. George Priya Doss, Hesham R. El-Seedi, Thomas Efferth, Siva Ramamoorthy. "The neuroprotective potential of carotenoids in vitro and in vivo", Phytomedicine, 2021	<1%
18	Isha Kalra, Xin Wang, Marina Cvetkovska, Jooyeon Jeong et al. " sp. UWO241 exhibits constitutively high cyclic electron flow and rewired metabolism under high salinity ", Cold Spring Harbor Laboratory, 2019 Publication	<1%
19	María Esther Pérez-Pérez, Stéphane D. Lemaire, José L. Crespo. "Reactive Oxygen Species and Autophagy in Plants and Algae", Plant Physiology, 2012	<1%

20	Yamori, Wataru, and Toshiharu Shikanai. "Physiological Functions of Cyclic Electron Transport Around Photosystem I in Sustaining Photosynthesis and Plant Growth", Annual Review of Plant Biology, 2016. Publication	<1%
21	lipidlibrary.aocs.org Internet Source	<1%
22	Advances in Photosynthesis and Respiration, 2014. Publication	<1%
23	Anish Kundu, Shruti Mishra, Jyothilakshmi Vadassery. "Spodoptera litura-mediated chemical defense is differentially modulated in older and younger systemic leaves of Solanum lycopersicum", Planta, 2018 Publication	<1%
24	p2receptor-signal.com Internet Source	<1%
25	orbi.ulg.ac.be Internet Source	<1%
26	Fujii, Ritsuko, Nami Yamano, Hideki Hashimoto, Norihiko Misawa, and Kentaro Ifuku. "Photoprotection vs. Photoinhibition of Photosystem II in Transplastomic Lettuce (Lactuca sativa) Dominantly Accumulating Astaxanthin", Plant and Cell Physiology, 2015.	<1%

Srilatha Nama, Sai Kiran Madireddi, Elsin Raju <1% 27 Devadasu, Rajagopal Subramanyam. "High light induced changes in organization, protein profile and function of photosynthetic machinery in Chlamydomonas reinhardtii", Journal of Photochemistry and Photobiology B: Biology, 2015 **Publication** Submitted to Trinity College Dublin <1% 28 Student Paper Inmaculada Couso, María Esther Pérez-Pérez, 29 Enrique Martínez-Force, Hee-Sik Kim et al. "Autophagic flux is required for the synthesis of triacylglycerols and ribosomal protein turnover in Chlamydomonas", Journal of Experimental Botany, 2017 Publication

Laura Klasek, Kentaro Inoue. "Dual Protein Localization to the Envelope and Thylakoid Membranes Within the Chloroplast", Elsevier BV, 2016

Publication

Paul H. M. Kullmann, Kristine M. Sikora, K.
Lyles Clark, Irene Arduini, Mitchell G. Springer,
John P. Horn. "HCN hyperpolarizationactivated cation channels strengthen virtual
nicotinic EPSPs and thereby elevate synaptic

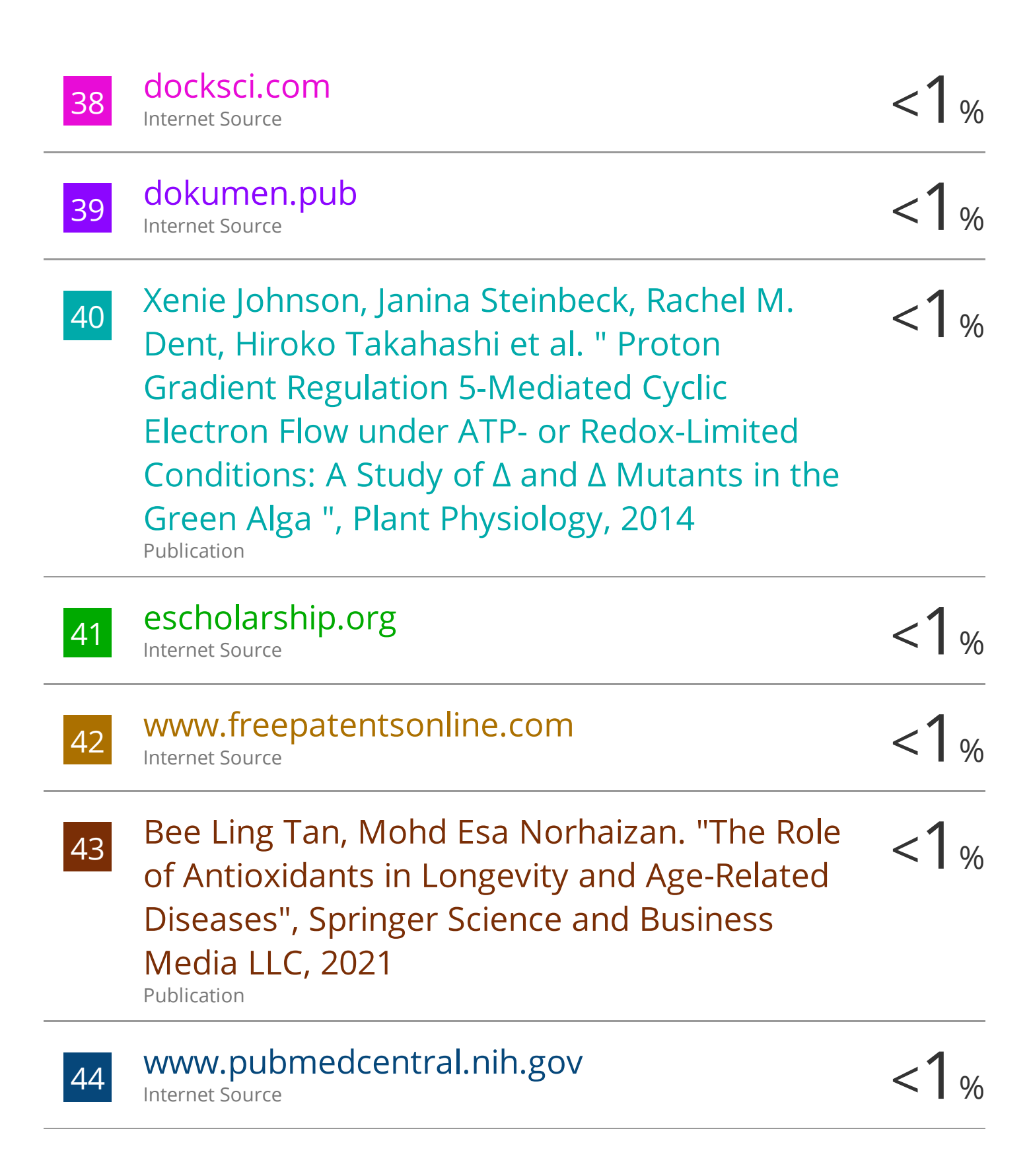
<1%

<1%

amplification in rat sympathetic neurons", Journal of Neurophysiology, 2016

Publication

32	cyberleninka.org Internet Source	<1%
33	dspace.unitus.it Internet Source	<1%
34	Mingzhu Ma, Yifei Liu, Chunming Bai, Yunhong Yang, Zhiyu Sun, Xinyue Liu, Siwei Zhang, Xiaori Han, Jean Wan Hong Yong. "The Physiological Functionality of PGR5/PGRL1-Dependent Cyclic Electron Transport in Sustaining Photosynthesis", Frontiers in Plant Science, 2021 Publication	<1%
35	Sureshbabu Marriboina, Kapil Sharma, Debashree Sengupta, Anurupa Devi Yadavalli et al. " Systematic hormone-metabolite network provides insights of high salinity tolerance in (L.) pierre ", Cold Spring Harbor Laboratory, 2020 Publication	<1%
36	www.koreascience.or.kr Internet Source	<1%
37	Advances in Photosynthesis and Respiration, 2003. Publication	<1%



Exclude quotes On Exclude bibliography On





Autophagy Induced Accumulation of Lipids in *pgrl1* and *pgr5* of Chlamydomonas reinhardtii Under High Light

Nisha Chouhan, Elsinraju Devadasu, Ranay Mohan Yadav and Rajagopal Subramanyam*

Department of Plant Sciences, School of Life Sciences, University of Hyderabad, Hyderabad, India

triggered lipid metabolism in microalgae has not being studied so far from a mutant of proton gradient regulation 1 like (PGRL1) and proton gradient regulation 5 (PGR5). In this study, C. reinhardtii cells (wild-type CC124 and cyclic electron transport dependant mutants pgr11 and pgr5) were grown photoheterotrophically in high light 500 µmol photons m⁻² s⁻¹, where pgr5 growth was retarded due to an increase in reactive oxygen species (ROS). The lipid contents were increased; however, carbohydrate content was decreased in pgr5. Further, the Nile Red (NR) fluorescence shows many lipid bodies in par5 cells under high light. Similarly, the electron micrographs show that large vacuoles were formed in high light stress despite the grana stacks structure. We also observed increased production of reactive oxygen species, which could be one reason the cells underwent autophagy. Further, a significant increase of autophagy ATG8 and detections of ATG8-PE protein was noticed in pgr5, a hallmark characteristic for autophagy formation. Consequently, the triacylglycerol (TAG) content was increased due to diacylglycerol acyltransferases (DGAT) and phospholipid diacylglycerol acyltransference (PDAT) enzymes' expression, especially in pgr5. Here the TAG synthesis would have been obtained from degraded membrane lipids in par5. Additionally, mono, polyunsaturated, and saturated fatty acids were identified more in the high light condition. Our study shows that the increased light induces the reactive oxygen

Chlamydomonas (C.) reinhardtii is a potential microalga for lipid production. Autophagy-

Dalian University of Technology, China Ayse Kose, Ege University, Turkey Justin Findinier, Carnegie Institution for Science, United States

São Paulo State University, Brazil

*Correspondence:

Rajagopal Subramanyam srgsl@uohyd.ernet.in

OPEN ACCESS

Edited by:

Milton Lima Neto

Reviewed by: Fantao Kong,

Specialty section:

This article was submitted to Plant Abiotic Stress, a section of the journal Frontiers in Plant Science

Received: 03 August 2021 Accepted: 20 December 2021 Published: 25 January 2022

Citation:

Chouhan N, Devadasu E, Yadav RM and Subramanyam R (2022) Autophagy Induced Accumulation of Lipids in pgrl1 and pgr5 of Chlamydomonas reinhardtii Under High Light. Front. Plant Sci. 12:752634. doi: 10.3389/fpls.2021.752634 Keywords: Chlamydomonas reinhardtii, cyclic electron transport, lipid bodies, Nile Red fluorescence, triacylglycerol

species, which leads to autophagy and TAG accumulation. Therefore, the enhanced

accumulation of TAGs can be used as feedstock for biodiesel production and aqua feed.

INTRODUCTION

Light is vital for microalgae for efficient photosynthesis. CO₂ fixation by Calvin Benson cycle occurs through photosynthesis that primarily synthesizes carbohydrates, leading to the synthesis of lipid stored as triacylglycerols (TAG) (Mondal et al., 2017). Microalgal species do not accumulate increased amounts of neutral lipids under normal growth conditions. Neutral lipid is accumulated under unfavorable conditions like nutrient, light, salt, and temperature stresses. Under normal light

1

ORIGINAL ARTICLE



Role of cyclic electron transport mutations *pgrl1* and *pgr5* in acclimation process to high light in *Chlamydomonas reinhardtii*

Ranay Mohan Yadav¹ · Sabit Mohammad Aslam¹ · Sai Kiran Madireddi¹ · Nisha Chouhan¹ · Rajagopal Subramanyam¹

Received: 4 February 2020 / Accepted: 15 April 2020 / Published online: 29 April 2020 © Springer Nature B.V. 2020

Abstract

Light is crucial for photosynthesis, but the amount of light that exceeds an organism's assimilation efficacy can lead to photooxidative damage and even cell death. In *Chlamydomonas* (*C*). *reinhardtii* cyclic electron flow (CEF) is very important for
the elicitation of non-photochemical quenching (NPQ) by controlling the acidification of thylakoid lumen. This process
requires the cooperation of proton gradient regulation (PGR) proteins, PGRL1 and PGR5. Here, we compared the growth
pattern and photosynthetic activity between wild type (137c, t222+) and mutants impaired in CEF (pgrl1 and pgr5) under
photoautotrophic and photoheterotrophic conditions. We have observed the discriminative expression of NPQ in the mutants
impaired in CEF of pgrl1 and pgr5. The results obtained from the mutants showed reduced cell growth and density, Chl
a/b ratio, fluorescence, electron transport rate, and yield of photosystem (PS)II. These mutants have reduced capability to
develop a strong NPQ indicating that the role of CEF is very crucial for photoprotection. Moreover, the CEF mutant exhibits
increased photosensitivity compared with the wild type. Therefore, we suggest that besides NPQ, the fraction of non-regulated
non-photochemical energy loss (NO) also plays a crucial role during high light acclimation despite a low growth rate. This
low NPQ rate may be due to less influx of protons coming from the CEF in cases of pgrl1 and pgr5 mutants. These results
are discussed in terms of the relative photoprotective benefit, related to the thermal dissipation of excess light in photoautotrophic and photoheterotrophic conditions.

Keywords Chlamydomonas reinhardtii \cdot Chlorophyll fluorescence \cdot Cyclic electron transport \cdot High light \cdot Non-photochemical quenching \cdot Photosystems

Introduction

Photosynthesis is the process that can harness solar energy to fix it as chemical energy in a biologically available form. This is a highly regulated process that involves different electron transfer pathways for the generation of ATP and NADPH. The major portion of electron flux required for the generation of ATP and NADPH is provided by linear electron flow (LEF). This process involves the transfer of

Electronic supplementary material The online version of this article (https://doi.org/10.1007/s11120-020-00751-w) contains supplementary material, which is available to authorized users.

electrons from water, the primary electron donor, via photosystem (PS) II, several redox carriers, and PSI to the terminal electron acceptor NADP⁺. These electron transfer reactions are coupled with proton translocation from stroma to thylakoid lumen that generates proton motive force for the production of ATP by ATP synthase. The ATP and NADPH produced in this process are utilized by the Calvin–Benson cycle and other downstream metabolic reactions.

The stoichiometric proportions of 3ATP to 2NADPH required for the carbon fixation is slightly imbalanced towards NADPH in LEF. Therefore, the additional demand for ATP is compensated by the cyclic electron flow (CEF) (Alric 2010). CEF involves the reoxidation of NADPH and/or ferredoxin (FD) through plastoquinone (PQ), cytochrome (Cyt) b_6 f complex and PSI. This process generates the transmembrane proton gradient utilized in the ATP synthesis (Kramer et al. 2004a, b). In vascular plants and green algae, the CEF occurs through two pathways, antimycin-sensitive



Rajagopal Subramanyam srgsl@uohyd.ernet.in

Department of Plant Sciences, School of Life Sciences, University of Hyderabad, Gachibowli, Hyderabad, Telangana 500046, India

ORIGINAL ARTICLE



Changes in the photosynthetic apparatus and lipid droplet formation in *Chlamydomonas reinhardtii* under iron deficiency

Elsinraju Devadasu¹ · Dinesh Kumar Chinthapalli^{1,3} · Nisha Chouhan¹ · Sai Kiran Madireddi¹ · Girish Kumar Rasineni² · Prabhakar Sripadi³ · Rajagopal Subramanyam¹

Received: 22 April 2018 / Accepted: 28 August 2018 / Published online: 14 September 2018 © Springer Nature B.V. 2018

Abstract

The unicellular photosynthetic alga *Chlamydomonas reinhardtii* was propagated in iron deficiency medium and patterns of growth, photosynthetic efficiency, lipid accumulation, as well as the expression of lipid biosynthetic and photosynthesis-related proteins were analysed and compared with iron-sufficient growth conditions. As expected, the photosynthetic rate was reduced (maximally after 4 days of growth) as a result of increased non-photochemical quenching (NPQ). Surprisingly, the stress-response protein LHCSR3 was expressed in conditions of iron deficiency that cause NPQ induction. In addition, the protein contents of both the PSI and PSII reaction centres were gradually reduced during growth in iron deficiency medium. Interestingly, the two generations of Fe deficiency cells could be able to recover the photosynthesis but the second generation cells recovered much slower as these cells were severely in shock. Analysis by flow cytometry with fluorescence-activated cell sorting and thin layer chromatography showed that iron deficiency also induced the accumulation of triacylglycerides (TAG), which resulted in the formation of lipid droplets. This was most significant between 48 and 72 h of growth. Dramatic increases in DGAT2A and PDAT1 levels were caused by iron starvation, which indicated that the biosynthesis of TAG had been increased. Analysis using gas chromatography mass spectrometry showed that levels of 16:0, 18:0, 18:2 and 18:3^{Δ9,12,15} fatty acids were significantly elevated. The results of this study highlight the genes/enzymes of *Chlamydomonas* that affect lipid synthesis through their influence on photosynthesis, and these represent potential targets of metabolic engineering to develop strains for biofuel production.

Keywords Electron transport · Iron deficiency · LHCSR3 · Major lipid droplet protein · Photosystems · Triacylglycerol

Electronic supplementary material The online version of this article (https://doi.org/10.1007/s11120-018-0580-2) contains supplementary material, which is available to authorized users.

- ☐ Rajagopal Subramanyam srgsl@uohyd.ernet.in
- Department of Plant Sciences, School of Life Sciences, University of Hyderabad, Hyderabad, Telangana 500046, India
- ² Center for Excellence in Medical Services Pvt. Ltd., Kineta Towers, Road No. 3, Banjara Hills, Hyderabad, Telangana 500034, India
- ³ Analytical Chemistry and Mass Spectrometry, CSIR-Indian Institute of Chemical Technology, Hyderabad, Telangana 500 007, India

Introduction

The microalgae, a diverse group of eukaryotic photosynthetic organisms, occupy diverse habitats including freshwater, marine and more extreme environments such as hot springs and frozen regions (Li et al. 2012a, b). This ability to adapt to different environmental conditions is due to the plasticity of algal physiology. Microalgae have been used as a source of biodiesel (Chisti et al. 2007) and they are considered promising candidates for large-scale biofuel production due to their high photosynthetic efficiency and oil accumulation ability (Borowitzka and Moheimani 2013; Moody et al. 2014).

Abiotic stress leads to a variety of cellular responses in eukaryotic photosynthetic algae, including changes to the photosynthetic apparatus (Glaesener et al. 2013). In addition, stress leads to increased accumulation of lipids, particularly triacylglycerides (TAG) (Juergens et al. 2015).

